Effect of Biochar Amended Soils on Infiltration Processes

Vom Promotionsausschuss der
Technischen Universität Hamburg
zur Erlangung des akademischen Grades
Doktor-Ingenieurin (Dr.-Ing.)
genehmigte Dissertation

von

Karolina Villagra-Mendoza

aus

San José, Costa Rica

2019

1. Gutachter:

Prof. Dr.-Ing. Ralf Otterpohl, Technische Universität Hamburg

2. Gutachter:

Prof. Prof. h .c. Dr. Dr. h. c. Rainer Horn, Christian-Albrechts-Universität zu Kiel

Vorsitzender des Promotionsverfahrens:

Prof. Dr.-Ing. Peter Fröhle, Technische Universität Hamburg

Tag der mündlichen Prüfung: 21.10.2019

Abstract

Climate change imposes new challenges on agricultural practices due to extreme and rapid changes in the environmental conditions. Soil conservation becomes a primarily task due to its importance for supporting agricultural sustainability and food security. This thesis deals with the analysis and simulation of the effect of biochar amendments on soil water dynamics. In a microscale, infiltration at the topsoil is analyzed; in a macroscale, its impact in catchment hydrology is assessed.

An analysis of the main soil parameters affected by the biochar amendments is presented. The role of the biochar chemical characteristics on the soil amendments and the effect of the biochar dosage as a function of the soil type are exposed. The impact of biochar of two different soil materials is analyzed in terms of the effect of the main soil physical and hydraulic properties. Simulation of intense and repetitive extreme climate conditions (by means of wetting and drying periods) are considered as a critical environmental parameter influencing the dynamics of soil aggregate formation in the topsoil.

The effect of biochar amendments on the soil water balance equation considers the infiltration process as a key factor on the surface runoff formation. The water infiltration response by the amendments is tested by conventional infiltration equations and a statistical regression model in order to determine the main parameters and mechanisms that deals with the transport of water at the surface and in the soil matrix.

Several scenarios of the complexity of the addition of biochar, as a soil conservation management option, at a macroscale level are evaluated. In this case, all the soil water balance parameters are included and the discharge outputs reveal that biochar as a source of organic carbon alters soil aggregation and pore characteristics enhancing or reducing the capacity of the soil matrix to conduct water; and these bulk changes are a function of intense periods of wetting and drying. It is shown that application of biochar as amendment as an option for soil conservation and water management has a complex relation of the biomass composition, application dosage, soil type and environmental conditions.

Author keywords: biochar; catchment hydrology; infiltration process; infiltration models; soil physical and hydraulic properties; wetting and drying periods.

Acknowledgment

Contents

List of Figures and Tables

Figures

Tables

List of Symbols and Acronyms

Notation

x, y, z	Cartesian coordinates

Symbols

PV	Porosity
ρ_d	Soil bulk density, *g/cm³*
ρ_s	Soil particle density, *g/cm³*
ρ_l	Density of the liquid, *g/cm³*
ε	Pore ratio, *cm³/cm³*
ϑ	Moisture ratio, *cm³/cm³*
h	Height of capillary rise, *cm*
r	Equivalent radius of the capillary, *cm*
γ_l	Surface tension between liquid/gas, *kg/s²*
δ	Contact angle between water and soil, *grads*
g	Gravitational acceleration, *m/s²*
R_e	Reynolds number
q	Specific flux vector, *m/s*
Q	Rate of flow, *m³/s*
A_c	Cross section area, *m²*
K	Saturated hydraulic conductivity tensor, *m/s*
∇H	Hydraulic gradient vector
H	Hydraulic head, *m*
θ	Volumetric soil water content, *cm³/cm³*
ψ_m	Soil matric potential, *kPa*
∇	Del operator
q_w	Specific flux vector for unsaturated condition, *m/s*
$K(\psi)$	Unsaturated hydraulic conductivity, *m/s*

z	Gravitational potential, *kPa*
$\theta(\psi)$	Soil-water content-pressure head function, *cm³/cm³*
θ_r	Residual soil water content, *cm³/cm³*
θ_s	Saturated soil water content, *cm³/cm³*
α'	Inverse of the air entry value, *1/cm*
n, m	Soil water retention curve empirical fitting parameters
K_{sat}	Saturated hydraulic conductivity, *m/s*
$K_r(\psi)$	Relative hydraulic conductivity
λ	Tortuosity or pore connectivity parameter
Δ_P	Contracting force, *kg cm/s²*
r_1, r_2	Radii of the grain size and the water meniscus between two grains, *cm*
χ, p, q	Soil shrinkage characteristic curve fitting parameters
ε_s	Void ratio at saturated water content, *cm³/cm³*
ε_r	Void ratio at residual water content, *cm³/cm³*
V_w	Volume of water, *cm³*
V_s	Volume of solids, *cm³*
V_p	Volume of pores, *cm³*
P	Precipitation, *mm*
R	Surface runoff, *mm*
E	Evaporation, *mm*
ΔS	Change in water storage, *mm*
i	Infiltration capacity, *mm/h*
$Intf$	Interflow, *mm*
$Perc$	Percolation, *mm*
Eva	Evapotranspiration, *mm*
CU	Capillary uprise, *mm*
$Icum$	Cumulative infiltration, *mm*
S_s	Sorptivity, *cm/d¹ᐟ²*
A	Philip empirical constant, *cm/d*
Ib	Final infiltration capacity, *mm/h*
I_o	Initial infiltration capacity, *mm/h*
β	Horton empirical parameter
C	Kostiakov empirical parameter
α	Kostiakov empirical parameter

b	Kostiakov empirical parameter
I_N	Rainfall intensity, *mm/h*
l	Flow length, *cm*
$\overline{\Delta\vartheta}$	Change of soil water content between two measurements, cm^3/cm^3
$grad\psi_m$	Hydraulic gradient between two points, *kPa/cm*
d	Parameter dependent on the diffusion of water in the soil
r	Internal radius of the infiltrometer, *cm*
f	Air-filled porosity, cm^3/cm^3
$S_{s\_Ethanol}$	Sorptivity of ethanol, $cm/d^{1/2}$
S_{s_water}	Sorptivity of water, $cm/d^{1/2}$
K_l	Air conductivity, *m/s*
ρ_l	Air density, kg/m^3
ΔV	Volume of air, m^3
Δp	Pressure, *hPa*
A_{cl}	Average area of the cylinder, m^2
K_a	Air permeability, cm^2
μ_l	Air dynamic viscosity, *g/cm s*
$\emptyset_i$	Internal diameter of infiltrometer, *cm*
ΔL	Water that infiltrates through the surface, *ml*
Δt	Time interval, *s*
R^2	Coefficient of determination
R	Correlation coefficient
A	inflection point
B	wet-side maximum curvature
C	dry-side maximum curvature
D	air entry
E	shrinkage limit
Ø	Diameter of pores, *µm*
R/P	Fraction of surface runoff from precipitation
R$_{BC}$/R	Fraction of surface runoff of the amended treatments respect to the unamended soil

Acronyms

1D	One-dimensional
AC	Air capacity
AICc	Small-sample-size corrected version of Akaike information criterion (AIC)
ANOVA	Analysis of variance
AWC	Available water capacity
BET	Multipoint Brunauer Emmett-Teller
C	Organic carbon
CEC	Cation exchange capacity
CN	Curve number
CV	Coefficient of variation
DEM	Digital elevation model
EC	Electrical conductivity
FC	Field capacity
GW	Groundwater
H	Hydrogen
HSD	Honestly-significant-difference
m.a.s.l	Meters above sea level
MSSE	Mean sum of square error
N	Nitrogen
O	Oxygen
PSD	Pore size distribution
RETC	RETention curve
RI	Repellency index
S	Sulfur
S	Sandy soil
SL	Sandy loam soil
SSA	Specific surface area
SSC	Soil shrinkage characteristic curve
SSQ	Sum of squares
SSS	Soil shrinkage simulator
SWAT	Soil and Water Assessment Tool
TC	Total carbon
TDR	Time domain reflectometry
TP	Total porosity

WD	Wetting and Drying cycle
WHC	Water holding capacity
WP	Wilting point
WRC	Water retention curve
wt.	Weight

1. Introduction

1.1. Motivation and Context of this Work

Land degradation due to wrong farming practices and contamination endangers soil productivity and aggravates the problem of food security. Drylands are expanding and it is expected that they will cover half of the global land surface by the end of the century (FAO and ITPS, 2015). Many dryland regions such as Mediterranean areas, Africa, China, Asia, and South America are the most sensitive facing climate change and are prompt to suffer soil desertification and degradation in the near future (Villagra-Mendoza et al., 2017). Agricultural activities are directly impacted by degraded soils that show lower retention capacity and require higher doses of fertilizers, increasing production costs (Glaser et al., 2001). Instability in the upper soil layer structure and percolation ratios are high in degraded soils, which can lead to groundwater contamination. Therefore, there is an urgent need to look for sustainable farming practices aimed to water and soil conservation (Villagra-Mendoza et al., 2017).

Biochar as a soil conditioner has been identified as a key factor to improve soil biochemical and physical - i.e., mechanical and hydraulic - characteristics (Abel et al., 2013; Ajayi and Horn, 2016a, 2016b; Brewer, 2012; Ding et al., 2016). However, many studies present different trends with regard to the biochar effects on physical properties depending on soil type. For instance, some studies found a positive correlation between soil properties - such as bulk densities, porosity, water retention, available water holding capacity, and structural stability- and the addition of biochar (Ajayi and Horn, 2016b; Barnes et al., 2014; Bayabil et al., 2015; Devereux et al., 2012; Glaser et al., 2001; Liu et al., 2017). In contrast, other studies demonstrated negative effects on the hydraulic soil conductivity, especially on coarser textures (Ajayi & Horn, 2016a; Herath et al, 2013; Jeffery et al., 2015; Lim et al., 2016). Some other studies have described the shrinkage effect on some soil properties such as bulk density, porosity and water retention (Ajayi et al., 2016; Horn et al., 2017; Peng et al., 2007).

Water and solute transports in the vadose zone depend on the distribution, size, shape and configuration of the pores. They impact the soil hydraulic properties and are directly related to processes such as water storage, infiltration, groundwater recharge, but also erosion and runoff. Soils amended with biochar have become an option to improve their physical and hydraulic properties. Therefore, it is important to understand how water moves in amended soils with biochar to make decisions on sustainable water availability for plants.

This work is a contribution to the topic of the modeling of infiltration dynamics in amended soils with biochar. Figure 1.1 depicts the overall approach of this work: the effect of biochar application on the physicochemical and hydraulic properties of two

textural soils and the effect of wetting and drying on the soil structure and water dynamics. The water infiltration capacity was analyzed through the comparison of experimental data with empirical and semi-empirical infiltration models. Moreover, a regression analysis was carried out to explain the main soil parameters that influence infiltration on biochar amendment soils. Finally, the contribution of biochar and repetitive wetting and drying periods on the hydrological response of a catchment at a macroscale level was analyzed.
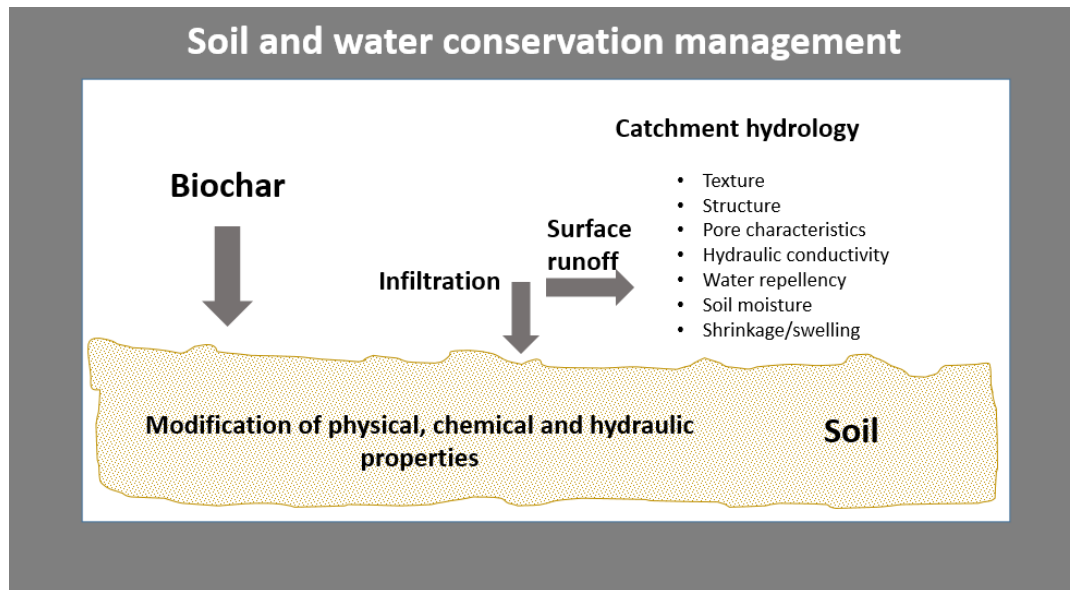
Figure 1.1. Overall scheme of the investigation of biochar application in the catchment hydrology as part of a soil and water conservation practice**.**

The hypothesis of this study is that biochar as part of a soil conservation option is able to overcome intense drought periods by improving soil physical and hydraulic properties. Moreover, it is thought that biochar enhances soil infiltration water capacity, reducing surface runoff and improving the watershed hydrology.

1.2. Organization of the Work

This thesis is organized into six chapters whose contents are detailed as follows:

Chapter 2 presents a brief introduction to soil physics and the main physical and hydraulic parameters related to the dynamics of non-rigid soils. It reviews the state of the art of biochar amendments and the related soil shrinkage effects.

Chapter 3 discusses biochar characteristics and effects on the most important soil physical and hydraulic properties. This chapter also reviews infiltration models and their physical interpretation.

Chapter 4 addresses the experimental validation, covering laboratory setup, methodology and mathematical formulation to compute soil physical and hydraulic parameters.

Chapter 5 deals with the analysis of the results and validation of the proposed model. The results are compared with respect to the outcome of different empirical infiltration models available in the literature. A regression analysis is performed to determine the main soil parameters that influence water infiltration in biochar amended soils. This chapter ends with the modelling of infiltration and runoff volume at a catchment scale, where a water dynamics pattern is obtained as a function of biochar dosage and wetting and drying cycles.

Chapter 6 discusses the main results obtained and addresses a detailed explanation of the main mechanisms that deals with water infiltration of biochar amended soils.

Chapter 7 summarizes the main findings of this study. The main contributions of this thesis regarding the effect of biochar on the soil properties and infiltration dynamics are reviewed. Recommendations for further work are also provided.

2. Water Behavior in Porous Media

Soil properties such as texture, structure and porosity play an important role on hydraulic functioning. This chapter provides an insight into the main physical and hydraulic soil characteristics, which influence the behavior of the soil water movement in the soil medium.

Soil is composed of inorganic and organic solids, water and air. Under optimal conditions the solid components constitute about 50% of the total volume, while water and air constitute about 25% each (Lal and Shukla, 2005). These solid-water-air components are non-rigid, and they change the relationship between their mass, volume and energy as the factors such as climate and management, interact with them. Figure 2.1 depicts the interaction of the solid components, water and air under three different moist conditions. When soil is completely dry, only solids and air interact and is called a two-phase system. As soil is moistened water starts filling partially the soil pores, and becomes a three phase (water, air and soil) system. Finally, as the soil medium reaches saturation, the pore spaces are filled with water interacting with the solids.

| Dry soil | Moist soil | Saturated soil |
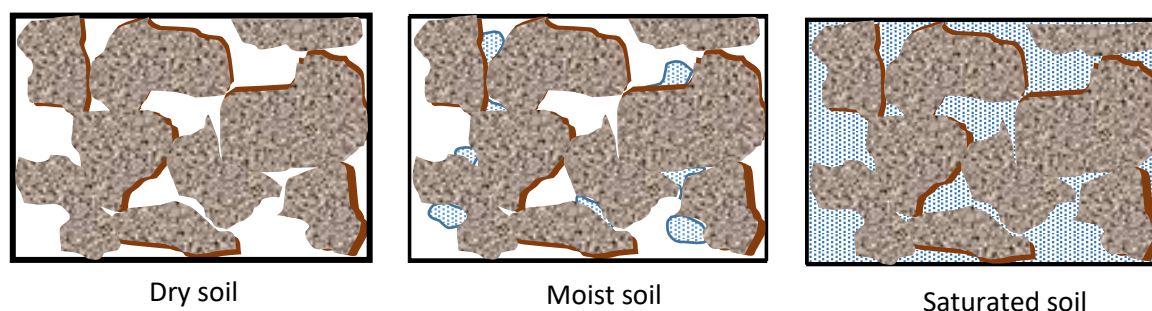
Figure 2.1. Interactions between solids, water and air for three moistened soil conditions (after Lal and Shukla, 2005).

The space between the solids filled with air and water constitute the pores. They are interconnected and represent a network of pore channels - with variable pore geometries of different shape, length and width- that enables water and air to move through (Warrick, 2003). These different pore diameters and interconnections may alter the fluxes to a great extent. Thus, the capacity parameters and the intensity values may differ intensely and influence the rate at which water can flow in the soil profile.

2.1. Capacity Parameters

Pore characteristics and interconnections limit their water filling and transport capacity. They create pathways within the soil matrix which may help the water to fill the pore spaces within the bulk.

2.1.1. Porosity

Porosity (PV) describes how densely the material is packed in a given volume of soil, and it is defined as the percentage of the total soil volume occupied by pores (Hartge and Horn, 2016; Lal and Shukla, 2005):

$$PV = 1 - \frac{\rho_d}{\rho_s}$$

(2.1)

where ρ_d (g/cm^3) is bulk density and ρ_s (g/cm^3) is the density of the solid particles (known as particle density). In general, porosity decreases as particle density increases, due to a bulk density increment; thus, sandy soils (coarse-grained solids) show lower porosity than clay rich soils (fine-grained solids).

Porosity is important in the building of corridors within the soil matrix, known as pore interconnectivity, enabling water and air to move into the soil. It plays a key role in the stability of the soil structure in terms of soil aggregation, which may cause an increase in available water capacity (Obia et al., 2016). Eusufzai & Fujii (2012) found an enhancement of hydraulic conductivity and water retention properties, due to increase in macro porosity of a clay loam soil by adding organic matter as amendment. Poor porosity facilitates soil erosion by runoff flow instead of allowing water to enters into the soil (Githinji, 2014).

The pore ratio (ε) is widely used in soil mechanics to express the ratio of pores compared to a volume of solids (Hartge and Horn, 2016; Lal and Shukla, 2005):

$$\varepsilon = \frac{\rho_s}{\rho_d} - 1$$

(2.2)

2.1.2. Pore Size Characteristics

.2.1.2.1   Pore Size Distribution

Pore size distribution associates the pore size with a particular matric potential at which the pore can be emptied. This is explained by the equation of capillary ascent or by the Young-Laplace equation (Hartge and Horn, 2016):

$$\text{h} = 2\gamma_l \frac{\cos \delta}{r\, \rho_l\, g} \tag{2.3}$$

where h is the height of capillary rise, r is the equivalent radius of the capillary, γ_l is the surface tension between liquid/gas (0.0727 kg/s^2 at 20°C), δ is the contact angle between water and soil (for a wettable surface it is assumed that $\delta = 0°$; $\cos \delta = 1$), ρ_l is the density of the liquid and g is the gravitational acceleration (9.8 m/s^2). The capillary rise is inversely proportional to the equivalent radius of the pores in a system and with the help of pressure (including ρ_l and g) the capillaries are drained.

Pores can be classified according to their origin, function or other attributes (Nimmo, 2004). They are commonly described by empirical limits of pore classes, based on pressure and equivalent pore diameter (Kutílek et al., 2006). In terms of their diameter, pore size is commonly classified in three categories. Micropores or fine pores with pore diameters of less than 0.2 μm and matric potentials more negative than -15000 hPa. These pores are typical for clayey soils, where water is retained mainly by adsorptive forces and do not participate in ordinary liquid flow phenomena. This water is referred as residual water, being not accessible for plants (Hillel, 1998). Capillary pores or mesopores, are in the range size of 0.2 and 50 μm with matric potentials between -60 and -15000 hPa (Hartge and Horn, 2016). These are medium-textured pores and fluid movement obeys capillarity and Darcy´s Law. Flow in these pores is, generally, laminar (Hillel, 1998). These pores are important for plant growth since they retain water against gravity. Macropores are pores with diameters greater than 50 μm. The water flow is, due to gravity forces, dominated by matric potentials less negative than -60 hPa (Hartge and Horn, 2016). They also can appear in the form of shrinkage cracks or fissures in clayey soils upon drying, or can be the product of biological activity (earth worms, root channels). The flow is often turbulent $(R_e > 1)$ in these pores when they are filled with water. Macropores increase infiltration rates and adequate aeration of plant roots.

The soil pore system can also be classified in terms of their aggregates (Alaoui et al., 2011; Kutílek et al., 2006; Nimmo, 2004): 1) matrix or textural pores (intra-aggregate pores) are within the soil aggregates and they do not contribute to the flow movement through the soil matrix; and, 2) structural pores (inter-aggregate pores), which are between the aggregates, contain macro pores or shrink/swell cracks and have a

significant effect on the pore interconnectivity and preferential flow, in terms of water flow and solute transport processes.

.2.1.2.2   Pore Geometry

Shape and continuity of the pore space play an important role on the air and water conductivity (Hartge and Horn, 2016). Differences in pore geometry and continuity affect the way pores are emptied. In some cases, larger pores surrounded by smaller pores drain after the latter drains first and air can pass through the finer pores. Tortuosity refers to the complexity of the fluid pathways through a porous media (Khabbazi et al., 2016). It depends on the arrangement of the soil aggregates (structural condition) and the soil water content; thus, it is associated to the soil permeability (Moldrup et al., 2001; Sun et al., 2013). Therefore, the interconnectivity of the pore systems plays an important role on the energy consumption as the fluid moves through the soil.

The complexity of the arrangement of the pores in natural soil systems (Figure 2.2), the formation of cracks, rootholes, and the soil structure (prismatic, polyhedral, sub-angular blocky, platy, column, etc.) may contribute to exhibit a pattern of micro pores and macro pores with varying directional bias. This leads to flow paths with changes in magnitude and flow direction (Dörner, 2005) and affects the water conductivity in the soil.
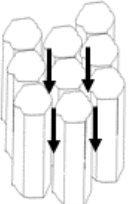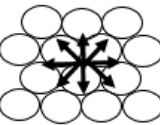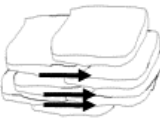
Aggregation	Prismatic	Spherical or granular	Blocky	Platy	Columnar
Dominant flow	Vertical anisotropic	Isotropic	Vertical anisotropic - isotropic	Horizontal anisotropic	Vertical anisotropic - isotropic

Figure 2.2. Example of different aggregate arrangements and their dominant flow direction (after Hartge and Horn, 2016).

2.2. Intensity Parameters: Water Movement in the Porous Media

2.2.1. Hydraulic Conductivity

Hydraulic conductivity influences the movement of water in the soil matrix (Hartge and Horn, 2016). It depends on texture, structure and pore properties (configuration, size, shape and distribution). Soils with large pore diameters drain off first, and react as barrier to the water flow at more negative matric potentials. At saturation, coarse textured soils conduct water more rapidly than finer textures (Jury and Horton, 2004). The same occurs for aggregated soils compared with poorly aggregated ones.

Depending on the characteristic of the pore system, the hydraulic conductivity flow may vary in all directions (*x, y, z*), as illustrated in Figure 2.2. It may be represented as a tensor where the horizontal component of the hydraulic conductivity may be greater or smaller than the vertical component. Hydraulic conductivity may be also asymmetrical and it may have different values for opposite directions of flow, known as soil anisotropy (Hillel, 1998). According to Dörner (2005) only spherical soil particle arrangements could exhibit isotropic behavior and anisotropy is generally observed in the scale of soil horizons. In individual soil horizons containing fine materials, platy structures or highly compacted, the horizontal hydraulic conductivity is greater than the vertical. In highly structured soils, the behavior may approach to isotropy.

Soil anisotropy affects the flow processes through the soil such as infiltration, interflow (known also as lateral flow), percolation and groundwater recharge. The rate at which many of these flow processes in the soil matrix occur depends on the pore diameter and its continuity.

Fluxes occur both under saturated and unsaturated conditions. They vary not only with the soil characteristics but also as a function of the soil water content. The main flow principles regarding these two water conditions are explained in the following subsections.

.2.2.1.1   Flow Movement under Saturated Conditions

Under steady, homogeneous, stable systems of intermediate pore size and saturated fluid conditions, the flow movement is described based on the potential concept and linear flow equation of Darcy´s Law (Hillel, 1998). The flux (q) through an isotropic medium is expressed as the product of the resistance to flow which characterizes the medium and forces acting to push the fluid to the medium (Selker et al., 1999):

$$q = \frac{Q}{A_c} = -K\nabla H \qquad (2.4)$$

where q is the specific flux vector (m/s), Q is the rate of flow (m³/s), A_c is the cross-section area of the medium at which the fluid moves through (m²), K is the saturated hydraulic conductivity tensor of the medium (m/s) and ∇H is the hydraulic gradient vector in the vertical and horizontal direction.

For one-dimensional systems it takes the form (Jury and Horton, 2004):

$$q = -K\frac{dH}{dx} = -K\frac{H_{i+1}-H_i}{x_{i+1}-x_i} \qquad (2.5)$$

or,

$$q = -K\frac{dH}{dz} = -K\frac{H_{i+1}-H_i}{z_{i+1}-z_i} \qquad (2.6)$$

where H_{i+1} and H_i are the hydraulic heads at two points in the dissolved directions, horizontal (x) or vertical (z).

The potential, expressed in equation 2.5 and 2.6, refers to the flow movement as a result of a change of potential energy, from areas of high potential towards areas of lower potential (denoted by a minus sign). This potential is driven by forces such as *pressure potential or pressure head*, described as the height of column of water that could be supported by the pressure measured at the point of interest; and *gravitational or elevation potential (z)*, which represents the height measured from a reference level (Selker et al., 1999).

The hydraulic conductivity K represents the slope of the linear relation between the hydraulic gradient (∇H) the flux (q) and they together influence the water movement. Structure and texture affect the hydraulic conductivity. For instance, highly porous and/or aggregated soils possess higher K values than compacted and dense soils (Hartge and Horn, 2016; Hillel, 1998).

Due to the highly spatial variability of the soil pore distribution rather than texture itself, K in the vertical direction may be different as K in the horizontal direction. Even it may change between soil horizons. Therefore, Darcy´s Law (eq. 2.4) may be rewritten for a homogeneous, anisotropic medium in three orthogonal spatial directions (Hartge and Horn, 2016):

$$q_x = -[K_{xx}\frac{dH}{dx} + K_{xy}\frac{dH}{dy} + K_{xz}\frac{dH}{dz}]$$

$$q_y = -[K_{yx}\frac{dH}{dx} + K_{yy}\frac{dH}{dy} + K_{yz}\frac{dH}{dz}] \qquad (2.7)$$

$$q_z = -[K_{zx}\frac{dH}{dx} + K_{zy}\frac{dH}{dy} + K_{zz}\frac{dH}{dz}]$$

where the hydraulic conductivity is represented as a 2nd order symmetrical tensor, expressed as a matrix $[K]$:

$$[K] = \begin{vmatrix} K_{xx} & K_{xy} & K_{xz} \\ K_{yx} & K_{yy} & K_{yz} \\ K_{zx} & K_{zy} & K_{zz} \end{vmatrix} \qquad (2.8)$$

Darcy´s Law is restricted to a linear relationship between the flux (q), the hydraulic gradient (dH/dx), the laminar flow (such as in silt or finer materials) and to a relative low Reynolds numbers (smaller than 1). Moreover, the flow must overcome a critical hydraulic gradient to be predicted by Darcy´s Law equation (Hillel, 1998) and it must be a rigid pore system. Under saturated and unsteady flow conditions magnitude, direction of the flux and hydraulic gradient vary in time, even for turbulent flow, the *law of mass conservation in combination to Darcy´s Law apply* (Hillel, 1998):

$$\frac{d\theta}{dt} = -\nabla \cdot q = \nabla \cdot K\nabla H \qquad (2.9)$$

Equation (2.9) expresses an equation of continuity which relates the rate of a fluid inflow-outflow in a volume element, where storing or decreasing may be observed in soil water content depending on this rate relation.

.2.2.1.2   Flow Movement in Unsaturated Soils

Water movement depends on soil texture, structure, pore geometry and the water content, because when the soil is not totally saturated, water flows downward by gravity through pores that are filled with water and, to a lesser extent, with air. As air increases its presence, the flow changes radically creating an irregular solid boundary and decreasing the cross-section of the flow. The flow becomes confined to the smaller pores increasing tortuosity as the water content decreases. Under unsaturated soil water conditions, larger pores in coarse-textured soils become nonconductive as matric potential develops, which steeply decreases the hydraulic conductivity. In contrast, in fine textured soils smaller pores dominate and conduct less water but more constantly, up to

more negative matric potential values. Thus, the hydraulic conductivity does not decrease as steeply as for coarse soils (Figure 2.3). Irrespective of the pore diameter, tortuosity affects the hydraulic conductivity in finer textured soils as it decreases the water fluxes and keeps it constant at a more negative matric potential. Thus, the more tortuous the pores are, the more is the water flux retarded (Hillel, 1998; Jury and Horton, 2004; Selker et al., 1999). This modifies the linear behavior of the hydraulic conductivity to a non-linear function of water content (θ) or matric potential (ψ_m) with a great impact on tortuosity and water-filled pores.
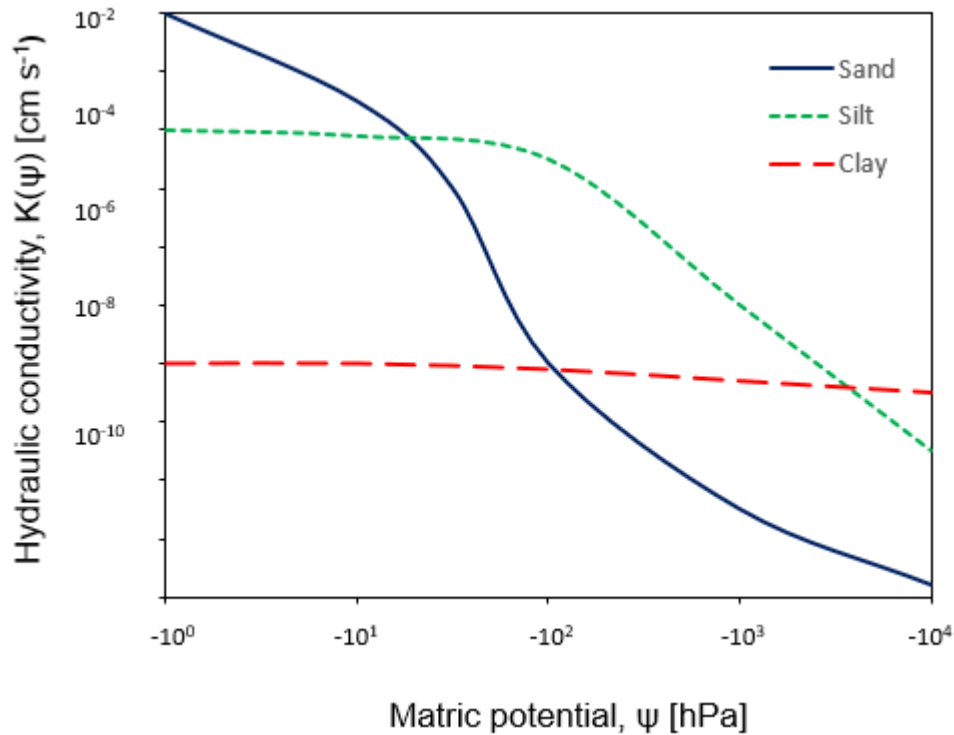
Figure 2.3. Unsaturated hydraulic conductivity curve for various soil classes (after Hartge and Horn, 2016).

Darcy´s Law refers to the movement of water under saturated conditions, however this is rather the exception of mostly soils in nature (Hartge and Horn, 2016). Soils, in general, present a certain degree of unsaturation, with water bounded partially by solid surfaces and by an interphase with the air phase (Jury et al., 1991). The Buckingham-Darcy law for unsaturated flow is expressed as (Selker et al., 1999):

$$q_w = -K(\psi)\nabla H \qquad\qquad (2.10)$$

where $K(\psi)$ is the unsaturated hydraulic conductivity as a function of the matric potential.

The main difference of Eq. (2.10) to Eq. (2.4) is that the primarily driving force is the gradient of a negative matric potential instead of the gradient of a positive matric potential (Hartge and Horn, 2016; Hillel, 1998).

Recalling Eq. (2.9) and modifying it for a transient flow (Hillel, 1998), the following expression holds:

$$\frac{d\theta}{dt} = -\nabla \cdot q = \nabla \cdot [K(\psi)\nabla H] \tag{2.11}$$

This equation is known as the *Richards equation*. For one-dimensional vertical flow, it is expressed as (Jury et al., 1991) follows:

$$\frac{d\theta}{dt} = \frac{d}{dz}\left[K(\psi)\left(\frac{d\psi}{dz} + 1\right)\right] \tag{2.12}$$

It may also be expressed in the general form for a three-dimensional space linking Darcy with the continuity equation flow as (Hartge and Horn, 2016):

$$\frac{d\theta}{dt} = \frac{d\left[K(\psi)\frac{d(\psi+z)}{dx}\right]}{dx} + \frac{d\left[K(\psi)\frac{d(\psi+z)}{dy}\right]}{dy} + \frac{d\left[K(\psi h)\frac{d(\psi+z)}{dz}\right]}{dz} \tag{2.13}$$

where θ is the water content (cm³/cm³), ψ_m and z are the matric and gravitational potentials (kPa), respectively, K is the hydraulic conductivity (m/s) and x, y, z are the spatial coordinates.

2.3. Modelling Soil Hydraulic Functions

Estimation of hydraulic functions is commonly based on models that consider Poiseuille´s law and the pore distribution of a soil described by pF-curve and the saturated hydraulic conductivity (Hartge and Horn, 2016). Many models have been developed to predict the soil water retention, and based on the additional information about the saturated hydraulic conductivity, derive also the unsaturated hydraulic conductivity curves (Brooks and Corey, 1964; Burdine, 1953; Gardner, 1958; Ghanbarian-Alavijeh and Hunt, 2012; Mualem, 1976; van Genuchten, 1980). Mostly, these models assume pore rigidity, and combine capacity (water retention curve) and intensity (e.g. hydraulic conductivity) parameters.

2.3.1. Modelling Water Retention

Van Genuchten (1980) proposed a soil-water content-pressure head curve, $\theta(\psi)$, based on the pore size distribution model of Mualem (1976). This expression was used to predict the unsaturated hydraulic conductivity in terms of soil water parameters. The soil water retention parameters, expressed by van Genuchten (1980) are:

$$\theta(\psi) = \theta_r + \frac{\theta_s - \theta_r}{[1+(\alpha'\psi_m)^n]^m}$$

(2.14)

where θ is the volumetric soil water content (cm³/cm³), ψ_m is the matric potential (kPa), θ_s is the saturated water content (cm³/cm³), θ_r is the residual water content (cm³/cm³), α' is the inverse of the air entry value (1/cm) and n, m are independent empirical parameters describing the S-shape steepness of the water retention curve. Parameter m may be restricted by Mualem´s model as $m = 1 - 1/n$ or Burdine´s model (1953) as $m = 1 - 2/n$.

2.3.2. Modelling Hydraulic Conductivity

Commonly, models consider the unsaturated hydraulic conductivity $K(\psi)$ divided into two parts; one is the saturated hydraulic conductivity and the other, the relative hydraulic conductivity as a function of the matric potential. Van Genuchten (1980) predicted the $K(\psi)$ model based on the capillary model of Mualem (1976), in combination with Eq.(2.14):

$$K(\psi) = K_{sat} \cdot K_r(\psi)$$

(2.15)

$$K(\psi) = K_{sat} \cdot \frac{[1-(\alpha'|\psi_m|)^{n-1}(1+(\alpha'|\psi_m|)^n)^{-m}]^2}{[1+(\alpha'|\psi_m|)^n]^{m\cdot\lambda}}$$

(2.16)

where $K(\psi)$ is the unsaturated hydraulic conductivity, K_{sat} is the saturated hydraulic conductivity (cm/d), $K_r(\psi)$ is the the relative hydraulic conductivity expressed as a function of the matric potential and λ (-) is a tortuosity or pore connectivity parameter.

2.3.3. Limitations of the Models

Environmental and anthropogenic conditions, such as shrinkage and swelling, mechanical deformation, plowing, biological and chemical processes may induce intense changes in the soil medium (Nimmo, 2004). Changes in the pore properties (distribution, shape and configuration) affect the hydraulic properties of the soil, such as hydraulic conductivity and soil water retention. These properties are important under field conditions, where the interconnected pores drain first and water flow is then influenced by the properties of the aggregates. Shrinkage and swelling contribute to the orientation of soil particles, affecting the formation of macro pores (enlarged by shrinkage and decreased by swelling) and the formation of aggregates with an intra-aggregate pore system. This aggregate re-formation enhances the contact between aggregates, which keeps the pores more conductive close to saturation. The intra-aggregate porosity and its hydraulic conductivity affect the fluxes in the soil. During the initial formation of aggregates new finer pores are formed and together with more contact points between the single particles promote a smaller flux; while more homogeneous and greater flux occur after the aggregate formation, together with a more continuous macroscopically homogeneous pore system, has reached the final stage of smallest entropy (Horn, 1994). As all fluxes, the hydraulic conductivity must be considered as a tensor with direction dependent values. Horn et al. (2014) described these interactions by means that the isotropic conditions are less frequent to be seen, whereas vertical or horizontal anisotropic flux conditions dominate in prisms, blocky or platy structures. Saturated hydraulic conductivity K_{sat} is mostly determined by large pores and greatly reduced when soil density increases. Contrary to K_{sat}, the unsaturated hydraulic conductivity $K(\psi)$ is enhanced by the increase in the pore connectivity (i.e. due to compaction) between smaller pores, due to the increase of the contact surface areas between the aggregates. (Alaoui et al., 2011; Hartge and Horn, 2016; Kutílek et al., 2006; Peng et al., 2007).

2.4. Soil Shrinkage

Swelling refers to the rewetting of the soil whereas shrinkage is the drying soil stage. Periods of swelling and shrinkage, referred as wetting and drying (WD), induce aggregate formation and rearrangement of particles. When soil dries, the soil particles and pores rearrange by contracting forces, reducing the soil matrix volume and changing particle shape (Hartge and Horn, 2016; Peng et al., 2016). Cracks or macro pores may be formed and depending on their magnitude they may damage plant root growth (Lal and Shukla, 2005) and trigger preferential flow (Saravanathiiban et al., 2014). In non-rigid soils, shrinkage may be present in the vertical, horizontal or even in both directions. Vertical shrinkage may result in the subsidence of the soil by compaction of the soil aggregates, while horizontal shrinkage produces soil cracks inducing preferential flow into deeper soil layers (Kutílek et al., 2006). When soil wets, the soil matrix increases its

volume, closing partially cracks and fissures. This deformation changes again the pore geometry and alters the dynamics of the soil hydraulic properties (Coppola et al., 2015).

Alternating periods of WD induces deformation of the pore geometry influenced by the pore rigidity characteristics and the intense capillary stress (Peng et al., 2016). The contracting force exerted during shrinkage is more pronounced in fine grained soils –with smaller pore diameter than coarser-grained soils – having a higher surface tension (γ_l). Since in nature pores have irregular shape and cross section, the contracting force (Δ_P) is expressed for non-spherical shape, as follows (Hartge and Horn, 2016):

$$\Delta_P = \gamma_l (\frac{1}{r_1} + \frac{1}{r_2}) \tag{2.17}$$

where r_1, r_2 are the radii of the grain size and the water meniscus between two grains. This equation shows that the contracting force is directly proportional to the surface tension of water and inversely proportional to the radii of the grain and meniscus formed.

Macropore or crack formation produces loss of water and nutrients to deeper zones, and reduce rewetting potential of the soil, affecting plant growth. According to Peng et al. (2007) changes in soil structure of organic and inorganic soils differ in their response to WD cycles followed by irreversible soil structure conditions; and textural properties – clayey particles more than silty – as well as soil organic compounds are more susceptible to deformation.

Assessing the shrinkage dynamics helps to provide a better agronomical management to understand and take the proper actions in terms of available water capacity of soil, nutrient retention, pollution control of groundwater, and irrigation and drainage.

2.4.1. Modelling Shrinkage in Soils

The way shrunk soils change their specific volume is a function of their water content (Boivin et al., 2006). It is represented by the soil shrinkage characteristic curve (SSC) characterized by the void ratio as a function of the moisture ratio (Cornelis et al., 2006; Peng and Horn, 2005). The general SSC, shown in Figure 2.4, exhibits four shrinkage phases (Hartge and Horn, 2016) ranging from saturation to drying conditions and exhibits different soil rigidity stages while shrinking (Peng and Horn, 2005). The *structural shrinkage* (I), is characterized by a constant void ratio in a changed moisture ratio interval from saturation to the shrinkage limit. These pores are emptied without changing the soil volume, representing soil rigidity. The *proportional or normal shrinkage* (II), represents the proportional decrease of the soil volume and the water content, and ranges from the structural shrinkage limit to the air entry point into the soil. During this phase the volume of air remains constant and the soil aggregates remain fully saturated. The *residual shrinkage* (III) refers to the segment when the air enters the pores of the soil aggregates,

and the soil volume decrease is smaller than the water loss. Finally, the *zero shrinkage* (IV) is the segment where the soil volume remains approximately constant as the last water volume is removed (Bronswijk, 1991; Lal and Shukla, 2005; Peng and Horn, 2005; Zolfaghari et al., 2016).
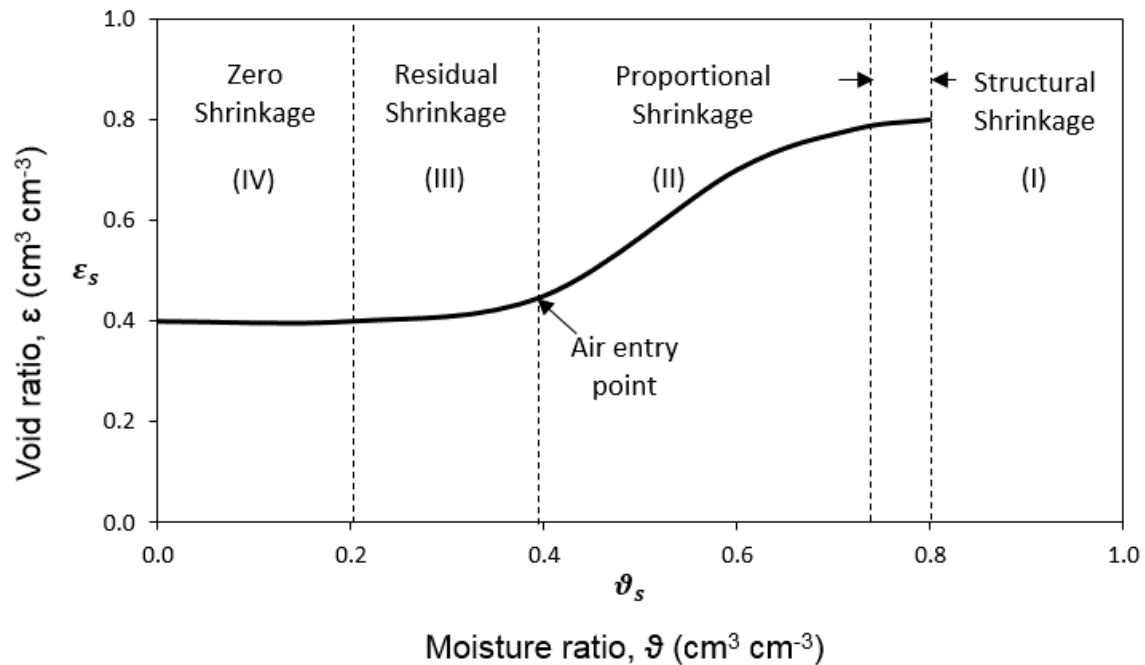
Figure 2.4. Typical soil shrinkage curve with all four phases (after Hartge and Horn, 2016).

The shape of the SSC may vary for structure and structureless soils. Whereas well-structured soils may exhibit the four phases with a sigmoidal shape, structureless soils may lack of structural shrinkage. Table 2.1 shows six shrinkage curve scenarios combining the four shrinkage zones (structural, proportional, residual, and zero shrinkage) based on the shrinkage curve model proposed by Peng and Horn (2013).

Table 2.1. Types of soil shrinkage curves based on four shrinkage zone (after Peng and Horn, 2013)

Soil Shrinkage Type	Shrinkage Zone	Example of SSC
Type A	Four Shrinkage Zones	
Type B	Structural, Proportional and Residual	
Type C	Structural and Proportional	
Type D	Proportional	
Type E	Proportional and Residual	
Type F	Proportional, Residual and Zero	

The shape of the shrinkage curve (SSC) is opposite to the water retention curve, therefore the sign of the n parameter (in the retention curve) is modified (and named as p in the SSC). Moreover, the parameter θ is substituted by the moisture ratio (ϑ) and ψ_m is substituted by the void ratio (ε) in the SSC, where ε_s and ε_r are the void ratios at saturation and at a residual water content, respectively. The following equation expresses the shrinkage curve followed by its boundary conditions (Peng and Horn, 2005):

$$\varepsilon(\vartheta) = \begin{cases} \varepsilon_r & \vartheta = 0 \\[2ex] \varepsilon_r + \dfrac{\varepsilon_s - \varepsilon_r}{[1+(\chi\vartheta)^{-p}]^q} & 0 < \vartheta < \vartheta_s, \quad n > 0 \\[2ex] \varepsilon_s & \vartheta = \vartheta_s \end{cases} \tag{2.18}$$

where χ, p, q are dimensionless fitting parameters, as in the water retention curve. The boundary conditions of Eq. (2.18) are:

$$\begin{aligned} \vartheta \to 0; \quad \frac{\vartheta}{\varepsilon_s - \vartheta} \to 0; \quad \varepsilon \to \varepsilon_r \\ \vartheta \to \vartheta_s; \quad \frac{\vartheta}{\varepsilon_s - \vartheta} \to \infty; \quad \varepsilon \to \varepsilon_s \end{aligned} \tag{2.19}$$

The relationship between the moisture ratio (ϑ, cm³/cm³) and the void ratio (ε, cm³/cm³) is defined as follows (Peng and Horn, 2005):

$$\vartheta = \frac{V_w}{V_s} \tag{2.20}$$

$$\varepsilon = \frac{V_p}{V_s} \tag{2.21}$$

where V_w, V_s and V_p are the volume of water (cm³), solid (cm³) and pores (cm³), respectively. The representation of the SSC requires simultaneous measurements of pore and water volume in a known volume of soil and in a range of water from saturation until dryness. The actual soil volume for each soil water stage is obtained by multiplying the soil height by the initial soil bulk area.

3. Effect of Biochar in the Infiltration Processes

Biochar as soil conditioner has been identified as a key factor to improve biochemical, physical, mechanical and hydraulic soil characteristics. The enhancement of these soil properties has demonstrated to impact related processes such as water storage, infiltration, groundwater recharge, erosion and runoff. This chapter, exposes the effect of biochar on soil properties and its effect on infiltration processes at the soil surface.

3.1. Biochar as Amendment

Biochar is a compound derived from the combustion of any carbon-containing material (manure, feedstock, green waste) in a zero or partial absence of oxygen (pyrolysis) (Brewer et al., 2011; Spokas et al., 2012).

The recent trend to use biochar as amendment is based on the findings in the Amazonian region, where the indigenous agricultural management practices lead to the creation of a black soil, called "terra preta do Indio" (Villagra-Mendoza and Horn, 2018a). This black soil was a mixture of biochar, animal manure, human excrements, human and animal bones, aquatic plants, fish residues, turtle shells, etc. (Factura et al., 2010; Glaser et al., 2001; Lehmann, 2009). Although several studies have been carried out in the Brazilian region, soil patches of terra preta have been found in other regions such as Ecuador, Peru and West and South Africa (Sohi et al., 2009). These anthropogenic soils have been identified as high fertile and of high quality in comparison to other soils. They contain high concentrations of nutrients and stable soil organic matter in form of char content, which is the main reason for their dark color (Glaser et al., 2001).

Sohi et al. (2009) have pointed out that biochar is a good alternative to protect soils against climate change due to its ability to increase the soil water absorption capacity. Figure 3.1 shows the direct relation of the quality of biochar as soil amendment to the variables mentioned above. Moreover, Brewer (2012) and Spokas et al. (2012) have emphasized the effect of biochar as soil conditioner and the strong relation that exists between quality of the biomass feedstock, thermal production processes, application rates and soil type to which it is amended.
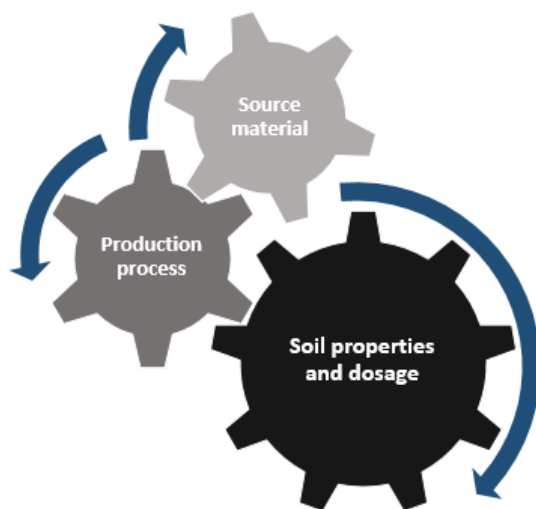
Figure 3.1. Scheme of the relation of the quality of biochar amendments to source material, production processes and soil properties.

3.1.1. Feedstock Characteristics and Production Processes

Biochar can be produced from a variety of biomass feedstock such as bioenergy crops, forest residues, organic waste, agricultural waste, kitchen waste, sewage sludge, among others. However, the properties of each biomass, as base material, may differ from the thermal conversion processes. The quality of the biomass feedstock depend on the ash and moisture content, caloric value, fraction of fixed carbon and volatile components, percentage of lignin, cellulose and hemicellulose, percentage and composition of inorganic substances, bulk density and particle size (Brewer et al., 2011; Nartey and Zhao, 2014). From those, lignin is a significant quality parameter because it is decomposed in a wide range of temperatures and contributes more to the biochar formation. Whereas cellulose and hemicellulose decompose rapidly at low temperatures (between 300 and 400°C) (Demirbas, 2006). The moisture content of the source material plays a key role specially to keep low the energy consumption during pyrolysis (Mašek et al., 2016). The contaminant level of the feedstock biomass influences the quality of the biochar, therefore it has to be free of any non-organic contaminant or non-organic waste (Lopez-Capel et al., 2016).

As mentioned in Villagra-Mendoza and Horn (2018a), independently of the thermal process used for biochar production – pyrolysis (slow or fast), gasification, torrefaction, hydrothermal carbonization, etc. (Brewer, 2012) – the process temperature has the greatest influence on the final biochar composition (Ronsse et al., 2013). Pyrolysis temperatures higher than 500 °C produce biochars with a carbon content greater than 80%, whereas the carbon content at temperatures between 400-500°C ranges between 60-80%, and at temperatures lower than 350°C the carbon content is between 15-60% (Laird et al., 2011; Ronsse et al., 2013). Elemental composition of N and S is lost when

pyrolysis temperatures increase from 300°C to 600°C (Laird et al., 2011). High temperatures (> 550°C) produce biochars with high surface areas (Joseph et al., 2010; Ronsse et al., 2013) of about >400 m^2/g, high ash content, and recalcitrant to decomposition. Low temperatures (< 550°C) produce biochars with more oxygen-containing and C-H functional groups, producing an amorphous C matrix that promote nutrient retention (Joseph et al., 2010; Laird et al., 2011; Verheijen et al., 2010) but as a negative property the hydrophobicity is increased, too (Kinney et al., 2012; Zornoza et al., 2016). The higher the pyrolysis temperature, the higher the pH is, due to more alkaline elements in the biochar, although it is highly dependent on the feedstock type, too (Ronsse et al., 2013). In general, Kinney et al. (2012) and Zornoza et al. (2016) proposed that ideal pyrolysis temperatures are between 400°C and 600°C, to promote appropriate hydrological conditions with high field capacity and low hydrophobicity.

Biochar has been recognized to be beneficial for agriculture and the environment. Thus, three functions can be recognized. Due to its ability to remain for a long time in the environment it is a source of carbon sequestration and can contribute to mitigate greenhouse gas emissions. As amendment, biochar changes the soil quality which depends on the soil type. It is a source of organic matter and may improve soil structure and water drainage, which enhance soil resilience to adverse climate change. Finally, it can also be beneficial for crop productivity by facilitating nutrient and water for an adequate plant growth (Figure 3.2).
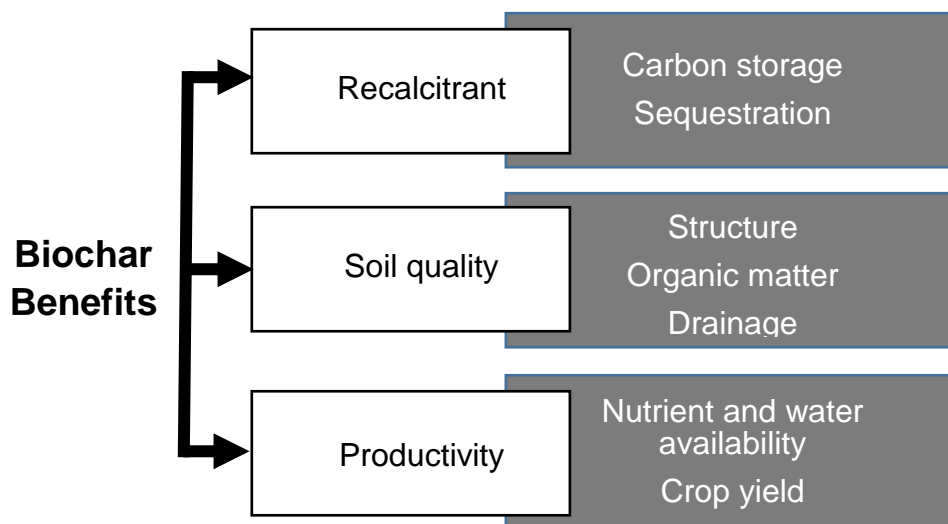
Figure 3.2. Key biochar beneficial effects to evaluate biochar properties (after Lopez-Capel et al., 2016).

3.1.2. Biochar Stability

Biochar has the potential to reduce carbon dioxide from the atmosphere and store it as a carbonaceous solid in the soil for hundreds or thousands of years (Brewer, 2012).

The biochar stability is based on the resistant of its molecules to decomposition by microorganisms. Therefore, the source material plays an important role on the capacity to store carbon in soils. Woody biochar contains more recalcitrant molecules than, for instance, green waste biochar. The latter contains more labile molecules that are easily decomposed by microorganisms. The process of pyrolysis converts carbon chemical composition to more resistant molecules able to support microbial break down for long time periods. One of the key properties to characterize biochar are the Hydrogen/Carbon (H/C) and the Oxygen/Carbon (O/C) ratios. While the H/C ratio indicates the degree of aromatization (molecular stability) the O/C ratio indicates the polarity (electrical charge). Molecular stability increases with increasing temperature. Thus, an optimal temperature to obtain recalcitrant woody biochar is approximately 450°C (Lopez-Capel et al., 2016).

The stable molecular composition that the biochar may reach enhances carbon sequestration and improves many soil functioning for long periods, relevant for agronomic and environmental performance (Lehmann, 2009; Major et al., 2010; Verheijen et al., 2010).

3.1.3. Effect of Biochar on Chemical Soil Properties

Biochar as amendment is known to enhance chemical soil properties aimed to increase soil fertility. Studies have cited that in infertile soils biochar applications improve cation exchange capacity (CEC) (Liang et al., 2006; Verheijen et al., 2010; Zornoza et al., 2016) enhancing the bounding nutrient-soil conditions, preventing leachate of nutrients to surface waters and deeper soil regions, reducing toxicity by immobilization of trace materials, and improving plant uptake (Villagra-Mendoza and Horn, 2018a). The increase of CEC is related to the oxidation of aromatic carbon molecules and formation of carboxyl groups (Ajayi and Horn, 2016a). Other studies have found that biochar addition increases pH producing a liming effect (due to cationic oxides) (Verheijen et al., 2010; Zornoza et al., 2016) and reduces the risk of some metal toxicity (i.e. aluminum). The availability of total carbon (TC) depends on the thermal process production and the characteristics of the feedstock source. Higher temperatures produce more recalcitrant forms of organic carbon (ash content) which may not be available for plants, however, can be critical to aggregation and structural development in amendment soils (Ajayi and Horn, 2016a). The more the ash content the higher the electrical conductivity (EC) related to an increase of soluble salts in the ash composition (Zornoza et al., 2016).

3.1.4. Effect of Biochar on Physical and Hydraulic Soil Properties

As mentioned by Villagra-Mendoza and Horn (2018a), biochar addition enhances physical and hydraulic soil properties by adding porous substances to the soil, modifying water retention, bulk density, total porosity and pore structure (Burrell et al., 2016; Novak

et al., 2012). This has implications in soil aeration, water holding capacity and soil workability (Ajayi and Horn, 2016c; Bodner et al., 2013; Verheijen et al., 2010). The more notable benefits have been observed in soils with coarse grained textures, with low pH and generally degraded (Abel et al., 2013; Jeffery et al., 2015). Ajayi et al. (2016) and Ajayi and Horn (2017) reported in coarse grained amended soils with biochar, an increase of total carbon, specific surface area (SSA) and buffer capacity of the soil (Burrell et al., 2016; Eibisch et al., 2015; Uzoma et al., 2011), micro porosity, plant available water and total porosity. Ajayi and Horn (2016a) also observed that the biochar dosage was positively correlated to the increase of SSA, total porosity, and available water content. They explained these results by a decrease of wide pores (as described in Villagra-Mendoza and Horn, 2018a). Since the benefits of biochar are dependent on many production parameters, Kinney et al. (2012) suggested that the best biochar materials are those that increase field capacity and have a minimal effect on wilting point. This condition is related to the modification of the pore size distribution (micro, meso and macropores) when biochar is applied. Fine biochar particles transform large pores to medium pores, because of the infilling of the large-sized pores by the small biochar particles (Eibisch et al., 2015; Hartge and Horn, 2016). This new relative soil condition makes water available as the soil dries leading to an increase of plant water availability during dry periods and increased water retention capacity (Ajayi et al., 2016; Ajayi and Horn, 2017; Jones et al., 2010; Verheijen et al., 2010).

Biochar particles, due to their fine pore structure, work similar to clay particles, raising strength of menisci with decreasing matric potential, producing a positive contracting force of particles (Ajayi and Horn, 2017).

As cited by Villagra-Mendoza and Horn (2018a), repetitive wetting and drying (WD) cycles influence soil shrinkage and swelling. This induces aggregate formation and rearrangement of particles, which make soils less sensitive to deformation. The impact of WD cycles on soils is highly dependent on the soil structure and texture (Horn et al., 2014). Organic soils have been reported to become more rigid, with less pore changes as soil dries, than mineral soils; presenting less swelling and keeping large pore formation during the WD periods (Peng et al., 2007). Similarly, it has been reported that biochar amended clayey soils are more suitable to reduce the effect of volume changes under wetting or drying conditions, reduce the crack formation and the size at which they are formed compared to unamended clay soils. The wider pore size distribution has been described as the mechanism to improve soil aggregation due to biochar addition (Lu et al., 2014; Zong et al., 2014). The improvement of soil aggregation may lead to an enhancement of the soil infiltration capacity (Verheijen et al., 2010) reducing runoff volume and erosion risk.

The formation of narrower pores when fine biochar particles are added to the soil tends to decrease saturated hydraulic conductivity (Yargicoglu et al., 2015). Some studies have reported that when biochar is added to coarse textured soils, saturated hydraulic conductivity decreases (Ajayi and Horn, 2016a; Barnes et al., 2014; Brockhoff et al., 2010; Herath et al., 2013; Lim et al., 2016). As mentioned in Villagra-Mendoza and Horn (2018a), authors such as Ajayi et al. (2016) also reported that during wetting and drying

cycles (WD) the saturated hydraulic conductivity decreased in coarse textures and increased in sandy loam and silty soils. This was attributed to the internal orientation of particles forming aggregates and inter-aggregates cracks.

Hartge and Horn (2016), Kutílek et al. (2006), Alaoui et al. (2011), and Peng et al. (2007) discussed the increase in the pore connectivity (e.g. due to compaction) between smaller pores, causing an increase of the contact surface areas between the soil aggregates. Castellini et al. (2015) found that in the near saturation (-1 to -12 hPa) biochar had a negligible effect on the unsaturated hydraulic conductivity of the soil. Kameyama et al. (2012) evaluated the effect of biochar addition on the unsaturated hydraulic conductivity ($K(\psi)$) and observed that the unamended soil compared to amendments up to 3% biochar, had the lowest values of $K(\psi)$ for matric potentials greater than -100 hPa. In contrast, biochar additions of 5% and 10% reported higher $K(\psi)$ than the unamended soil in the entire matric potential range. Bayabil et al. (2015) observed that charcoal incorporation increased the relative hydraulic conductivity ($K_r(\psi)$) of fine textured degraded soils, at matric potentials greater than -100 hPa. Hardie et al. (2014) reported that the addition of biochar, to a sandy loam soil, increased $K(\psi)$ near saturation at -2.5 and -1 hPa. Uzoma et al. (2011) observed that in amended sandy soils $K(\psi)$ increased, but it was dependent on the pyrolysis temperature and dosage applied.

3.1.5. Biochar Field Application

The benefits of biochar addition apart from depending on the soil type, and the biochar composition, also depend on the application rates of the biochar (Mukherjee and Lal, 2013; Verheijen et al., 2010). However, there is still a discussion regarding the relation between application effects, biochar dosage and soil type (Verheijen et al., 2010).

Also in various soil classes hydrophobicity has increased as the addition of biochar increased (Verheijen et al., 2010). Mukherjee & Lal (2013) reported that application rates of 1-2% biochar (by wet weight) were sufficient to increase the soil physical quality (i.e. available water capacity). Abel et al.(2013) mentioned that fractions of 2.5 dry wt.% produced the highest rise of available water content in sandy soils. Gaskin et al. (2007) found that biochar additions of 2% did not significantly change the available water content in a sandy loam soil, but by increasing it up to 8% the effect was evident. Ajayi & Horn (2016a) recommended a threshold application rate of 5% biochar (by dry weight) for sandy silt and fine sand soils to improve physical soil properties. Abrol et al. (2016) proposed a biochar addition of 2 dry wt.% was sufficient to enhance the hydrology of a loamy sand and loamy soil.

3.2. The role of Biochar in Soil Hydrology

Changes in the distribution, frequency and intensity of rainfall in combination with intensified soil degradation become a challenge to look for new forms of water management locally and at macroscale level. In agriculture, there is a need to look for new irrigation system designs able to supply the crop water needs using less amount of water. On the other hand, drainage systems must be able to evacuate water properly under water excess and retain it under water scarcity. Regarding water scarcity, biochar has shown to enhance soil physicochemical and hydraulic characteristics (Abel et al., 2013; Ajayi et al., 2016; Ajayi and Horn, 2017, 2016a; Bayabil et al., 2013; Burrell et al., 2016; Eibisch et al., 2015; Hardie et al., 2014) that may ameliorate soil water retention, nutrient and pollutant lixiviation and water transmissivity under adverse weather conditions. This is important since water infiltrated is expected to be retained longer in the soil, increasing the final infiltration rate and reducing the potential for surface runoff.

The hydrological cycle describes the movement and different states of the water and its interaction between the earth and atmosphere. The amount of water that is transported within the system is quantified in terms of the water balance equation, as follows:

$$P = R + E + \Delta S \tag{3.1}$$

where P is the height of precipitation (mm), R is the average height of runoff (mm) E is the evaporation (mm) and ΔS is the change in water storage (mm). Precipitation is the main influencing element of the hydrological components. When precipitation occurs, water does not infiltrate totally through the surface, since there are either losses in between or it runs directly as surface runoff.

From an overall view of the soil water budget, as water infiltrates important processes take place that influence changes in the soil water regime ($d\theta/dt$). Infiltrated water (i) penetrates through the soil surface and becomes part of the water content of the soil; interflow ($Intf$) moves parallel to the surface into the first layers; percolation ($Perc$) moves deeper into the lower soil layers; evapotranspiration (Eva) generates a loss of moisture from the direct surface; and capillary uprise (CU) increases soil moisture through the upward movement of fluids by capillarity (Villagra-Mendoza et al., 2017). These processes are summarized in the well-known 1D-water balance equation:

$$\frac{d\theta}{dt} = i(t) - [Intf(t) + Perc(t)] - Eva(t) + CU(t) \tag{3.2}$$

all these processes influence the hydrological response of the catchment.

Infiltration is the water that enters into the soil profile per unit of soil surface area (Hillel, 1998) and it influences the major mechanisms governing water availability for plants (Adeniji et al., 2013). It decreases with time from the beginning of the input of water. Two

forces – matric as well as gravitational potentials – are in charge of moving the water flux from the surface into the soil profile. These forces produce, besides a downward movement, an upward and lateral movement (Baver et al., 1972) depending on the topographical conditions and the given anisotropy of the hydraulic functions. Initially, the water infiltration is high. Especially when the soil is initially dry the hydraulic gradient as the sum of matric and gravitational potential dominates. At this stage, water infiltrates into the soil by capillary attraction as well as being pulled down by gravity but it fades off with time until it reaches a steady rate. As water penetrates deeper, it moves as a wetting front through the soil profile, the matric potential gradient decreases and the gravitational gradient becomes the only force that moves the water downward (Hillel, 1998; Jury and Horton, 2004). At this moment the flux tends to approach the hydraulic conductivity as a limiting value and the slope of the infiltration curve becomes flat. This steady condition is considered the maximum depth of water that can infiltrate the soil in a unit of time (Hillel, 1998). In the unsaturated zone, besides the main forces – capillary and gravitational – there are different mechanisms like absorption that helps to bind the water molecules to the soil bulk reducing the drainage of water into deepest layers.

Infiltration is influenced by many factors that may hinder or enhance the way and time water enters in the soil surface:

a. Rainfall intensity and amount, drop diameter and drop size distribution may induce surface sealing, especially due to raindrop impact, reducing permeability and slowing down infiltration (Assouline and Mualem, 1997). Rainfall may also cause soil compaction, destruction of the surface aggregates, particle detachment, dispersion, and clogging of pores (Hillel, 1998).

b. Soil properties such as texture, organic matter, structure and initial wetness alter the velocity at which infiltration occurs. Coarser soil textures are associated with high infiltration rates due to their larger pores and clay-rich soils are associated with lower infiltration (Chartier et al., 2011). For instance, studies such as from Adeniji et al. (2013) associated the soil fine fraction (< 500 µm) as a key factor to estimate infiltration. The latter soils however can also have a very high infiltration rate if they are well structured and if they have continuous coarse pores in the vertical direction. Organic matter, swell and shrink processes amongst others, all enhance soil structure and its strength and provide pores that are important for infiltration and water retention (Bens et al., 2007). Deterioration of soil structure may reduce capacity of infiltration and high initial soil moisture may cause an early constant infiltration rate (Hillel, 1998).

c. Vegetation exerts a first-order control on infiltration and runoff dynamics by direct interaction with soil quality and surface characteristics. It stabilizes soil aggregates and is associated to nutrient conservation which is a positive effect for infiltration (Chartier et al., 2011).

d. Management practices such as tillage vary the composition of the top soil (Adeniji et al., 2013) enabling preferential flow (Hillel, 1998) or destroying macropores (Nimmo,

2004) reducing water transmissivity. Subsoiling or chiseling may form cracks that are pathways for preferential flow (Hillel, 1998), and horizontal plough changes the pore size distribution of the top layer, creating narrower pores.

e. Pore characteristics such as pore size distribution and connectivity, hydraulic conductivity and sorptivity are the most important parameters that influence infiltration capacity (Elrick and Reynolds, 1992; Jačka et al., 2016). Pore connectivity plays a key role by enabling the infiltrated water and solutes to reach deeper soil depths (Bens et al., 2007). Soils with high saturated hydraulic conductivity are associated with high infiltration rates (Hillel, 1998). Figure 3.3 shows a graphical effect of the soil texture and hydraulic conductivity on water infiltration. In coarse soil textures hydraulic conductivity is higher and the wetting front moves faster in vertical direction due to gravity forces. In fine grained soils the vertical wetting front moves more slowly because the gradient is controlled by the matric potential.
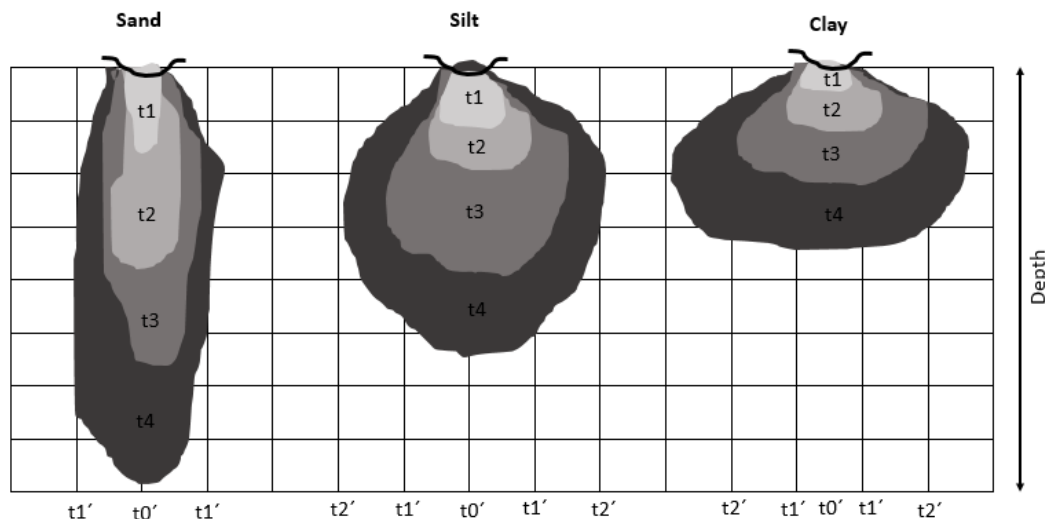
Figure 3.3. Pattern behavior of infiltration according to soil type and hydraulic conductivity (after Hartge & Horn, 2016).

f. Soil water repellency may delay initial infiltration rates with a later increase over time, due to air entrapment and flow instabilities (Bens et al., 2007; Carrick et al., 2011; Dohnal et al., 2009; Hillel, 1998). Contrary to non-repellent soils which show initially high infiltration rates and a decrease over time (Bens et al., 2007).

g. Soil profile heterogeneity affects infiltration because the flow path may face abrupt discontinuities at the boundary of the different layers and may decrease the infiltration rate and downward movement in the soil profile (Hillel, 1998). Depending on the permeability of the layers and the hillslope gradient, lateral flow may be greater than vertical flow. Additionally, the spatial orientation of soil aggregates within the soil

profile affects the function of the porous media with the development of continues bias inducing soil anisotropy (Dörner, 2005).

h. Repetitive wetting and drying (WD) facilitate the formation of preferential flow paths (Peng et al., 2007) making the soil matrix sensitive to soil deformation and changing the configuration of structural pores affecting transport of water and air (Dörner, 2005). Wetting and drying cycles modify the pore size distribution in response to internal capillary stress and infiltration decreases due to the collapse of the soil aggregates (Hillel, 1998). Rewetting periods increase structural instability and shrunk soils may form cracks and fissures, highly sensitive to soil deformation, acting as large pores contributing to a faster water penetration (Hillel, 1998). Shrinkage changes the configuration of structural pores (anisotropic or isotropic behavior), affecting the transport of water and air (Dörner, 2005).

3.2.1. Infiltration Modelling

Infiltration can be predicted by several models; however, some general restrictions must be considered when they are applied. In general, models assume the soil profile as deep, homogeneous and with constant initial wetness (Angelaki et al., 2013; Barrera & Masuelli, 2011; Jačka et al., 2016). Heterogeneity of the profile, cracks, wormholes and root channels are not considered in the models since they provide unrealistic and invalid hydraulic conductivity and flux potential values. Soil structure and pore size distribution are assumed to be temporally stable, and the soil bulk is considered rigid, thus any shrinkage/swelling behavior (Clothier and Scotter, 2002; Elrick and Reynolds, 1992) nor preferential flow is taking in consideration (Clothier and Scotter, 2002; Dohnal et al., 2009). The effect due to hysteresis, entrapped air or soil water repellency is ignored, too (Clothier and Scotter, 2002). Ponding surface conditions are considered constant (Jačka et al., 2016), and uniform rainfall or irrigation rate must be assumed (Uloma et al., 2014).

Infiltration models are generally classified in three groups. *Physically based models* are those models that rely on the Law of Conservation of Mass and Darcy´s Law, under some assumptions as described above. Examples of these models are Green-Ampt, Philips or Smith Parlange. *Semi-empirical models* employ simple forms of the continuity equation, such as the Horton model. *Empirical models* are simple models which derive from observed field or laboratory data, such as Kostiakov or Holtan (Uloma et al., 2014). The use of one model over another depends on the data collected and the quality of fitting. Jačka et al. (2016) mentioned that empirical models perform better than physically based models and the latter perform better when using laboratory data than field data.

.3.2.1.1   Philip Model

Philip (1958) derived a two parameter equation to express the cumulative infiltration ($Icum$) and the infiltration rate (i) (cited by Lal & Shukla, 2005):

$$Icum = S_s t^{1/2} + At \tag{3.3}$$

$$i = \frac{1}{2} S_s t^{-1/2} + A \tag{3.4}$$

where both parameters have physical meaning: S_s is an estimate of sorptivity (cm/d$^{1/2}$) and A is an empirical constant known as the soil-water transmissivity and is related to saturated hydraulic conductivity (cm/d). While S_s represents the effect of matric potential, A represents the gravity-driven flow (van De Genachte et al., 1996). Equation (3.3) is widely used for the evaluation of data measured with ring infiltrometers. In heterogeneous soils, this equation can result in unrealistic negative estimate parameters (Jačka et al., 2016). When $t \to \infty$ the coefficient A can be replaced by K_{sat}. Soil water repellency may decrease parameters S_s and A, providing unreasonable negative values of A due to slow infiltration (Li et al., 2017). This model neglects two important factors which are the air entrapment in the soil profile during infiltration and the existence of a surface crust. Therefore this model may predict a much slower rate of decay compared to field data (Baver et al., 1972)

.3.2.1.2   Horton Model

Horton (1940) assumed that the shape of the infiltration curve was similar to an exponential function and assumed also a finite initial rate value at $t = 0$ (Jačka et al., 2016). He proposed the following expression for cumulative infiltration ($Icum$) and infiltration rate (i) (cited by Baver et al., 1972):

$$Icum = Ibt + \frac{(I_o - Ib)}{\beta}[1 - \exp(-\beta t)] \tag{3.5}$$

$$i = Ib\,t + (I_o - Ib)\exp(-\beta t) \tag{3.6}$$

where I_o is the initial infiltration capacity at $t = 0$, Ib is the final infiltration capacity and β is a constant which describes the decreasing rate of infiltration capacity; controlled by

variables such as soil type, water content, surface conditions, slope and rain characteristics. This formula applies when rain intensity is higher than infiltration capacity (Xue and Gavin, 2008).

.3.2.1.3   Kostiakov Model

The Kostiakov model is an empirical model with any physical explanation for the infiltration process (van De Genachte et al., 1996). Kostiakov (1932) suggested an expression that assumes that infiltration rate is infinite at $t = 0$, and approaches to zero when $t = \infty$ (cited by Uloma et al., 2014). The expression for cumulative infiltration ($Icum$) is given by (cited by Baver et al., 1972):

$$Icum = Ct^{\alpha} \tag{3.7}$$

where C and α ($0 < \alpha < 1$) are empirical constants and function of texture, soil water content and bulk density; and t is the infiltration time. This expression has the disadvantage that the fitting parameters can only be obtained by direct infiltration measurements (Hartge and Horn, 2016). Soil water repellency affects the model fitting parameters by decreasing α and increasing C with the increase of water repellency (Li et al., 2017).

In 1972, the Kostiakov equation was modified by (cited by Hasan et al., 2015):

$$Icum = Ct^{\alpha} + b \tag{3.8}$$

where b is another empirical constant which depends on soil conditions. Equation 3.8 is most commonly used in irrigation applications than equation 3.7.

3.2.2. Effect of Biochar on the Infiltration Dynamics

Biochar addition not only enhances processes such as soil water storage and conductivity, but it may also improve the soil infiltration capacity (Igbadunh et al., 2016; J. Novak et al., 2016). However, not all biochar feedstocks are optimal for improving initial water infiltration. Soil structure, texture and hydraulics may also affect water infiltration by enhancing or delaying the water flow. Infiltration may also be affected by soil hydrophobicity (Assouline and Mualem, 1997). High repellency (specially on very dry soils) may induce to low initial infiltration rates increasing over time, contrary to non-water-repellent soils that shows high initial infiltration rates. Few studies have

investigated the effect of biochar on infiltration and runoff formation. Itsukushima et al. (2016) reported higher initial and final infiltration rates in amended soils with bamboo charcoal and humus than in unamended soils. Hamidreza Sadeghi et al. (2016) indicated that the effectiveness of biochar in reducing surface runoff was influenced by the time of biochar application before the rainfall event, and suggested that the effect of biochar in the decrease of surface runoff resulted from increasing water holding capacity or increasing infiltration capacity of the topsoil. Hardie et al. (2011) and Doerr and Thomas (2000) suggested that hydrophobic soils affected the soil hydrology by producing a lower response in time to infiltration and accelerating time to runoff generation. Zhi-guo et al. (2017) agreed on the benefits of agricultural and forest residues, in the form of biochar, on the decrease of surface runoff and its time of occurrence. Abrol et al. (2016) demonstrated that biochar is also useful as a soil conservation measure by ameliorating infiltration and controlling soil erosion. Although many studies have pointed out the positive effects of biochar amendments on the soil hydrology; it is still not clear the potential contribution of biochar as an agricultural management practice, especially under extreme weather conditions.

Figure 3.4 shows the behavior of the infiltration rate after biochar addition. Initial and final infiltration rates are higher than unamended soils. When rainfall occurs (I_N) the amount of soil water increases at the surface (surface runoff shadowed over the infiltration capacity curve, i) of the unamended soil compared to the amended one (i'), enhancing the water storage capacity of the soil (Itsukushima et al., 2016). These scenarios may help to prevent or reduce flooding at a catchment level.
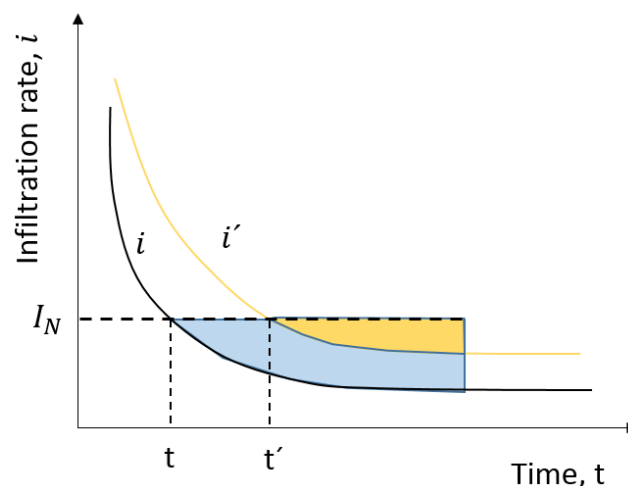
Figure 3.4. Change of the infiltration capacity after biochar addition. Infiltration rate (i) corresponds to a treatment without biochar and infiltration rate (i') corresponds to a treatment with biochar (after Itsukushima et al., 2016).

4. Methods to Evaluate the Biochar Amendment on Soil Functioning

4.1. Sample Preparation

Two materials were used: medium sand (S) with grain size diameter mainly between 0.20 -0.63 mm (99% sand and 1% clay) and a sandy loam soil (SL) (54% sand, 13% clay and 33% silt) collected in Schleswig-Holstein, in the northern part of Germany (Figure 4.1). Sediments were first air dried, macerated and passed through a 2 mm sieve. Mango wood was used as biochar source material (with minimum age of 30 years), pyrolyzed at a temperature of about 600°C. It was crushed into finer fractions and passed through a 63 µm sieve (Villagra-Mendoza and Horn, 2018a).

Figure 4.1. Base materials used for sample preparation: a) biochar; b) sandy loam (SL); c) sand (S).

As mentioned by Villagra-Mendoza and Horn (2018a), test samples were prepared by adding biochar (2.5 and 5% by dry mass) to the two soil materials. Thus, the treatments consisted of S0 (control-unamended sand), S2.5 (sand + 2.5% biochar), S5 (sand + 5% biochar), SL0 (control-unamended sandy loam), SL2.5 (sandy loam + 2.5% biochar) and SL5 (sandy loam + 2.5% biochar). Samples were packed as follows:

a. The first group of 40 replications per treatment was prepared by packing 100 cm^3 stainless steel cylinders (about 4 cm height and 5.6 cm diameter) with the homogenized substrates. The sandy substrates, S were packed to an initial bulk

density of 1.5 g/cm^3 and the sandy loam substrates, SL were refilled to bulk densities of 1.35 g/cm^3 using an Instron 5569 loading frame (Instron, 2008). Water content, sorptivity, air conductivity and shrinkage, at each matric potential were determined (Figure 4.2).

b. Ten samples per treatment (100 cm^3 cylinder) were prepared (to the same bulk densities as in point a) to characterize saturated hydraulic conductivity after different wetting and drying (WD) cycles.

c. Another 10 ring samples of about 2 cm diameter (ca. 2.6 cm^3), for each treatment, were prepared to quantify the water content by weight at -1500 kPa, equivalent to the permanent wilting point (Figure 4.3).
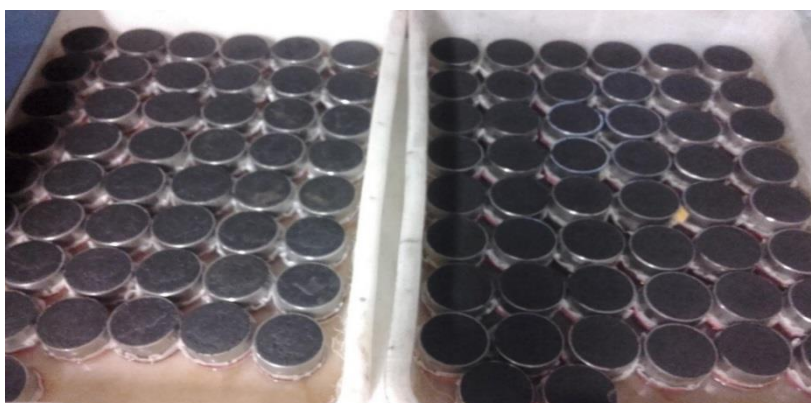
Figure 4.2. Example of sample preparation of the sandy substrates with 2.5% and 5% biochar addition. Bulk density was achieved by using the Instrom 5569 loading frame.

Figure 4.3. Sample ring preparation for all mixtures to obtain water content values at -1500 kPa.

4.2. Parameter Analysis

The dry bulk density (ρ_d) was determined by the soil core method (Soil Survey Staff, 2014). The particle density (ρ_s) was measured with the Pycnometer method. The organic carbon and nitrogen content were determined with a C/N Element-Analyzer. The inorganic carbon fraction was estimated by determining the $CaCO_3$ content by measuring the volumetric gas production of CO_2 after adding HCl. Soil texture was analyzed by the combined sieve (> 63 µm) and pipette method (Blume et al., 2010) and soil classification was based on the German Standard (AG Boden, 2005). The pH was measured in a 0.01 M $CaCl_2$ solution and cation exchange capacity (CEC) followed the method of (Blume et al., 2010) and it was determined by the atomic absorption spectrophotometer method (Villagra-Mendoza and Horn, 2018a).

The specific surface area (SSA) was determined with the Multipoint Brunauer Emmett-Teller (BET) method. In this method, as explained by Ajayi and Horn (2016a), samples are subjected to N_2 adsorption at 77 K (-196.15°C) and CO_2 adsorption at 273 K (-0.15°C), in a Quantachrome Autosorb-1 analyser. The micropore surface area is calculated with the linear form of Dubinin-Radushkevich equation, based on the CO_2 molecules monolayer in the micropore space. Prior to measurement, the samples are degassed at 40°C for several hours to remove volatile substances and make them water free.

4.3. Moisture Retention and Shrinkage Behavior

Samples were saturated with water by capillary rise for 48 h and thereafter drained to matric potentials of -3, -6, -15, -30 and -50 kPa. Water desorption up to -6 kPa was done in a sand bed, whereas for more negative matric potentials, the samples were desiccated on ceramic plates. To estimate the gravimetric water content, the weight of the samples was recorded at each matric potential. After the last matric potential, samples where oven dried at 105°C for 16 h. To obtain the gravimetric water content at the matric potential of -1500 kPa, samples were packed in small rings, saturated and thereafter drained for about four weeks on ceramic plates under pressure and later oven dried at 105°C for 16 h (Villagra-Mendoza and Horn, 2018a).

Based on the guidelines in AG Boden (2005), air capacity was calculated as the water content at saturation minus the water content at a matric potential of -6 kPa (pore diameter > 50 µm). Available water capacity was calculated as the water content at -6 kPa minus -1500 kPa (pore diameter between 50 and 0.2 µm) (Villagra-Mendoza and Horn, 2018a).

The water retention curve was fitted with the Van Genuchten-Mualem equation (van Genuchten, 1980) – see Eq. 2.14 – with the help of the RETC software (van Genuchten et al., 1991) to obtain the fitting parameters θ_s, θ_r, α, n and m.

Soil shrinkage was estimated by measuring the height changes of the bulk soil of each sample after each matric potential and at the end (after oven drying at 105°C.) (Figure 4.4). The height was measured at five consistent points on the soil surface using a digital caliper (resolution 0.05 mm). The soil volume after each matric potential was obtained by multiplying the soil height by the initial soil core area reported by Peng and Horn (2005). The relation between the moisture ratio (ϑ, cm^3/ cm^3) and void ratio (ε, cm^3/ cm^3) was used to characterize the volume changes by a shrinkage curve (Villagra-Mendoza and Horn, 2018a):

$$\vartheta = V_w V_s^{-1} \qquad\qquad (4.1)$$

$$\varepsilon = V_f V_s^{-1} \qquad\qquad (4.2)$$

where V_w , V_s and V_f are the volume of water, solid and pores, respectively. The soil shrinkage model (Peng and Horn, 2005) was used to estimate the shrinkage curves for all three treatments:

$$\varepsilon(\vartheta) = \varepsilon_r + \frac{\varepsilon_s - \varepsilon_r}{[1+(\chi\vartheta)^{-p}]^q} \quad 0 \leq \vartheta \leq \vartheta_s \qquad (3)$$

where χ, p, and q are dimensionless fitting parameters, ϑ_s is the moisture ratio at saturation; ε_r and ε_s are the residual and saturated void ratios, respectively. The parameters of the shrinkage curve were obtained with the soil shrinkage simulator (SSS) developed by (Peng and Horn, 2013).
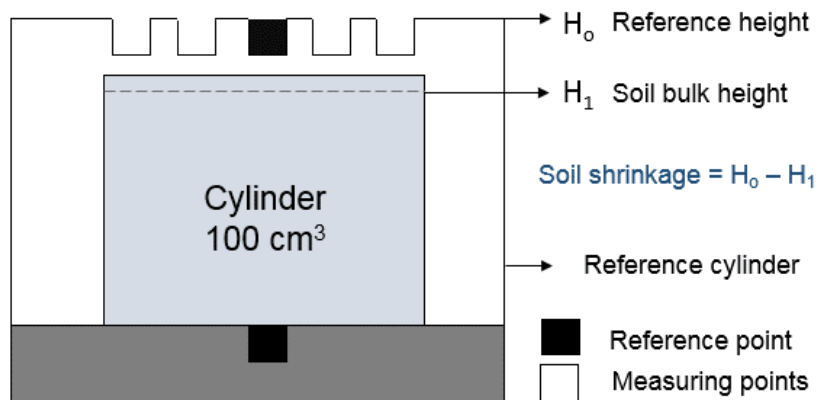
Figure 4.4. Diagram of the procedure for measuring the height changes of the bulk soil after each matric potential (after Dörner, 2005).

4.4. Soil Hydraulic Conductivity

Four wetting and drying (WD) cycles were simulated, separately. For each WD cycle a new set of 10 samples per treatment, with same bulk densities (as in 4.1a), was prepared. Samples were saturated (wetting period) by capillary rise, then dried (in an oven at 30°C for 72 h), and thereafter sorptivity was measured to determine the degree of repellency of the sample. This was repeated depending on the number of cycles applied. After each drying period, the weight changes were registered in order to quantify the changes in bulk density. Finally, after completing the corresponding cycle, the saturated hydraulic conductivity was measured. The sequence used for each WD cycle is described in table 4.1 (Villagra-Mendoza and Horn, 2018a).

Table 4.1. Description of the sequence of the WD cycles applied to a set of 10 samples per treatment (in total 60 samples tested for each WD) to determine the effect of different WD cycles on the saturated hydraulic conductivity (after Villagra-Mendoza and Horn, 2018a).

Cycle	Description of the cycles													
WD0	W	K_{sat}												
WD1	W	D	Sorp	W	K_{sat}									
WD2	W	D	Sorp	W	D	Sorp	W	K_{sat}						
WD4	W	D	Sorp	W	D	Sorp	W	D	Sorp	W	D	Sorp	W	K_{sat}

WD: wetting and drying cycle; W: wetting up to saturation by capillary rise; D: drying at 30°C for 72 h; Sorp: sorptivity after drying; K_{sat}: saturated hydraulic conductivity.

As presented in table 4.1, the saturated hydraulic conductivity (K_{sat}) was measured with the falling-head method (Hartge, 1966), after simulating different wetting and drying cycles (WD). Water flow over time through each soil sample was replicated 3 times (at three upper and lower gradient limits), and the geometric mean was calculated for the 10 samples. After each cycle K_{sat} and the weight changes were determined (Villagra-Mendoza and Horn, 2018a).

The unsaturated hydraulic conductivity $K(\psi)$ was determined with a modification of the evaporation method (Hartge and Horn, 2009). A scheme of this method is depicted in Figure 4.5. Soil samples (three replicates per treatment) were packed in 472 cm^3 stainless steel cylinders (about 6 cm height and 10 cm diameter) and put on a metal plate. At the bottom an o-ring sealed the soil cores and avoided both evaporation or water leakage from the sample. Thus, the water loss only occurred from the top surface by a continuous horizontal air flow and was registered by TDR mini probes and micro tensiometers, installed horizontally at two different depths. Soil water content (θ, cm^3/cm^3) and matric potential (ψ_m, kPa) were monitored continuously by a real-time

computer. Tensiometers were lined with Kaolinite, in order to guarantee a good contact soil-sensor. Before starting the measurements, the samples were saturated.

The unsaturated hydraulic conductivity was obtained according to a transformed Darcy´s equation:

$$K(\psi) = \frac{1}{t_1 - t_2} * \frac{\overline{\Delta\vartheta}}{grad\psi_m} \tag{4.4}$$

where $K(\psi)$ is the unsaturated hydraulic conductivity (cm/s), l is the flow length (cm), $t_1 - t_2$ is the time interval between two measurements (s), $\overline{\Delta\vartheta}$ is the change of soil water content between two measurements (cm³/cm³), $grad\psi_m$ is the hydraulic gradient between two points (kPa/cm) and equals to $\frac{\psi_2 - \psi_1}{l}$.
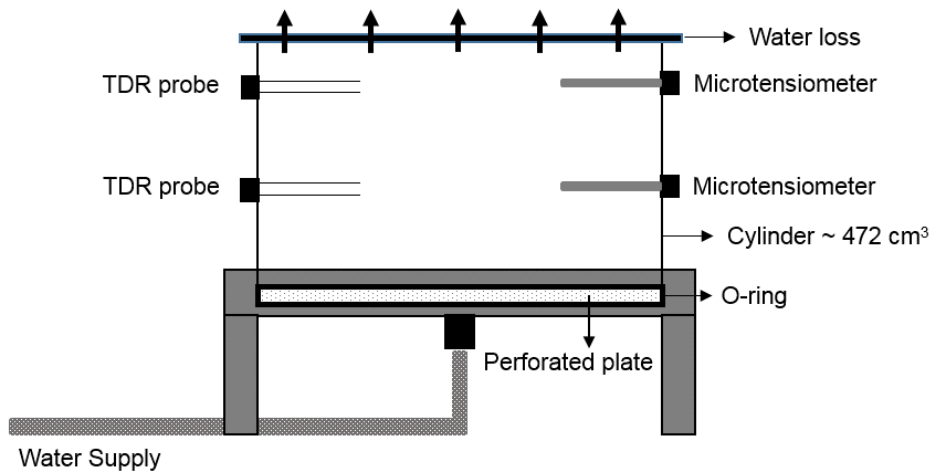
Figure 4.5. Diagram of the experiment set up for determination of the unsaturated hydraulic conductivity (after Dörner, 2005).

The observed hydraulic properties at different matric potential values were fitted with the expression of Van Genuchten-Mualem (van Genuchten, 1980) using the software RETC (van Genuchten et al., 1991). Referred to Eqs. 2.15 and 2.16. The Mualem restriction $m = 1 - 1/n$, and Burdine restriction $m = 1 - 2/n$ were compared and the best fitted values (using as criteria the SSQ) was chosen.

4.5. Water Repellency

As shown in table 4.1, after each drying cycle, water repellency (by means of the measurement of sorptivity of water and ethanol using a micro- infiltrometer) was estimated simultaneously (Hallett, 2007; Tillman et al., 1989). Sorptivity for both, water and ethanol was quantified as follows:

$$S_S = \sqrt{\frac{Qf}{4dr}} \qquad (4.5)$$

where Q is the rate of uptake of the liquid (m³/s), d is a parameter dependent on the diffusion of water in the soil and was taken as 0.55 (White and Sully, 1987), r is the radius of the tip of infiltrometer (cm), and f is the air-filled porosity (cm³/cm³), which depends on the degree of saturation and bulk density of the soil sample. The repellency index RI, was estimated as follows:

$$RI = 1.95 \frac{S_{S\_Ethanol}}{S_{S\_water}} \qquad (4.6)$$

where the constant 1.95 is obtained from the relation of the surface tension and the viscosity of ethanol and water (Villagra-Mendoza and Horn, 2018a).

4.6. Air Permeability

Air flux was measured at each matric potential using a steady flow meter and the air conductivity (K_l, m/s) calculated as follows (Peth, 2004):

$$K_l = \rho_l \cdot g \frac{\Delta V \cdot l}{\Delta t \cdot \Delta p \cdot A_{cl}} \qquad (4.7)$$

where ρ_l is the air density (kg/m³), g is the gravitational acceleration (m/s²), ΔV is the volume of air that flows in a time Δt (m³), l is the length of the soil sample (m), Δp is the pressure applied at which the airflow passes through the soil sample (hPa) and A_{cl} is the average area of the cylinder (m²). Air pressure and temperature were registered at every flux measurement.

Air permeability (K_a, cm²) was determined as follows:

$$K_a = K_l \cdot \frac{\mu_l}{\rho_l \cdot g}$$ (4.8)

where μ_l is the air dynamic viscosity (g/cm s) (Villagra-Mendoza and Horn, 2018a).

4.7. Water Infiltration at the topsoil

The study was carried out in two parts: 1) Determining the water infiltration behavior at laboratory scale for different soil amendments applying simulated wetting and drying (WD) cycles; and 2) Evaluating the watershed hydrological response, in the long term, with six biochar amendment treatments.

4.7.1. Measuring Infiltration at Laboratory Scale

Soil cores of 100 cm³ with the homogenized soil were compacted to obtain average soil densities of 1.51 g/cm³ for the sandy soil and 1.39 g/cm³ for the sandy loam. Each treatment was prepared with three replicates. A sequence of WD cycles were simulated. Infiltration capacity was first measured after sampling preparation (WD0) and then oven dried at 30°C for 72 h. Thereafter, infiltration capacity was measured again followed by an oven dry period of 72 h at 30°C (WD1, WD2 WD3 and WD4). After each drying period the height changes were registered in order to quantify changes in bulk density. Moreover, weight of each sample was obtained to determine the initial soil water content. The sequence used for each WD cycle is depicted in Figure 4.6. All infiltration tests were performed under similar initial moisture conditions (~2 vol-%).

WD0		WD1		WD2		WD3		WD4	
Sample preparation	Infiltration capacity	Drying 30°C	Infiltration capacity	Drying 30°C	Infiltration capacity	Drying 30°C	Infiltration capacity	Drying 30°C	Infiltration capacity

Figure 4.6. Simulated WD cycles to measure infiltration capacity. A WD cycle consisted of saturation during infiltration and thereafter oven dry at 30°C for 72 h.

Infiltration rate was measured with a disc infiltrometer with an internal diameter ($\emptyset_i$) of 23 mm. Time (s) and water volume changes (ml=cm^3) in the graduated disk infiltrometer were registered until volume changes reached a steady flow. Infiltration rate (i) was determined as follows:

$$i = \frac{\Delta L}{\Delta t} = \frac{\frac{Vw_{i+1}-Vw_i}{\pi r^2}}{t_{i+1}-t_i} \tag{4.9}$$

where ΔL is the amount of water that infiltrates through the surface (mm) measured between two consecutive readings; Δt is the time interval at which water infiltrates between two consecutives readings (h); Vw_i is the volume of water that infiltrates at a specific time (cm^3) and r is the internal radius of the mini-disc infiltrometer (cm).

Cumulative infiltration ($Icum$) was determined with the following expression:

$$Icum = \frac{Vw_i-Vw_o}{\pi r^2} \tag{4.10}$$

where Vw_o is the initial volume of water (cm^3) at $t = 0$.

The infiltration time series were fitted to the models of Philip (Eqs. 3.3 and 3.4), Horton (Eqs. 3.5 and 3.6) and Kostiakov (Eq. 3.7). A linear regression analysis was performed to fit the infiltration data to a pedotransfer function.

4.7.2. Modeling of Catchment Hydrology with Biochar Amendments

.4.7.2.1 Description of the Study Area

To evaluate the effect of biochar addition (as a soil conservation option) on the hypothetical hydrological response of a catchment, the geometry, landuse and climate data of the Birris subcatchment (Figure 4.7) were used and the soil data parameters were hypothetically set as the six soil scenarios obtained in the laboratory (Appendix F, Table F.1). The aim of this study was to evaluate the impact of biochar amendments to overcome dry long periods in terms of water infiltration, surface runoff, water storage and water discharge at a gauging station.

The Birris watershed is located in the northern part of the Reventazón watershed which is the main source of hydropower production in Costa Rica. The 83.5 km^2 watershed is located between the coordinates 551 000 – 561 000 East and 205 000 – 218 000 North based on the Lambert North Costa Rica. This sub basin yields 16% of the

total sediments that arrive at the Reventazón main reservoir (Lianes et al., 2009). The drainage system has an order of 4, which means that this catchment has a quick response to rain events.
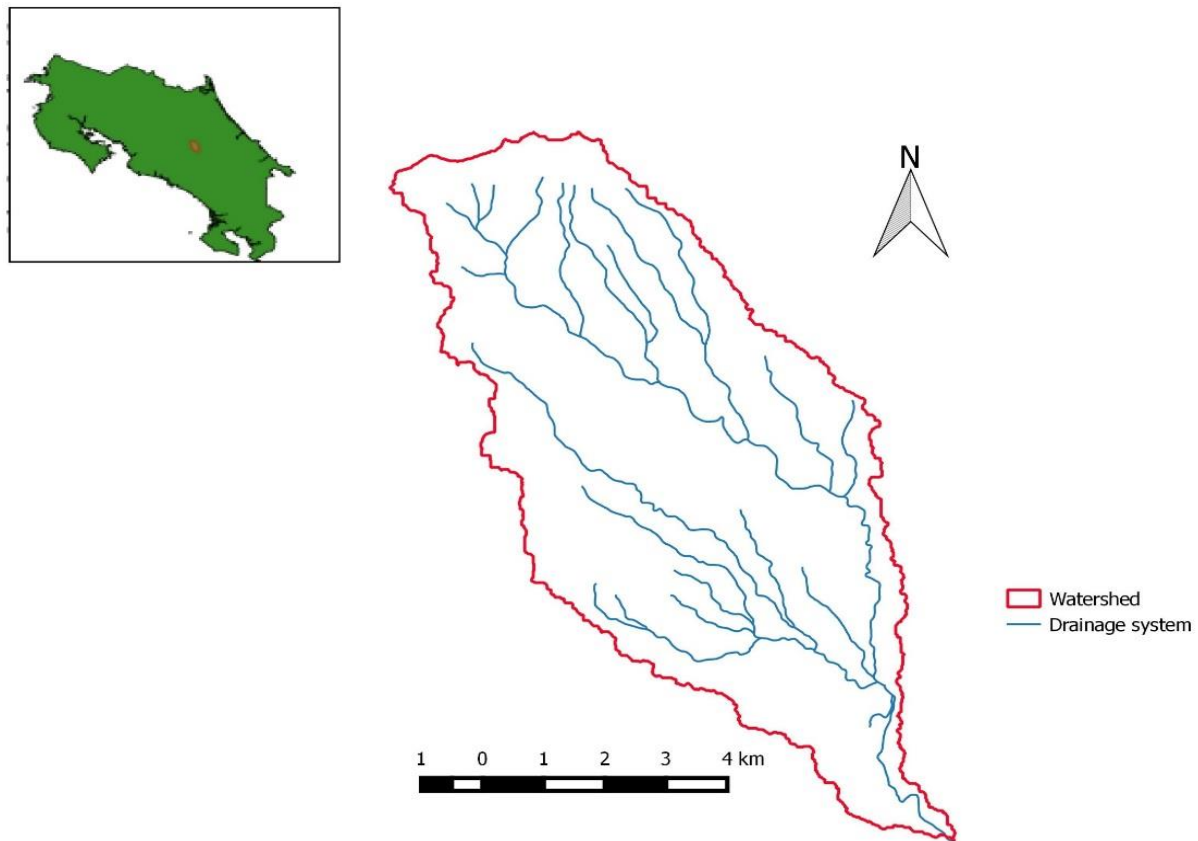
Figure 4.7. Birris subcatchment and drainage system.

This subcatchment was selected to analyze the runoff generated in a catchment when degraded soils are enhanced with biochar. It is occupied by 30% agriculture (crops) 39% by cattle raising (grass land) 27% forest, and 4% other uses such as residential areas and roads (Lianes et al., 2009) (Figure 4.8).
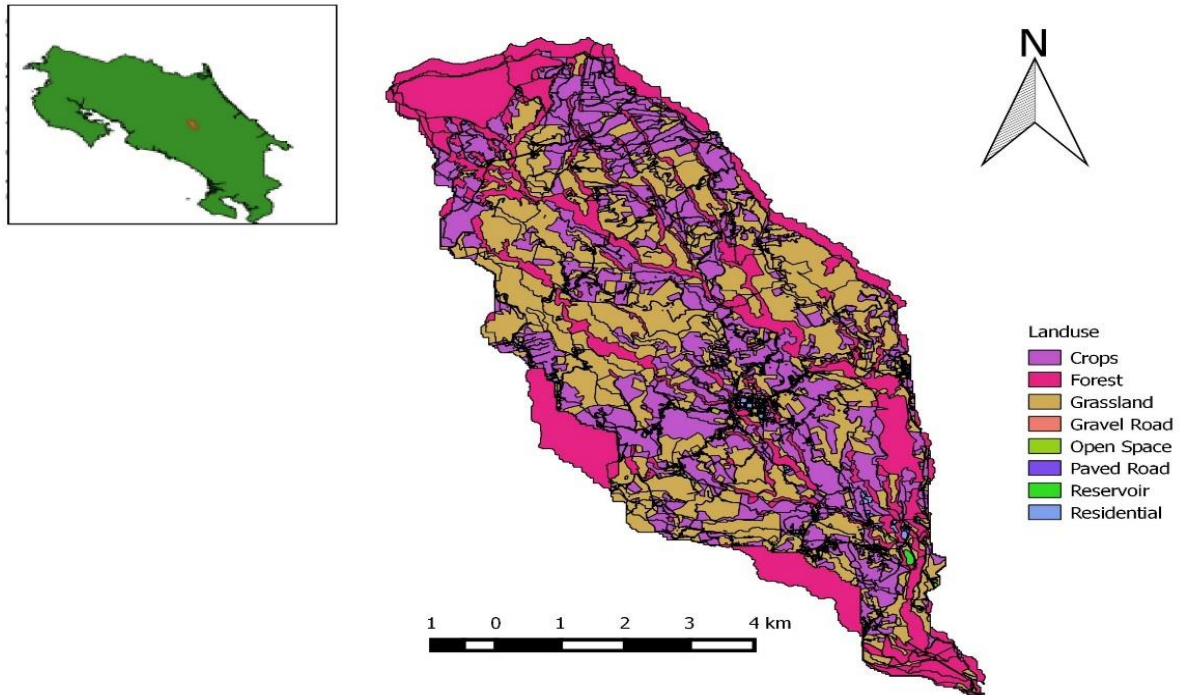
Figure 4.8. Landuse classification of the Birris sub basin. Most of the area of subcatchment is occupied by Crops and Grassland.

The hypsometric curve was obtained by plotting the relative area along the abscissa vs. elevation along the ordinate (Figure 4.9a). The relative area was obtained as a ratio of the area above a contour line to the total area of the catchment. Figure 4.9a shows the stage, of the watershed, between youthful and mature, with a slight S-shape. Reaching the outlet, the surface elevation changes abruptly, observed by a steep decay in the curve. Figure 4.9b depicts that the elevation range is between 900 and 3400 m.a.s.l, being 1700 m.a.s.l the most frequent elevation.
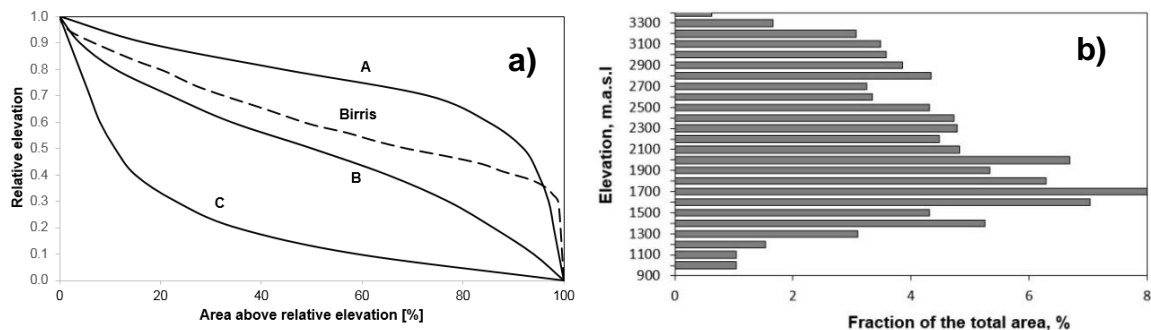
Figure 4.9. Hypsometry of the Birris watershed, a) Hypsometric curve and b) Elevation frequency. Labels in the curves correspond to: A) Youthful stage: high erosion potential; B) Mature stage: watershed in equilibrium; C) Old-age stage: sedimentary watershed.

From the Digital Elevation Model (DEM) it was obtained that the hillslopes were between 70% in the upper part of the catchments and between 4-8% in the lowlands, being 17% the average hillslope (Figure 4.10).
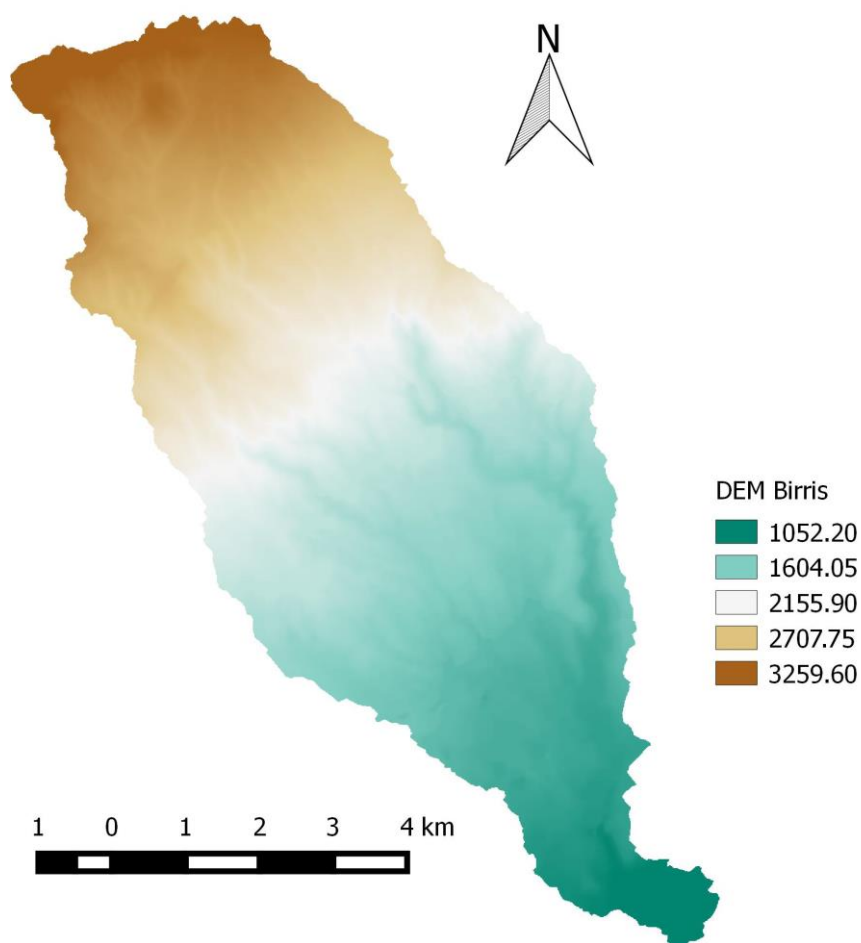
Figure 4.10. Digital Elevation Model (DEM) of the Birrís Watershed.

Average annual precipitation is 2325 mm and average daily month precipitation is between 2 and 14 mm. Average monthly precipitations vary between 65 mm in march and 300 mm in October. The Atlantic coast has a strong influence on the climate conditions of the sub catchment with a mean daily temperature value of about 13 °C during the year and an average relative humidity of 88%. Figures 4.11 and 4.12 show the average daily month precipitation and temperature, respectively; from two gauging stations located along the sub catchment from a period of 2006 to 2017.
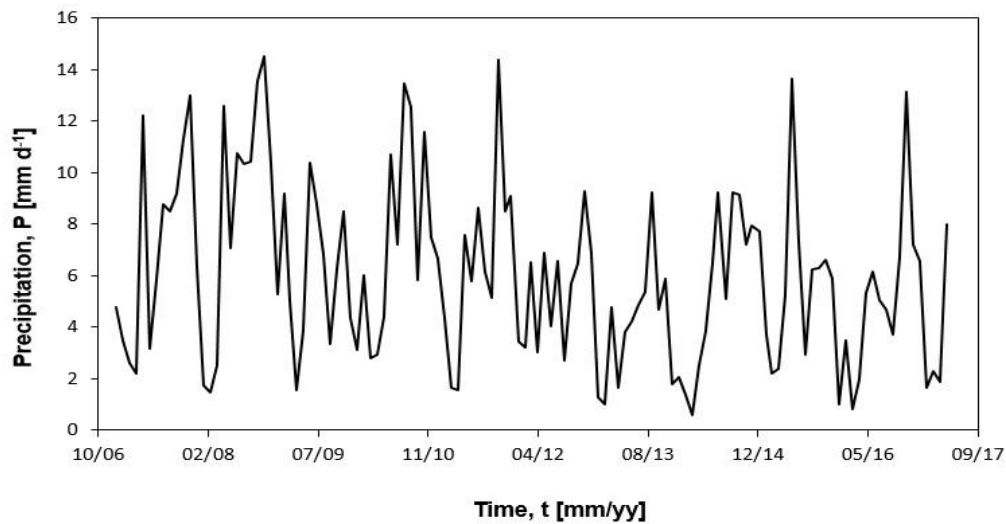
Figure 4.11. Average daily month precipitation of the Birris sub basin obtained from five gauging stations located within the study area.
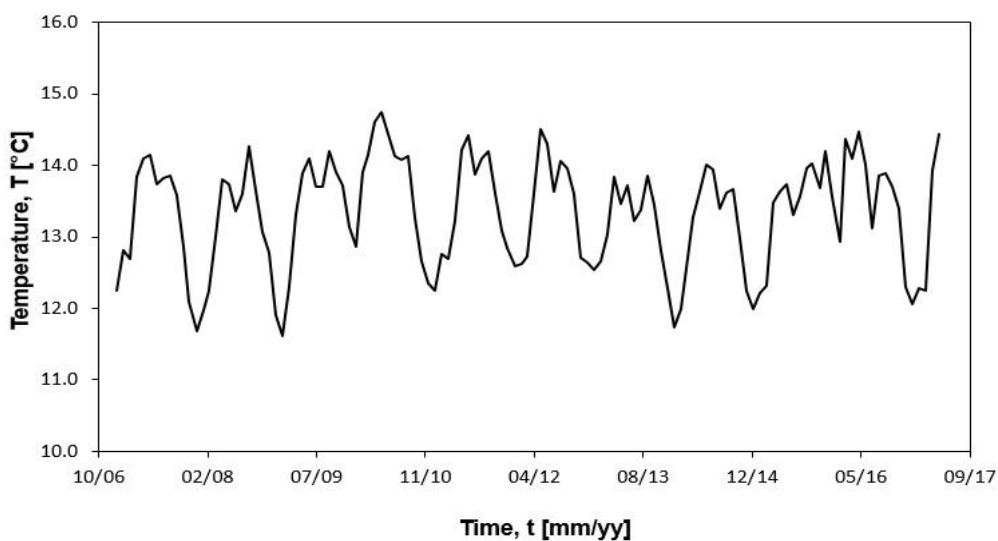
Figure 4.12. Average daily month temperature of the Birris sub basin obtained from five gauging stations located within the study area**.**

.4.7.2.2   Model Description

The Soil and Water Assessment Tool (SWAT) version 2009 (Neitsch et al., 2009) was used to model the catchment hydrology and to obtain the differences in surface runoff (R) and water discharge (Q) at the outlet, for each treatment studied. SWAT is a physically based, long term yield model; and predicts the impact of land management

practices on water, sediment and chemical yields. Figure 4.13 shows the main model modules and input data required for the "Land phase of the hydrologic cycle".

Six scenarios were identified, sharing the same climate and landuse data and differentiating only on the soil input data for the areas occupied by Crops and Grassland. Thus, for these specific landuse types six different conditions (based on the treatments set for this study) were identified: unamended sand (S0); sand + 2.5 biochar (S2.5), sand + 5% biochar (S5), only sandy loam (SL0), sandy loam + 2.5% biochar (SL2.5) and sandy loam + 5% biochar (SL5). Six different output scenarios, in terms of water discharge and surface runoff volume were obtained and discussed.

Precipitation and temperature time series from 2006 to 2017 from two gauging stations located inside the subcatchment, where used to run the models. Landuse data was obtained using satellite images and soil data (for all landuse types except for Crops and Grassland) was obtained from digital maps according to (Ortiz-Malavassi, 2014).

Figure 4.13. Schematic of the SWAT model structure for the land phase of the hydrologic cycle to obtain the water yield at the catchment outlet (after Neitsch et al., 2009).

4.8. Statistical Analysis

The mean and standard deviations were calculated. The analysis of variance (ANOVA) with $p < 0.05$ was used to assess the effect of the pore size distribution of the different amendment conditions. The differences of means were assessed by the HSD Tukey´s test ($p < 0.05$). The non-parametric Kruskal- Wallis test was applied to assess

the differences of the water retention and hydraulic conductivity data. The Dunn test was used to find significant differences in the means. The test of Shapiro-Wilk was applied to demonstrate the normality of the data ($p < 0.05$). All statistical analyses were performed with the free software R studio v.1.0.136 (Villagra-Mendoza and Horn, 2018a).

5. Results

5.1. Physical, Chemical and Hydraulic Properties of the Amended Soils

This chapter gathers the main results related to the effect, of two soil types (sandy and sandy loam) amended with two different fractions (2.5 and 5% dry wt.) of biochar, on some physical, chemical and hydraulic soil properties. It also presents the effects of the biochar amendments on soil water infiltration by comparing three different infiltration models (empirical and semi empirical) and a statistical model. Finally, the hydrological response of a catchment is analyzed to understand the effect of soil management, in a macroscale perspective, with biochar addition on areas occupied by crops and grassland.

5.1.1. Chemical Properties

Table 5.1 shows the chemical properties of the amendments and the pure biochar. The woodchip pyrolyzed biochar with a neutral pH had a C/N ratio of 163 and, as the biochar is added, the C/N ratio increases in the amendments. Sand (S) was slightly alkaline and sandy loam (SL) was neutral according to AG Boden (2005). The addition of 2.5% and 5% biochar did not produce any significant effect on the pH in both soils. As expected, biochar increased the total carbon content significantly in all treatments. The applied biochar with a specific surface area (SSA) of 42 m^2/g increased the SSA of the sand amendments (S) as biochar dosage increased ($p < 0.05$). The SSA of the sandy loam (SL) increased significantly with the addition of 2.5% of biochar (Villagra-Mendoza and Horn, 2018a).

Table 5.1.Chemical properties and specific surface area for two soils sand (S) and sandy loam (SL) with two doses of biochar addition (2.5% and 5%) (Villagra-Mendoza and Horn, 2018a).

Treatment	pH	TC	C/N	$^*C_{inorg}$	Na^+	K^+	Ca^{2+}	Mg^{2+}	Multipoint BET-SSA
		%				$cmol_c/kg$			m^2/g
S0	7.54	0.16 ± 0.01^a	62.97 ± 16.49^a	0.14	0.22 ± 0.01^a	0.12 ± 0.014^a	5.94 ± 0.32^a	0.21 ± 0.02^a	0.32 ± 0.07^a
S2.5	7.47	1.83 ± 0.02^b	461.11 ± 25.74^b	0.02	0.17 ± 0.02^a	1.55 ± 0.05^b	5.10 ± 0.07^a	0.70 ± 0.01^b	0.49 ± 0.19^a
S5	7.50	3.56 ± 0.03^c	435.09 ± 84.52^b	0.04	0.14 ± 0.01^a	2.86 ± 0.09^c	6.80 ± 0.04^a	1.14 ± 0.01^c	1.53 ± 0.25^b
SL0	6.83	1.35 ± 0.01^d	10.07 ± 0.39^c	n. d	0.40 ± 0.003^b	6.73 ± 0.12^d	92.23 ± 2.06^b	19.82 ± 0.25^d	4.73 ± 0.48^c
SL2.5	6.98	3.27 ± 0.03^e	23.17 ± 0.06^c	n. d	0.43 ± 0.03^b	8.20 ± 0.09^e	$94.91 \pm 2.04^{b,c}$	$18.93 \pm 0.10^{e,f}$	3.95 ± 0.12^d
SL5	7.08	4.85 ± 0.04^f	35.47 ± 1.44^c	n. d	0.36 ± 0.01^b	9.53 ± 0.22^f	97.21 ± 2.46^c	19.03 ± 0.16^f	4.71 ± 0.25^c
Biochar	7.12	78.36	163	n. d	n. d	n. d	n. d	n. d	42.07 ± 0.69

TC: total carbon; C/N: ratio Carbon/Nitrogen; C_{org}: inorganic carbon; SSA: specific surface area (Multipoint BET Surface method); n.d: not determined.

Variables with different letters in a column are significantly different (p<0.05)

5.1.2. Physical Properties

Figure 5.1 shows the grain size distribution of the base materials and the amended soils. Texture classification was based on the German standard (AG Boden, 2005). Treatments with the initial S were classified as fine-medium sand (*mSfs*) and treatments named SL were classified as sandy loam (*Sl4*) (Appendix A, Table A.1).

Table 5.2 includes the initial average bulk density and particle density values, as well as pore size distribution of the treatments based on the water content at different matric potentials. Addition of biochar modified the pore size distribution, being more significant in the sandy soil (S). For all treatments, the increase of the biochar fraction decreased the fraction of wide coarse pores (pores drained between 0 and -6 kPa). The fraction of narrow pores (pores drained between -6 and -30 kPa) increased significantly for the sandy and amendments (S), whereas in the sandy loam (SL) treatments the differences were small. Medium pores (pores drained between -30 and -1500 kPa) increased significantly in the sandy mixtures (S) whereas in the SL mixtures non-significant differences were observed (Villagra-Mendoza and Horn, 2018a). Fine pores increased in the sandy (S) treatments but in the sandy loam (SL) treatments no changes were

observed with respect to the unamended soil. These changes on the pore size distribution are explained with the fill in of pores with the smaller grained biochar (Ajayi et al., 2016; Ajayi and Horn, 2017).
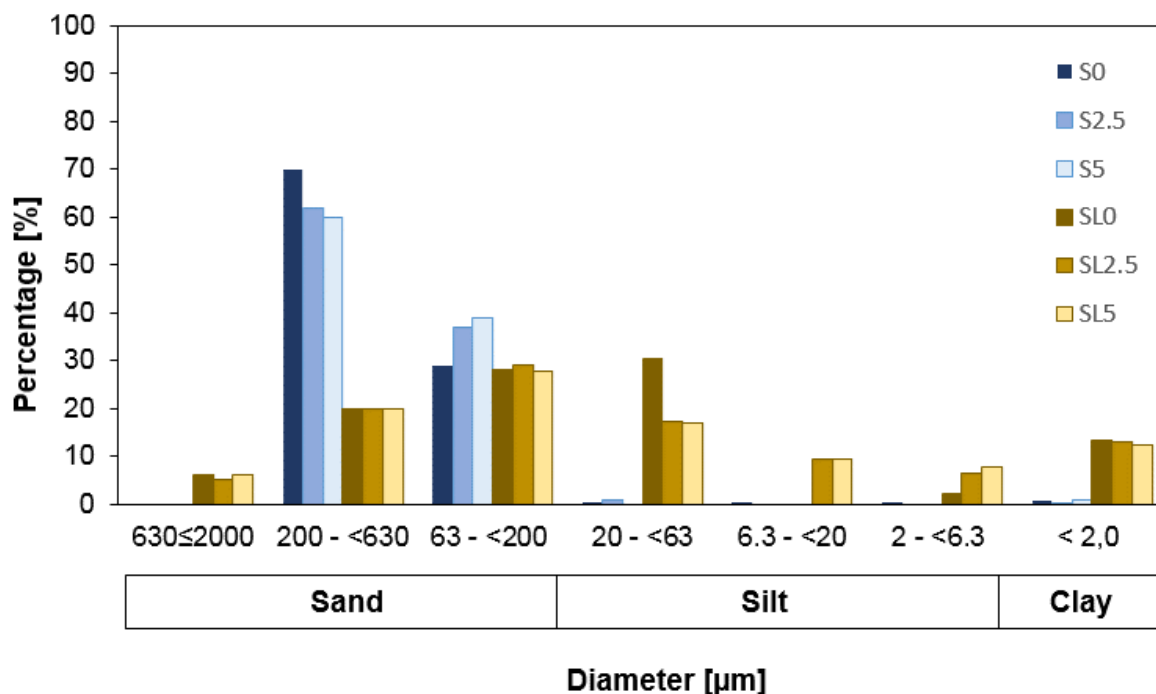
Figure 5.1. Grain size distribution of the base soil materials and amendments.

The addition of biochar enhanced moisture retention as a function of the amended rate, and the effect was more pronounced in the sand (S) than in the sandy loam (SL) treatments. The available water capacity (AWC) increased significantly as the dosage of biochar increased in sandy treatments (S), whereas in the sandy loam (SL) treatments significant differences were observed only between SL0 and SL5 (Table 5.3). There was no significant alteration of the total porosity by the increase of biochar. Air capacity decreased in all treatments, being more pronounced in the sandy amendments (S) (Villagra-Mendoza and Horn, 2018a). Biochar addition significantly enhanced field capacity in the sandy treatments and had not significantly effect in the sandy loam. Wilting point did not change significantly as the fraction of biochar increased, except for sand, which showed a slight increase.

Table 5.2. Bulk and particle density; and pore size distribution of the treatments.

Treatment	Particle density	Bulk density	Pore size distribution			
			Wide coarse pores	Narrow coarse pores	Medium pores	Fine pores
			> -6 kPa	-6 to -30 kPa	-30 to -1500 kPa	< -1500 kPa
		g/cm^3	> 50 µm	50-10 µm	10-0.2 µm	< 0.2 µm
S0	2.51	1.56±0.07	28.24±3.03	4.24±1.19	4.72±0.54	0.61±0.06
S2.5	2.41	1.51±0.06	20.08±2.57	8.27±1.34	7.75±0.85	1.29±0.16
S5	2.35	1.49±0.07	13.87±3.67	10.67±1.79	9.95±0.79	2.12±0.09
SL0	2.65	1.39±0.03	4.16±1.48	14.34±3.51	15.18±0.97	13.96±1.09
SL2.5	2.65	1.39±0.02	3.00±1.56	16.92±2.26	13.98±0.71	13.95±0.54
SL5	2.65	1.36±0.04	2.48±1.86	15.13±2.26	17.53±1.49	13.47±0.26
Biochar	1.61			n.d		

Particle density of the Sandy mixtures (S) was obtained by the pycnometer method, whereas the particle density of the sandy loam mixtures (SL) was assumed to be 2.65 g/cm^3.

Standard deviation corresponds to the variability of the core samples regarding the matric potential applied.

Table 5.3. Total porosity, available water content, air capacity and water constants of the sandy (S) and sandy loam (SL) amendments with 0%, 2.5% and 5% biochar (Villagra-Mendoza and Horn, 2018a).

Treatment	TP	AWC	AC	FC	WP
S0	37.81 ± 2.98[f]	8.83 ± 0.97[a]	28.37 ± 1.96[a]	9.44 ± 1.02	0.61 ± 0.06
S2.5	37.39 ± 2.40[f]	15.83 ± 0.87[b]	20.27 ± 1.37[b]	17.12 ± 1.03	1.29 ± 0.16
S5	36.61 ± 2.93[f]	20.95 ± 1.46[b,c]	13.91 ± 1.48[c]	23.07 ± 1.55	2.12 ± 0.09
SL0	47.64 ± 0.98[g]	29.27 ± 0.61[d]	4.38 ± 0.50[d]	43.26 ± 0.48	13.96 ± 1.09
SL2.5	47.85 ± 0.74[g]	30.99 ± 0.17[d]	2.90 ± 0.03[d,e]	44.95 ± 0.71	13.95 ± 0.54
SL5	48.61 ± 1.69[g]	32.66 ± 0.8[e]	2.48 ± 0.64[e]	46.13 ± 1.05	13.47 ± 0.26

TP: total porosity; AWC: available water content (water content at -6 kPa minus water content at -1500 kPa); AC: air capacity (water content at saturation minus water content at -6 kPa); FC: field capacity; WP: wilting point.

Variables with same letters in a column are not significantly different (p<0.05).

5.1.3. Parameterization of the Water Retention Curve

The observed retention values with the Mualem restriction ($m = 1 - 1/n$) fitted better, in general, than the Burdine restriction ($m = 1 - 2/n$). The SSQ (sum of squares) of the Mualem restriction reflected a better performance of the retention model (Table 5.4). All parameters (θ_r, θ_s, α', n, λ) except K_{sat}, were fitted to the retention curve. Parameter K_{sat} was not fitted since it was determined in the laboratory and the obtained results were reliable enough to be used. Most of the treatments showed a good correlation, except for treatment SL5 where the Burdine´s model provided an unacceptable fit.

Table 5.4. Fitted soil hydraulic parameters for the retention curves plotted in Fig. 5.2.

Treatment	θ_r	θ_s	α'	n	λ	R^2	SSQ
	[cm³/cm³]		[1/cm]	[-]	[-]		
S0							
m=1-1/n	0.000	0.37	0.03726	2.46724	1.43059	0.987	0.03058
m=1-2/n	0.000	0.36	0.04115	3.35166	2.44842	0.987	0.02981
S2.5							
m=1-1/n	0.065	0.36	0.02431	2.77771	-0.88037	0.995	0.03624
m=1-2/n	0.000	0.37	0.02681	3.82111	0.0001	0.994	0.05532
S5							
m=1-1/n	0.073	0.31	0.00670	12.64024	-1.36287	0.942	0.15842
m=1-2/n	0.000	0.32	0.00660	9.53769	0.0001	0.936	0.17703
SL0							
m=1-1/n	0.162	0.46	0.00656	2.64802	0.0001	0.968	0.19002
m=1-2/n	0.000	0.49	0.00873	4.17136	0.0001	0.950	0.34166
SL2.5							
m=1-1/n	0.141	0.47	0.00711	2.20506	0.0001	0.984	0.06755
m=1-2/n	0.000	0.41	0.01002	3.04382	0.0001	0.975	0.13845
SL5							
m=1-1/n	0.148	0.47	0.00414	3.18801	0.0001	0.982	0.01269
m=1-2/n	-	-	-	-	-	-	NR

θ_r: residual water content, when less than 0.001, changed to fit with 0.000; θ_s: saturated water content; α', n, λ: fitted parameters; R^2: coefficient of determination; SSQ: sum of squares; NR: poor correlation.

The van Genuchten model fitted the water retention curve better for the measured data of the sandy loam (SL) than for the sand (S) (Figure 5.2). In the sandy mixtures (S2.5 and S5) the fitting was less accurate than for the unamended sand (S0). The observed data revealed that the biochar addition of 2.5 and 5% enhanced the retention properties of the sandy mixtures (S). The biochar addition amplified the retention ability of the sandy soil. Water content at saturation and at wilting point did not increase but the field capacity range increased (although not significantly) with a higher dosage of biochar.

If we compare the fitting parameter α', it becomes obvious that in the sandy treatments, the air entry value $1/\alpha'$ increased as the biochar dosage increased. The higher the dosage of biochar the more negative the matric potential at which air starts entering the soil matrix (Table 5.4). In the sandy loam, the fitted curve shows a longer flat pattern than in sandy soil, with air entry values starting at a matric potential of about -30 kPa compared to -3 kPa in the sandy soil.
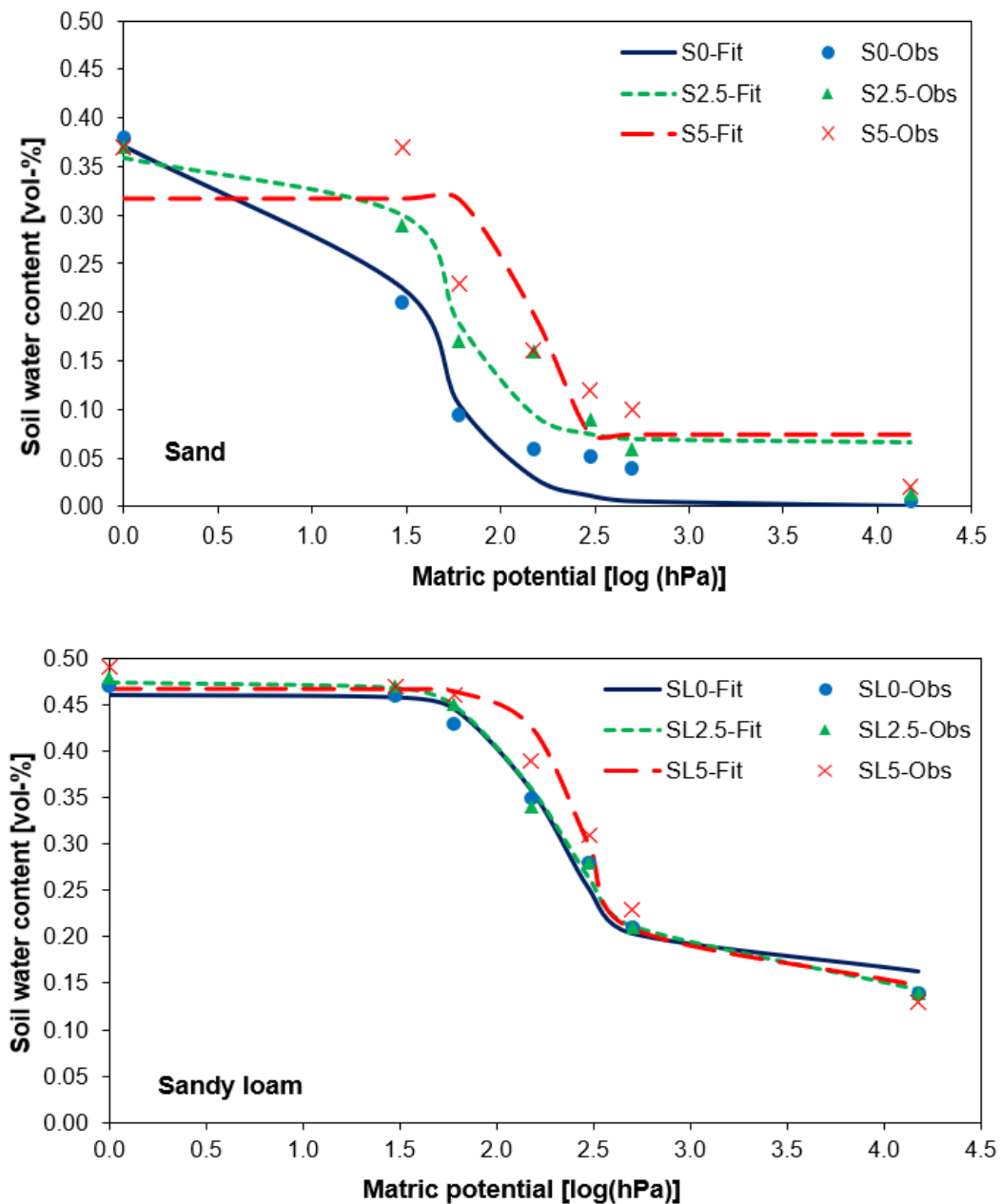
Figure 5.2. Fitted soil water retention curves of the sand (S) and sandy loam (SL) and their amendments at biochar application rates of 2.5 and 5%.

5.1.4. Soil Water Repellency as a Function of Biochar and Intense Wetting and Drying Cycles

Amended soils, under dehydration, were tested for hydrophobicity using the water repellency index (RI) (Hallett, 2007). Hydrophobicity is initially observed, in Table 5.5, in the sandy loam (SL), whereas sand (S0 and S2.5) is hydrophilic. A 5% biochar fraction resulted in a hydrophobic amended sand (S5). As the water drained and the matric potential decreased S0 and S2.5 continued under hydrophilic conditions and treatment S5 oscillated between hydrophobic and hydrophilic conditions along the dehydration. In the sandy loam (SL) there was no clear relation regarding the fraction of biochar added and the hydrophobic condition.

Additionally, amended soils were submitted to four repetitive wetting and drying (WD) cycles simulated by oven-drying the samples at 30°C for 72h. Table 5.6 shows that the water repellency index, RI, oscillated with the different WD cycles and no clear trend was observed for any of the treatments studied. There was also no clear correlation observed between hydrophobicity and the biochar content along the WD cycles applied. Except for WD2 in the unamended sandy treatment (that we assume was an experimental error) and WD4 for treatment S5, all sandy mixtures remained hydrophilic during all WD cycles. It was also observed that, in general, in the sandy mixtures a higher dosage of biochar increased RI, although most of the treatments kept their hydrophilic condition. The unamended sandy loam (SL0) was already hydrophobic and biochar increased slightly the hydrophobicity of the mixtures. However, no clear trend was observed between the effect of WD cycles and the hydrophobic condition of these treatments.

Table 5.5. Repellency index, RI, for different matric potentials and biochar amendments of sand (S) and sandy loam (SL) samples (Villagra-Mendoza and Horn, 2018a).

Treatment	-3 kPa	-6 kPa	-15 kPa	-30 kPa	-50 kPa
			RI		
S0	0.68	0.41	0.97	0.85	0.66
S2.5	0.91	0.50	0.68	0.61	0.52
S5	1.26	0.89	0.83	1.84	0.85
SL0	1.66	3.32	2.92	3.77	2.62
SL2.5	2.41	3.28	2.76	2.73	3.12
SL5	1.23	3.42	2.07	2.55	3.16

Table 5.6. Effect of three intense wetting and drying (WD) periods on the repellency index RI, of the sand (S) and sandy loam (SL) treatments.

Treatment	WD1	WD2	WD4
S0	0.60	2.27	0.38
S2.5	0.94	0.69	0.78
S5	0.48	0.99	1.10
SL0	1.76	2.28	1.52
SL2.5	1.99	3.14	2.51
SL5	1.89	1.64	2.33

5.1.5. Shrinkage of the Amended Soils

Figure 5.3 presents the shrinkage behavior of the six treatments after applying different matric potentials. Swelling was observed during saturation, whereas shrinkage occurred as more negative matric potentials were applied. The measured data was fitted to the Peng and Horn´s model (Peng and Horn, 2013) with a relation coefficient of 0.68 < r < 0.99 (Table 5.7). Only treatment S0 presented the proportional phase, while treatments SL0 and SL2.5 presented additionally the residual phase, because the wet-side maximum point was outside the curve. Treatment S2.5 included the first three shrinkage phases (structural, proportional and residual) and treatments S5 and SL5 presented all the shrinkage curve phases. In the sandy soil, the structural shrinkage appeared as biochar was added and increased its range as the fraction of biochar increased. In the sandy loam, structural shrinkage occurred until 5% biochar dose. The presence of zero shrinkage was only observed in both amendments with 5% biochar (S5 and SL5), being related to the dosage of biochar (Villagra-Mendoza and Horn, 2018a).
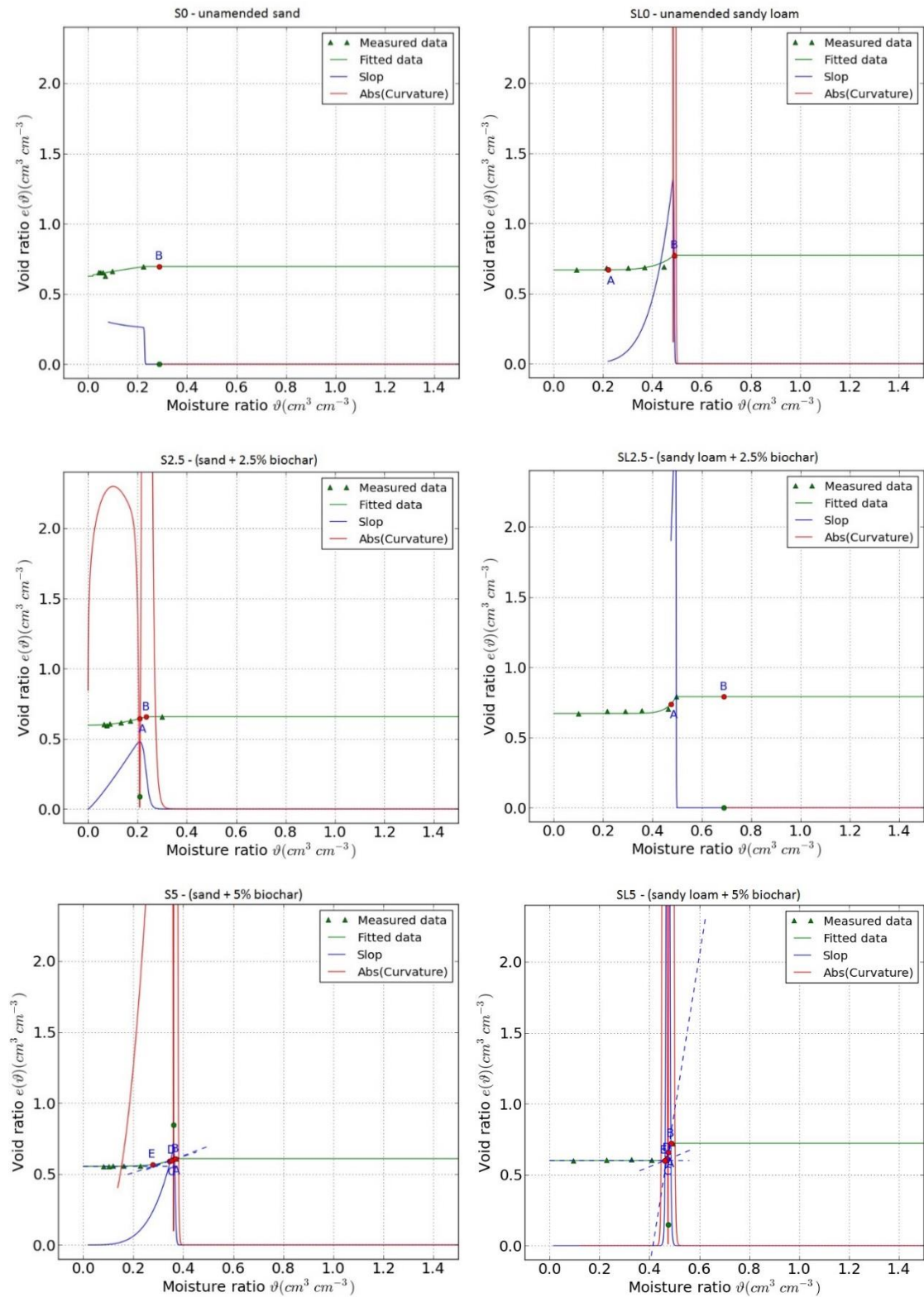
Figure 5.3. Shrinkage response in the unamended sand (S0) and sandy loam (SL0) and the corresponding amendments (S2.5, S5, SL2.5, SL5).

Table 5.7. Parameters of the shrinkage curve for each treatment at initial bulk density of 1.5 g/cm^3 for sand and 1.35 g/cm^3 for sandy loam (Villagra-Mendoza and Horn, 2018a).

Parameter/ Treatment	S0	S2.5	S5	SL0	SL2.5	SL5
r	0.68	0.98	0.99	0.89	0.89	0.98
e_s	0.696	0.659	0.608	0.773	0.789	0.722
e_r	0.627	0.597	0.554	0.668	0.671	0.599
ϑ_s	0.222	0.299	0.373	0.489	0.496	0.495
ϑ_r	0.068	0.075	0.081	0.093	0.099	0.095
χ	4.374	4.262	2.716	2.046	2.018	2.108
p	282.565	28.416	178.192	468.333	952.451	169.028
q	0.003	0.076	0.028	0.014	0.014	1.011
A	n.a	0.209, 0.645	0.360, 0.602	0.220, 0.669	0.475, 0.739	0.474, 0.657
B	0.287, 0.696	0.236, 0.656	0.369, 0.607	0.490, 0.773	0.690, 0.790	0.486, 0.720
C	n.a	n.a	0.345, 0.593	n.a	n.a	0.463, 0.601
D	n.a	n.a	0.352, 0.597	n.a	n.a	0.469, 0.616
E	n.a	n.a	0.277, 0.567	n.a	n.a	0.460,0.600
Shrinkage curve type (after Peng and Horn, 2013)	II	I+II+III	I+II+III+IV	II+III	II+III	I+II+III+IV

Correlation coefficient (r); Void ratio saturation (e$_s$); Void ratio residual (e$_r$); Moisture ratio saturation (ϑ_s); Moisture ratio residual (ϑ_r); shrinkage curve parameters χ,p,q; inflection point (A); wet-side maximum curvature (B); dry-side maximum curvature (C); air entry (D); shrinkage limit (E).

5.1.6. Effect of Biochar on the Hydraulic Conductivity

The saturated hydraulic conductivity (K_{sat}) values decreased significantly ($p < 0.05$) in the amended soils (Table 5.8). The decrease of K_{sat} was more pronounced in the sandy mixtures than in the sandy loam. The effect of the wetting and drying (WD) cycles caused in most cases an initial general decrease followed by an increase in the K_{sat} values (Villagra-Mendoza and Horn, 2018a).

Swelling was present during wetting in all amended mixtures, decreasing bulk density. In the sandy loam, it was observed an inverse relation between bulk density and K_{sat}. As bulk density decreased, K_{sat} increased with increasing WD cycles. In the sandy mixtures although bulk density decreased at each WD cycle, K_{sat} showed an oscillating behavior, which in most cases was not significantly different. The weaker structure of sand (S0)

promoted an increase of bulk density. On the other hand, biochar improved rigidity and after saturation (during desiccation), the sand mixtures resisted more the vertical height reduction (Villagra-Mendoza and Horn, 2018a).

Table 5.8. Saturated hydraulic conductivity (K_{sat}) for sand S and sandy loam SL and their amendments at 25 and 50 g kg-1 biochar for four repeated wetting and drying cycles (Villagra-Mendoza and Horn, 2018a).

	K_{sat}	ρ_d	K_{sat}	ρ_d	K_{sat}	ρ_d	K_{sat}	ρ_d
	cm/d	g/cm³	cm/d	g/cm³	cm/d	g/cm³	cm/d	g/cm³
	WD0		WD1		WD2		WD4	
S0	1471.88 ± 226.45[a]	1.50	1020.13 ± 115.62[a]	1.50[a]	1333.94 ±219.49[a]	1.50[a]	1576.58 ±194.05[a]	1.60[b]
S2.5	343.71 ± 75.36[b]	1.50	346.33 ± 31.10[b]	1.48[c]	288.60 ± 15.78[b]	1.46[d]	1018.40 ±261.19[c]	1.45[e]
S5	167.82 ± 17.44[d]	1.50	142.55 ± 13.27[d]	1.47[f]	106.68 ± 9.57[d]	1.46[d]	113.89 ±16.82[d]	1.43[g]
SL0	35.18 ± 3.40[e]	1.35	18.24± 1.42[f]	1.35[h]	34.38 ± 5.33[e]	1.35[h]	45.98 ±6.57[e]	1.33[i]
SL2.5	23.11 ± 3.41[g]	1.35	11.61 ±1.25[h]	1.33[i]	20.87 ± 2.70[g]	1.33[i]	27.00 ±3.59[g]	1.30[j]
SL5	12.66 ± 2.26[i]	1.35	8.75 ± 0.95[i]	1.33[i]	12.70 ± 1.69[i]	1.30[j]	31.66 ± 4.34[i]	1.27[k]

Same letters in a column are significantly similar (p<0.05).

The effect of biochar and texture affected the pattern of the hydraulic conductivity matric potential (Figures 5.4 and 5.5). In the sandy mixtures, the increase of field capacity (in average 200% in the observed data), coincided with a more continuous unsaturated hydraulic conductivity pattern ($K(\psi)$). The higher the dosage of biochar the more constant and relatively higher was $K(\psi)$ up to -50 kPa (according to the fitting curve). In the sandy mixtures, the changes in the field capacity were less pronounced than in the unamended sand (S0); this is attributed to the fact that biochar increased the frequency of narrow and medium pores, by clogging larger pores with smaller biochar particles, enhancing the ability of the amended sand to retain water at more negative matric potentials. Moreover, the sorption capacity of the biochar, due to a higher specific surface area (Table 5.1) increased water retention at more negative matric potentials compared to the unamended sand. The sandy loam (SL) showed a relatively constant $K(\psi)$ up to a matric potential of – 30 kPa and the unamended sandy loam (SL0) showed a slightly higher (non-significant) $K(\psi)$ compared to the amended soil. The $K(\psi)$ curve pattern is relatively flat in the near saturated range, but decreases rapidly at more negative matric potentials.
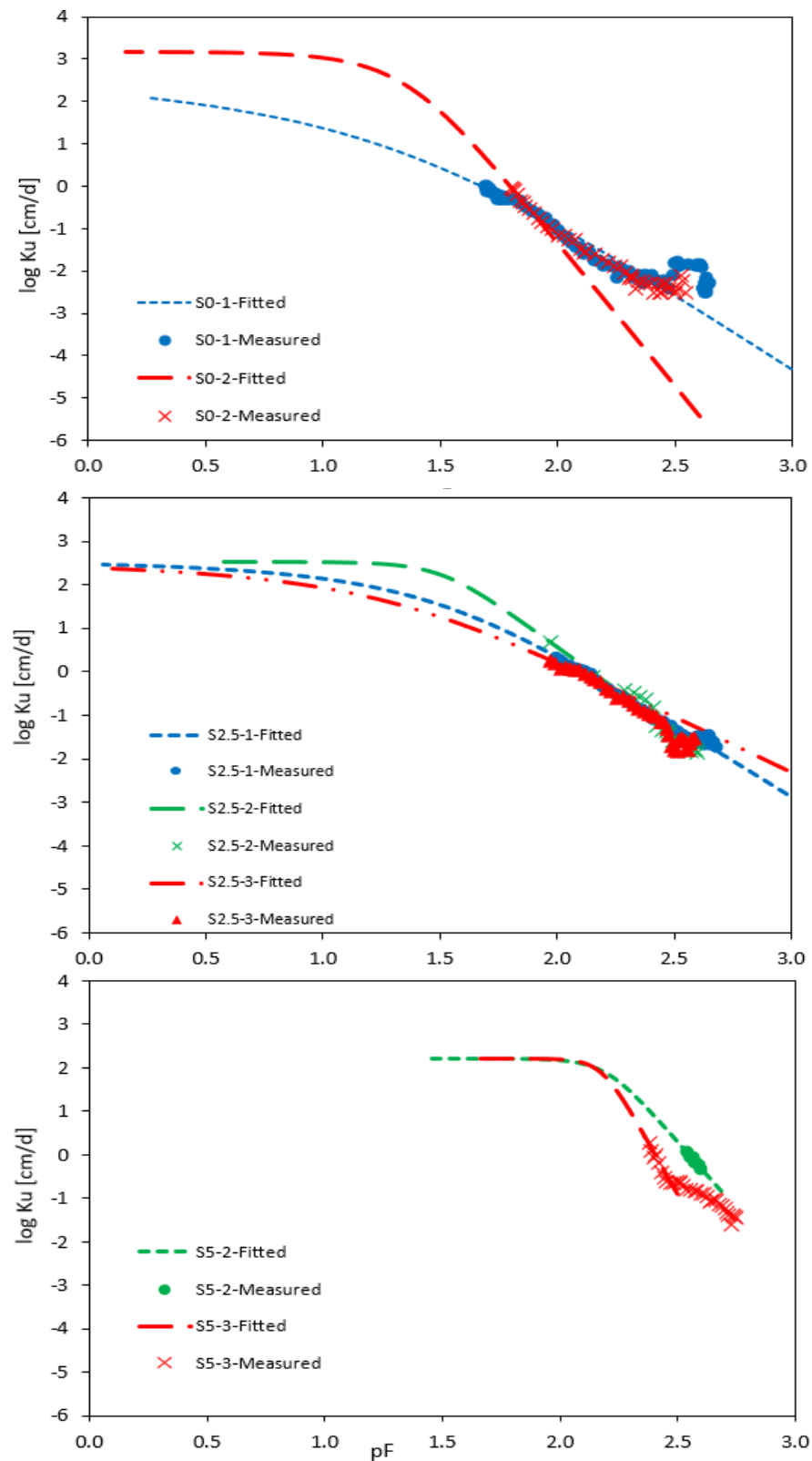
Figure 5.4. Fitted unsaturated hydraulic conductivity for the sandy amendments (S) with the van Genuchten model (fitted) and measured unsaturated hydraulic conductivity (measured) with the modified Evaporation Method (Hartge, 1966). The numbers after the treatment codes (S0, S2.5 and S5) correspond to the replica number.
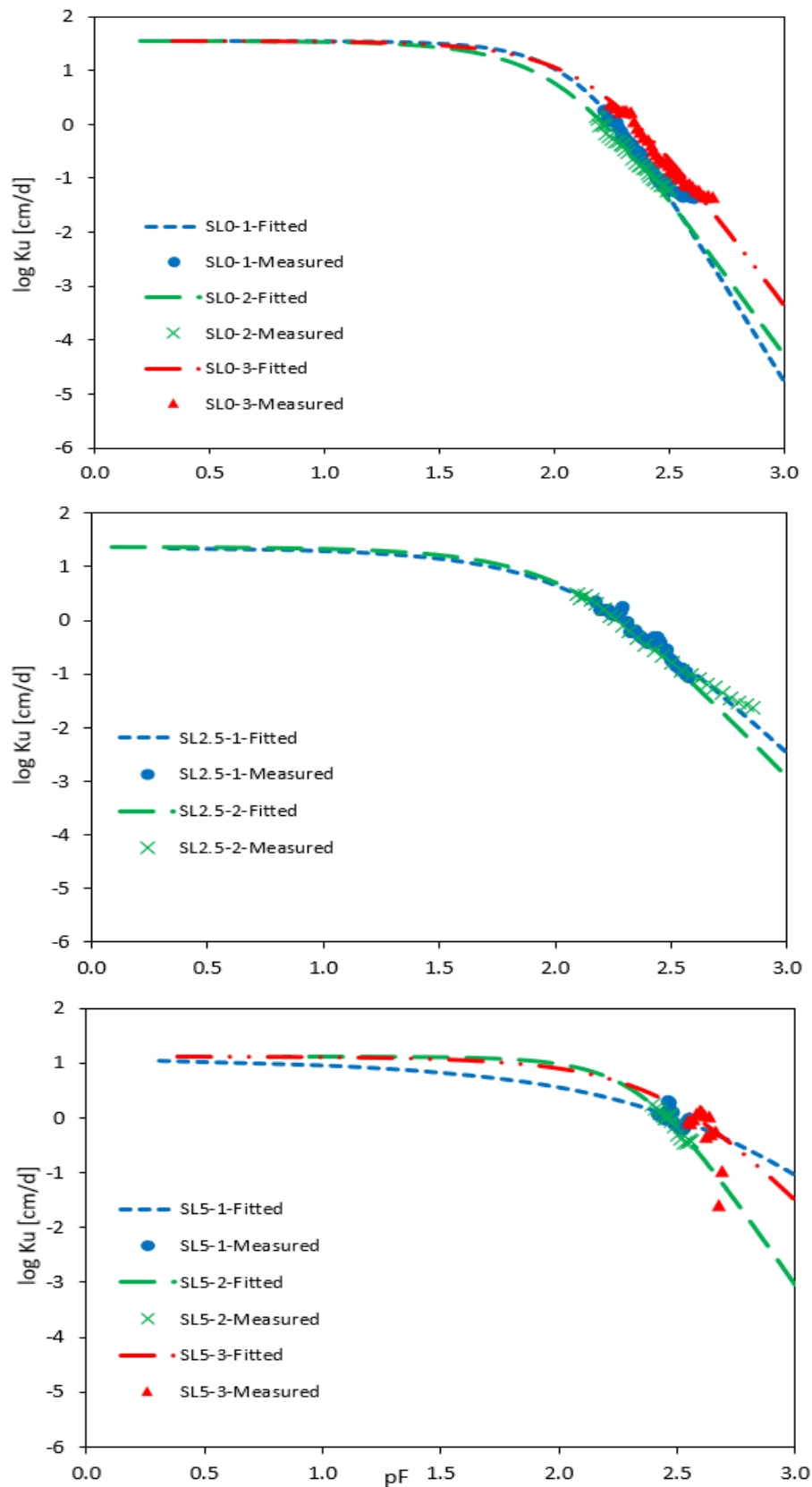
Figure 5.5. Fitted unsaturated hydraulic conductivity for the sandy loam amendments (SL) with the van Genuchten model (fitted) and measured unsaturated hydraulic conductivity (measured) with the modified Evaporation Method (Hartge, 1966). The numbers after the treatment codes (SL0, SL2.5 and SL5) correspond to the replica number.

The fitted $K(\psi)$ data of the van Genuchten-Mualem model (Figures 5.4 and 5.5) predicted very well the range of the measured data if the decreasing K_{sat} values of the initial wetting drying cycle (WD0) – due to biochar addition – were included (Table 5.8).

Furthermore, the increase in surface area (Table 5.1) of the amended sandy mixtures (S) also contributed to a relative constant $K(\psi)$ due to the delayed entrance of air in the soil matrix. Although the matric potential at which air enters the sandy loam (SL) mixtures was more negative than in the sandy mixtures (S), $K(\psi)$ was not significantly higher when compared to $K(\psi)$ of the sandy mixtures. This may be also related to the measured K_{sat} which was higher for sand and decreased as biochar was added. Between a matric potential of -30 and -100 kPa the decline of $K(\psi)$ in the sandy loam was less than for sand. This was due to the presence of finer pores which reduced the draining process and contributed to retain more water in the soil bulk.

5.1.7. Effect of Biochar on the Air Permeability

The relation between air filled porosity and air permeability showed the dynamic changes of the mixtures with respect to gas flux during drying from -3 kPa to -50 kPa (Figure 5.6). Unamended sand (S0) and its amended mixtures (S2.5 and S5) showed a steeper slope than the corresponding sandy loam variants (SL), indicating a higher air permeability as pores are filled with gas. At less negative matric potentials, it was possible to have some air flux through the pores. The unamended sand (S0) even at nearly saturated conditions was able to permit the flow of air, while a decrease of the flow path occurred at the same matric potentials with increasing biochar fraction (Figure 5.7). On the other hand, in the sandy loam, it was necessary to reduce the matric potential at least to -15 kPa (drainage of narrow coarse pores) to start any flux. At the same low matric potentials, air permeability was lower than the one of the sandy material (Villagra-Mendoza and Horn, 2018a). Air permeability increased as the volumetric water content decreased and air-filled porosity increased; air permeability was greater in the unamended treatments (S0 and SL0) in comparison to the amendments.
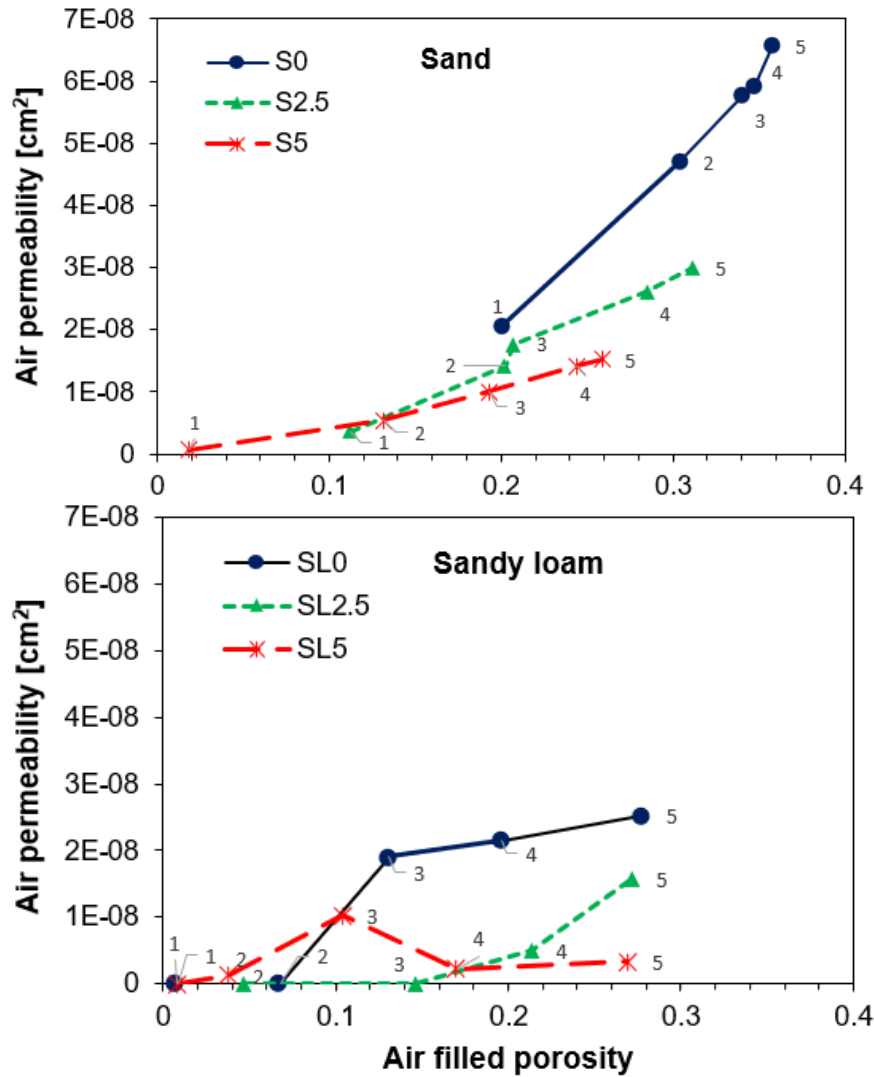
Figure 5.6. Relation of air permeability and air-filled porosity as a function of soil texture (sand S and sandy loam SL) and two different biochar dosages (2.5% and 5%). Numbers referred to 1 (-3 kPa), 2 (-6 kPa), 3 (-15 kPa), 4 (-30 kPa), 5 (-50 kPa).

Figure 5.8 shows that the effect of repetitive wetting and drying periods (WD) did not affect the soil functioning in terms of air permeability. In the sandy loam and amendments, it was found out that although there is a slight significant effect of the WD cycles on the air permeability it can be observed a pattern effect. As the WD cycle increases air permeability increases, too.

It is also observed that repetitive WD changes the pore structure of the substrates. While in figures 5.6 and 5.7 the sandy materials conducted more air than the sandy loam substrates through the soil bulk, the opposite occurred under different WD periods. This suggests a modification of the pore system under drying conditions that permitted a higher air flux through the sandy loam substrates.
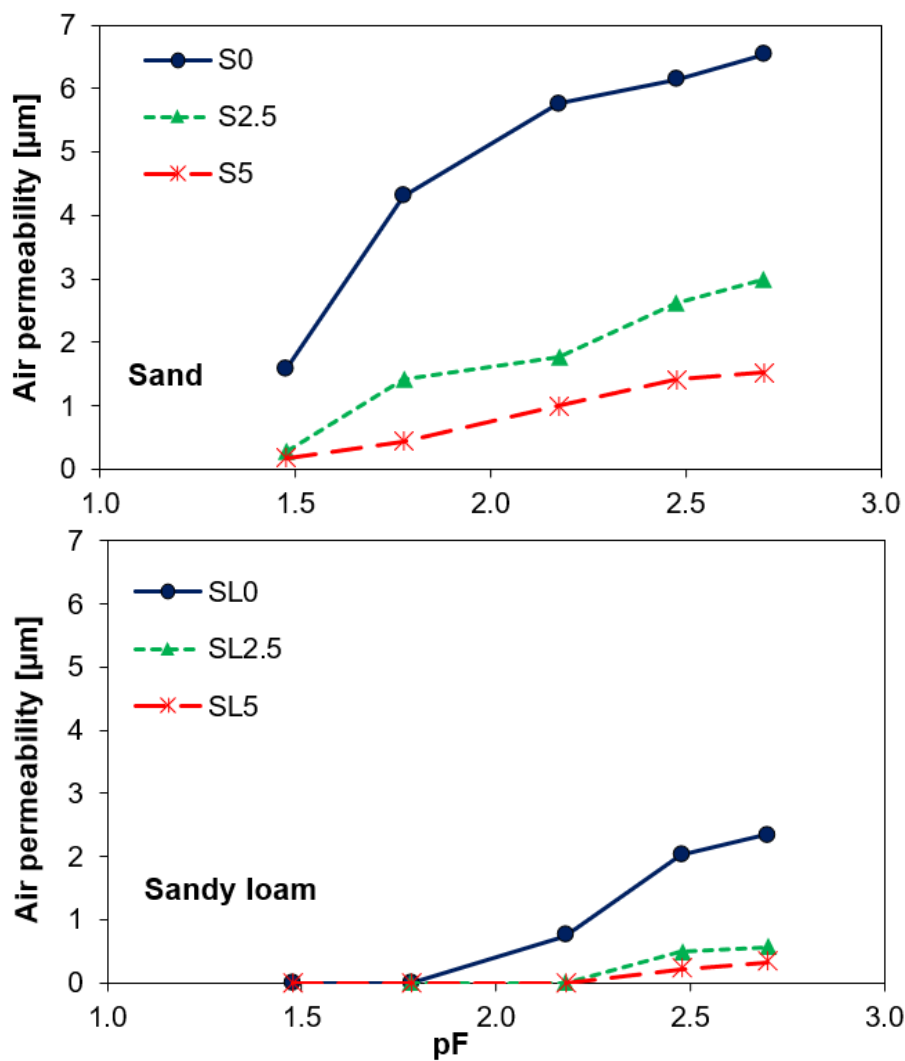
Figure 5.7. Air permeability in the amendments sandy (S) and sandy loam (SL) substrates at pF 1.5; 1.8; 2.2; 2.5 and 2.7.
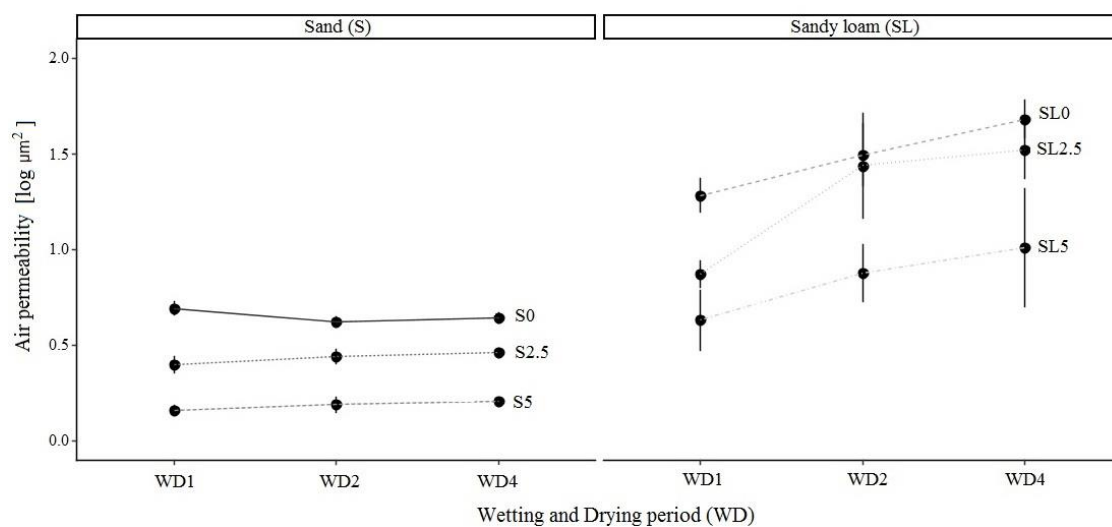
Figure 5.8. Air permeability in the amendments sandy (S) and sandy loam (SL) substrates for repetitive wetting and drying.

5.2. Effect of Biochar Amendments on Water Infiltration at the Topsoil

This section presents the results of the water infiltration behavior of a sandy (S) and a sandy loam (SL) soil amended with biochar fractions of 2.5 and 5% dry wt. The measured infiltration and cumulative rates, and comparison to empirical and statistical models were elaborated.

5.2.1. Measured Infiltration Data

Figures 5.9 and 5.10 show the observed cumulative infiltration, obtained from repetitive WD cycles. Cumulative infiltration ($Icum$) varied according to the different fractions of biochar applied and it was higher in the sandy substrates. The WD cycles for the infiltration experiments and the WD cycles for the K_{sat} experiments (Section 1.1.6) were simulated with similar procedures. For K_{sat} during wetting, the soil bulk was saturated by the upward flow due to capillarity; whereas for infiltration, soil samples were saturated downward by the hydraulic gradient and gravity.

Due to the lack of measured bulk density in the third WD cycle (WD3), the following infiltration analyses were performed only for cycles WD0, WD1, WD2 and WD4.

Cumulative infiltration tended to be higher and straight in the unamended treatments during WD0 (previous to any wetting and drying cycle), and as the biochar fraction increased the cumulative infiltration curves decreased. Repetitive wetting and drying (WD) periods decreased infiltration showing an oscillating behavior as the WD cycles were applied. However, this oscillating behavior was less significant as the biochar fraction increased (Figure 5.9). Cumulative infiltration values, after 15 and 45 minutes for repetitive WD cycles, are shown in Appendix B, tables B.1 and B.2. In the first 15 minutes, cumulative infiltration decreased in all treatments as the wetting and drying occurred, with exception of SL0. In the unamended sandy loam (SL0), $Icum$ oscillated, along the WD cycles, without being able to reach the cumulative infiltration obtained during WD0. In the sandy treatments the addition of biochar reduced the impact of the WD cycles on $Icum$. For instance, for WD4 $Icum$ decreased (with respect to WD2) 35% in S0, whereas in S2.5 the decrease was of 28.5% and in S5 4.4%. The same pattern, except for S0 during WD1, was observed in the other WD cycles. These changes suggest an increase on pore rigidity as the biochar fraction increased. In the sandy loam treatments, there was not a significant decrease of $Icum$ with the addition of biochar.

At 45 minutes, $Icum$ decreased as the biochar dosage increased. Data of $Icum$ for the unamended sand (S0) is not shown in this table, since the infiltration test ran in a time shorter than 45 minutes. However, data from a shorter time (15 minutes) confirmed the same $Icum$ pattern. During different wetting and drying, for a same treatment, $Icum$

tended to decrease in all cases. In the sandy treatments (S) the changes were more significant than in the sandy loam treatments (SL).
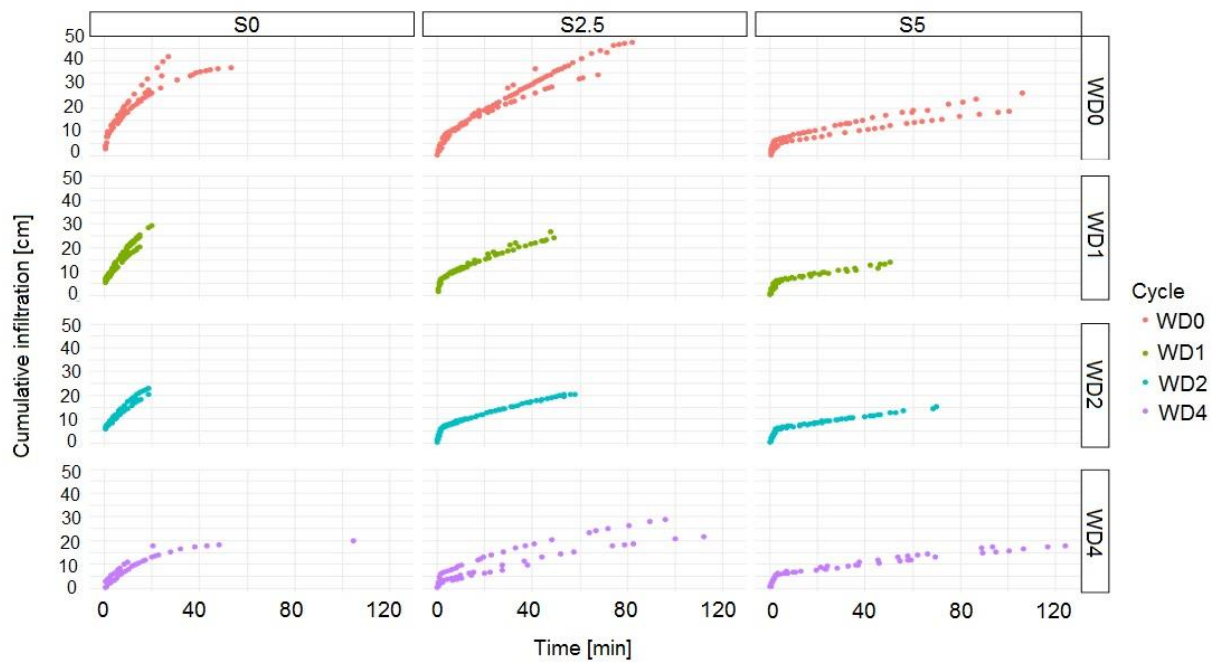
Figure 5.9. Observed cumulative infiltration for the amended sandy soil (S) for different WD periods. Initial values of soil water content for all treatments are about 2 vol-%.
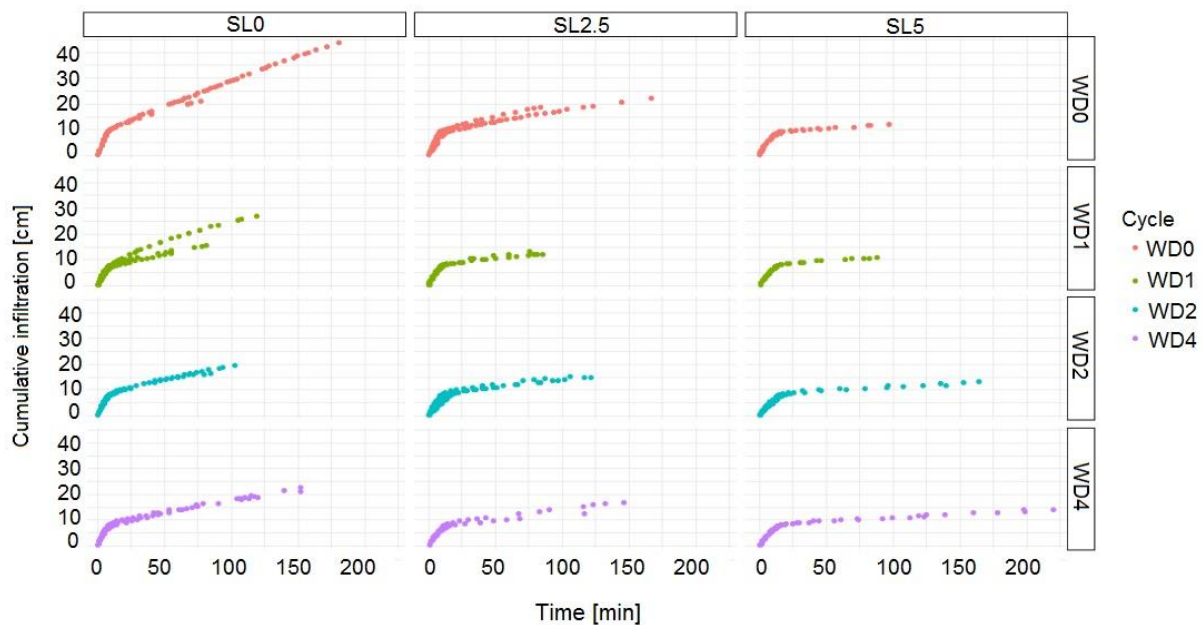
Figure 5.10. Observed cumulative infiltration for the amended sandy loam soil (SL) for different WD periods. Initial values of soil water content for all treatments are about 2 vol-%.

Figures 5.11 and 5.12 show the observed values of the infiltration capacity curves for all treatments and for different WD cycles. After sampling preparation (WD0) the curve of decay in the sandy loam (SL) was not as steep as in the sandy (S) treatments; even the initial infiltration was much lower than the sandy substrates (S2.5 and S5). The point of inflection, in the sandy treatments (S), occurred very fast near the starting infiltration time. As biochar increased (S2.5 and S5), the inflection point of the infiltration curve occurred slightly earlier than in the unamended S0, taking the form of the letter "L". In the sandy loam amendments (SL2.5 and SL5), the slope of the curve before the inflection point was not as steep as for the unamended SL0, but the inflection point did not change significantly.

In the sandy materials (S), during repetitive WD (WD1, WD2 and WD4), the point of inflection was not significantly delayed but the rate at which it occurred, tended slightly to decrease, with exception of S5. Whereas in the sandy loam substrates (SL) non-significant changes were observed. The time delay of the inflection point may be beneficial since the amended soils may be able to absorb water at the surface for longer time, reaching basic infiltration may take longer, thus surface runoff volume may decrease; however, the decrease of the rate at which it occurs may be not beneficial since it may increase surface runoff.

Figures B.1 and B.2 (in Appendix B) show the initial infiltration rate (I_0) and the steady final rate flow. Figure B.1 illustrates that during WD0 the initial infiltration rate (I_o) in the sandy treatments decreased as the biochar fraction increased whereas in the sandy loam the opposite was observed. In the sandy treatments there was an oscillating behavior when increasing wetting and drying. The highest rate of infiltration (~5000 mm/h) was observed in the unamended sand, for cycles WD0 and WD2. In the sandy treatments, an oscillating pattern was observed for the initial infiltration rates in S2.5 and S5, but the steady rate (Ib) tended in all WD cycles to decrease with a higher biochar dosage (Figure B.2). The amended sandy loam (SL2.5 and SL5) tended to increase the initial infiltration rate during WD0 but non-significant changes were observed on the other WD cycles. In general, final infiltration rate decreased as biochar application rate increased. In SL5 during WD4 steady infiltration rate tended to decrease. For other WD, there were no observed clear differences.

As observed in figure 5.11 and figure B.2, final infiltration rate of the sandy mixtures (S2.5 and S5), during WD0 and WD1 cycles may be potentially able to infiltrate rain water with intensities of 100 mm/h or less, without occurring overland flow. As more WD cycles were applied (WD2 and WD4), in all sandy treatments (S), final infiltration rates (Ib) decreased and overland flow may occur. Sandy loam mixtures (SL) are potentially able to infiltrate water but at lower rainfall intensities. Treatment SL0 (without facing any shrinkage and swelling, during the WD0 cycle) was the only treatment able to overcome a rain event of 100 mm/h without producing overland flow. Because the final infiltration capacity decreased for all SL treatments, with different wetting and drying, overland flow may occur.
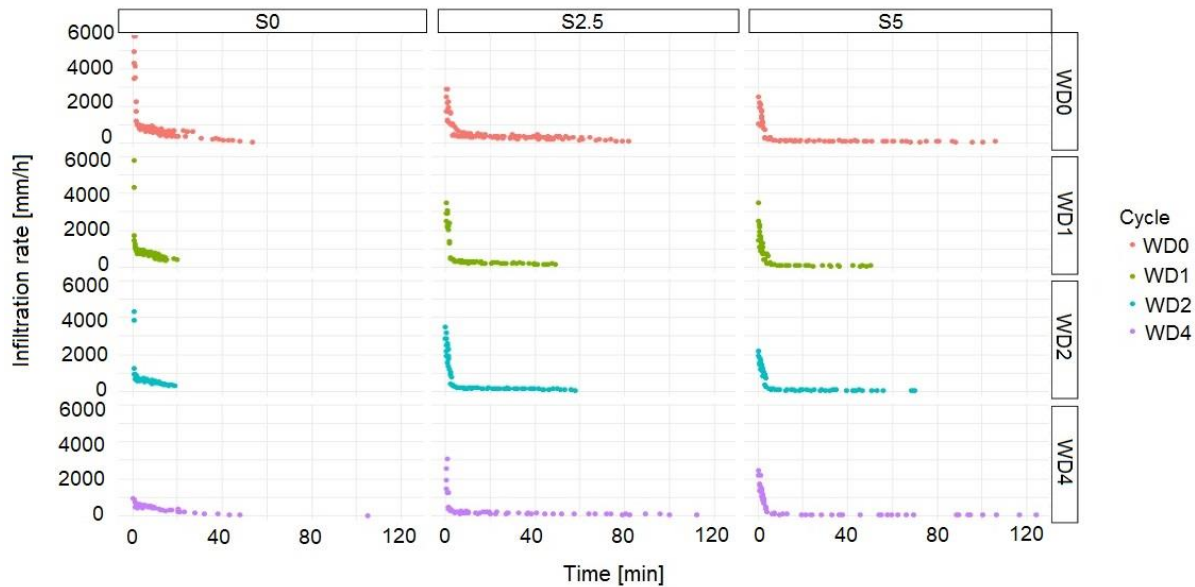
Figure 5.11. Observed infiltration capacity for the amended sand (S) for different WD periods. Initial values of soil water content for all treatments are about 2 vol-%.
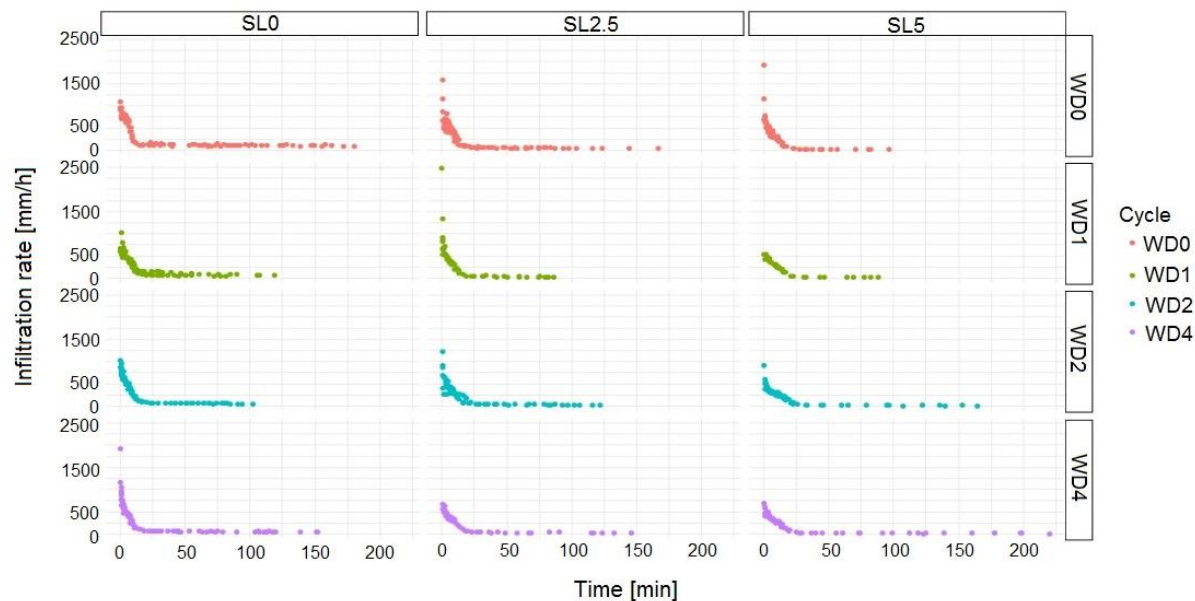
Figure 5.12. Observed infiltration capacity for the amended sandy loam (SL) for different WD periods. Initial values of soil water content for all treatments are about 2 vol-%.

Table 5.9 presents the effect of the simulated WD cycles on the bulk density. As the WD cycles occurred, bulk density increased considerably in the unamended sand (S0) whereas in the sandy mixtures (S2.5 and S5) the opposite occurred. As biochar dosage increased, it was determined, by visual observation, that the amendments were able to swell during wetting (reducing bulk density) but during drying the amendments did not

shrink enough to produce the opposite effect. Thus, the net bulk density, of the sandy mixtures, along the WD cycles, did not vary considerably. In the sandy loam mixtures (SL), bulk density did not vary as significantly as in the sandy mixtures and it oscillated along the different WD cycles. Although bulk density decreased (especially in the sandy treatments) as the WD cycles occurred, cumulative infiltration decreased, too. Initial soil moisture was kept constant, about 2 vol-%, for all treatments along the WD cycles, with the exception of WD0, which corresponded to the soil moisture content before applying any wetting and drying condition.

5.2.2. Validation of the Infiltration Dynamics Using Three Different Models

The measured infiltration rates (i) and cumulative infiltration ($Icum$) were validated with three different models (Kostiakov, Horton and Philip) under different wetting and drying (WD) cycles. Average values of i and $Icum$ for the different repetitions per treatment were plotted against time. Results of the time series for two extreme wetting and drying cycles (WD0 and WD4) are shown in figures 5.13 to 5.16. Results for WD1 and WD2 are included in figures C.1 to C.4 in Appendix C.

Table 5.9. Effect of the simulated WD cycles on the bulk density (ρ_d) and soil water content (θ) on the sandy (S) and sandy loam (SL) mixtures.

Treatment	Wetting/Drying Cycle (WD)							
	WD0		WD1		WD2		WD4	
	ρ_d	θ	ρ_d	θ	ρ_d	θ	ρ_d	θ
S0	1.55	1.3±0.54	1.54±0.03	1.1±0.45	1.61±0.07	1.2±0.46	1.71	1.0±0
S2.5	1.52±0.03	2.0±1.32	1.49±0.03	1.7±1.14	1.47±0.03	1.1±0.31	1.48	0.7±0
S5	1.48±0.01	1.7±0.31	1.46±0.02	1.1±0.28	1.46±0.02	1.1±0.21	1.43	0.8±0
SL0	1.38±0.02	4.6±0.72	1.36±0.02	1.8±0.10	1.37±0.01	2.1±0.17	1.38	1.9±0
SL2.5	1.40±0.05	5.5±0.86	1.39±0.06	1.9±0.04	1.38±0.05	2.4±0.12	1.35	1.6±0
SL5	1.40±0.04	5.2±0.79	1.36±0.05	1.9±0.11	1.35±0.02	2.3±0.11	1.37	1.9±0

ρ_d: bulk density (g/cm^3); θ: initial volumetric soil moisture (cm^3/cm^3).

In general, the three models fitted very well the curves of infiltration rate (i) vs. time, especially after the inflection point, except for treatment S0 where the Philip model was

the least accurate (Figure 5.13 and Tables 5.10 to 5.12). Before the inflection point none of the models were able to predict the initial infiltration rate (I_o) and all of them tended to underestimate it during WD0 and WD4; whereas during WD1 and WD2 the Kostiakov model overestimated the initial infiltration rate (I_o) of the sandy loam mixtures. In general, the Kostiakov model overestimated the I_o while the Horton and Philip models underestimated it. This condition produced a significant increase on the mean sum of square error (*MSSE*) for all the models (Tables 5.10 to 5.12).

The Horton model approximated better the cumulative infiltration ($Icum$) in most of the cases, but this approximation was not enough to explain the behavior of the infiltrated water (Figures 5.15 and 5.16). Cumulative infiltration in the unamended sand (S0) showed a more straight line compared to the sandy amendments (S2.5 and S5). Treatment S2.5 showed a straight line but after 60 min a curvature was observed. In treatment S5, the slope of the curve was flatter than the sandy mixture S2.5. Between WD cycles the curvature trend was kept similar but with lower cumulative infiltration values. The sandy loam mixtures also showed that as the biochar dosage increased the curvature was flatter and by comparing WD0 against WD4; WD4 had lower cumulative infiltration values.
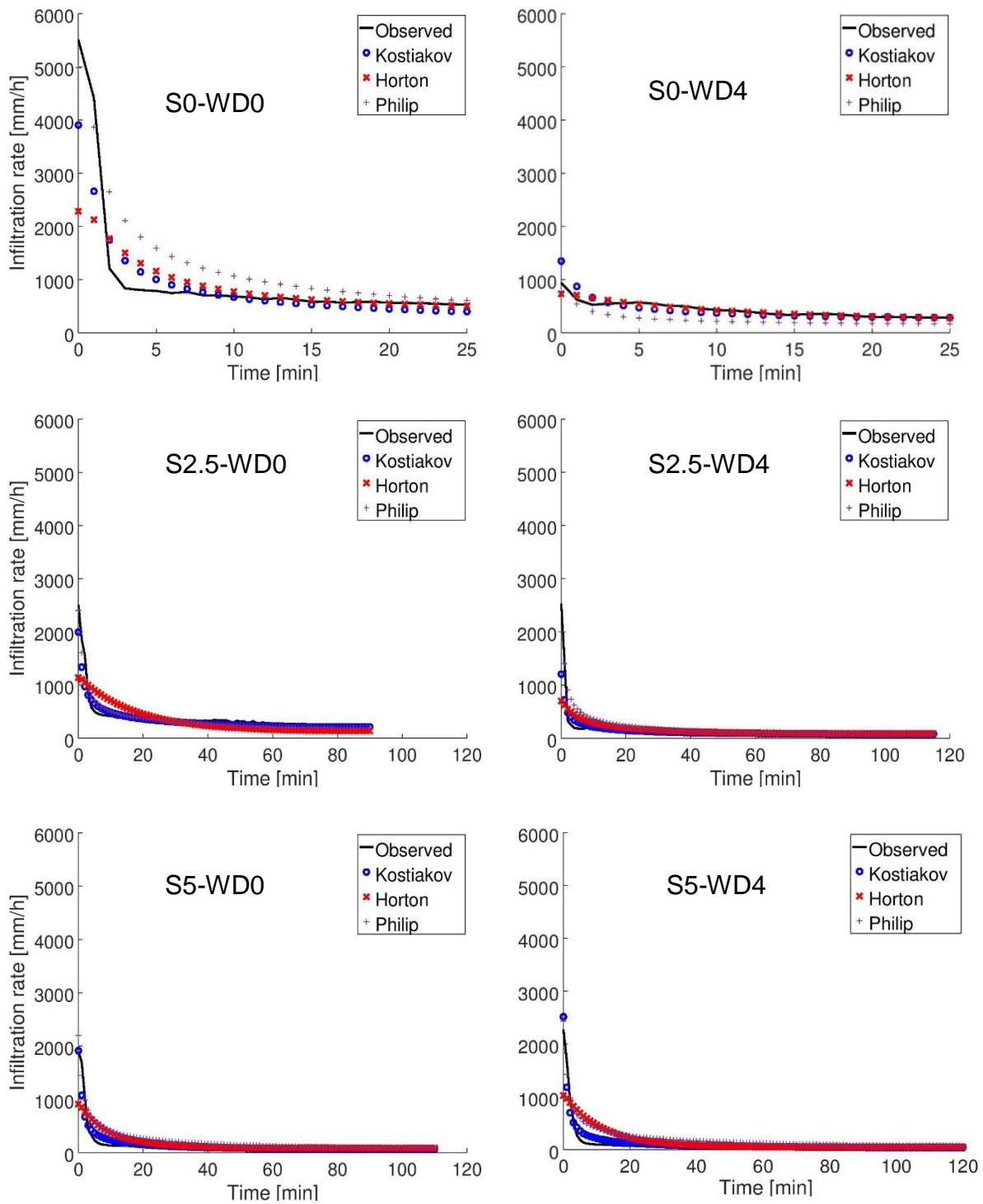
Figure 5.13. Comparison of the average values of the infiltration rate for the sandy treatments (S) obtained with the models of Kostiakov, Horton and Philip for two extreme wetting and drying (WD) cycles.
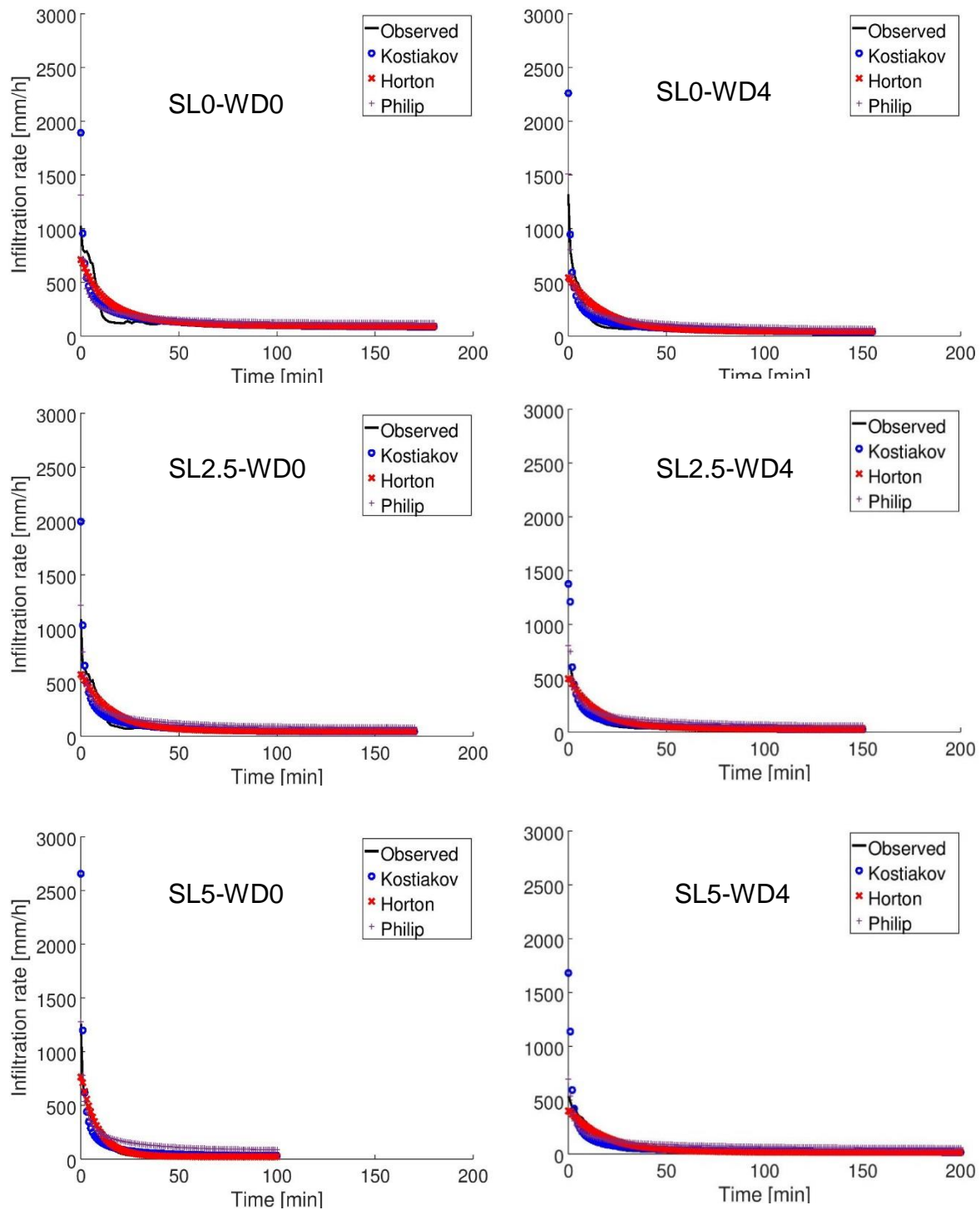
Figure 5.14. Comparison of the average values of the infiltration rate for the sandy loam (SL) treatments obtained with the models of Kostiakov, Horton and Philip for two extreme wetting and drying (WD) cycles.
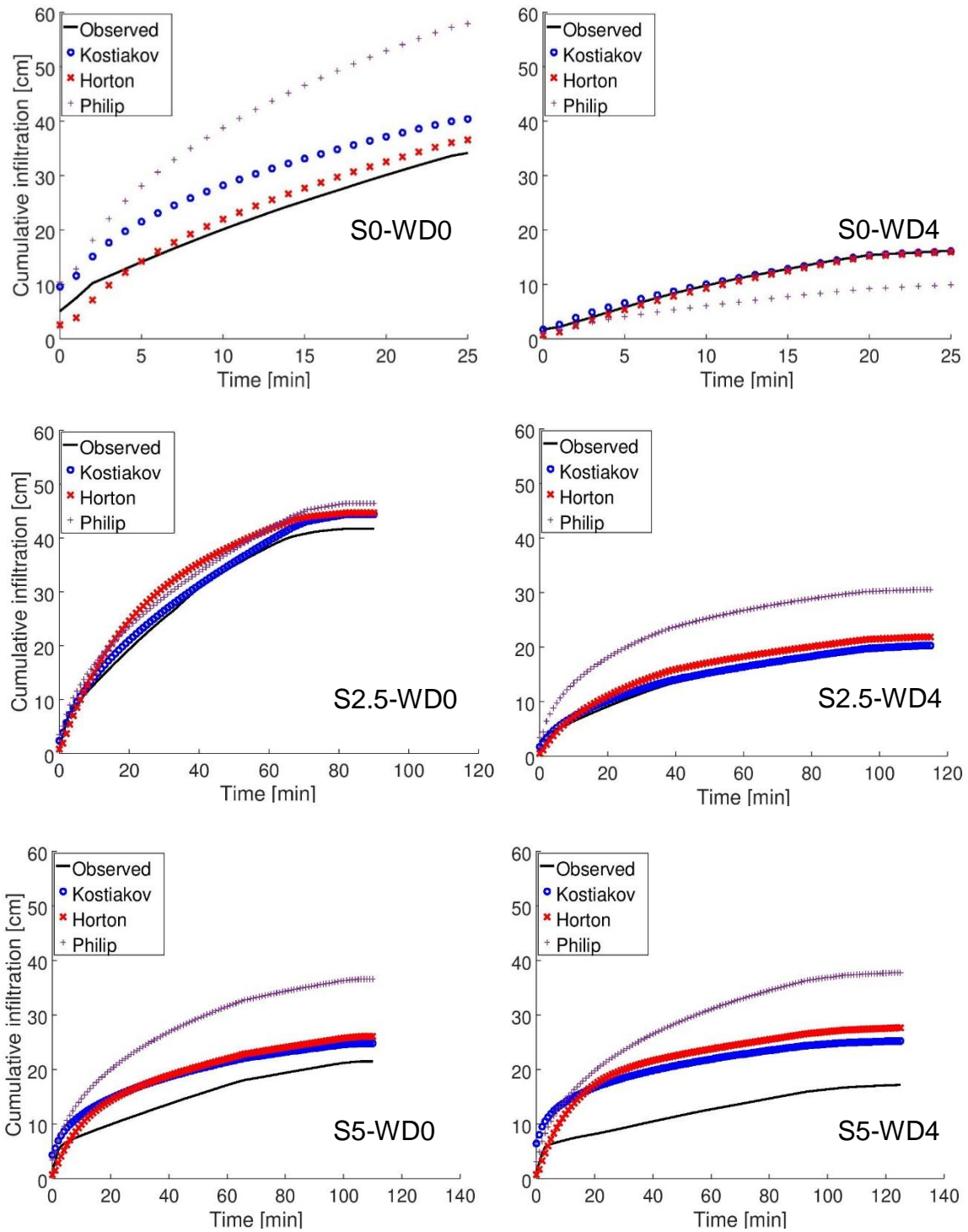
Figure 5.15. Comparison of the average values of cumulative infiltration for the sandy treatments (S) obtained with the models of Kostiakov, Horton and Philip for two extreme wetting and drying (WD) cycles.
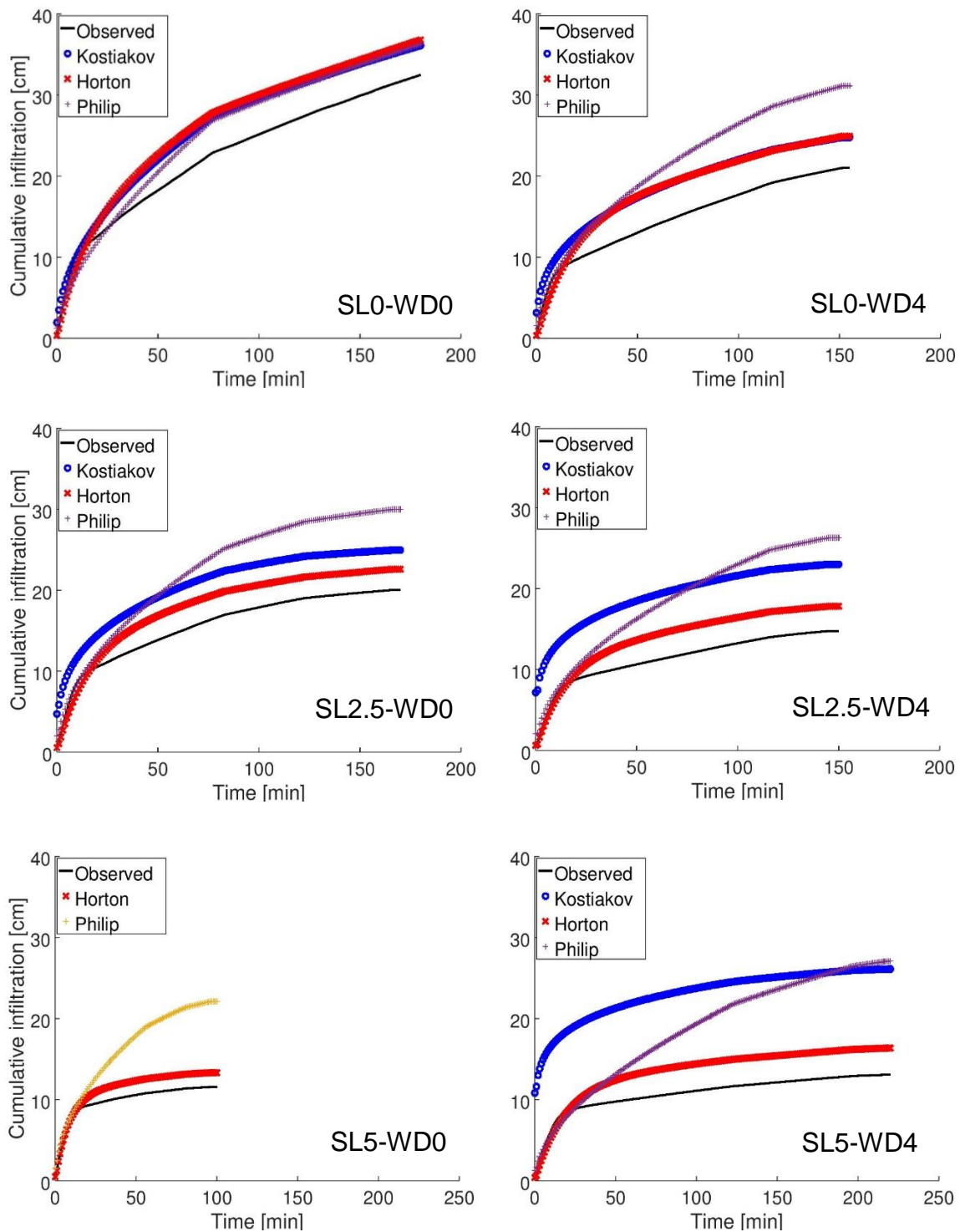
Figure 5.16. Comparison of the average values of cumulative infiltration for the sandy loam (SL) treatments obtained with the models of Kostiakov, Horton and Philip for two extreme wetting and drying (WD) cycles.

The fitting parameters of the different models (Kostiakov, Horton and Philip) for WD0 and WD4 cycles are shown in Tables 5.10 to 5.12. Fitting parameters for the cycles WD1 and WD2 are included in Tables C.1 to C.3 in Appendix C. In general, all the models faced problems fitting the initial infiltration rate resulting in high MSSE values. From all the models, the Horton model presented the least MSSE for the sandy loam mixtures (SL), whereas Kostiakov resulted in better fitting parameters for the sandy mixtures (S).The Philip model showed inconsistency on the parameter estimation related to the hydraulic conductivity, A (Table 5.12). In some cases, it revealed unrealistic negative results and very high coefficients of variation.

Table 5.10. Mean, standard deviation and coefficient of variation (%) of the fitted infiltration parameters for the model of Kostiakov for WD0 and WD4 cycles.

Treatment	Cycle	C			α			MSSE	
		Mean	Std. dev	CV %	Mean	Std. dev	CV %	i	Ic
$S0$	WD0	2609.4	229.7	8.8	-0.6	0.12	20.2	$3.7 \cdot 10^5$	59.
	WD4	866.9	126.3	14.6	-0.4	0.23	59.6	$2.6 \cdot 10^4$	4.3
$S2.5$	WD0	1299.6	147.2	11.3	-0.4	0.08	17.8	$5.6 \cdot 10^4$	3.6
	WD4	689.6	146.9	21.3	-0.5	0.05	9.0	$1.3 \cdot 10^5$	1.8
$S5$	WD0	1058.1	313.7	29.6	-0.6	0.10	15.1	$7.9 \cdot 10^4$	17.
	WD4	1172.2	281.8	24.0	-0.7	0.03	4.5	$5.9 \cdot 10^4$	62.
$SL0$	WD0	956.6	180.8	18.9	-0.5	0.12	22.4	$5.9 \cdot 10^4$	7.8
	WD4	926.5	94.0	10.2	-0.6	0.05	7.4	$5.4 \cdot 10^4$	10.
$SL2.5$	WD0	1056.6	27.7	2.6	-0.7	0.02	3.4	$6.6 \cdot 10^4$	20.
	WD4	1032.4	133.4	12.9	-0.8	0.02	2.0	$3.4 \cdot 10^4$	50.
$SL5$	WD0	1100.8	109.4	9.9	-0.8	0.03	3.3	$1.4 \cdot 10^5$	10.
	WD4	1032.2	135.8	13.2	-0.8	0.06	7.5	$7.3 \cdot 10^4$	15.

Table 5.11. Mean, standard deviation and coefficient of variation (%) of the fitted infiltration parameters for the model of Horton for WD0 and WD4 cycles.

Treatment	Cycle	I_o			β			MSSE	
		Mean	Std. dev	CV %	Mean	Std. dev	CV %	i	$Icum$
$S0$	WD0	2609.0	1120	42.9	0.23	0.15	67.9	$7.7 \cdot 10^5$	13.0
	WD4	763.14	107.8	14.1	0.12	0.09	73.0	$5.1 \cdot 10^3$	1.6
$S2.5$	WD0	1160.1	207.2	17.9	0.06	0.01	16.3	$1.5 \cdot 10^5$	32.9
	WD4	718.5	369.6	51.4	0.12	0.12	102.1	$2.1 \cdot 10^5$	6.4
$S5$	WD0	950.0	416.4	43.8	0.11	0.1	54.2	$1.7 \cdot 10^5$	15.9
	WD4	1056.9	111.6	10.6	0.09	0.01	15.5	$1.7 \cdot 10^5$	58.4
$SL0$	WD0	N.D							
	WD4	551.6	87.2	15.8	0.06	0.01	11.8	$4.1 \cdot 10^4$	8.9
$SL2.5$	WD0	588.6	144.3	24.5	0.07	0.02	30.2	$2.0 \cdot 10^4$	3.8
	WD4	516.2	74.6	14.4	0.07	0.04	48.5	$4.4 \cdot 10^3$	4.2
$SL5$	WD0	797.7	125.7	15.8	0.12	0.02	19.5	$2.8 \cdot 10^4$	0.9
	WD4	410.9	22.5	5.5	0.06	0.01	16.8	$4.7 \cdot 10^3$	3.4

Table 5.12. Mean, standard deviation and coefficient of variation (%) of the fitted infiltration parameters for the model of Philip for WD0 and WD4 cycles.

Treatment	Cycle	S			A			MSSE	
		Mean	Std. dev	CV %	Mean	Std. dev	CV %	i	$Icum$
$S0$	WD0	7974.4	1387.9	17.4	-196.9	30.5	15.5	$4.6 \cdot 10^5$	328.1
	WD4	928.9	10.8	1.2	67.9	0.94	1.4	$4.5 \cdot 10^4$	12.0
$S2.5$	WD0	3062.2	1542.4	50.4	21.18	138.5	654	$4.7 \cdot 10^4$	50.6
	WD4	2815.5	1104.5	39.2	-88.12	33.4	37.9	$8.6 \cdot 10^4$	80.8
$S5$	WD0	3006.9	1393.5	46.3	-72.83	62.9	86.3	$6.8 \cdot 10^4$	113.2
	WD4	2990.5	473.6	15.8	-75.7	9.4	12.5	$4.7 \cdot 10^4$	158.8
$SL0$	WD0	1330.6	17.4	1.3	57.6	11.4	19.7	$3.2 \cdot 10^4$	3.9
	WD4	1584.3	208.3	13.2	0.10	13.3	-	$9.3 \cdot 10^3$	21.2
$SL2.5$	WD0	1584.4	175.8	11.1	7.9	27.0	341	$1.5 \cdot 10^4$	20.1
	WD4	1376.7	467.0	33.9	0.15	16.9	-	$6.2 \cdot 10^3$	25.7
$SL5$	WD0	1512.4	586.8	38.8	0.75	45.2	-	$1.8 \cdot 10^4$	16.4
	WD4	994.4	127.5	12.8	16.6	6.4	38.4	$8.6 \cdot 10^3$	28.2

5.2.3. Regression Analysis of Infiltration Capacity and Cumulative Infiltration

To explore the correlation of the observed soil parameters to the dependent variables: infiltration rate (i) and cumulative infiltration ($Icum$) a multivariate principal component analysis was performed (Figure 5.17). As it is ibserved, the variables are located in a circle with a center 0 and radius 1, and there are mainly two groups formed. Group 1 enclosed variables such as sand, bulk density (ρ_d) and saturated hydraulic conductivity (K_{sat}), whereas group 2 included variables such as silt and clay content, total carbon (TC), total porosity (TP), specific surface area (SSA), and field capacity (FC). Both groups have coordinate values with respect to the first axis (Dim 1) near to -1 and 1 respectively. This means that the coordinates of the individuals of these two groups of variables are directly and inversely proportional, respectively; to the deviation between the average of the variables and the values of the individuals in those variables.

Within each group (1 and 2), the correlation between variables that belong to each group is near to one. This means that in group 1 the individuals that have high sand contents, have also high saturated hydraulic conductivity and bulk density.

The variables cycle (with respect to Dim 2) and TC (with respect to Dim 1) are close to cero, therefore they do not represent a lineal relation with respect to the values of the individuals over these variables.

Figure 5.17a illustrates the correlation of the soil parameters to infiltration rate (i). The two first components (Dim 1 and Dim 2) conserved 74% of the original information. Component 1 (Dim 1) contained time, WD cycle and infiltration rate (i). Component 2 (Dim 2) included soil parameters divided in the two groups 1 and 2, described above. From those variables, time had a strong and negative correlation with respect to i, whereas WD had a weak and negative correlation to i. Parameters in group 1 had a strong and positive correlation among them and strongly negative to parameters in group 2. Group parameters 1 presented a weak and positive correlation to i. Parameters in group 2, showed a strong and positive correlation among them, except for TC that was not well represented in the correlation circle. Variables in this group had a weak and negative correlation to i.

Figure 5.17b depicts the principal component analysis for the cumulative infiltration ($Icum$) with respect to the soil parameters. It is observed that the two first components (Dim 1 and Dim 2) conserved 77.11% of the original information. Component 1 (Dim 1) contained the variables time, WD cycle and cumulative infiltration rate ($Icum$). Component 2 (Dim 2) included soil parameters divided in the same two groups as in figure 5.17a and with a similar correlation as explained for Figure 5.17a. However, TC had a higher negative correlation to group 1, than in figure 5.17a.

An AICc analysis confirmed that the best statistical model, with an explanation of approximately 80%, should include $K_{sat}, \rho_d, Sand, TP, logtime$ and $WD\ cycle$. However

due to the high collinearity of K_{sat}, ρ_d and $Sand$; only K_{sat} was selected as input parameter for the statistical model (Figures E.1 and E.2, Appendix E).

From this information, the average values of the four correlated variables (i, $Icum$, TP and K_{sat}) were determined (Table 5.13). As the biochar fraction increased all the dependent (i and $Icum$) and independent variables (K_{sat} and TP) decreased.
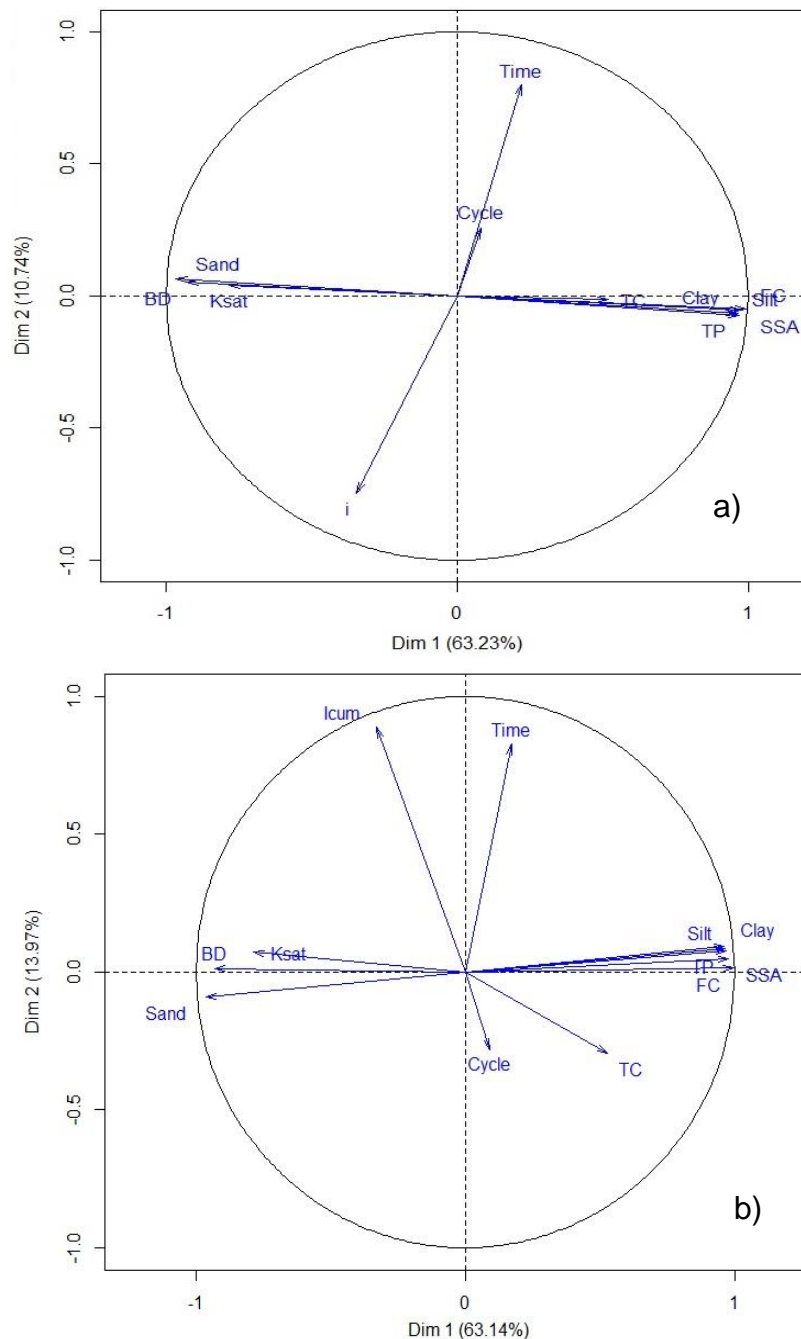
Figure 5.17. Principal component analysis of some chemical, hydraulic, and physical soil parameters with respect to a) infiltration rate (i) and b) cumulative infiltration ($Icum$).

Table 5.13. Mean and standard deviation of infiltration rate (i), cumulative infiltration ($Icum$), saturated hydraulic conductivity (K_{sat}) and total porosity (TP) for the sandy (S) and sandy loam (SL) treatments. Average values belong to the initial soil condition WD0.

Measured parameter	Treatments					
	*S*0	*S*2.5	*S*5	*SL*0	*SL*2.5	*SL*5
i (mm/h)	1085.78 ± 1323.54[a]	539.22 ± 553.88[b,d]	463.64 ± 659.16[c,d]	318.12 ± 293.44[e]	289.84 ± 291.93[e]	357.35 ± 318.60[e]
$Icum$ (mm)	N.D	32.72 ± 4.81	14.51 ± 2.46	17.38 ± 1.14	13.32 ± 1.10	10.38 ± 0.28
K_{sat} (mm/h)	613.28 ± 94.35[a]	143.21 ± 31.40[b]	69.93 ± 7.27[c]	14.66 ± 1.42[d]	9.63 ± 1.42[e]	5.28 ± 0.94[f]
TP (cm^3/cm^3)	37.81 ± 2.98	37.39 ± 2.40	36.61 ± 2.93	47.64 ± 0.98	47.85 ± 0.74	48.61 ± 1.69
Ib (mm/h)	314.89 ± 282.41	110.87 ± 23.72	79.35 ± 13.89	92.84 ± 7.41	44.34 ± 9.09	20.57 ± 0.81

I is the infiltration rate at 15 minutes during WD0

$Icum$ is the cumulative infiltration set to 45 min for all treatments during WD0.

Same letters in a row are significantly similar (p < 0.05).

Tables B.3 and B.4 in Appendix B, provides a more complete information about the average infiltration rates (i) at 15, 30, 45 and 60 minutes, for the four WD cycles. In general, in the sandy treatments (S), i decreased at all times by repetitive WD. In the sandy loam treatments (SL), at 15 and 30 minutes, there was observed an oscillating pattern explained by the rearrangement of the particles and formation of preferential flow. During 45 and 60 minutes dominated a decreasing i by repeating WD.

A linear regression analysis was performed for each soil type. In order to perform the analysis, a logarithmic transformation of the main variables, i, $Icum$ and time were used. Once the regression analyses were carried out, the transformed variables were expressed in their original variables. The regression equations used for i and $Icum$ were:

$$\log Icum = K_{sat} + TP + \log time + WDcycle \tag{5.1}$$

$$\log i = K_{sat} + TP + \log time + WDcycle \tag{5.2}$$

Tables 5.14 and 5.15 show the regression coefficients for the sandy (S) and sandy loam (SL) treatments for the infiltration rate and cumulative infiltration. All the models explained more than 80% of the original data.

Table 5.14. Coefficients of the linear regression for the logarithm of cumulative infiltration ($Icum$).

Coefficient	Sand (S)			Sandy loam (SL)		
	Estimate	Std.error	R^2	Estimate	Std.error	R^2
Intercept	-0.43820	0.11710		-0.01351	0.41469	
K_{sat}	0.00059	0.00002		0.01637	0.00119	
TP	0.02474	0.00307		0.00295	0.00872	
$logTime$	0.47430	0.00712	0.88	0.54288	0.00601	0.92
WD1	-0.01910	0.01300		-0.00090	0.01410	
WD2	-0.09634	0.01286		-0.09090	0.01340	
WD4	-0.29610	0.01332		-0.19454	0.01480	

Table 5.15. Coefficients of the linear regression for the logarithm of the infiltration rate (i).

Coefficient	Sand (S)			Sandy loam (SL)		
	Estimate	Std.error	R^2	Estimate	Std.error	R^2
Intercept	2.54900	0.18220		-0.22137	0.74004	
K_{sat}	0.00052	0.00004		0.02670	0.00212	
TP	0.01499	0.00477		0.06389	0.01557	
$logTime$	-0.60760	0.01108	0.82	-0.69727	0.01073	0.84
WD1	-0.10120	0.02022		-0.04634	0.02516	
WD2	-0.17780	0.02001		-0.17731	0.02391	
WD4	-0.31030	0.02073		-0.32946	0.02642	

Figures 5.18 and 5.19 show the fitting results of the linear regression for infiltration capacity (i) comparing two extreme simulated WD (WD0 and WD4). Figures D.1 to D.4 (in Appendix D) show the infiltration curves for WD1 and WD2. The model tended to fit well the observed infiltration data, especially for the sandy (S) treatments being very accurate simulating the shape of the curve, the inflection point and the steady flow rate. However, it overestimated, more significantly in the sandy loam (SL), the initial infiltration rate.
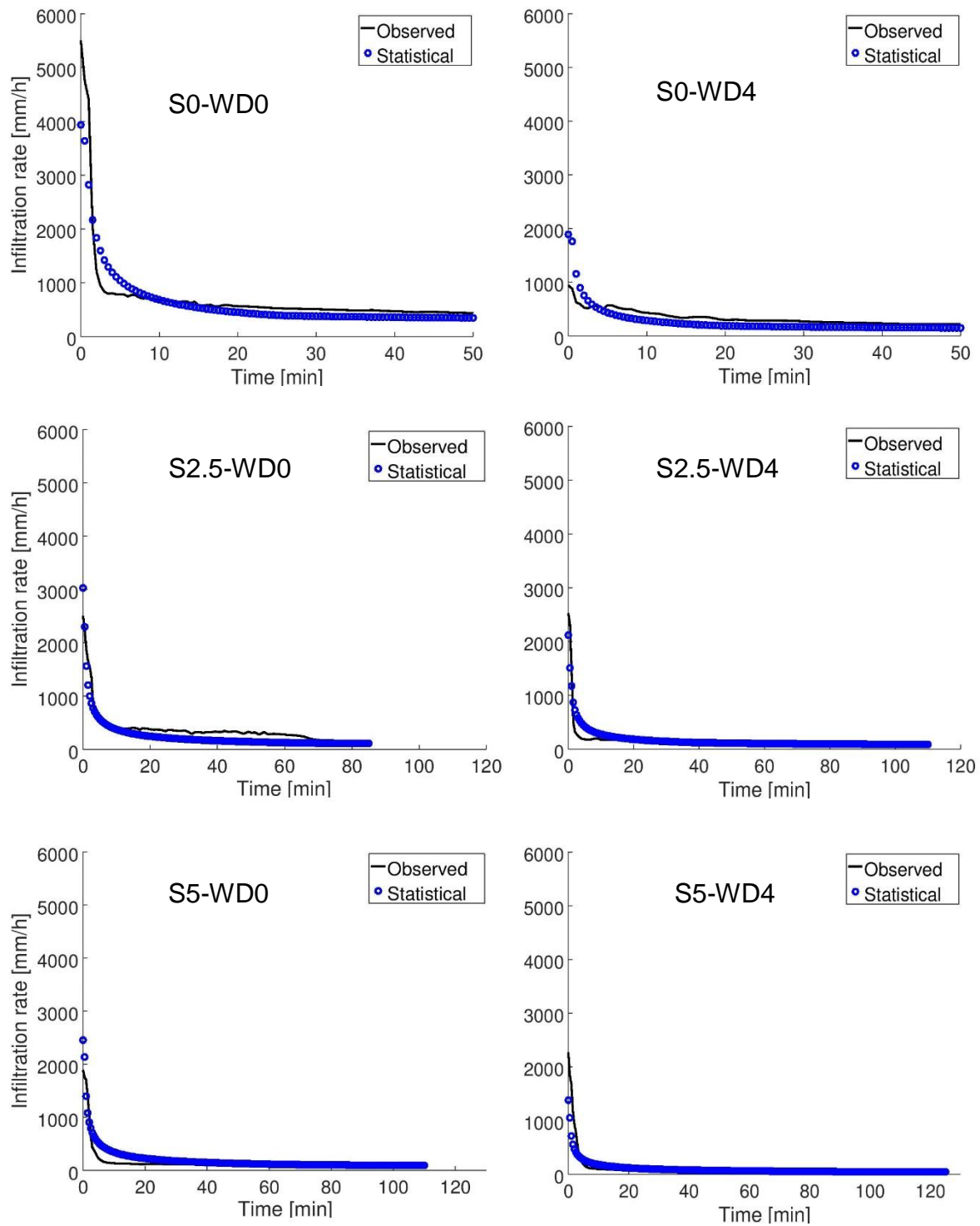
Figure 5.18. Comparison of the average observed data and the statistical model of the infiltration rate for the sandy treatments (S) for two extreme wetting and drying (WD) cycles.
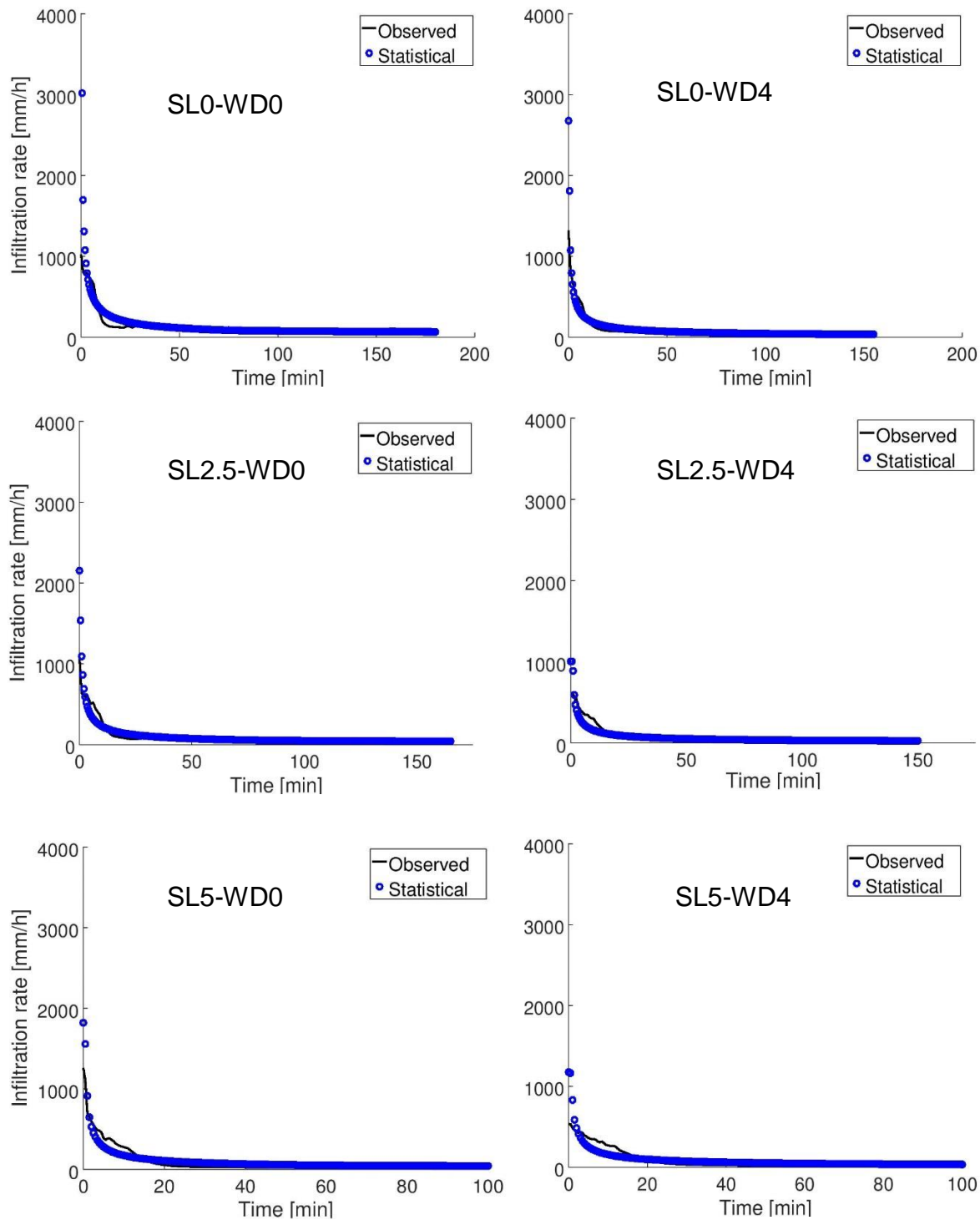
Figure 5.19. Comparison of the average observed data and the statistical model of the infiltration rate for the sandy loam treatments (SL) for two extreme wetting and drying (WD) cycles.

The linear regression model fitted better the cumulative infiltration curves of the sandy mixtures (S) and the unamended sandy loam (SL0) during WD0 (Figures 5.20 and 5.21) and WD1 (Figures D.3 and D.4, Appendix D); however, by repeating the WD, the accuracy of the model decreased, especially in treatments S2.5 and S5. In the sandy

loam mixtures (SL2.5 and SL5) as the biochar fraction and WD increased, the linear regression was not able to explain the observed data. It was also observed that the cumulative infiltration tended to decrease drastically between WD0 and the subsequent WD cycles. Between WD1, WD2 (Figures D.3 and D.4, Appendix D) and WD4, changes in cumulative infiltration were not significant. In figure 5.20 it is also observed that cumulative infiltration in the SL5 treatment did not change significantly along the WD cycles, which may be an indicator of enhancement of soil rigidity.
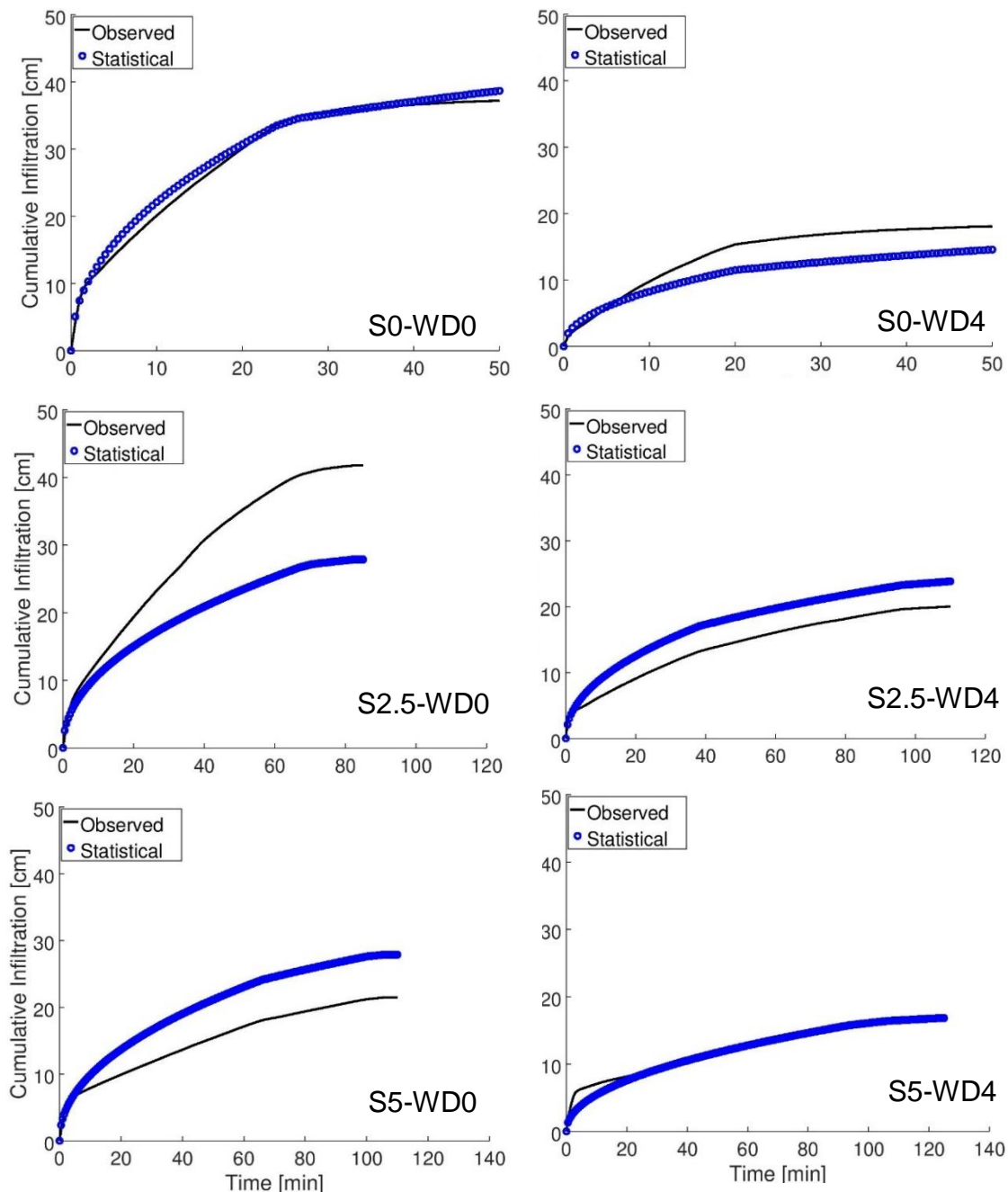
Figure 5.20. Comparison of the average observed data and the statistical model of the cumulative infiltration for the sandy treatments (S) for two extreme wetting and drying (WD) cycles.
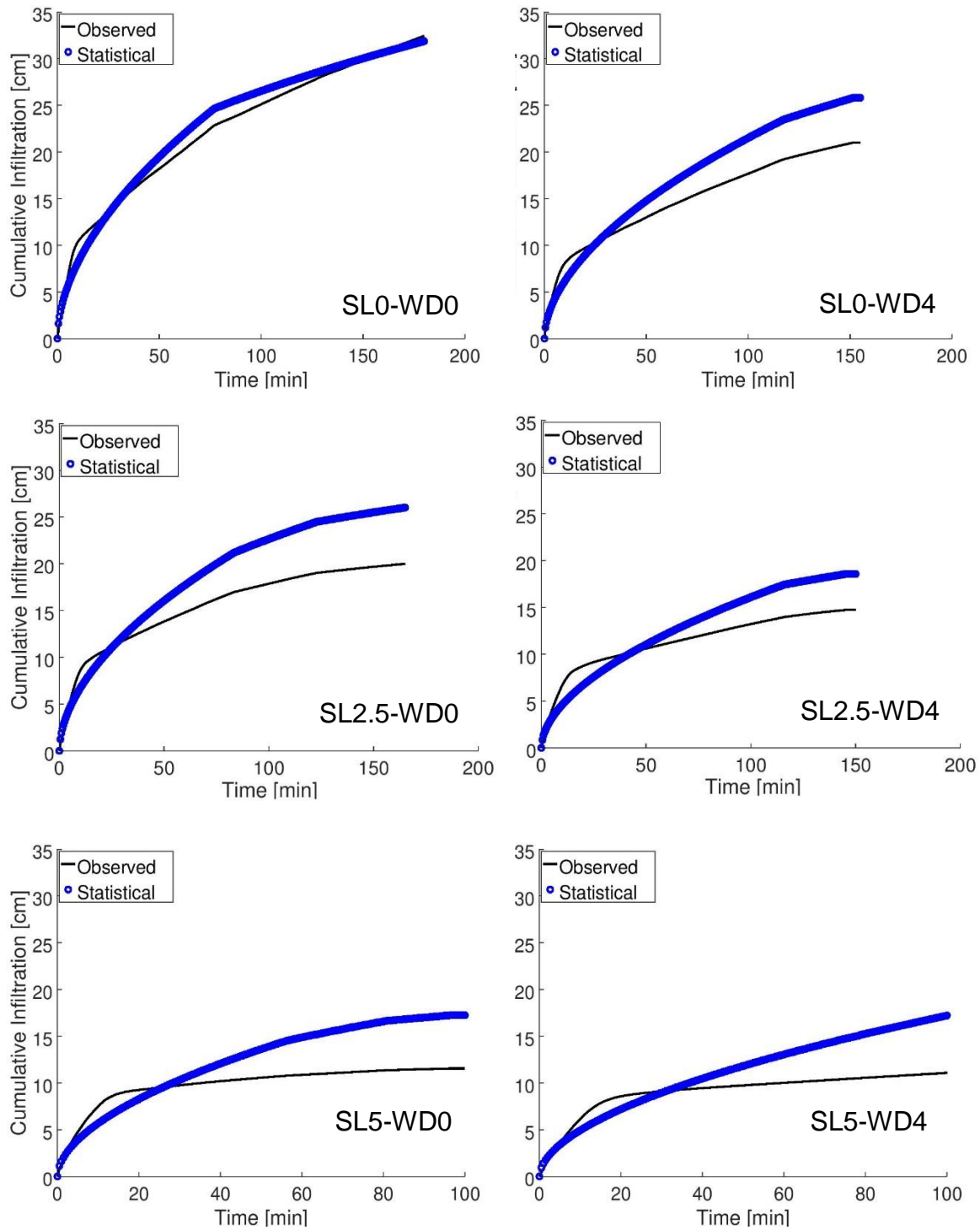
Figure 5.21. Comparison of the average observed data and the statistical model of the cumulative infiltration for the sandy loam treatments (SL) for two extreme wetting and drying (WD) cycles.

Figures 5.22 and 5.23 show the determination coefficient R^2 for the cumulative infiltration of both soil treatments (S and SL) and two WD (WD0 and WD4). Figures D.5 and D.6 (Appendix D) presented the scatter plots for WD1 and WD2. By plotting the observed and predicted data of cumulative infiltration, using the linear regression

analysis, it is observed that in the sandy mixtures (S) the fit was highly acceptable with a coefficient of determination greater than 0.98. In the sandy loam (SL), the statistical model represented very well the unamended sandy loam (S0) and SL2.5 for WD0, but as biochar increased as well as the frequency of WD, the coefficients of determination tended to decrease up to 0.82. In general, as the biochar dosage increased, the model tended to explain with more deficiency the observed data.
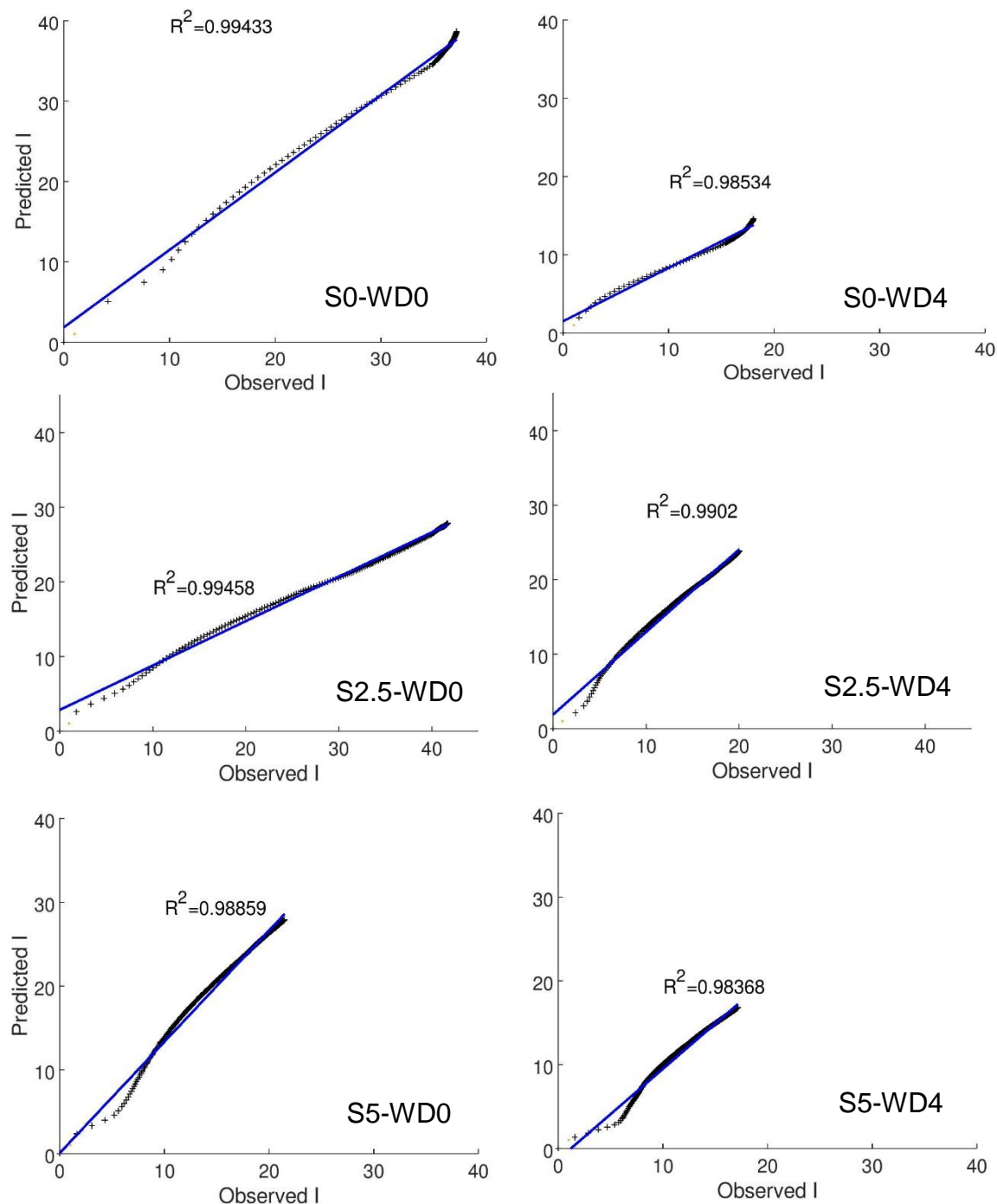
Figure 5.22. Scatter plots of the observed and predicted cumulative infiltration using the statistical model for the sandy (S) treatments for two extreme wetting and drying cycles (WD0 and WD4). The diagonal line represents the line of best fit.
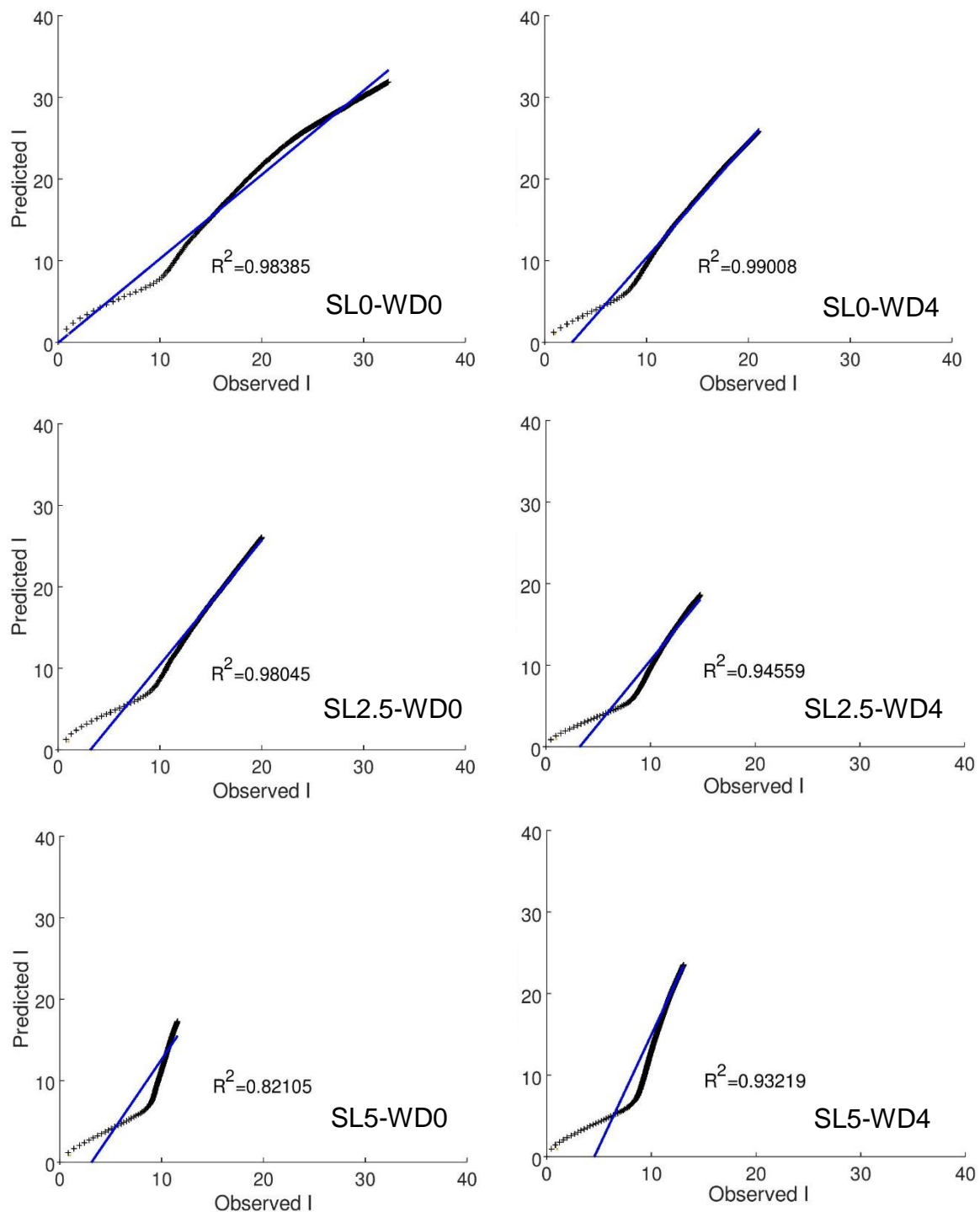
Figure 5.23. Scatter plots of the observed and predicted cumulative infiltration using the statistical model for the sandy loam (SL) treatments for two extreme wetting and drying cycles (WD0 and WD4). The diagonal line represents the line of best fit.

5.3. Effect of biochar addition at catchment level

This section explains the results of a catchment hydrological response under six scenarios – based on the six biochar amended soils studied – and the effect of wetting and drying on the total outflow and surface runoff volume produced by each scenario. All hydrological units (landuse, soil type and slope) were kept constant and each scenario consisted on changing the soil characteristics of the landuse Crops and Grassland, by including the characteristics of each amended soil. The main input model parameters are detailed in Appendix F, table F.1.

The Birris catchment is mostly agricultural, being crop cultivation the main agricultural activity. Based on the landuse map (Figure 4.8) crops and grassland correspond to the 30% and 39% of the total occupied area, respectively. Crops and grassland are distributed along all the catchment. The hypsometric curve depicted an instable topographic condition with high risk of erosion. Catchment topography goes gradually from a high level (3400 m.a.s.l) to about 1100 m.a.s.l; then decreased drastically to 900 m.a.s.l. Moreover, the order of the drainage system contributed to a short time response at the catchment outlet.

Based on the precipitation regime of the Birris subcatchment, the period from November to April was considered as dry season and from May to October as rainy season. Because SWAT is a long-term hydrological model, the simulations referred to the response of the catchment to daily and monthly cumulative precipitation. Figure 5.23 illustrates the time series of the water discharge at the outlet of the Birris subcatchment for a period of 7 years. Figure 5.24a shows the time series of the water discharge (Q) for the sandy amendments (S) and figure 5.24b the time series corresponding to the sandy loam amendments (SL). The runoff regime of the Birris subcatchment showed that dry-season events produced significant smaller runoff peaks than rainy-season events. The high peaks occurred during the rainy season and the low outflows during the dry season. For the sandy (Figure 5.24a) and sandy loam mixtures (Figure 5.24b) the catchment had the same water discharge shape, but the magnitude of Q varied, occurring a higher discharge in the sandy mixtures (S), mainly during the rainy season. Four high peaks during the rainy season (numbered from 1 to 4) and three low outflows during the dry season (numbered from 5 to 7) were chosen to compare the flow patterns.
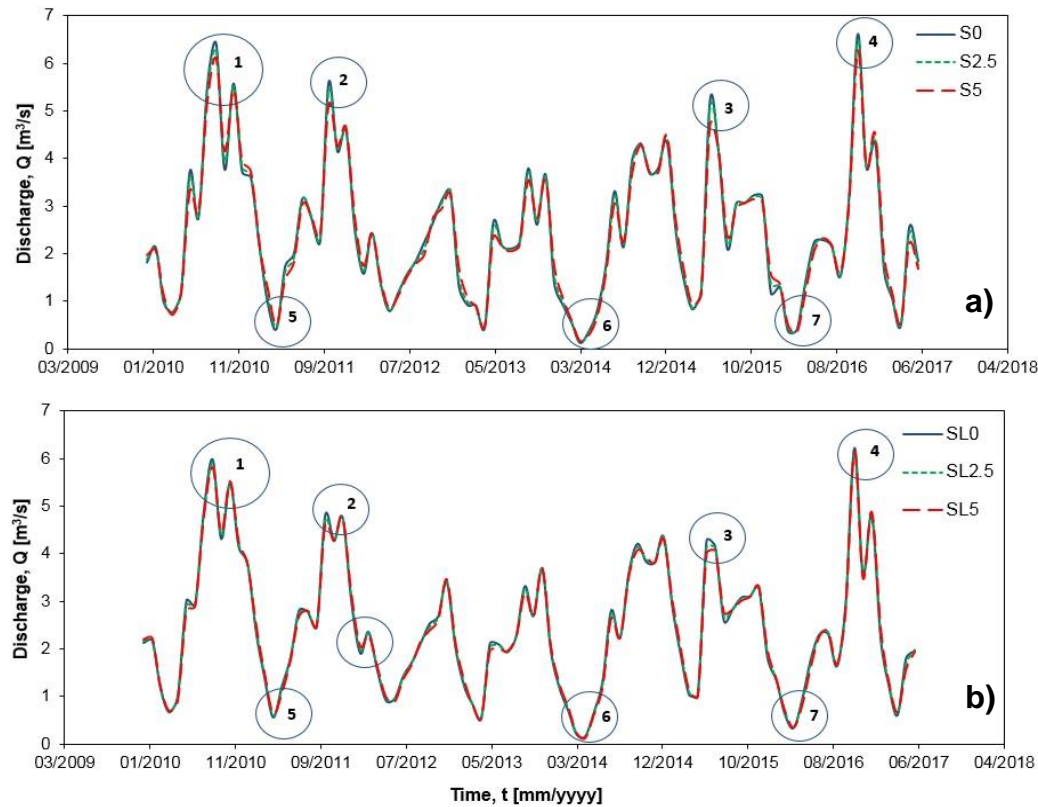
Figure 5.24. Simulated water discharge Q for the period 01/2010 to 06/2017 applying six scenarios (S0, S2.5, S5, SL0, SL2.5, SL5) for the land occupied by Crops and Grassland in the Birris sub basin. The circled high and low peaks are taken as example considered for further analysis**.**

Figure 5.25 shows four examples of high peaks corresponding to the water discharge of the sandy mixtures (left) and sandy loam mixtures (right), during the rainy season (numbers 1 to 4 relates to the corresponding position in figure 5.24). The unamended soils (S0 and SL0) had the highest peaks with respect to their amendments. The sandy loam mixtures (SL) produced less water discharge than the sandy treatments (S), for the same rainfall conditions. During the time, where rainy season prevailed and soil remained saturated, the sandy loam mixtures produced 10% less discharge (Q) than the sandy mixtures. This suggests that the sandy loam (SL) substrates were able to retain more water in the soil and transport less water within the soil bulk than the sandy (S) amendments, although they produced in general more surface runoff (Table 5.16). In the sandy treatments, the water discharge differences between the unamended sand (S0) and the amendments (S2.5 and S5) were more significant than the differences between the unamended sandy loam (SL0) and the sandy loam amendments (SL2.5 and SL5). Treatments S2.5 and S5 generated up to 7% and 20%, respectively, less water discharge than the unamended sand, whereas, SL2.5 and SL5 produced up to 6% and 12% less water discharge than the unamended sandy loam.
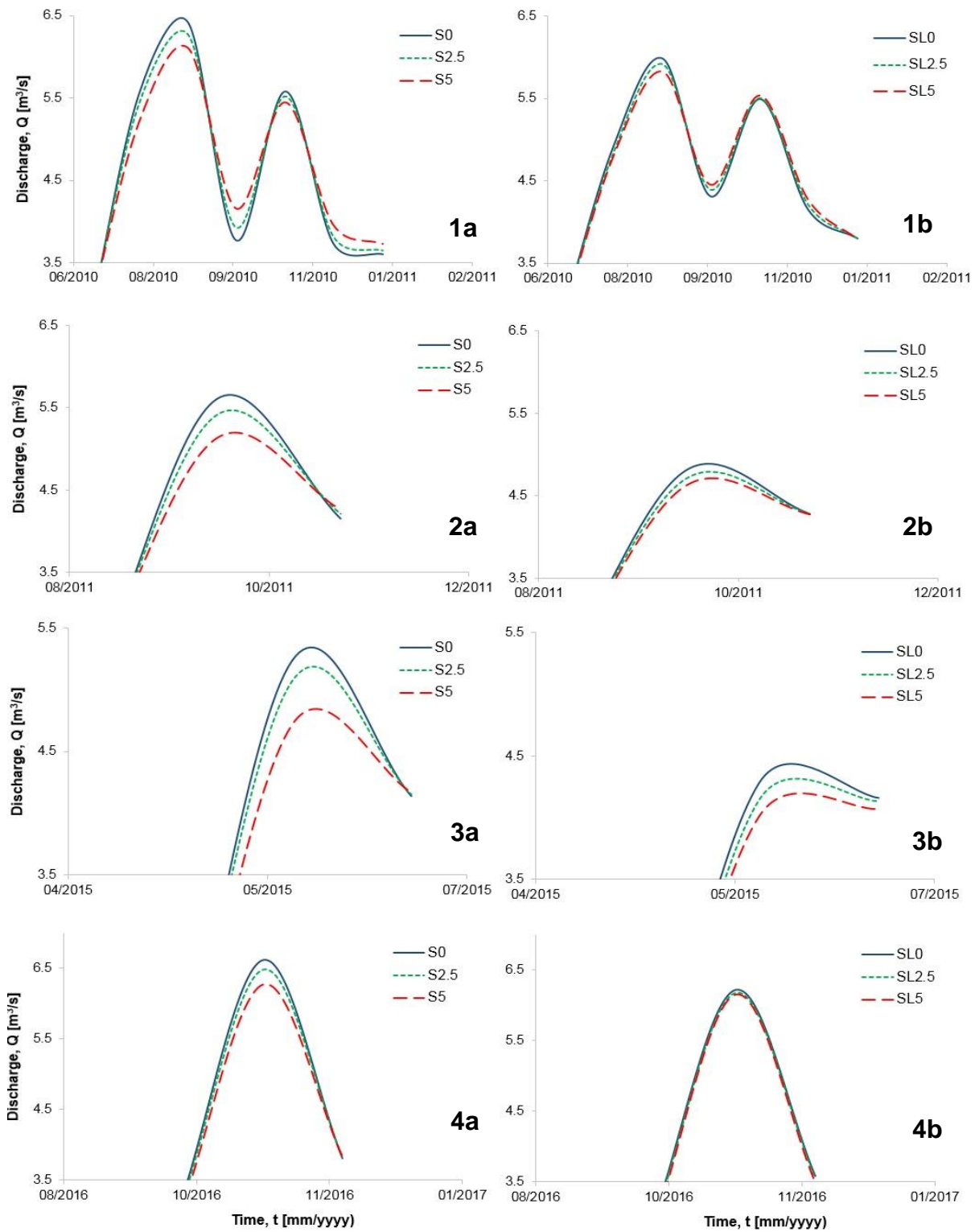
Figure 5.25. Comparison of four high outflow peaks Q for six scenarios (S0, S2.5, S5, SL0, SL2.5, SL5) for the land occupied by Crops and Grassland in the Birris sub basin. Numbers follow the order in Figure 5.24, where "a" correspond to sandy mixtures (S) and "b" to the sandy loam mixtures (SL).

During the dry season (figure 5.26), contrarily to the rainy season, the low outflows were slightly higher in the sandy loam amendments (SL) than in the sandy treatments (S). On average, in the dry season the sandy loam mixtures (SL) generated 21%, 18% and 14% more discharge with respect to the unamended sand (S0), and the sandy amendments with 2.5 and 5% biochar, respectively. This suggests that during the dry season, although precipitation is low, the sandy loam mixtures continue contributing to the drainage system greater than the sandy amendments.
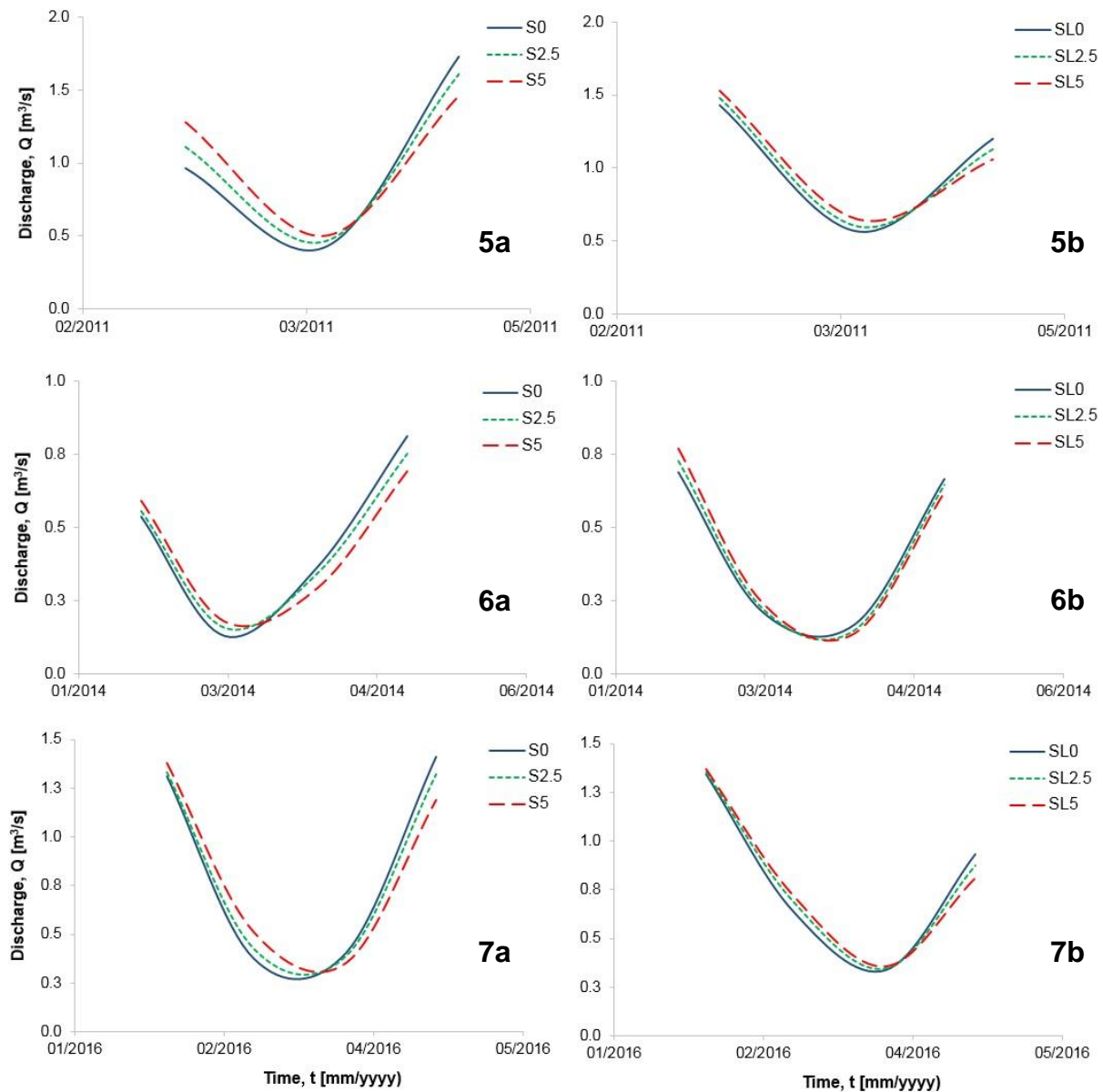
Figure 5.26. Comparison of four low outflow peaks Q for six scenarios (S0, S2.5, S5, SL0, SL2.5, SL5) for the land occupied by Crops and Grassland in the Birris sub basin. Numbers follow the order in Figure 5.24, where "a" correspond to sandy mixtures (S) and "b" to the sandy loam mixtures (SL).

Table 5.16 provides the average output values of the 1-D water balance parameters for the six soil scenarios, considering all landuse types (forest, crops, grassland, permeable and impermeable roads and infrastructure). In overall, the sandy loam (SL) treatments produced more surface runoff than the sandy (S) treatments, whereas interflow (sub surface flow) was higher in the sandy treatments. The runoff coefficient (ratio of surface runoff volume with respect to precipitation) was higher for the sandy loam mixtures (SL) reflecting high soil moisture conditions, whereas the interflow coefficient (ratio of interflow with respect to precipitation) was double the higher in the sandy treatments (S) than in the sandy loam substrates (SL). For the 7 years studied, in average, the sandy substrates (S) produced between 40 and 47% surface runoff volume from the total precipitation, whereas the sandy loam mixtures (SL) produced between 28 and 33%.

Table 5.16. Water movement within the catchment associated to water infiltration obtained from the simulated hydrological cycle using swat model, for six scenarios, in the Birris subcatchment.

Treatment	P	Eva	R	$Intf$	CU	Shallow aquifer	Deep GW recharge	R/P	$Intf$/P
S0		536.0	168.69	769.1	12.77	460.04	24.85	8.6	39.0
S2.5		536.8	172.54	710.73	12.77	510.9	27.53	8.7	36.0
S5		538.7	178.36	612.67	12.77	596.47	32.03	9.0	31.1
SL0	1972.3	545.3	347.33	295.15	12.77	731.51	39.14	17.6	15.0
SL2.5		545.7	350.25	250.97	12.77	770.38	41.18	17.8	12.7
SL5		546.3	353.96	205.77	12.77	809.23	43.22	17.9	10.4

P: precipitation; Eva: evapotranspiration; R: surface runoff; $Intf$: interflow CU: capillary uprise; GW: groundwater. All parameters are in mm. R/P: runoff coefficient (%); $Intf$/P: interflow coefficient (%).

In Appendix F, table F.2, it can be found the summarized information regarding all parameters interfering in the hydrological cycle, but only considering the land use Crops and Grassland for WD0. Available water content is higher in the sandy loam mixtures than in the sandy treatments, due to the presence of a greater number of smaller pores able to retain water infiltrated by capillarity for a longer period. For the same precipitation amount, surface runoff tended to increase as the biochar fraction increased and was higher in the sandy loam mixtures (SL) probably due to their lower infiltration capacity and a lower final infiltration rate with respect to the sandy treatments. In the sandy amendments the fraction of surface runoff was more significantly higher than in the sandy loam amendments. Thus, a dosage of 5% produced nine times mores surface runoff than the unamended treatment in the sandy soil, compared to 2 times more surface runoff in the sandy loam amendment.

6. Impact of Biochar Addition on the Infiltration Processes

Infiltration is an important process within the water balance of a catchment, since it contributes to its water recharge and surface runoff. The process of infiltration, in amended soils, is influenced by diverse soil parameters such as texture, organic carbon content, surface area of the soil particles, water repellency (sorptivity), initial soil moisture, soil hydraulic conductivity, surface conditions (i.e. sealing), and wetting and drying (WD) periods, which greatly contribute to define soil structure (Canarache et al., 1968; Hartge and Horn, 2016; Hillel, 1998; Jačka et al., 2016; Uloma et al., 2014). Most of these parameters are influenced by the soil pore size distribution (PSD), their connectivity, and structural conformation of the aggregates that affect the intensity and direction of the water infiltrated. In biochar amended soils, biochar characteristics such as particle size, specific surface area (SSA) and hydrophobicity, as well as its chemical composition may also alter the intensity and magnitude of the infiltration process. Biochar may increase or decrease soil drainage and enhance the soil-water-plant relationship, but this is dependent on soil type, biochar amendment rate, and biochar properties (Barnes et al., 2014; Brewer, 2012).

6.1. Changes on Chemical Soil Properties

Biochar properties and their effects on the soil depend on soil texture, feedstock characteristics, and thermal processes (Brewer, 2012). The degree of the biochar at which it may alter the soil hydrology depends first on the biochar properties, and second, on the soil type that is amended. This section addresses the findings of this work on how the main biochar properties affect directly some soil chemical properties.

Adequate pH values help nutrients to be absorbed and contribute to soil structure; cation concentration is important for water and nutrient retention, and SSA refers to the biochar pore architecture, important for soil water holding and adsorption capacity, too.

Heating rate and residence time influence SSA of the biochar particles. This affects the water holding and adsorption capacity for nutrients and contaminants. As mentioned by Villagra-Mendoza and Horn (2018a), the present study used mango wood as biomass source, pyrolized at 600°C, with a relatively low SSA, which shows similar properties with respect to a pyrolyzed woody biomass source prepared at temperatures between 350-400°C (Ronsse et al., 2013). According to Ronsse et al. (2013), only in case of higher temperatures during the pyrolyzation process, a much more widened surface and a higher SSA can be expected, because of the increased porosity of the biochar particles.

The sandy (S) material´s specific surface area increased with the added dosage of biochar. This condition enhances the soil-biochar particle bindings, having a relative effect on the coarse textured soil. These findings are in agreement with Ajayi et al. (2016) who related the increase of the micropore surface area to a significant increase in soil moisture retention even at small biochar dosages. In the sandy loam (SL), however, biochar addition did not affect significantly the SSA of the soil because even the finer mineral substrate provided already a high SSA due to the properties of the clay. Some studies have found that biochar produced at high temperatures have a higher SSA with a larger proportion of micropores, whereas longer residence time reduces SSA due to ash fusion filling micropores (Lopez-Capel et al., 2016; Ronsse et al., 2013; Sohi et al., 2009). These results contradict the SSA obtained at the mentioned heating process; therefore, it is assumed that the thermal process of this mango wood biochar was carried out at temperatures not greater than 400°C. The increase of SSA in all treatments enhanced soil water retention (Eibisch et al., 2015), which could have reduced the final infiltration rate, especially in the coarser texture material. Ajayi and Horn (2016a) indicated that the increase of total carbon in recalcitrant form is critical to aggregation and structural soil formation. This is reported as an improvement on water retention and infiltration rate by Abrol et al. (2016), Essien (2011) and Itsukushima et al. (2016), contrary to the results of this study, where higher water retention influenced the decrease of the steady rate flow (Ib). However, these results are in agreement to the different hydraulic effects reported on the biochar amendments by Abel et al. (2013); Ajayi and Horn (2016a); Bayabil et al. (2013) and Githinji (2014), highly related to the quality of the source material, thermal process, application rate, and soil type (Brewer, 2012).

In this study, due to the similarity of the neutral pH of the biochar and the base materials (sand and sandy loam), there was no significant effect on the pH of the amended mixtures. The neutral pH of the soil materials kept constant due to the presence of high levels of alkalines – Ca^{2+} in the sand and Ca^{2+} and Mg^{2+} in the sandy loam – (Laird et al., 2011; Lopez-Capel et al., 2016; Yargicoglu et al., 2015). Several studies have determined that biochar pH is typically larger than 6 for a wide variety of source biomass such as wood, green wastes, crop residues, sewage sludges and litter with pyrolysis temperatures between 350-500°C (Brewer et al., 2011; Verheijen et al., 2010) and most of the studies coincide in that biochar pH increases as temperature increases (Brewer et al., 2011; Jindo et al., 2014; Oh et al., 2012).

Cation concentration plays a role on shrinkage and swelling. In the sandy loam substrates (SL0, SL2.5 and SL5) swelling occurred more as biochar increased. Swelling depends mainly on the presence of ions and cations. Bivalent cations (Ca^{2+} and Mg^{2+}) are capable of hydrating more than monovalent cations (Hartge and Horn, 2016). Xing et al. (2017) observed that low concentrations of K^+ and Na^+ reduced the soil water retention capacity and that higher concentration of K^+, Na^+ and Ca^{2+} helped to produce less cracks. Although higher concentrations of Ca^{2+} reduce cracking (because it enhances soil rigidity) it also may reduce water retention depending on the aggregation status (Hartge and Horn, 2016).

Generally, total carbon content in biochar ranges between 172 to 905 g/kg, and C/N (carbon to nitrogen) ratio in biochar varies between 7 and 500. As expected in this study, total carbon, TC in the amendments (which is mostly organic), increased as the dosage of biochar increased, as expected since biochar is a source of organic carbon (Glaser et al., 2001). An acceptable C/N relation was observed in the sandy loam (SL) mixtures being beneficial for plants, since an adequate amount of N can be released in the soil, as reported by Tammeorg et al. (2014) and Verheijen et al. (2010). Contrarily, a greater C/N ratio was obtained in the sandy (S) treatments, due to a lack of nitrogen in the base material. In the sandy loam mixtures (SL2.5 and SL5) and in a lower degree in the unamended treatment (SL0), the microbial growth observed during dehydration is an indicator of this acceptable C/N ratio. A limit ratio in organic matter is often set between 20 and 30 to support microbial growth (Brewer, 2012; Lopez-Capel et al., 2016).

6.2. Effect of Biochar Dosage on Soil Properties

In this study, 2.5 and 5% (dry wt.) of biochar were applied to the sandy and sandy loam substrates resulting in an enhancement of field capacity and water holding capacity (WHC). These results are consistent with the ones of Novak et al. (2009) and Peake et al. (2014). Several studies have tested the influence of different biochar fractions on the physical and hydraulic characteristics of soil amendments, but contradictory results have been obtained mainly due to the varying soil characteristics and biochar source biomass used. Similar to this study, Peake et al. (2014) applied 0.1, 0.5 and 2.5% biochar to eight particle size distribution classes (ranging from loamy sand to silty clay loam), obtaining in the sandy soils a remarkable decrease on bulk density (because of a low bulk and specific density of the biochar) at the highest application rate, and with an increase of field capacity and available water content. Novak et al. (2009) applied a biochar dose of 2% to a loamy sand soil and observed an increase up to 15% of water retention in the amendments. Githinji (2014) amended a sandy loam soil with 25%, 50%, 75% and 100% v/v of biochar and reported a decrease of bulk density, an increase of porosity and water holding capacity (WHC), and a decreasing trend of cumulative infiltration and saturated hydraulic conductivity as the biochar fraction increased. The decreasing infiltration rate was explained by the hydrophobic nature of the biochar used. Moreover, similar to this research, Ajayi et al. (2016) added 2%, 5% and 10% (dry wt.) of biochar to a fine sand and sandy loam silt soil. They reported more pronounced changes on water retention on the fine sand soil. They also obtained contrary responses on the saturated hydraulic conductivity with an increase on the sandy loam silt and a decrease on the fine sand soil, which corroborates findings of the hydraulic soil properties changes of this research. Similarly, Eibisch et al. (2015) associated an increase on saturated hydraulic conductivity and available water content with biochar fractions of 2%. Masiello et al. (2014) summarized results of different biochar application rates on different soil textures exposing an increase on water holding capacity (WHC) on coarser textures and on increasing biochar doses. Brockhoff et al. (2010) added 5% and 25% biochar to a sand

material and reported an increase on water retention and saturated hydraulic conductivity as biochar rate increased. In general, most of the studies reported acceptable improvements on sandy based soils and biochar dosages no greater than 10%.

The EBC (2012) suggests a maximum biochar application of 50 ton/ha over a 100 year period, but some authors have referred to a wide range of biochar and charcoal applications from 0.5 up to 135 ton/ha (Agegnehu et al., 2017; Chan et al., 2007; Glaser et al., 2002) with positive crops yields. Ruysschaert et al. (2016) compiled a wide range of biochar dosages, from 2.5 to 300 ton/ha, applied in European fields; with positive crop responses in terms of productivity with dosages up to 90 ton/ha, whereas other tests have shown the opposite with biochar dosages of 50 ton/ha.

It is important to point out that beyond the soil type and the biochar source material, the optimal biochar dosage should also depend on the economical and feedstock accessibility to guarantee a sustainable production capacity.

6.3. Effect of Biochar and the Environment on Soil Characteristics and on Infiltration Dynamics

In soil hydrology, soil structure affects porosity, water holding capacity, hydraulic conductivity, infiltration and might impact erosion rates. Soil structure is largely controlled by the actual and maximum pre-drying intensity (Hartge and Horn, 2016) and it is also complemented by biological processes (root formation and decomposition), which alter soil volume and produce soil aggregates.

6.3.1. Effect of Wetting and Drying on Water Infiltration

The environment plays a role on the way infiltration occurs. Intense dried periods followed by wetting alter the internal bulk pore distribution, shape and geometry; forming cracks and producing varying responses to the water flux and facilitating preferential flow. During drying, matric forces act on the pores inducing capillary stress. This pore contraction pulls aggregates together, collapsing larger pores and forming cracks. On the other hand, during wetting, soil particles tend to adsorb water and Van der Waals forces disperse soil particles and colloids. These drying and wetting processes are responsible for changing constantly soil aggregation and are significantly prominent in clay-rich soils (Hartge and Horn, 2016; Tang et al., 2011). Some authors suggest the incorporation of these temporal changes on the hydrological response analyses of catchments (Gebhardt et al., 2012).

The impact of cracks on infiltration at the topsoil depends on the crack volume and depth. Zhang et al. (2014) reported that soils with high clay content presented more fine cracks, while in soils with more organic carbon content cracks are larger and deeper.

Authors such as Alaoui et al. (2011), Zhang et al. (2014) and Zhao et al. (2015) agreed that cracks are formed during drying and close after rewetting –due to pore structural changes by the rearrangement of the soil aggregates– resulting in decrease of the infiltration rate. Zhao et al. (2015) also observed that infiltration rate oscillated with different wet-dry cycles. They concluded that changes on macroporosity (due to clogging of pores also reported by Itsukushima et al. (2016) that changes pore distribution and connectivity) and near-saturated hydraulic conductivity were responsible for the same oscillation trend of water infiltration.

Peng et al. (2007) reported that differences on shrinkage behavior of clay and silt soils with respect to organic rich soils were caused by the formation of large pores in organic soils during intense drying and wetting periods, which resulted in more rigidity in comparison to clay soils. Other authors have also reported intense swelling and shrinkage in sandy and organic soils (Ajayi et al., 2016; Gebhardt et al., 2012; Peng et al., 2007). From the shrinkage curves obtained in this study (Section 5.1.5), it was found that the unamended sand (S0) lacked of structural shrinkage, which means that this soil had a high non-rigidity condition and a weaker structure compared to the sandy amendments S2.5 and S5. The greater void ratio in the unamended sand (S0) produced a greater volume reduction at the drainage levels applied, implying a smaller aggregate strength (Horn et al., 2014).

The addition of biochar and repetitive wetting and drying produced changes on the intensity parameters and the soil materials became even more rigid. In the sandy loam mixtures (SL), the more biochar was added, the less shrinkage occurred in both vertical and horizontal directions. In SL2.5 and SL5, biochar functioned as a binding material (because of its swelling capacity), providing a more rigid soil structure. These shrinkage and swelling processes produced a net effect on the temporal bulk density, which kept the mixtures with bulk densities similar to the initial bulk density previous to the application of the WD periods. Therefore, as the biochar dosage increased, soil rigidity was enhanced and showed some resilience to repetitive wetting and drying (WD) in S and SL mixtures. The presence of more fine pores in the sandy loam materials slowed down water infiltration but contrary to the sandy treatments, did not change the initial infiltration rate with the WD periods. The sandy loam substrates also presented a more pronounced but narrower proportional phase, caused by the finer pore sized distribution when compared to sand. If considered only the effect of biochar, it is explained as the ability of pure biochar to hold water if it has enough porosity and low hydrophobicity (Gray et al., 2014). During drying, because of the higher surface area of the biochar particles with respect to the soil particles, biochar is capable to adsorb and retain water at higher (more negative) matric potentials, keeping the biochar pore spaces with a greater water film around particles (Eibisch et al., 2015), reducing pore stress and consequently deformation. On the opposite, when water enters into the biochar pores, it generates an extra positive capillary pressure (to exceed the entry pressure) (Gray et al., 2014; Kinney et al., 2012; Sun and Lu, 2014) higher than the pore tension. Then, the water film expands the pores and decreases bulk density, lifting the particles and enabling the biochar to hold water up to ten times its own mass (Kinney et al., 2012).

The sandy materials (S) had a smoother slope up to more negative matric potentials or moisture ratio values, allowing the substrates to deform for a longer water range (Villagra-Mendoza and Horn, 2018a). These findings are in agreement with Ajayi et al. (2016) that reported slightly changes on the rigidity of an amended sandy soil with biochar as the biochar rate increased and observed volume changes on an unamended and amended sandy loamy silt. The presence of macropores made the sandy materials more sensitive to deformation than smaller pores which resist higher capillary stress (Bodner et al., 2013). This is why when the dosage of biochar increased, the soil strength increased too in the amended sandy soils (S2.5 and S5), presenting relatively higher rigidity at a higher moisture ratio and less bulk deformation at higher drying conditions. This pattern was contrary to the high non-rigidity condition of the sandy control (S0) corresponding to a high sensitivity to deformation of the wider coarse pores with different WD periods, during the proportional shrinkage phase. These changes varied infiltration rates, especially initial infiltration rate (I_o); whereas final infiltration rate (Ib) stayed similar with repetitive wetting and drying. Similarly, Bottinelli et al. (2016) observed an increase of macropore formation during the proportional shrinkage phase, due to the formation of cracks and enlargement of pre-existing macropores. They also concluded that shrinkage enhanced pore connectivity by moving macropores closer together and by new interconnections among new cracks.

Drying and wetting periods as well as biochar amendments change significantly soil physical and hydraulic properties by forming a more rigid pore system increasing water absorption at more negative matric potentials in coarse soils and producing a net effect of the bulk volume.

6.3.2. Effect of Soil Characteristics on Infiltration

.6.3.2.1   Soil Water Content

Texture and pore size distribution (PSD) affect the hydrological behavior of soils (FAO and ITPS, 2015; Hartge and Horn, 2016; Hillel, 1998; Lal and Shukla, 2005; Wesseling et al., 2009). Texture is an inherent factor affecting infiltration capacity, especially by the soil PSD that strongly influences soil water transmissivity (Ritzema, 2006). As expected, finer soil textures had higher holding capacity than coarse textured soils due to the presence of more capillary pores, which enabled soil to hold water for longer time and at more negative matric potentials. Under saturated conditions, finer textures (like the sandy loam mixtures) had lower saturated hydraulic conductivity than coarser textures (sandy mixtures), slowing down infiltration rates, as mentioned by Hartge and Horn (2016), that might potentially increase surface runoff. Adeniji et al. (2013) recommended to estimate infiltration considering only the fine soil particles with grain size no greater than 500 μm. Coarse textured soils are dominated by coarse pores (pores > 10 μm) counting for up to 40 percent of the total bulk volume, while fine grained soils (such as clay) are dominated by fine capillary pores (pores < 0.2 μm) with 35±10 percent of the bulk volume (Blume et

al., 2010; Hartge and Horn, 2016). These fine capillary pores, additionally to the soil structure, are responsible to retain water under more negative matric potentials.

PSD changes alter infiltration rates. From section 5.1.2., it was determined that in the amended sandy treatments (S2.5 and S5), biochar addition decreased the fraction of wide pores related to a matric potential > -6 kPa (Ø > 50 µm) and increased the narrow (50 – 10 µm) and medium pores (10-0.2 µm) corresponding to matric potentials of -6 to -30 kPa and -30 to -1500 kPa, respectively. These PSD changes reduced infiltration by a reduced substrate permeability, due to the fill in of pores with the smaller grained biochar as explained by Ajayi et al. (2016), Ajayi and Horn (2017), Novak et al. (2016) and Verheijen et al. (2010). Contrarily, Ayodele et al. (2009) reported an enhancement of infiltration and reduction of runoff volume with charcoal addition on a loamy sand soil, attributed to changes in soil structure, increased porosity and decreased bulk density.

Water storage by the formation of new pores with diameters smaller than 0.2 µm was not altered significantly in the sandy loam substrates (SL) as expected, since the addition of biochar in this case introduced particles with similar particle size, introducing little impact on the variation of the initial PSD (Villagra-Mendoza and Horn, 2018a). The nearly identical pattern of the retention curves between saturation and -6 kPa in the sandy loam treatments (SL) was not surprising, as the larger quantity of finer particles, already in the unamended sandy loam substrate, was responsible for determining the overall pattern.

Biochar addition decreased air capacity more in the sandy loam (~40%) than in sand (~25%), although the absolute values were negligible small; these results were in agreement with findings of Ajayi and Horn (2017). The smaller the newly formed pores and the greater the accessible biochar outer and inner pore surfaces were, the greater the storage of extra water, especially at less negative matric potential. Thus, the reduction of the air capacity and increase of field capacity is attributed to these processes, as well as the approximate 180-230% increase of the available water capacity in the amendments compared to the unamended materials. This corresponds to an enhancement of the soil particles bonding characteristics and a flatter and constant behavior of water content near saturation (Villagra-Mendoza and Horn, 2018a).

When biochar is added to soil, it changes the soil pore structure of the amendment materials. Authors such Ajayi et al. (2016) suggested that the PSD and the degree at which it changes depend on the dosage, the base material, and wetting and drying. The results of this study also indicated that also the biochar particle size must be taken in consideration. If the biochar particles are smaller than the soil grain size, they reduce the fraction of wide coarse pores due to the fill-in of the soil pores; and they increase the medium and fine pores especially in the coarse textured substrates (Ajayi et al., 2016; Ajayi and Horn, 2017). This pore fill-in dynamics has been also studied by Brodowski et al. (2007) stating that biochar tends to degrade, over time, into silt sized particles changing porosity and even altering the saturated hydraulic conductivity of the amendments (Villagra-Mendoza and Horn, 2018a). Several studies have reported significant changes on the PSD of coarse-grained soils passing from coarse pores to medium pores, while in fine-grained soils, the changes are less pronounced. As the biochar dosage increases, the PSD changes are greater increasing the amount of pores

able to hold water (Abel et al., 2013; Ajayi and Horn, 2017; Burrell et al., 2016; Githinji, 2014; Masiello et al., 2014; Teβin, 2016; Zhang et al., 2016).

Changes on the PSD to more frequent finer pores may impede the hydrological performance of catchments, promoting instantaneous surface runoff.

.6.3.2.2   Hydraulic Conductivity

Initial soil moisture and hydraulic conductivity account together for a greater part of the water flux that enters the soil surface (Barnes et al., 2014; Brockhoff et al., 2010; Canarache et al., 1968; Lim et al., 2016; Novak et al., 2016). Hydraulic conductivity, as an indicator of structural stability, highly depends on the conformation of the pore system (PSD). Although grain size strongly influences the primary pore configuration, other components such as shrinkage, swelling, and biological activity facilitate the formation of secondary pores, which changes the PSD and its connectivity.

Under saturated conditions, coarse soils have larger saturated hydraulic conductivity values than finer textures, because the first soils have larger connecting pores that enable a faster water conduction, and a rapid displacement of air filled in the larger pores. Additionally, in coarse textured soils, infiltration occurs mostly through non-capillary pores and the fill-in of water depends on the drainage capacity of the pores and the permeability of underneath layers. As main findings of this work in section 5.1.6., it was observed that in sandy (S) and sandy loam (SL) substrates, saturated hydraulic conductivity (K_{sat}) was reduced due to blockage of pores by biochar particles, reduction of pore throat size and available space for flow. This slowed down infiltration in advance stages and decreased the final infiltration rate. The effect of the hydraulic conductivity on infiltration was clearer observed in the sandy amendments (S), by the delay of the inflection point of the infiltration curve as biochar dosage increased. Changes of K_{sat} with the addition of biochar are consistent with findings of Obia et al. (2017) under the circumstances that the application of smaller biochar particles caused a change in the pore size distribution and reformation of the pore continuity of the soil amended. This effect was mainly produced on the sandy mixtures that varied significantly the fraction of large pores to fine and medium pores, although total porosity did not change significantly in the amendments. Authors such as Ajayi et al. (2016), Barnes et al. (2014), Brockhoff et al. (2010) and Uzoma et al. (2011) agreed with the results of this work, since they reported that in coarse textured soils biochar amendments decreased saturated hydraulic conductivity with biochar dosages up to 10% and 0.85 mm grain size due to the increase of fine pores. However, other authors such as Ouyang et al. (2013) reported opposite effects on K_{sat}. They observed that biochar helped to form stabilized soil macro-aggregates especially in coarse textures, acting as a binding agent and producing higher hydraulic conductivity. Studies from Barnes et al. (2014), Castellini et al. (2015) and Herath et al. (2013) documented a positive effect in K_{sat} on fine textured soils with high clay and silt contents due to an improvement in the macropore volume, contrary to the

results of the sandy loam mixtures (SL) obtained in this study. The reason for these contradictory results may be due to the incubation time of the biochar mixtures that may introduce a soil structure dynamics effect, but also on the soil and biochar particle size distribution, the particle shape and amount of biochar added.

Saturated hydraulic conductivity depends on the mobility of the particles during wetting and drying (WD), too. The first wetting and drying (WD) cycle collapsed the initial particle conformation, clogged pores and reduced $Ksat$ values. During the following WD cycles, particles rearranged to form a new configuration with paths allowing the water to flow through the bulk. The arrangement of particles during the WD cycles, due to the formation of aggregates and secondary pores (Horn, 1994), might have affected more the particle size distribution on the sandy mixtures (S) than on the sandy loam (SL) (Villagra-Mendoza and Horn, 2018a).

By visual examination, all amendments swelled at saturation and the sandy loam shrunk forming cracks at the surface. Crack formation was less evident as biochar dosage increased. During the repeated WD cycles, cracks tended to disappear and formed again when dried. This responded to a rearrangement of the particles during swelling and strengthening of the soil matrix during drying, allowing a dynamical formation of cracks and varying the intensity of the water flow. This was expressed by an oscillating behavior of the hydraulic conductivity of the samples, contrary to the decreasing trend observed by Ajayi et al. (2016) (Villagra-Mendoza and Horn, 2018a). The rearrangement of particles agrees with statements done by Dörner and Horn (2009) and Horn (2004) that changes of structural soil configuration contributes to the formation of direction-dependent secondary pores enhancing pore rigidity and water conductivity.

Biochar and texture affect the pattern of the hydraulic conductivity matric potential, too. In general, unsaturated conductivity is higher in clay soils at more negative matric potentials than in coarser soils (Amer et al., 2009), implying that smaller pores increase hydraulic conductivity at more negative matric potentials (Mohawesh et al., 2017). Generally, the higher the unsaturated hydraulic conductivity, the finer the pore system of the biochar amended is. As presented in section 5.1.6., in the sandy mixtures (S) the increase of field capacity (in average 200% in the observed data), coincided with a more continuous unsaturated hydraulic conductivity pattern ($K(\psi)$). The higher the dosage of biochar the more constant and relatively higher was $K(\psi)$ up to -50 kPa (according to the fitting curve). In the sandy mixtures (S2.5 and S5), the changes in the field capacity were less pronounced than in the unamended sand (S0) because biochar increased the frequency of narrow and medium pores, by clogging larger pores with smaller biochar particles, and enhancing the ability of the amended sand to retain water at more negative matric potentials. With the addition of biochar the unsaturated hydraulic conductivity ($K(\psi)$) reached K_{sat} quickly as far as the soil bulk became saturated; producing an abrupt slope decay of the infiltration rate at initial infiltration times on the sandy amendments.

Moreover, the sorption capacity of the biochar, due to a higher SSA, increased water retention of the amendments (S2.5 and S5) at more negative matric potentials when compared with the unamended sand (S0). The sandy loam (SL) showed a relatively constant $K(\psi)$ up to a matric potential of − 30 kPa; the unamended sandy loam (SL0)

showed a slightly higher (non-significant) $K(\psi)$ compared to the amendments (SL2.5 and SL5). In the sandy loam (SL), $K(\psi)$ changed smoothly when the soil bulk became moistened and the decay slope of the infiltration rate occurred not as abrupt as in the sandy soils. This agrees with Canarache et al. (1968) who stated that the influence of the hydraulic conductivity on infiltration rate was also soil dependent and affirmed that the infiltration rate was inversely proportional to the volume of pores filled with water, decreasing as increasing moisture content because of the fill-in of pores with water.

In the water retention curve (WRC), in section 5.1.3., the air entry value – that defines the matric potential at which air starts entering the soil pores (Fredlund et al., 2002) – differed as the WRC shape changed. Biochar changed the WRC of the amended soils by changing the PSD. Therefore, it was expected a delay of the air entry value in the retention curve due to the enhancement of the water retention. This aspect enhances the unsaturated hydraulic conductivity since pores remain filled with water at more negative matric potentials. By comparing the fitting parameter α, it becomes obvious that in the sandy treatments (S), the air entry value $1/\alpha$ increased as the biochar dosage increased. The higher the dosage of biochar, the more negative the matric potential at which air starts entering the soil matrix. In the sandy loam (SL), the fitted curve showed a longer flat pattern than in sandy soil, with air entry values starting at a matric potential of about -30 kPa compared to -3 kPa in the sandy soil. Assuming saturated hydraulic conductivity as the limiting value for the final infiltration rate (Ib), it was expected a decrease of Ib. Final infiltration rates (Ib) in the sandy treatments were considerably lower than K_{sat} as a result of air entrapped within the pores. In the sandy loam mixtures, Ib was greater than K_{sat}, suggesting that infiltration tests could have been prolonged to obtain lower steady conditions. The increase of soil water retention at more negative matric potentials helps to retard drainage, decreasing the rate at which water enters at the soil surface.

.6.3.2.3   Air Permeability

Air permeability controls the gas flux via convective flow in response to a pressure gradient (Amoakwah et al., 2017) and is influenced by the same larger pores that influence the water flow under saturated conditions (Huang et al., 2015); therefore, coarser textures have better air permeability than finer soil textures. Pore diameters between 50 and 10 µm are responsible to contribute to air flow at field capacity and they are also dominant pathways for water flow at saturated conditions (Huang et al., 2015).

As resulted from section 5.1.7, the sandy loam mixtures presented a lower air permeability than the sandy mixtures and it was more affected as an increased quantity of smaller biochar particles was added to the base materials. This could have been affected by a better pore connectivity in the unamended treatments. If this observation is related to water infiltration, it suggests that the higher the pore connectivity, the higher the infiltration rate is. Air permeability differences between sandy and sandy loam were mainly due to differences of the pore characteristics between both soil types. The gas

flux in the sandy mixtures (S) occurred between saturation and -3 kPa corresponding to a pore volume greater than 75 μm radius according to Ball (1981), and was much greater than the sandy loam substrates at any given matric potential. These differences between the air flux of the sand (S) and sandy loam (SL) substrates are related to the higher dependency of air permeability to 1) soil type; 2) soil total porosity; 3) the radius and continuity of the larger pores; 4) tortuosity and in a lesser extent 5) on total air filled porosity; as reported by Amoakwah et al. (2017), Ball (1981) and Moldrup et al. (2003).

In the sandy loam (SL), although the retention curves of the three treatments (SL0, SL2.5 and SL5) did not show significant differences, the unamended sandy loam (SL0) presented higher permeability than the amendments; these findings are in agreement with Ajayi et al. (2016). The reason for these differences referred to the presence of a greater quantity of small pores in the sandy loam substrates as biochar was added (Ball, 1981), due to a clogging of soil pores by biochar particles.

In general, in all treatments air permeability increased as air filled porosity increased and water content decreased, which is in agreement with findings by Masís-Meléndez et al. (2014) and Amoakwah et al. (2017) because gas flux occurs preferentially in water-drained pores and due to a better interconnection of inter-pores as soil dries out.

Intense periods of shrinkage and swelling modifies soil structure. It was demonstrated that by wetting and drying the soil materials changed the ability to conduct air under unsaturated conditions, especially in the sandy loam mixtures. This was due to the formation of a secondary pore system that improved pore continuity and enhanced soil structure. While studies such as the one from Ajayi et al. (2016) indicated that biochar addition — in terms of higher dosages and smaller particle size than soil grains — reduces air permeability because of the formation of new small capillary pores; this study revealed that WD was able to enhance the air flux in finer textures by a reconfiguration of the pore system.

Biochar as amendment improves soil structure and soil hydraulic properties in terms of water retention and hydraulic conductivity in coarse soils and in a lesser extend in medium graded materials. Moreover, repetitive wetting and drying contribute to improve soil aeration. It is not well defined a minimum biochar particle size capable to potentiate the hydraulic properties of amended soils, but the selection of the biochar particle must be soil grain size specific. Since fine textures already have high water retention, biochar addition must be aimed to enhance hydraulic conductivity and their chemical properties, resulting in a better hydrological watershed response in terms of greater infiltration capacity and less runoff volume.

6.3.3. Soil Water Repellency

Soil water repellency is largely associated with low infiltration rates and increased runoff (Li et al., 2017; Lopez, 2014; Verheijen et al., 2010). It has been reported that soil water repellency is more prominent in coarse textured soils (sandy soils) due to their

relative small SSA and in soils with less than 10% of clay, although in some cases fine textures have shown some repellency degree due to the formation of soil aggregates, which reduce the surface area covered later by a hydrophobic skin (Doerr et al., 2000; Doerr and Thomas, 2000).

The addition of biochar to mineral soils may result in diverse effects on soil hydrophobicity. Already a dosage of 5% biochar affected the wettability of the sandy material (S), while in the sandy loam (SL) biochar did not have any additional impact on its hydrophobicity, since the increase of the accessible particle surface in the finer textured soil was small (Villagra-Mendoza and Horn, 2018a). In the sandy loam mixtures (SL), hydrophobicity tended to decrease with increasing water content, resulting from a decrease of both the matric potential gradient and the available water storage capacity (Carrick et al., 2011). The hydrophilic condition of the unamended sand (S0) did not evidence any opposition to the flow entering the soil surface during infiltration and presented the higher initial infiltration rates. In the sandy loam (SL), all treatments had hydrophobic conditions which may had helped to reduce the rate at which water entered the soil. These findings partially agreed with the results of Doerr et al. (2000) that reported an increase on the hydrophobicity of amended coarse textured soils as the dosage of biochar increased and Herath et al. (2013) reporting no effect on finer textures, suggesting that the effect of biochar addition on hydrophobicity is soil type dependent. Githinji (2014) concluded that an increasing rate of biochar application produced a decreasing trend of cumulative infiltration in a sandy loam soil, and attributed this trend to biochar hydrophobicity. He observed a linear decrease of K_{sat} with increasing biochar dosage, which also caused the reduction of the cumulative infiltration.

Hardie (2011) reported an increase of soil water repellency after intense drying (using heating oven-dry) conditions. These reports are contrary to the results of this study since the sandy mixtures (S) did not show any water repellency with repetitive wetting and drying, and it slightly appeared with a biochar dosage of 5%. In the sandy loam (SL) a higher repellency index was observed at more negative matric potentials (although the unamended sandy loam was already hydrophobic), but after simulating repetitive wetting and drying, the SL mixtures presented an oscillating behavior. The dynamics of this behavior assumes that wetting periods decreased hydrophobicity and dry periods produced a re-distribution of the organic molecules that restored hydrophobicity of the SL samples to some degree, as suggested by Doerr and Thomas (2000).

6.3.4. Empirical Modelling of Water Infiltration

Understanding infiltration patterns and their influencing parameters, such as environmental, soil, and management are important for designing and taking decisions for erosion, pollution control, irrigation projects, as well as for flood protection. Since the interrelation of these parameters are highly complex, there is a need to simplify these relations and identify the main mechanisms in terms of parameters that are likely to

represent the water movement at the topsoil. Therefore, infiltration models have become a valuable tool to save time and avoid costs on field measurements.

Empirical models, such as Kostiakov, has proved to fit well to measure data although its parameters lack of physical meaning (Adindu et al., 2014; Canarache et al., 1968; Hasan et al., 2015; Igbadun et al., 2016a). Li et al. (2017) adduced this good performance because the fitting parameters are not related to the wetting front depth. Authors such as Haghiabi et al. (2011) suggested to use the logarithmic characteristic of infiltration to estimate the parameters of Kostiakov, since this modification provides better estimations.

The Kostiakov model was found to be suitable for simulating cumulative infiltration in sandy amendments up to 2.5% biochar addition (S2.5), while Horton and Philip had a better fit in the sandy loam amendments (SL) up to the inflection point of the curve (after this point the Philip model was less accurate than Horton). These results partially agree with findings of van De Genachte et al. (1996) that reported a better estimation of infiltration in high clay content soils, by Philip, Green-Ampt, Kostiakov and Horton equations; while for coarse sand Philip and Green-Ampt described better the infiltration behavior. They found some heterogeneities in parameter A (hydraulic conductivity) because of the poor structure of the coarse soil dominated by the matrix flow, while in the high clay content soils, a high contribution of preferential flow was present due to the formation of subangular blocky structures with abundant channels.

Other studies have obtained good estimations of infiltration using Philip model. For instance, Ayodele et al. (2009) observed good fitting results of the Philip equation in an amended loamy fine sand soil. Likewise Carrick et al. (2011) confirmed that hydrophobicity (by means of sorptivity) was the main mechanism affecting early-time infiltration, being sorptivity one of the main parameters of the Philip infiltration model. In the unamended sandy loam SL0 and SL2.5, due to the formation of some small cracks at the surface (after intense WD cycles), Horton equation performed better because it was able to estimate better the initial preferential flow, as suggested by (van De Genachte et al., 1996).

In the Philip model an increase in parameters S (Sorptivity) and A (transmissivity) are related to improved macro-porosity and effective porosity, respectively (Eastman, 2011; Mbagwu, 1994). In the sandy loam substrates (SL), parameter A was applicable to predict the measured data but the oscillating values suggested that porosity could have changed along the WD cycles. Lower total porosity (smaller A) implied a lower saturated flow. This effect was observed specially in the unamended treatment by the formation of small cracks at the surface. The oscillating behavior of parameter A (in the sandy loam, SL), suggested that biochar influenced saturated flow due to the enhancement of soil rigidity and rearrangement of pores during the WD cycles. Flow in all treatments was dominated by the matrix flow because the study was performed with disturbed samples, as mentioned by van De Genachte et al. (1996). In the sandy mixtures (S), the predicted S decreased with the occurrence of the WD cycles corresponding to the decrease of the wide pores. In some cases, predicted negative A values suggested that this model is not applicable to sandy substrates.

The fitted model parameters for the Kostiakov, Horton and Philip models differ considerably between sand (S) and sandy loam (SL). The coefficient of variation (CV, %), revealed that the parameters of the models of Philip and Horton exhibited a higher variability than the parameters of Kostiakov. The lower number of parameters (2 instead of 3) theoretically decreased the fitting ability of the measured infiltration data, as reported by Jačka et al. (2016).

6.3.5. Regression Analysis of Water Infiltration

Cumulative infiltration showed, in all wetting and drying scenarios, a convexity pattern, characteristic of soils with high initial infiltration rate that decreases gradually with time because of a decrease of capillary driving forces as the wetting front advances (Bughici and Wallach, 2016).

The linear regression provided an insight into the soil hydrology influenced by biochar application that could help to predict soil response changes due to a soil management with biochar. It was determined that in the soil amendments the major soil and water characteristics affecting infiltration were hydraulic conductivity, organic matter as total carbon, periods of shrinkage and swelling (described as wetting and drying), and bulk density. However, bulk density, as a capacity parameter, may not be sufficient to explain the infiltration behavior (intensity parameter) and may lead to misunderstand the real mechanisms influencing water infiltration. If only bulk density is considered, the changes on the mass per volume are considered but not the effect of the connectivity or the distribution of the pores that may also influence the water transmissivity within the bulk soil (Horn and Kutilek, 2009). Under these circumstances, intensity parameters such as hydraulic conductivity may explain better the decrease of water infiltration. Nonetheless, authors such as Uloma et al. (2014) and Novak et al. (2016) linked infiltration rate with bulk density changes by the formation of more pore space (assuming pores are connected). Other studies from Clothier and Scotter (2002) affirmed that sorptivity and macroscopic capillary length were the main soil properties that better explained water transmission in unsaturated soils. Canarache et al. (1968) observed that infiltration presented a negative correlation with soil moisture content and positive correlations with hydraulic conductivity, non-capillary porosity, and total porosity. Gray and Norum (1967) recognized that there were several factors affecting infiltration rate, by indirectly affecting hydraulic gradient (fluid properties, moisture content, pore shape, geometry and continuity, and surface conditions) and the hydraulic gradient (pressure and gravitational gradient). Mbagwu (1994) identified effective porosity as the most important soil property affecting the fitting parameters of the Philip and Kostiakov infiltration models. Van De Genachte et al. (1996) determined that bulk density, porosity, initial moisture content and organic carbon content explained better infiltration capacity and emphasized that detailed information of the soil particle size distribution was necessary to obtain good fitting results for the infiltration pedotransfer functions. In the sandy amendments (S), the statistical models for infiltration capacity and cumulative infiltration fitted well with coefficients of

determination (R^2) greater than 0.82, being an indication of close agreement between the measured and predicted statistical data. In the sandy loam amendments (SL5), the statistical model was not able to predict accurately the cumulative infiltration curves, probably because other soil parameters (not measured in this study) could have had a stronger effect, such as micro and macro porosity and effective porosity (Mbagwu, 1994).

Although the empirical models have been well documented to explain the infiltration processes, it is obvious that the complexity that brings the biochar properties to the amended soils must be further investigated. These models as well as the regression analysis were not able to explicitly explain the influence of biochar particle properties and pore architecture in the soil pore system. Moreover, wetting and drying demonstrated some soil instabilities not capable to be represented by any conventional model, neither by the regression model. Information about crack volume and length after each wetting and drying period, rearrangement of soil aggregates, and unsaturated hydraulic conductivity should be included in future work. Models with separation of flow domains (soil matrix and macropores) may provide better results, albeit more soil parameters may be required.

6.3.6. Effect of Biochar Amendments on Watershed Hydrology

Modelling the water discharge of a catchment depended on biochar dosage, soil type, and weather condition. During the wet season, the unamended treatments tended to produce more water discharge. During dry conditions, water discharge at the catchment outlet was higher as the biochar dosage increased.

The unamended soil materials (S0 and SL0) discharged a higher water volume (Q) than the amended soils, with an increasing surface runoff and a decreasing subsurface flow (interflow) as biochar dosage increased. The increasing surface runoff was a result of the decrease of water infiltration as the biochar dosage increased. The processes behind these phenomena can be explained both by the reduced pore diameter, due to the added biochar, as well as by the increased water saturation or stronger menisci forces, due to the smaller pore diameter (Hartge and Horn, 2016). Zhang and Hartge (1995) carried out infilling experiments and proved the more pronounced strength but also altered water uptake rates. Hydrophobicity may also have played a role on the higher formation of runoff in the SL amendments, but further research is still needed, since SWAT does not consider this parameter.

As observed by Grayson et al. (1997), the Birris subcatchment presented a two regime surface runoff generation, associated with wet and dry conditions. It is assumed that this bimodal surface runoff regime is mainly dependent on the pore size distribution measured by the hydraulic conductivity parameter.

The decrease of interflow with the biochar addition is related to the decrease of saturated hydraulic conductivity in the amendments. These results agree with findings of Lee et al. (2015) that observed a significant increase of runoff on biochar soil

amendments compared to the unamended treatments. Others, such as Hamidreza Sadeghi et al. (2016) reported an amelioration of water infiltration in biochar amendments. Thus, the controversy results concerning the infiltration behavior may be finally attributed and explained by: 1) ageing effects for soils amended with biochar and the formation of soil aggregates which changes the infiltration capacity; and 2) the effect of soil water repellency not revealed under laboratory, but under in situ conditions (reported also by several authors like Bughici and Wallach, 2016; Chau et al., 2012; Doerr et al., 2003; Doerr and Thomas, 2000; Hallin et al., 2015; Miyata et al., 2007). Under full saturation during the rainy season, the sandy loam mixtures generated less water discharge (Q) than the sandy mixtures. Although the runoff coefficient (R/P) of the sandy loam treatments (SL) was higher than the sandy mixtures (S), the interflow coefficient was twice as high in the sandy substrates. We explain this as the effect of a multidimensional flow in the subsurface hillslope – under in situ conditions –, and a higher hydraulic conductivity in the sandy mixtures due to a greater amount of wider pores than in the sandy loam substrates (as reported in Villagra-Mendoza and Horn, 2018a). These findings also agree with observations of Imhoff and Akbar Nakhli (2017), with a decrease of saturated hydraulic conductivity in an amended silt loam (30%) and sandy loam (54%) and an increase in a loamy sand (17%). They associated it with changes on the inter-pore volume, because small biochar particles filled the large pores between the sand particles, increasing the portion of finer pores.

Under partially saturated soil conditions (dry season), the sandy loam mixtures generated more water discharge (Q) than the sandy mixtures. When the soil is not completely dry, the movement of water in the sandy loam is higher than in the sandy mixtures. This is due to the higher available water content and more formation of narrow and medium pores in the sandy loam mixtures, which increased the unsaturated hydraulic conductivity and enhanced the water flux under unsaturated soil conditions. After large pores and inter-particle pores drain, water is retained in small pores and biochar intra-particle pore spaces. Thus, biochar increase water retention in the capillary region, which enhances the water conduction under partially saturated soil conditions (Imhoff and Akbar Nakhli, 2017). The more narrow and medium pores are formed due to biochar addition, the higher the unsaturated hydraulic conductivity gets (Villagra-Mendoza and Horn, 2018b). Finally, Imhoff and Akbar Nakhli (2017) observed that when soil was not fully saturated, the unsaturated hydraulic conductivity was higher, due to an increase of the available water content in the loamy sand (70%) and sandy loam (20%), resulting in a less surface runoff.

This work aimed to understand the effect of biochar amendments on the catchment hydrology by means of the dynamics of the infiltration process on the topsoil. It was analyzed the relation between the biochar production process, biochar amendment dosages and soil type, the effect of the environment, as well as the main mechanisms that affect the soil physico-chemical and hydraulic properties that influence soil structure and aggregation. Moreover, infiltration models were tested in order to identify their ability to explain infiltration on soils amended with biochar (Figure 6.1).
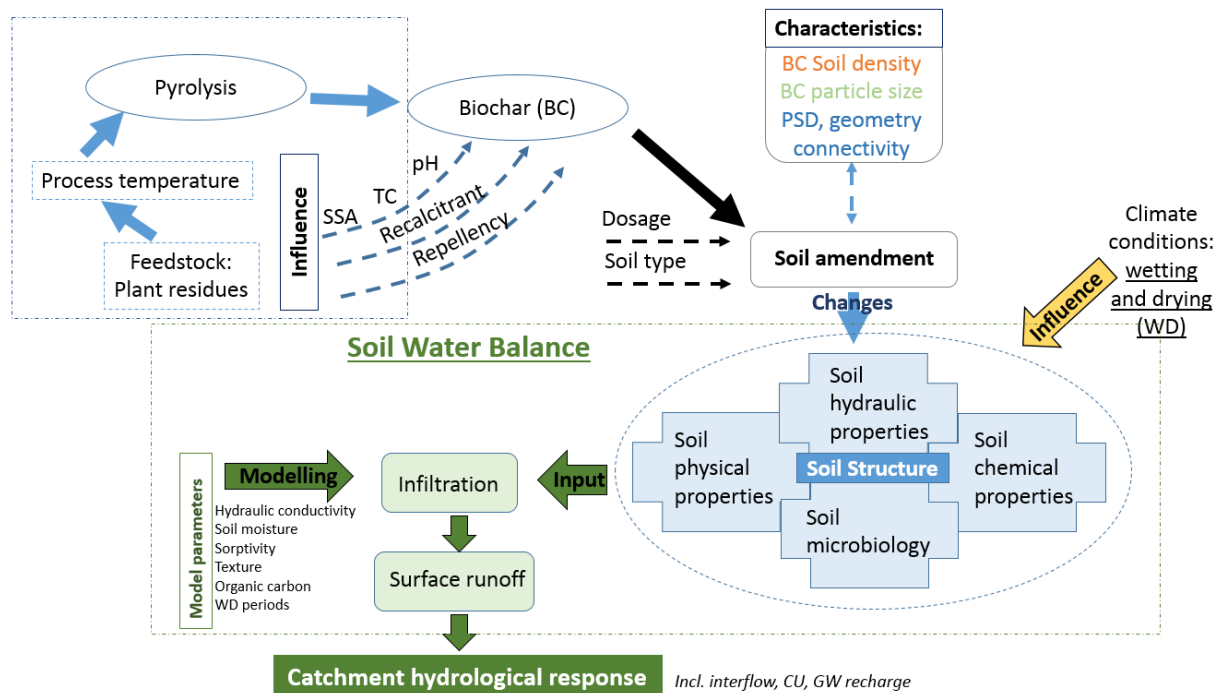
Figure 6.1. Scheme of the effect of biochar amendments on the catchment hydrology.

7. Conclusions and Outlook

This thesis addressed the effect of biochar addition on the chemical, physical, and hydraulic characteristics of sandy and sandy loam soils. The effect of intense and repetitive wetting and drying on the soil hydraulic properties, for the two types of amended soils was explored. The main mechanisms of the resilience of the amended soils to simulated adverse climate conditions were also identified based on the infiltration behavior of the amended soils. These results were compared with conventional empirical and semi empirical models; a regression analysis was carried out to identify the main soil properties that better described the water movement at the soil surface of biochar amended soils. Six scenarios with amended soils were evaluated at catchment level to understand the role of biochar on the hydrological response of the watershed, and the impact that climate change may have on a watershed with an exclusive biochar management. In summary, the main conclusions presented in this thesis are:

- Biochar particle size is of great importance. In the case of coarse textured soils, small biochar particle size improves soil properties such as water holding capacity and saturated as well as unsaturated hydraulic conductivity, enhancing the conductive capacity of coarse-textured soils under drying conditions. Nevertheless, it decreases soil aeration and saturated hydraulic conductivity, because of the fill-in of larger pores and formation of more narrow and medium pores. In finer soil texture amendments, fine biochar particles presented negative or no effects on the soil hydraulic properties. Therefore, before any biochar inclusion to fine soil textures, the soil particle size should be known (D_{50}) to incorporate biochar particles of greater size.

- The formation of small pore diameters by biochar addition, has a positive impact on water retention especially in coarse grained soils.

- In general, a biochar dosage of 5% produced more significant changes (positive or negative) on the soil physical and hydraulic properties than a dosage of 2.5%. But just a dosage of 2.5% was enough to produce changes on the soil functioning. Small dosages of about 2.5%, applied to a degraded soil at a depth of 20 cm, which corresponds to about 75 ton/ha (with a bulk density of 1.5 g/cm^3), is enough to noticeably improve soil properties (in coarse grained degraded soils). However, biochar doses must be according to the biomass availability, to guarantee a sustainable biochar production.

- Wetting and drying contribute to the rearrangement of the soil aggregates forming new pores. Since biochar increases rigidity of coarse-grained soils, water loss and the solute flux in the soil matrix are enhanced especially under drying conditions.

- The addition of biochar enhances the transport of water under unsaturated conditions by reducing the formation of larger pores (draining pores) and promoting finer inter-particle pore formation. In coarse textured biochar amendments, water content increased within the pore diameter in the range of 50-10 μm. This enhances the unsaturated hydraulic conductivity for the same matric potentials when compared to the unamended soils.

- Infiltration capacity decreases due to biochar inclusion, due to the formation of narrower pores, and is further enhanced during repeated wetting and drying periods by the rearrangement of soil aggregates.

- The correlation analysis of the soil parameters, that influence the infiltration process in the topsoil, derived from a combination of intensity and capacity parameters (saturated hydraulic conductivity and total porosity) with the additional effect of the wetting and drying periods.

- Conventional models are not able to make a good description of the infiltration processes on biochar amendment soils. It is suggested to include in further analyses information about crack volume and length after each wetting and drying period, rearrangement of soil aggregates, unsaturated hydraulic conductivity and antecedent soil moisture content. It is recommended as future work, to use models with separation of flow domains (soil matrix and macropores) that may provide better results, albeit more soil parameters may be required.

- The watershed runoff analysis revealed that biochar amended soils are more sensitive to higher runoff generation than the unamended soils; and hydraulic conductivity (saturated and unsaturated) plays a key role on the hydrological response of catchments.

- The impact of the addition of biochar on the soil hydraulic functioning is soil type dependent and it helps to overcome extreme climate conditions. Under fully wetting conditions sandy loam amendments generate more surface runoff (low infiltration capacity) and less interflow than the sandy treatments. Under dry soil conditions, biochar enhances the conducting and retention capacity of both soil materials. Fresh biochar addition will initially reduce infiltration capacity until re-formation of soil aggregates is well developed.

This study confirms that biochar is an attractive alternative for soil conservation management and a valuable resource to improve soil physical functions that can help to mitigate the impact of extreme drying conditions.

Appendices

Appendix A

Table A.1. Grain size distribution of the base soil materials and amendments.

Treatment	Sand			Silt			Clay
μm	$630 \leq 2000$	$200 \leq 630$	$63 \leq 200$	$20 \leq 63$	$6.3 \leq 20$	$2 \leq 6.3$	$< 2,0$
				[%]			
$S0$	0.0	70.0	29.0	0.1	0.1	0.2	0.6
$S2.5$	0.0	62.0	37.0	0.7	0.0	0.0	0.3
$S5$	0.0	60.0	39.0	0.0	0.0	0.0	1.0
$SL0$	6.0	20.0	28.1	30.2	0.0	2.3	13.4
$SL2.5$	5.0	20.0	29.0	17.1	9.3	6.5	13.1
$SL5$	6.0	20.0	27.7	16.8	9.4	7.7	12.4

Appendix B
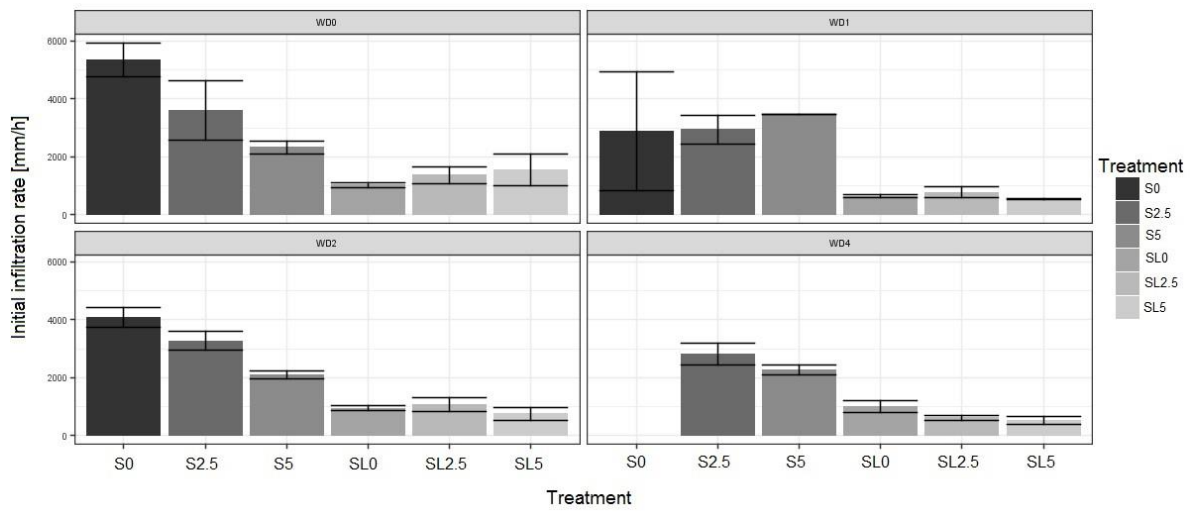
Figure B.1. Initial infiltration rate (I_o) for the amended sandy (S) and sandy loam (SL) at different wetting and drying (WD) cycles.
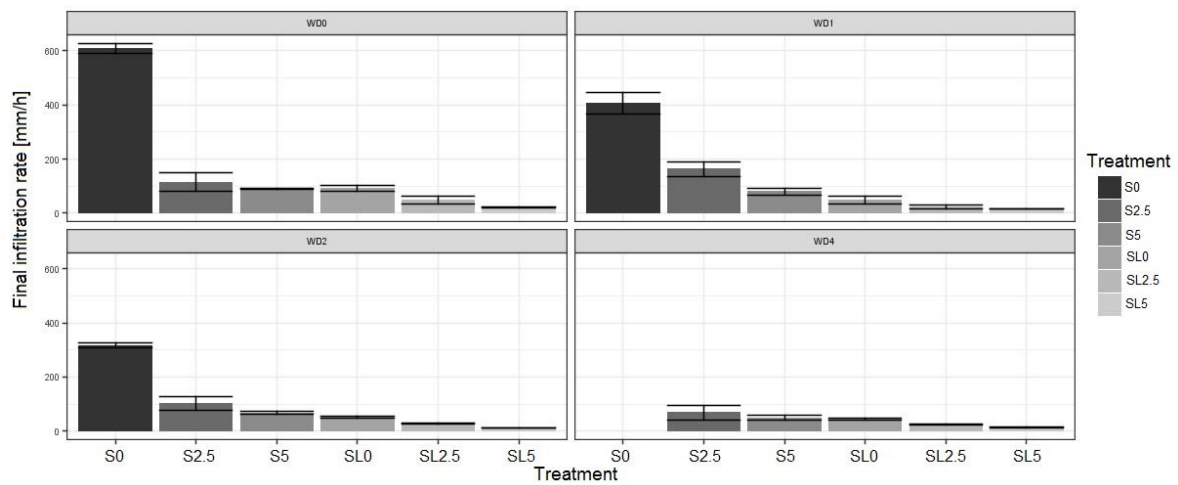
Figure B.2. Final infiltration rate (I_b) for the amended sandy (S) and sandy loam (SL) at different wetting and drying (WD) cycles.

Table B.1. Cumulative infiltration (cm) at 15 minutes for all treatments, after applying the four wetting and drying periods.

Treatment	Wetting and Drying Period (WD)			
	0	1	2	4
S0	25.3 ± 3.09	25.07 ± 0.79	19.69 ± 2.05	12.67 ± 2.60
S2.5	16.16 ± 1.06	13.68 ± 0.69	10.86 ± 0.17	7.77 ± 3.14
S5	8.91 ± 1.51	8.28 ± 0.38	7.95 ± 0.33	7.60 ± 0.50
SL0	11.55 ± 0.07	8.99 ± 0.94	9.62 ± 0.32	9.07 ± 0.71
SL2.5	9.83 ± 0.77	8.53 ± 0.28	8.38 ± 1.12	8.14 ± 0.88
SL5	8.85 ± 0.32	8.01 ± 0.18	7.63 ± 0.66	7.83 ± 0.22

Table B.2. Cumulative infiltration (cm) at 45 minutes for all treatments, after applying the four wetting and drying periods.

Treatment	Wetting and Drying Period (WD)			
	0	1	2	4
S0	ND.	ND.	ND.	ND.
S2.5	32.72 ± 4.81	24.10 ± 1.68	18.38 ± 0.24	16.38 ± 4.57
S5	14.51 ± 2.46	12.50 ± 0.87	11.86 ± 0.16	11.01 ± 0.83
SL0	17.38 ± 1.14	13.52 ± 2.70	13.18 ± 0.59	12.45 ± 0.51
SL2.5	13.32 ± 1.10	10.64 ± 0.61	11.16 ± 0.62	10.34 ± 1.22
SL5	10.38 ± 0.28	9.63 ± 0.07	9.77 ± 0.31	9.59 ± 0.22

Table B.3. Comparison of the infiltration rate at 15, 30, 45 and 60 minutes for the amended sandy (S) at different WD cycles.

Treatment	WD	Infiltration rate (mm/h)				
		$\dfrac{\rho_d}{g/cm^3}$	15 min	30 min	45 min	60 min
$S0$	WD0	1.55	581.03	286.25	133.89	
	WD1	1.54±0.03	459.98			
	WD2	1.61±0.07	373.66			
	WD3	N.D.	351.51	166.87	50.17	
	WD4	1.71	332.61	154.93	58.71	
$S2.5$	WD0	1.52±0.03	404.13	340.80	240.87	246.45
	WD1	1.49±0.03	274.47	221.37	159.59	
	WD2	1.47±0.03	179.47	149.16	116.81	
	WD3	N.D.	185.04	148.17		
	WD4	1.48	175.75	147.73	127.10	104.35
$S5$	WD0	1.48±0.01	123.71	106.61	108.89	108.67
	WD1	1.46±0.02	94.68	85.78	73.21	
	WD2	1.46±0.02	83.01	76.27	73.58	64.91
	WD3	N.D.	75.39	68.80	69.60	68.07
	WD4	1.43	81.80	63.12	55.53	57.04

Table B.4. Comparison of the infiltration rate at 15, 30, 45 and 60 minutes for the amended sandy loam (SL) at different WD cycles.

Treatment	WD	$\dfrac{\rho_d}{g/cm^3}$	Infiltration rate (mm/h)			
			15 min	30 min	45 min	60 min
$SL0$	WD0	1.38±0.02	116.25	132.39	97.32	98.03
	WD1	1.36±0.02	138.52	108.05	79.74	74.56
	WD2	1.37±0.01	111.45	71.78	66.02	63.33
	WD3	N.D.	128.39	71.09	67.69	64.25
	WD4	1.38	102.91	68.39	64.08	63.94
$SL2.5$	WD0	1.40±0.05	109.85	74.52	61.46	58.39
	WD1	1.39±0.06	115.09	47.26	35.34	31.72
	WD2	1.38±0.05	165.01	45.77	39.93	37.58
	WD3	N.D.	159.92	54.77	41.77	40.64
	WD4	1.35	141.37	41.68	35.60	32.18
$SL5$	WD0	1.40±0.04	121.55	31.16	24.50	20.59
	WD1	1.36±0.05	157.82	31.90	22.16	16.85
	WD2	1.35±0.02	190.48	31.61	23.51	17.05
	WD3	N.D.	177.75	34.40	22.46	18.71
	WD4	1.37	132.29	32.98	20.10	16.39

Appendix C

Figure C.1. Comparison of the average values of the infiltration rate for the sandy treatment (S) obtained with the models of Kostiakov, Horton and Philip for two wetting and drying (WD) cycles.

Figure C.2. Comparison of the average values of the infiltration rate for the sandy loam (SL) obtained with the models of Kostiakov, Horton and Philip for two wetting and drying (WD) cycles.

Figure C.3. Comparison of the average values of the cumulative infiltration for the sandy treatment (S) obtained with the models of Kostiakov, Horton and Philip for two wetting and drying (WD) cycles.
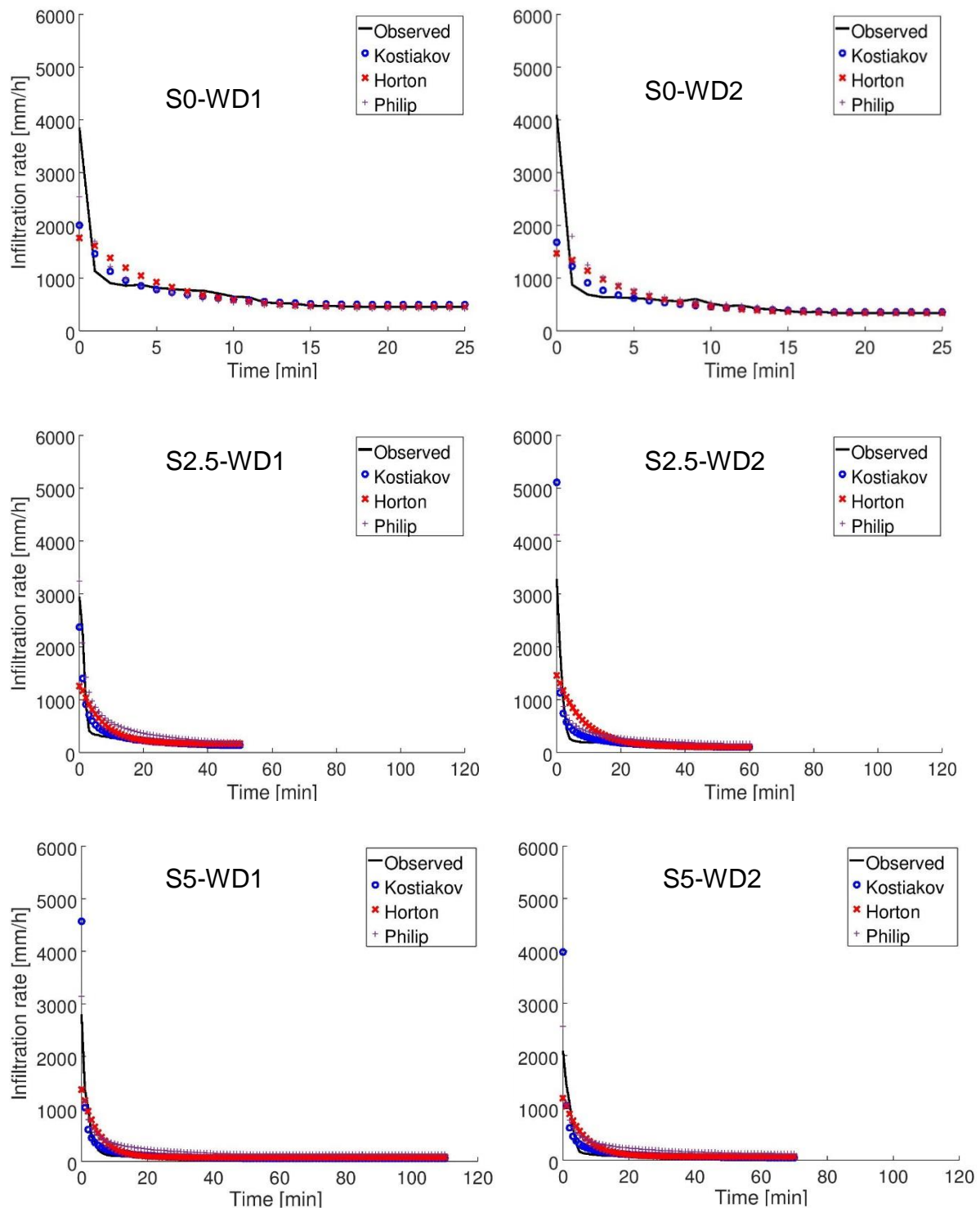
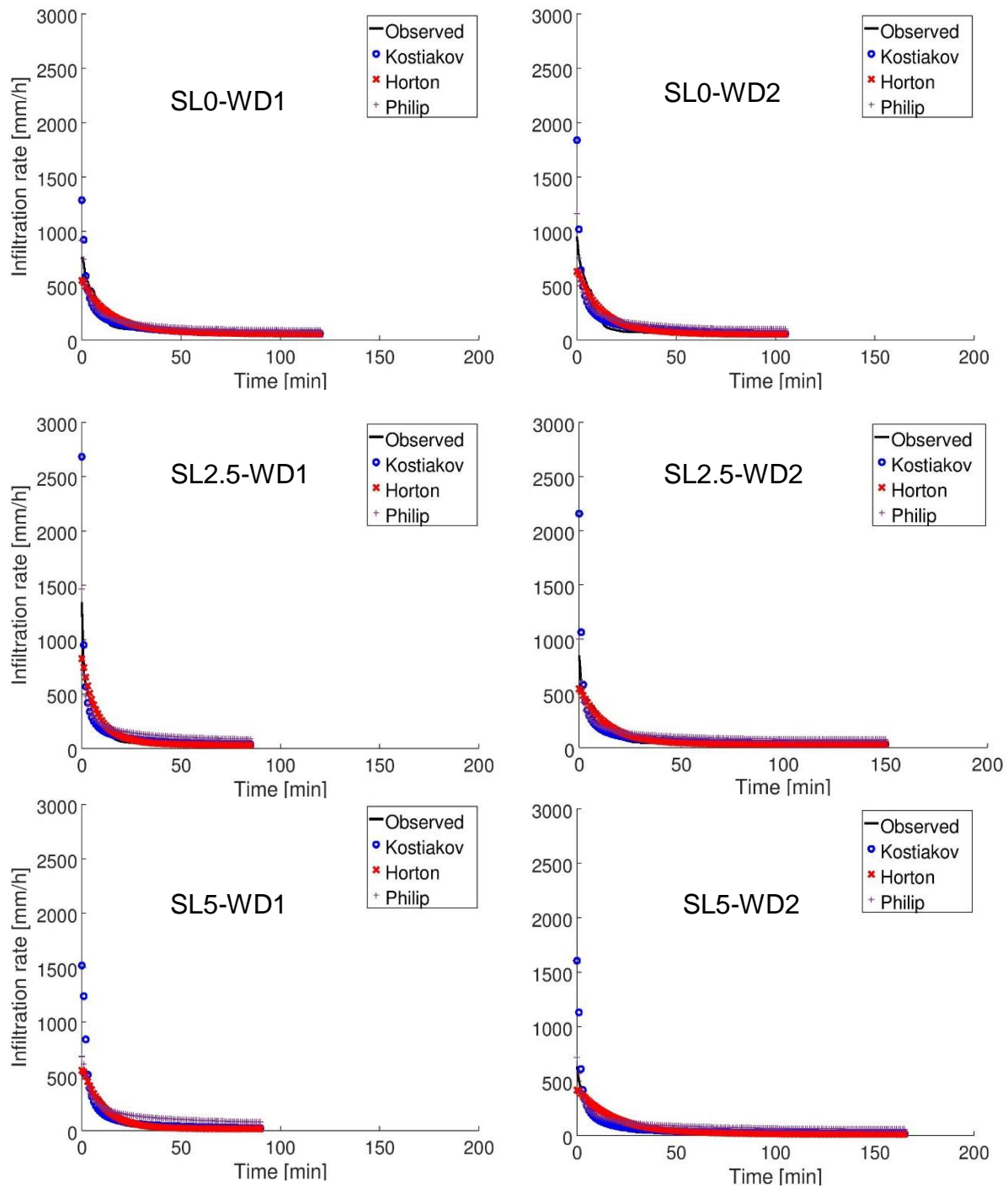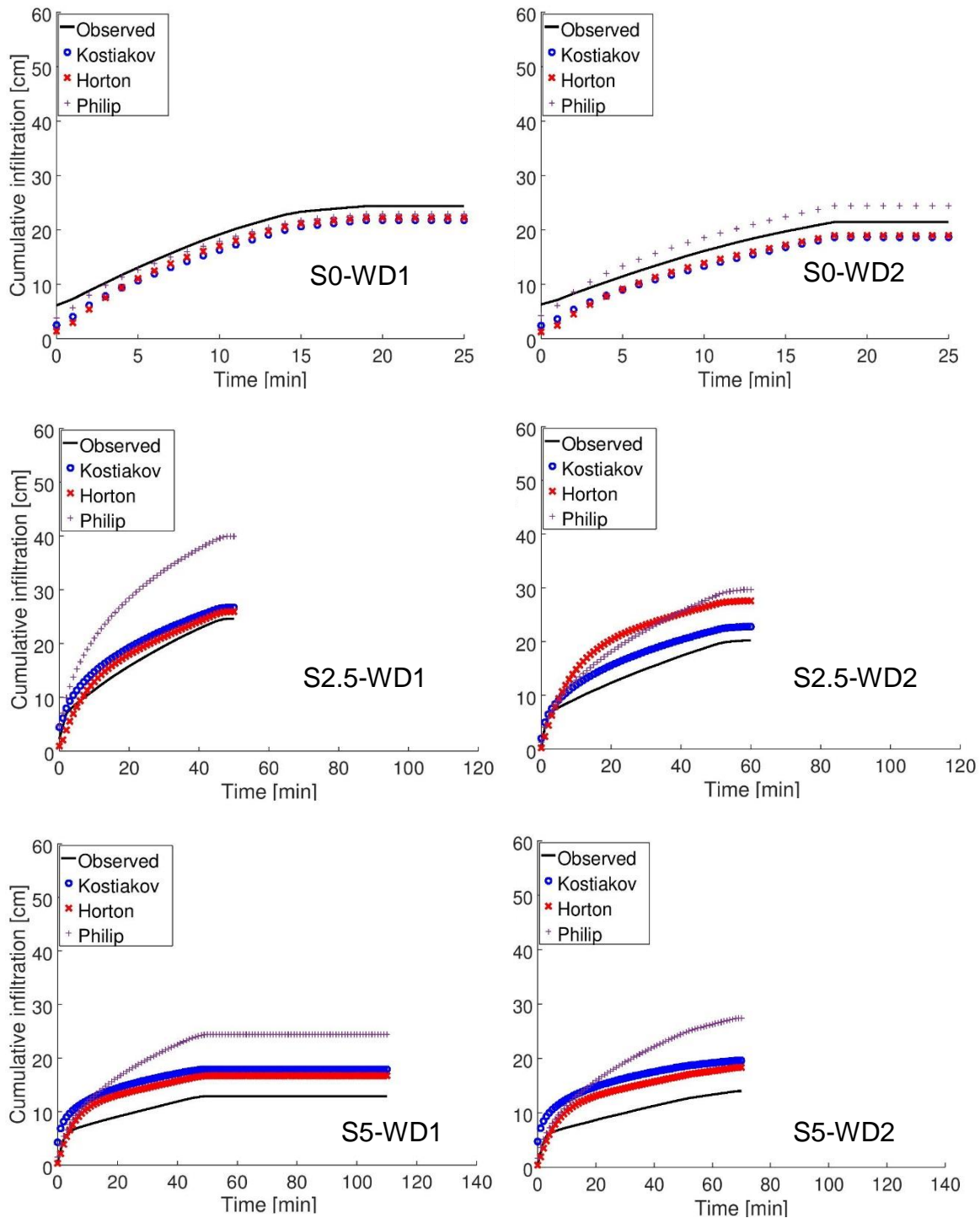Figure C.4. Comparison of the average values of cumulative infiltration for the sandy loam (SL) obtained with the models of Kostiakov, Horton and Philip for two wetting and drying (WD) cycles.

Table C.1. Mean, standard deviation and coefficient of variation (%) of the fitted infiltration parameters for the model of Kostiakov for WD1 and WD2 cycles.

| Treatment | Cycle | C | | | α | | | MSSE | |
		Mean	Std. dev	CV %	Mean	Std. dev	CV %	i	$Icum$
S0	WD1	1459.9	299.8	20.5	-0.4	0.04	10.7	$3.0\cdot10^5$	8.3
	WD2	1222.7	193.5	15.8	-0.4	0.04	9.6	$2.8\cdot10^5$	8.5
S2.5	WD1	1389.7	143.2	10.3	-0.6	0.06	9.9	$1.6\cdot10^5$	10.2
	WD2	1126.4	121.1	10.7	-0.6	0.05	8.8	$2.8\cdot10^5$	6.5
S5	WD1	1015.5	122.5	12.1	-0.7	0.03	3.9	$2.8\cdot10^5$	20.5
	WD2	1041.6	110.1	10.6	-0.8	0.01	1.6	$3.1\cdot10^5$	28.1
SL0	WD1	901.3	167.0	18.5	-0.6	0.03	5.6	$2.4\cdot10^4$	8.4
	WD2	1012.4	151.8	15.0	-0.7	0.07	10.0	$4.3\cdot10^4$	17.7
SL2.5	WD1	948.7	60.5	6.4	-0.7	0.06	8.4	$1.0\cdot10^5$	29.4
	WD2	961.3	83.3	8.7	-0.7	0.05	6.3	$9.3\cdot10^4$	29.2
SL5	WD1	1501.1	641.0	42.7	-0.9	0.17	17.7	$5.1\cdot10^4$	1112.8
	WD2	1053.8	209.2	19.8	-0.8	0.04	5.0	$6.5\cdot10^4$	159.2

Table C.2. Mean, standard deviation and coefficient of variation (%) of the fitted infiltration parameters for the model of Horton for WD1 and WD2 cycles.

| Treatment | Cycle | I_o | | | k | | | MSSE | |
		Mean	Std. dev	CV %	Mean	Std. dev	CV %	i	$Icum$
S0	WD1	1896.8	418.9	22.1	0.22	0.02	7.6	$3.8\cdot10^5$	8.6
	WD2	1594.1	178.2	11.2	0.22	0.02	7.7	$3.5\cdot10^5$	9.2
S2.5	WD1	1323.8	29.6	2.2	0.15	0.01	8.4	$3.6\cdot10^5$	4.2
	WD2	1471.6	192.2	13.1	0.12	0.02	12.6	$3.6\cdot10^5$	33.6
S5	WD1	1404.2	321.0	22.8	0.20	0.02	10.8	$2.2\cdot10^5$	7.0
	WD2	1218.4	166.2	13.6	0.17	0.02	11.1	$1.0\cdot10^5$	9.6
SL0	WD1	567.6	48.4	8.5	0.08	0.04	51.5	$8.5\cdot10^3$	2.5
	WD2	648.6	54.6	8.4	0.08	0.02	23.2	$1.0\cdot10^4$	3.4
SL2.5	WD1	847.0	331.6	39.1	0.12	0.05	43.9	$3.8\cdot10^4$	2.6
	WD2	555.4	130.4	23.5	0.08	0.02	26.0	$9.7\cdot10^3$	1.8
SL5	WD1	600.0	98.9	16.5	0.10	0.02	21.6	$1.9\cdot10^3$	0.7
	WD2	429.4	79.7	18.6	0.05	0.01	21.4	$4.7\cdot10^3$	3.1

Table C.3. Mean, standard deviation and coefficient of variation (%) of the fitted infiltration parameters for the model of Philip for WD1 and WD2 cycles.

Treatment	Cycle	S			A			MSSE	
		Mean	Std. Dev	CV %	Mean	Std. dev	CV %	i	$Icum$
S0	WD1	3393.7	1555.8	45.8	0.05	64.2	-	$2.5 \cdot 10^5$	13.4
	WD2	3709.5	473.8	12.8	-62.1	0.51	0.82	$2.2 \cdot 10^5$	5.1
S2.5	WD1	4380.3	947.9	21.6	-128.6	55.0	42.8	$1.5 \cdot 10^5$	115.2
	WD2	2438.0	283.0	11.6	-2.5	6.7	270.0	$1.5 \cdot 10^5$	31.0
S5	WD1	2331.7	890.2	38.2	-30.9	68.7	222.5	$6.6 \cdot 10^4$	35.9
	WD2	2198.1	446.1	20.3	-15.6	56.18	359.0	$7.6 \cdot 10^4$	45.0
SL0	WD1	1430.4	633.5	44.3	9.6	23.7	246.7	$9.5 \cdot 10^3$	10.5
	WD2	1468.2	421.0	28.7	16.3	28	172.0	$1.4 \cdot 10^4$	12.8
SL2.5	WD1	1339.2	303.6	22.7	7.63	17.8	233.0	$1.1 \cdot 10^4$	9.9
	WD2	1120.8	293.4	26.2	18.7	5.8	30.9	$1.1 \cdot 10^4$	9.5
SL5	WD1	1337.3	598.1	44.7	5.93	27.3	460.0	$8.1 \cdot 10^3$	26.8
	WD2	1083.9	315.3	29.1	10.0	13.8	138.3	$5.6 \cdot 10^3$	20.1

Appendix D
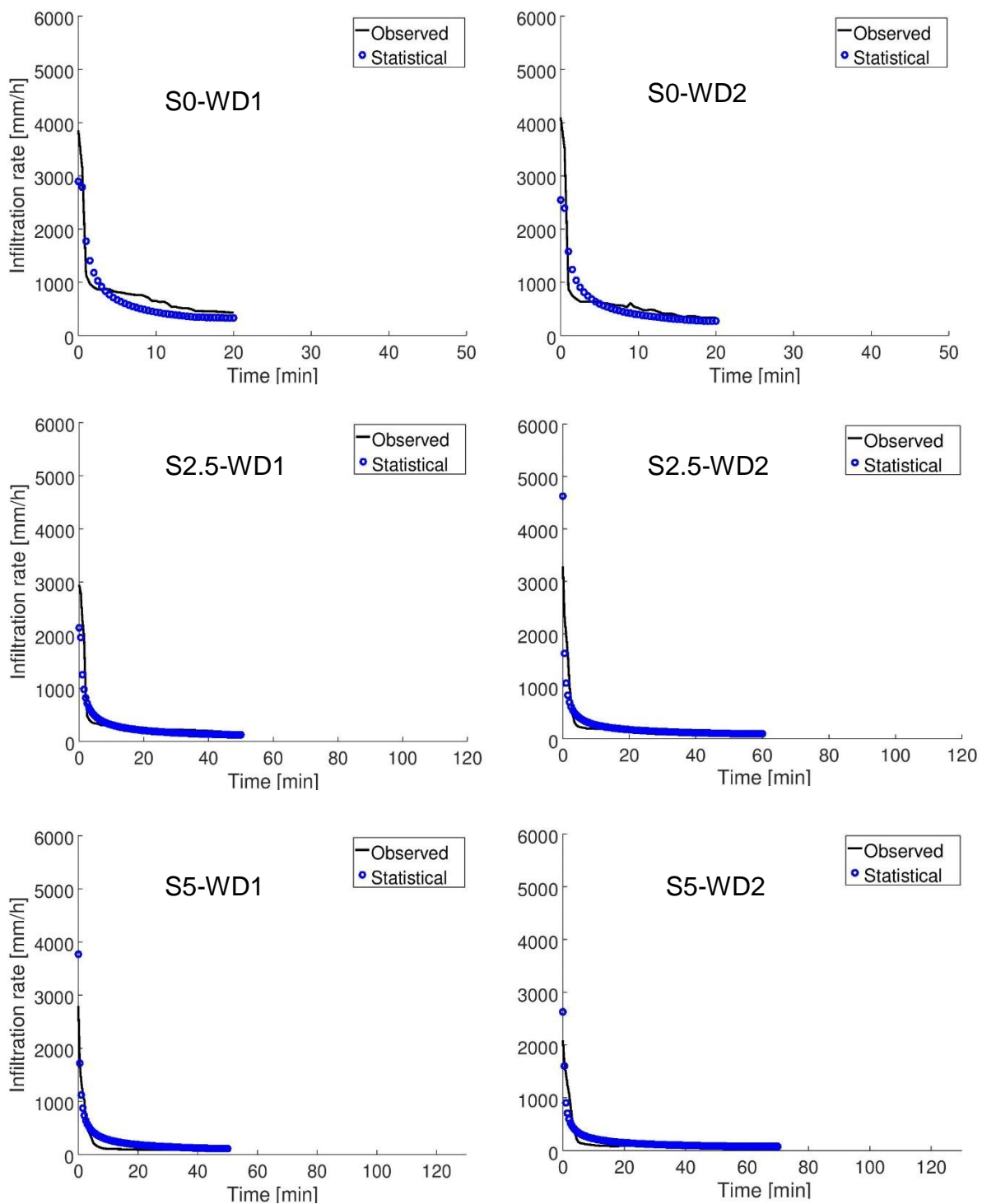
Figure D.1. Comparison of the average values of the infiltration rate for the sandy treatment (S) obtained with the models of Kostiakov, Horton and Philip for two wetting and drying (WD) cycles.
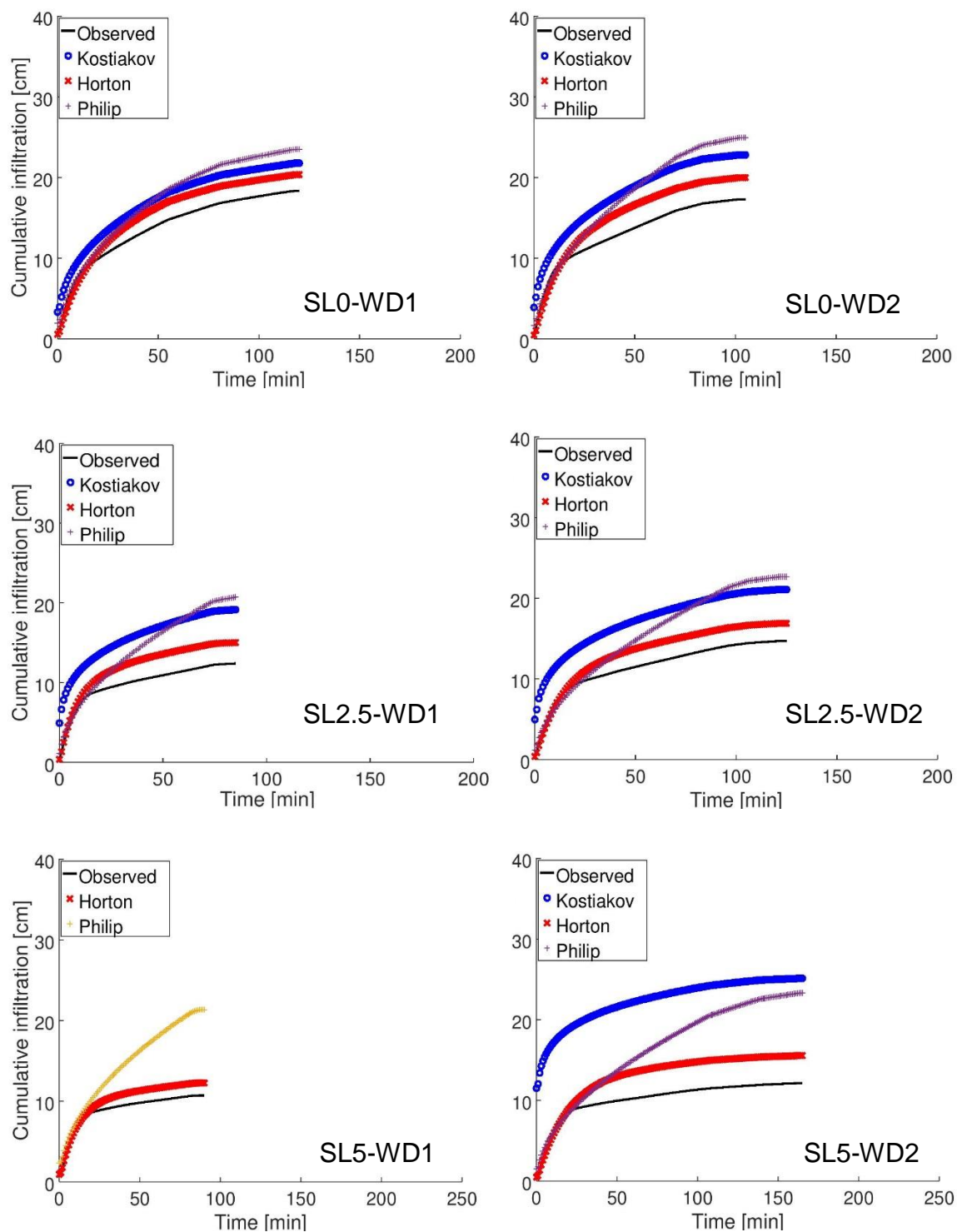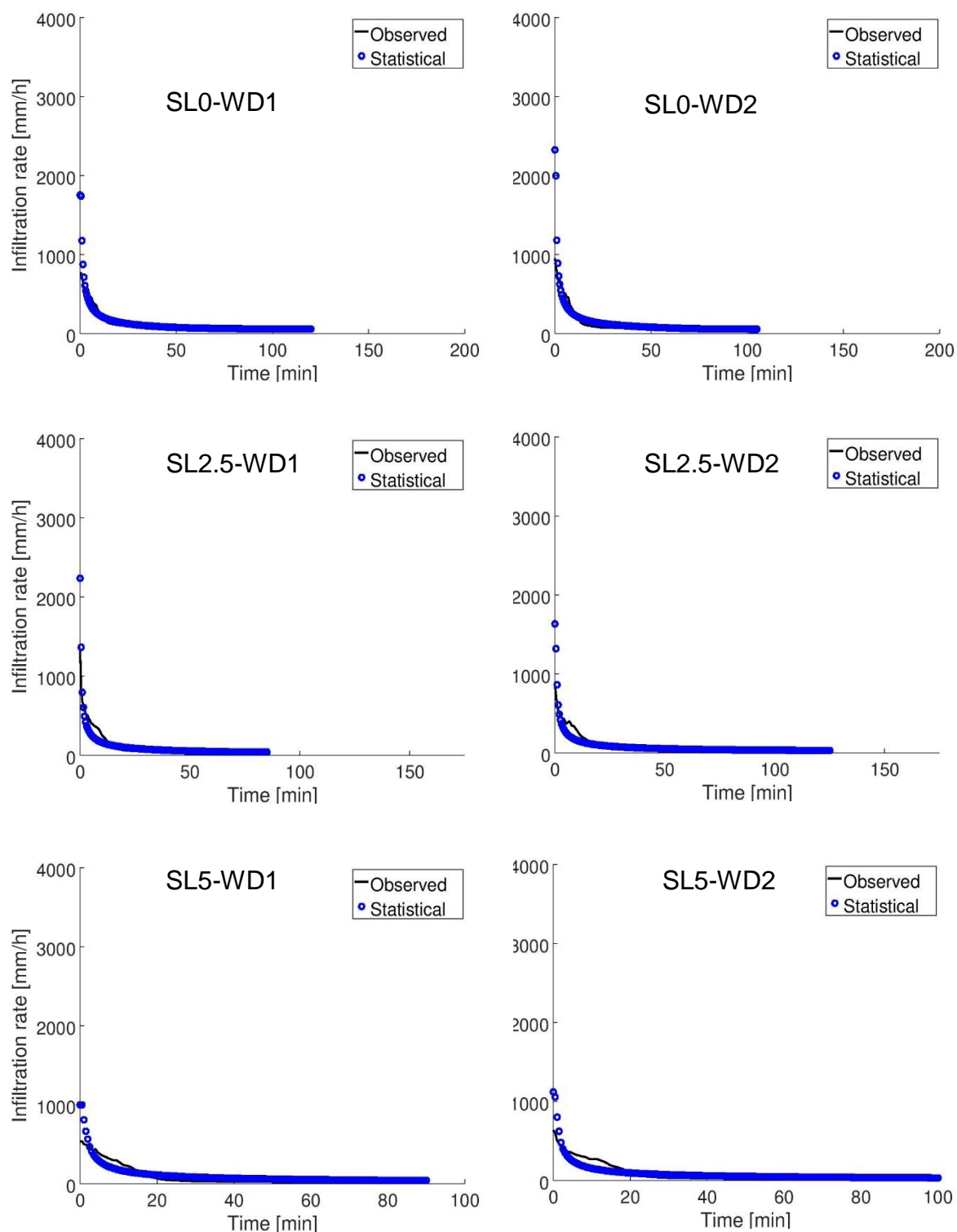
Figure D.2. Comparison of the average values of the infiltration rate for the sandy loam (SL) obtained with the models of Kostiakov, Horton and Philip for two wetting and drying (WD) cycles.
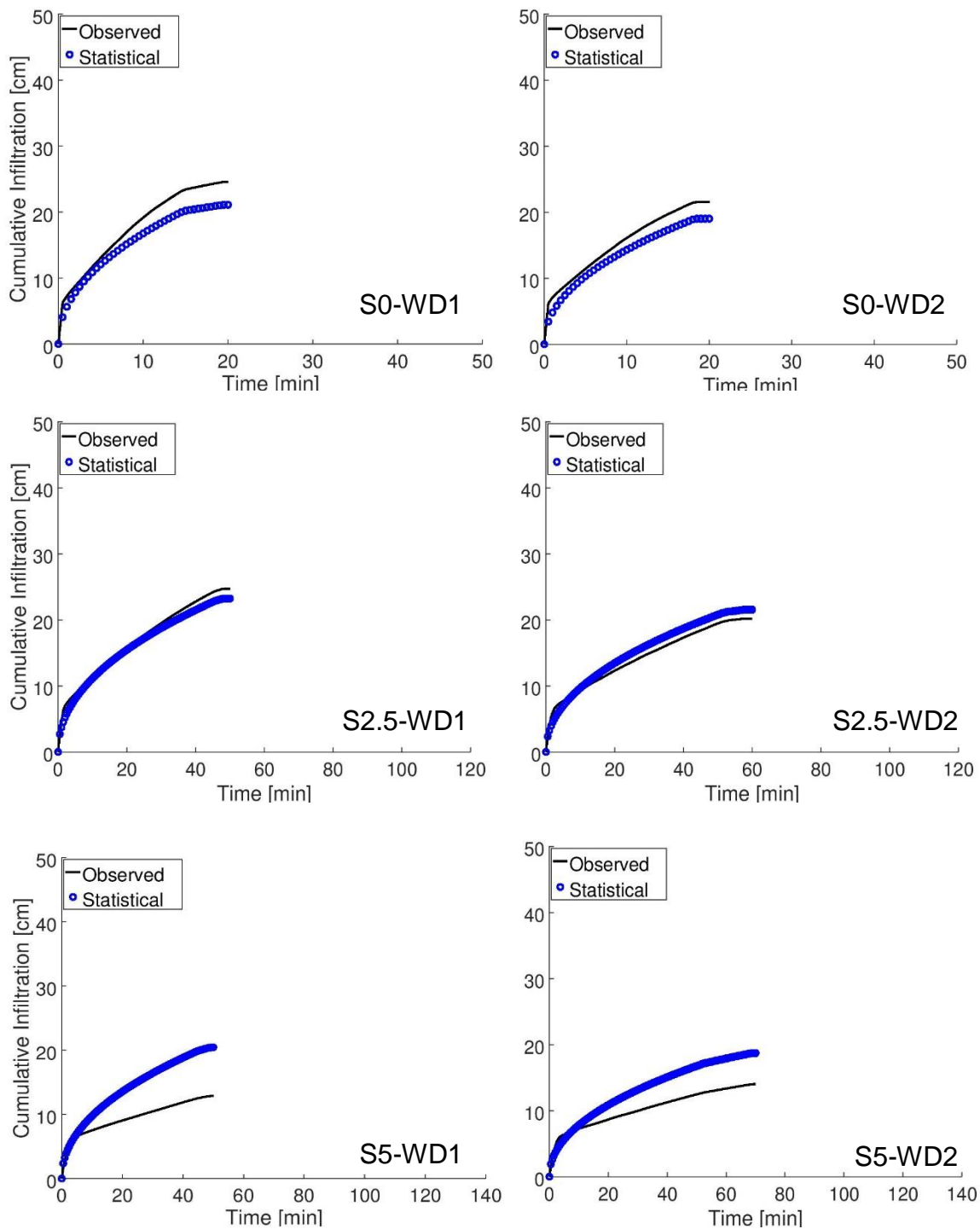
Figure D.3. Comparison of the average values of the cumulative infiltration for the sandy treatment (S) obtained with the models of Kostiakov, Horton and Philip for two wetting and drying (WD) cycles.
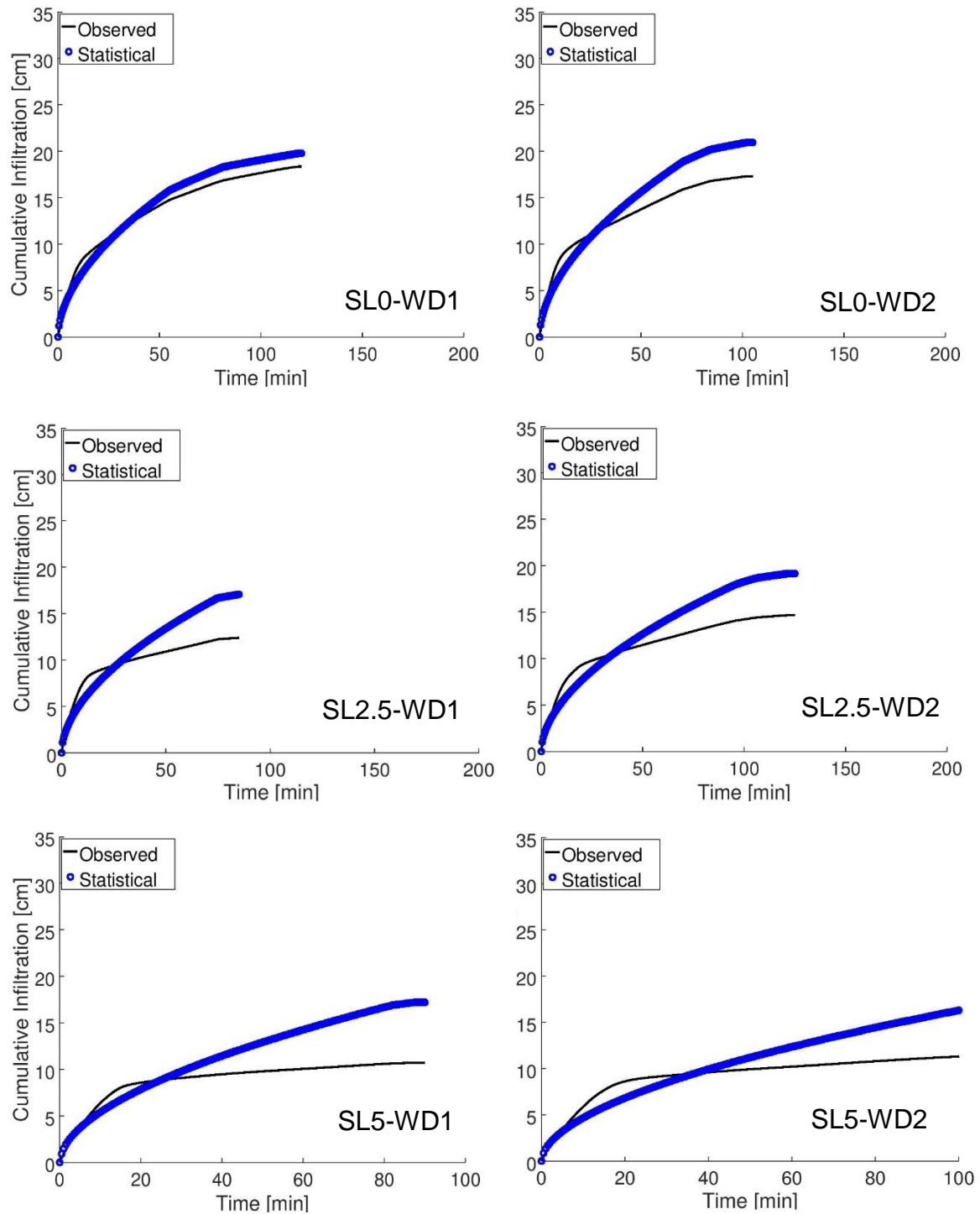
Figure D.4. Comparison of the average values of cumulative infiltration for the sandy loam (SL) obtained with the models of Kostiakov, Horton and Philip for two wetting and drying (WD) cycles.
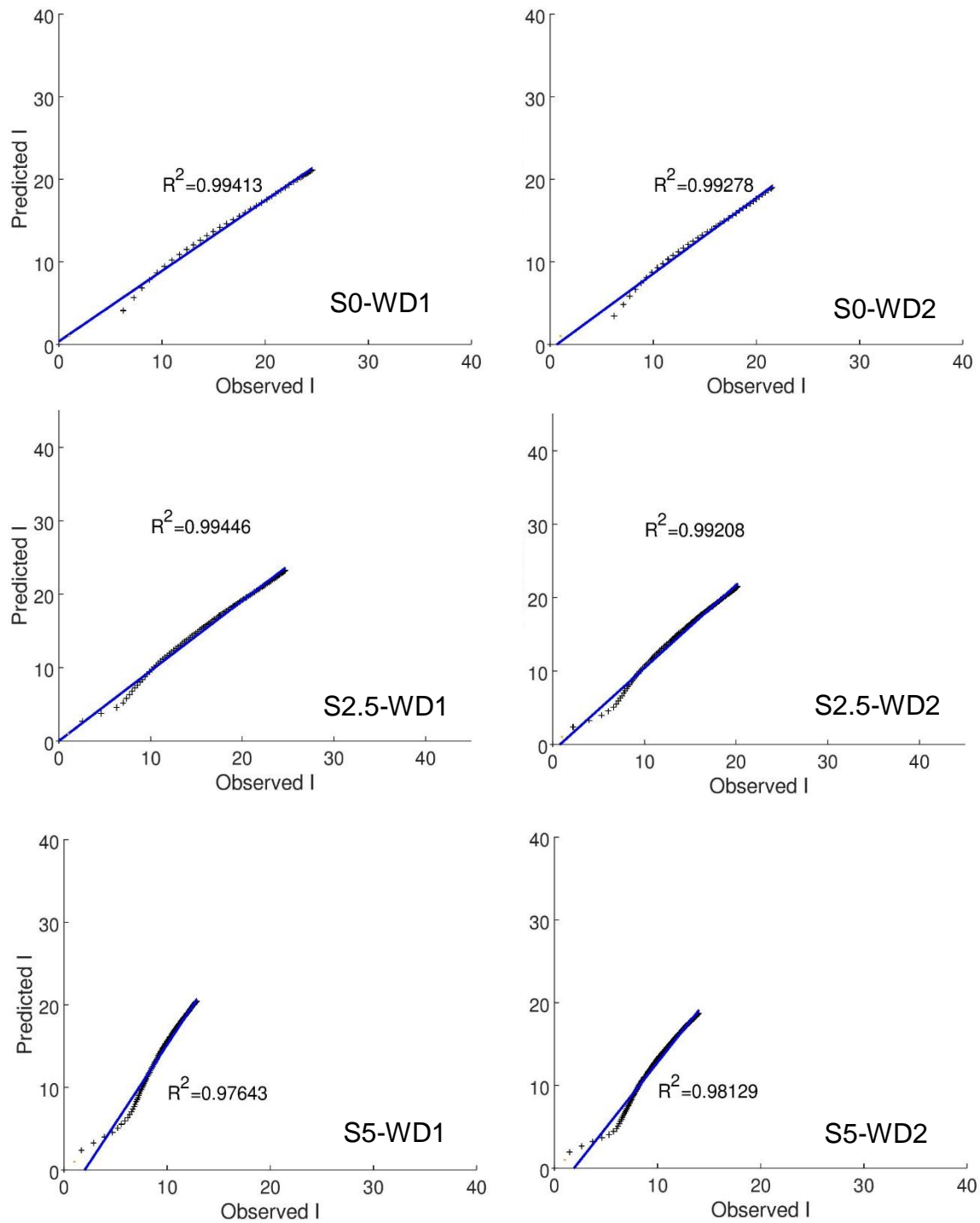
Figure D.5. Scatter plots of the observed and predicted cumulative infiltration using the statistical model for the sandy (S) treatments for two wetting and drying cycles (WD1 and WD2). The diagonal line represents the line of best fit.
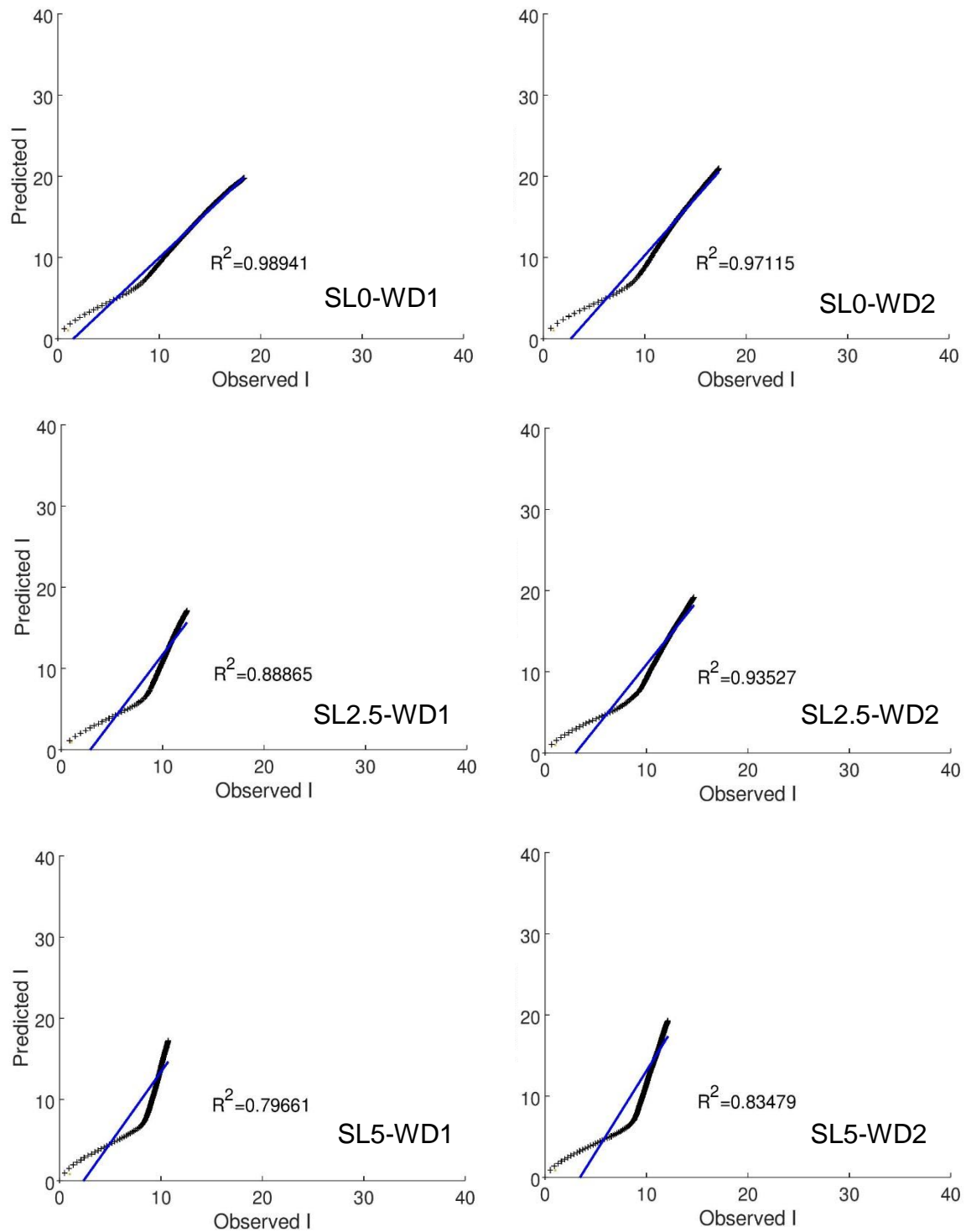
Figure D.6. Scatter plots of the observed and predicted cumulative infiltration using the statistical model for the sandy loam (SL) treatments for two wetting and drying cycles (WD1 and WD2). The diagonal line represents the line of best fit.

Appendix E
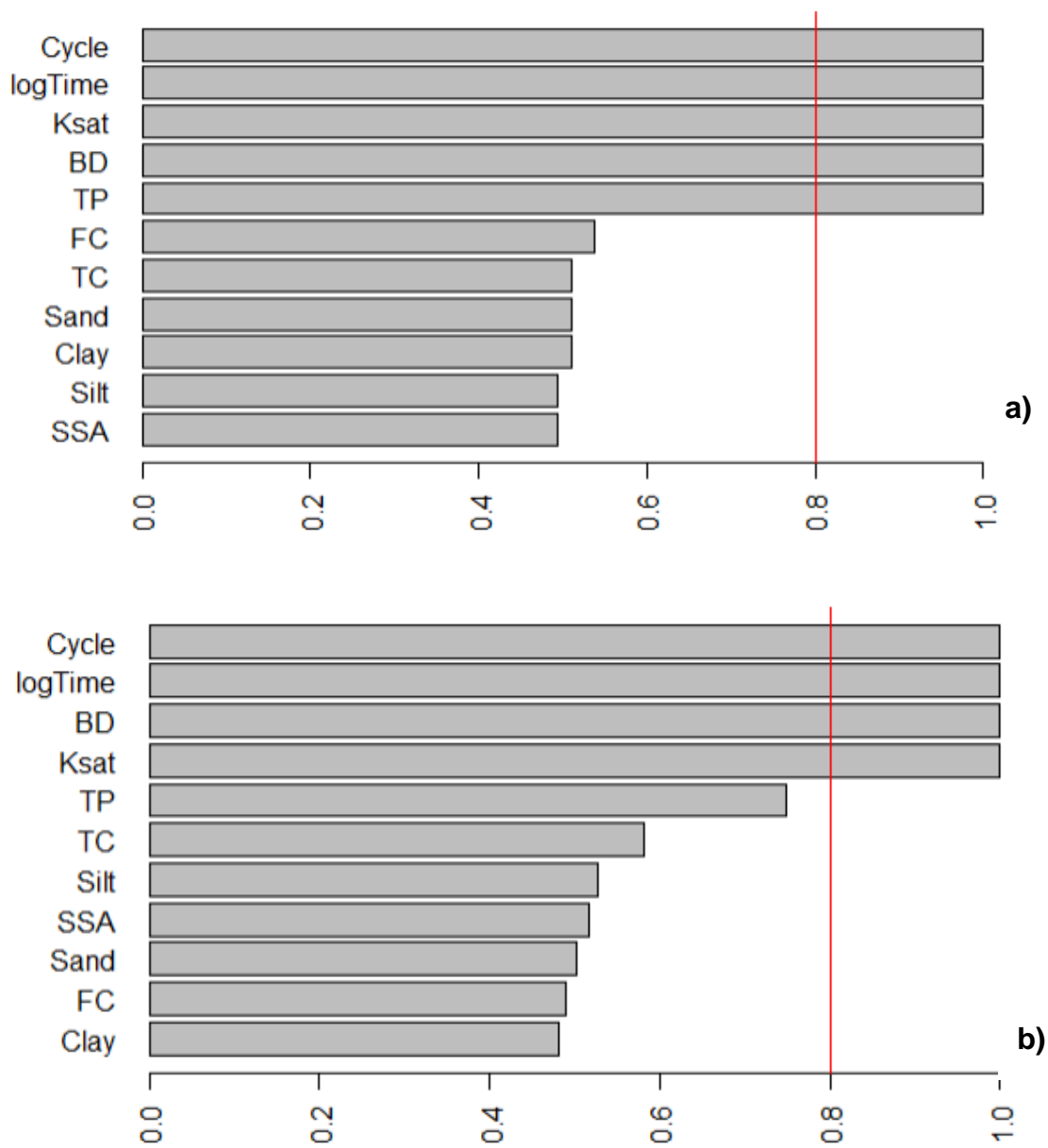
Figure E.1. Studied parameters that explain more than 80% of the infiltration rate (i) for a) the sandy treatments and b) the sandy loam treatments.
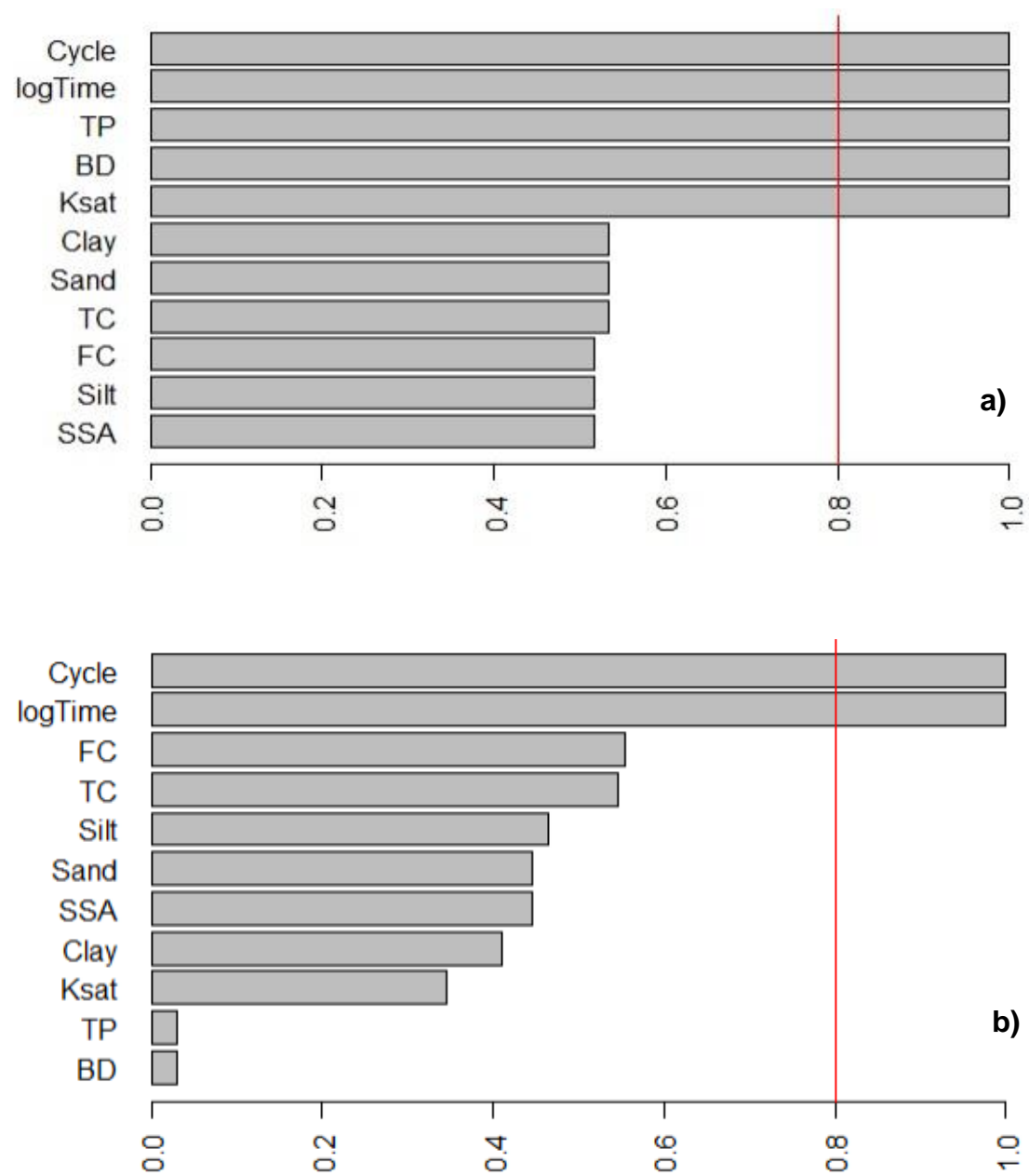
Figure E.2. Studied parameters that explain more than 80% of the cumulative infiltration ($Icum$) for a) the sandy treatments and b) the sandy loam treatments.

Appendix F

Table F.1. Main input parameters used in the SWAT model to explain the hydrological response of the catchment.

Land use type	Layer	Soil depth	Treatment	Hydrological group (CN)	K_{sat}	ρ_d	AWC	Biochar amount
		cm			*mm/h*	*g/cm³*	*%*	*ton/ha*
			S0		613.33	1.50	30.00	-
			S2.5	A	143.33	1.50	53.00	112
			S5		70.00	1.50	69.83	225
Crops and grassland	1	30	SL0		14.56	1.37	97.57	-
			S2.5	B	9.63	1.37	103.30	102
			SL5		5.28	1.36	108.87	204
	2	70			3.75	1.60	43.33	
	3	120			2.64	1.60	62.00	
	1	30			16.88	1.05	55.50	
Forest	2	100	Clay loam	A,B	4.17	1.45	90.15	
	3	133			4.48	1.65	42.09	
	1	16			6.08	1.75	18.11	
Residential and roads	2	46		C,D	2.21	1.80	32.68	
	3	78			3.33	1.75	35.53	

CN: curve number; K_{sat}: saturated hydraulic conductivity; ρ_d: bulk density; AWC: available water content.

Table F.2. Summary of the parameters associated to water infiltration obtained from the simulated hydrological cycle using SWAT model for six scenarios, in the Birris subcatchment.

Treatment	CN	P	AWC	R	R/P	R_{BC}/R
		mm			%	
S0				148.73	7.54	-
S2.5	57.74		262.89	153.73	7.79	3.36
S5		1972.30		162.46	8.24	9.23
SL0				403.25	20.45	-
SL2.5	73.15		270.24	407.37	20.65	1.02
SL5				412.59	20.92	2.32

CN: SCS runoff curve number for moisture condition II; P: precipitation; AWC: available water capacity of the soil layer; R: surface runoff; R/P: fraction of surface runoff from precipitation; R_{BC}/R: fraction of surface runoff of the amended treatments respect to the unamended soil.

References

Abel, S., Peters, A., Trinks, S., Schonsky, H., Facklam, M., Wessolek, G., 2013. Impact of Biochar and Hydrochar Addition on Water Retention and Water Repellency of Sandy Soil. Geoderma 202–203, 183–191.

Abrol, V., Ben-Hur, M., Verheijen, F.G.A., Keizer, J.J., Martins, M.A.S., Tenaw, H., Tchehansky, L., Graber, E.R., 2016. Biochar Effects on Soil Water Infiltration and Erosion nder Seal Formation Conditions: Rainfall Simulation Experiment. J. Soils Sediments 16, 2709–2719.

Adeniji, F.A., Umara, B.G., Dibal, J.M., Amali, A.A., 2013. Variation of Infiltration Rates with Soil Texture . A Laboratory Study. Int. J. Eng. Innov. Technol. 3, 454–459.

Adindu, R.U., Igbokwe kelechi, K., Chigbu Timothy, O., Ike-Amadi, C.A., 2014. Application of Kostiakov's Infiltration Model on the Soils of Umudike, Abia State - Nigeria. Am. J. Environ. Eng. 4, 1–6. https://doi.org/10.5923/j.ajee.20140401.01

AG Boden, 2005. Bodenkundliche Kartieranleitung, 5. Aufl. E. Schweizerbart´sche Verlagsbuchhandlung, Stuttgart.

Agegnehu, G., Srivastava, A.K., Bird, M.I., 2017. The Role of Biochar and Biochar-Compost in Improving Soil Quality and Crop Performance: A Review. Appl. Soil Ecol. 119, 156–170. https://doi.org/10.1016/j.apsoil.2017.06.008

Ajayi, A.E., Holthusen, D., Horn, R., 2016. Changes in Microstructural Behaviour and Hydraulic Functions of Biochar Amended Soils. Soil Tillage Res. 155, 166–175. https://doi.org/10.1016/j.still.2015.08.007

Ajayi, A.E., Horn, R., 2017. Biochar-Induced Changes in Soil Resilience: Effects of Soil Texture and Biochar Dosage. Pedosphere 27, 236–247. https://doi.org/10.1016/S1002-0160(17)60313-8

Ajayi, A.E., Horn, R., 2016a. Modification of Chemical and Hydrophysical Properties of Two Texturally Differentiated Soils due to Varying Magnitudes of Added Biochar. Soil Tillage Res. 164, 34–44. https://doi.org/10.1016/j.still.2016.01.011

Ajayi, A.E., Horn, R., 2016b. Comparing the Potentials of Clay and Biochar in Improving Water Retention and Mechanical Resilience of Sandy Soil. Int. Agrophysics 30, 391–399. https://doi.org/10.1515/intag-2016-0009

Ajayi, A.E., Horn, R., 2016c. Transformation of Ex-Arable Land to Permanent Grassland Promotes Pore Rigidity and Mechanical Soil Resilience. Ecol. Eng. 94, 592–598. https://doi.org/10.1016/j.ecoleng.2016.06.104

Alaoui, A., Lipiec, J., Gerke, H.H., 2011. A Review of the Changes in the Soil Pore System due to Soil Deformation: A Hydrodynamic Perspective. Soil Tillage Res. 115–116, 1–15. https://doi.org/10.1016/j.still.2011.06.002

Amer, A.M., Logsdon, S.D., Davis, D., 2009. Prediction of Hydraulic Conductivity as Related to Pore Size Distribution in Unsaturated Soils. Soil Sci. 174, 508–515. https://doi.org/10.1097/SS.0b013e3181b76c29

Amoakwah, E., Frimpong, K.A., Okae-Anti, D., Arthur, E., 2017. Soil Water Retention, Air Flow and Pore Structure Characteristics after Corn Cob Biochar Application to a Tropical Sandy Loam. Geoderma 307, 189–197. https://doi.org/10.1016/j.geoderma.2017.08.025

Angelaki, A., Sakellariou-Makrantonaki, M., Tzimopoulos, C., 2013. Theoretical and Experimental Research of Cumulative Infiltration. Transp. Porous Media 100, 247–257. https://doi.org/10.1007/s11242-013-0214-2

Assouline, S., Mualem, Y., 1997. Modeling the Dynamics of Seal Formation and its Effect on Infiltration as Related to Soil And Rainfall Characteristics. Water Resour. Res. 33, 1527–1536.

Ayodele, A., Oguntunde, P., Joseph, A., De Souza Dias Junios, M., 2009. Numerical Analysis of the Impact of Charcoal Production on Soil Hydrological Behavior, Runoff Response and Erosion Susceptibility. Rev. Bras. Ciência do Solo 33, 137–145.

Ball, B.C., 1981. Pore Characteristics of Soils from Two Cultivation Experiments as Shown by Gas Diffusivities and Permeabilities and Air-Filled Porosities. J. Soil Sci. 32, 483–498.

Barnes, R.T., Gallagher, M.E., Masiello, C.A., Liu, Z., Dugan, B., 2014. Biochar-Induced Changes in Soil Hydraulic Conductivity and Dissolved Nutrient Fluxes Constrained by Laboratory Experiments. PLoS One 9, e108340.

Barrera, D., Masuelli, S., 2011. An Extension of the Green-Ampt Model to Decreasing Flooding Depth Conditions, with Efficient Dimensionless Parametric Solution. Hydrol. Sci. J. 56, 824–833. https://doi.org/10.1080/02626667.2011.585137

Baver, L.D., Gardner, W.H., Gardner, W.R., 1972. Soil Physics, 4th ed. John Wiley & Sons, USA.

Bayabil, H.K., Lehman, J.C., Yitaferu, B., Stoof, C.R., Steenhuis, T.S., 2013. Hydraulic Properties of Clay Soils as Affected by Biochar and Charcoal Amendments, in: Mekuria, W. (Ed.), Rainwater Management for Resilient Livelihoods in Ethiopia: Proceedings of the Nile Basin Development Challenge Science Meeting. Addis Adaba, 9-10 July. NBDC Technical Report 5. Nairobi, Kenya: International Livestock Research Institute.

Bayabil, H.K., Stoof, C.R., Lehmann, J.C., Yitaferu, B., Steenhuis, T.S., 2015. Assessing the Potential of Biochar and Charcoal to Improve Soil Hydraulic Properties in the Humid Ethiopian Highlands: The Anjeni Watershed. Geoderma 243–244, 115–123. https://doi.org/10.1016/j.geoderma.2014.12.015

Bens, O., Wahl, N.A., Fisher, H., Hüttl, R.F., 2007. Water Infiltration and Hydraulic Conductivity in Sandy Cambisols: Impacts of Forest Transformation on Soil Hydrological Properties. Eur. J. For. Res. 126, 101–109.

Blume, H.P., Brümmer, G.W., Horn, R., Kandeler, E., Kögel-Knabner, I., Kretzschmar, R., Stahr, K., Wilke, B.M., 2010. Scheffer/Schachtschabel: Lehrbuch der Bodenkunde, 16. Auflag. ed. Spektrum Akademischer Verlag, Heidelberg. https://doi.org/10.1017/CBO9781107415324.004

Blume, H.P., Stahr, K., Leinweber, P., 2010. Bodenkundliches Praktikum, 3rd. ed. Spektrum Akademisher Verlag, Heidelberg.

Bodner, G., Scholl, P., Kaul, H.P., 2013. Field Quantification of Wetting-Drying Cycles to Predict Temporal Changes of Soil Pore Size Distribution. Soil Tillage Res. 133, 1–9. https://doi.org/10.1016/j.still.2013.05.006

Boivin, P., Garnier, P., Vauclin, M., 2006. Modeling the Soil Shrinkage and Water Retention Curves with the Same Equations. Soil Sci. Soc. Am. J. 70, 1082–1093. https://doi.org/10.2136/sssaj2005.0218

Bottinelli, N., Zhou, H., Boivin, P., Zhang, Z.B., Jouquet, P., Hartmann, C., Peng, X., 2016. Macropores Generated during Shrinkage in Two Paddy Soils using X-Ray Micro-Computed Tomography. Geoderma 265, 78–86. https://doi.org/10.1016/j.geoderma.2015.11.011

Brewer, C.E., 2012. Biochar Characterization and Engineering. Dissertation. Iowa State University. Paper12284. https://doi.org/12284

Brewer, C.E., Unger, R., Schmidt-Rohr, K., Brown, R.C., 2011. Criteria to Select Biochars for Field Studies based on Biochar Chemical Properties. Bioenergy Res. 4, 312–323. https://doi.org/10.1007/s12155-011-9133-7

Brockhoff, S.R., Christians, N.E., Killorn, R.J., Horton, R., Davis, D.D., 2010. Physical and Mineral-Nutrition Properties of Sand-Based Turfgrass Root Zones Amended with Biochar. Agron. J. 102, 1627–1631. https://doi.org/10.2134/agronj2010.0188

Brodowski, S., Amelung, W., Haumaier, L., Zech, W., 2007. Black Carbon Contribution to Stable Humus in German Arable Soils. Geoderma 139, 220–228.

Bronswijk, J., 1991. Relation between Vertical Soil Movement and Water-Content Changes in Cracking Clays. Soil Sci. Soc. Am. J. 55, 1220–1226. https://doi.org/10.2136/sssaj1991.03615995005500050004x

Brooks, R.H., Corey, A.T., 1964. Hydraulic Properties of Porous Media. Hydrology Paper 3. Colorado State Univ., Fort Collins.

Bughici, T., Wallach, R., 2016. Formation of Soil – Water Repellency in Olive Orchards and its Influence on Infiltration Pattern. Geoderma 262, 1–11.

Burdine, N.T., 1953. Relative Permeability Calculations from Pore Size Distribution Data. Pet. Trans. AIME 198, 71–78. https://doi.org/10.2118/225-G

Burrell, L.D., Zehetner, F., Rampazzo, N., Wimmer, B., Soja, G., 2016. Long-Term Effects of Biochar on Soil Physical Properties. Geoderma 282, 96–102.

Canarache, A., Motoc, E., Dumitriu, R., 1968. Infiltration Rate as Related to Hydraulic Conductivity , Moisture Deficit and other Soil Properties. Soil Sci. March, 392–401.

Carrick, S., Buchan, G., Almond, P., Smith, N., 2011. Atypical Early-Time Infiltration into a Structured Soil Near Field Capacity: The Dynamic Interplay between Sorptivity, Hydrophobicity, and Air Encapsulation. Geoderma 160, 579–589. https://doi.org/10.1016/j.geoderma.2010.11.006

Castellini, M., Giglio, L., Niedda, M., Palumbo, A.D., Ventrella, D., 2015. Impact of Biochar Addition on the Physical and Hydraulic Properties of a Clay Soil. Soil Tillage Res. 154, 1–13. https://doi.org/10.1016/j.still.2015.06.016

Chan, K.Y., Van Zwieten, L., Meszaros, I., Downie, A., Joseph, S., 2007. Agronomic Values of Greenwaste Biochar as a Soil Amendment. Aust. J. Soil Res. 45, 629–634. https://doi.org/10.1071/SR07109

Chartier, M.P., Rostagno, C.M., Pazos, G.E., 2011. Effects of Soil Degradation on Infiltration Rates in Grazed Semiarid Rangelands of Northeastern Patagonia, Argentina. J. Arid Environ. 75, 656–661. https://doi.org/10.1016/j.jaridenv.2011.02.007

Chau, H.W., Goh, Y.K., Vujanovic, V., Si, B.C., 2012. Wetting Properties of Fungi Mycelium alter Soil Infiltration and Soil Water Repellency in A Γ-Sterilized Wettable and Repellent Soil. Fungal Biol. 116, 1212–1218.

https://doi.org/10.1016/j.funbio.2012.10.004

Clothier, B., Scotter, D., 2002. Unsaturated Water Transmission Parameters obtained from Infiltration, in: Dane, J.H., Topp, G.C. (Eds.), Methods of Soil Analysis, Part 4: Physical Methods. Soil Science Society of America, Madison, WI, pp. 879–898.

Coppola, A., Comegna, A., Dragonetti, G., Gerke, H.H., Basile, A., 2015. Simulated Preferential Water Flow and Solute Transport in Shrinking Soils. Vadose Zo. J. 14, 1–22. https://doi.org/10.2136/vzj2015.02.0021

Cornelis, W.M., Corluy, J., Medina, H., Díaz, J., Hartmann, R., Van Meirvenne, M., Ruiz, M.E., 2006. Measuring and Modelling the Soil Shrinkage Characteristic Curve. Geoderma 137, 179–191. https://doi.org/10.1016/j.geoderma.2006.08.022

Demirbas, A., 2006. Production and Characterization of Bio-Chars from Biomass Via Pyrolysis. Energy Sources, Part A Recover. Util. Environ. Eff. 28, 413–422. https://doi.org/10.1080/009083190927895

Devereux, R., Sturrock, C., Mooney, S., 2012. The Effects of Biochar on Soil Physical Properties and Winter Wheat Growth. Earth Environ. Sci. Trans. R. Soc. Edinburgh 103, 13–18.

Ding, Y., Liu, Y., Liu, S., Li, Z., Tan, X., Huang, X., Zeng, G., Zhou, L., Zheng, B., 2016. Biochar to Improve Soil Fertility. A Review. Agron. Sustain. Dev. 36, 1–18. https://doi.org/10.1007/s13593-016-0372-z

Doerr, S.H., Ferreira, A.J.D., Walsh, R.P.D., Shakesby, R.A., Leighton-Boyce, G., Coelho, C.O.A., 2003. Soil Water Repellency as a Potential Parameter in Rainfall-Runoff Modelling: Experimental Evidence at Point to Catchment Scales From Portugal. Hydrol. Process. 17, 363–377. https://doi.org/10.1002/hyp.1129

Doerr, S.H., Shakesby, R.A., Walsh, R.P.D., 2000. Soil Water Repellency: Its Causes, Characteristics and Hydro-Geomorphological Significance. Earth Sci. Rev. 51, 33–65. https://doi.org/10.1016/S0012-8252(00)00011-8

Doerr, S.H., Thomas, A.D., 2000. The Role of Soil Moisture in Controlling Water Repellency: New Evidence from Forest Soils in Portugal. J. Hydrol. 231–232, 134–147. https://doi.org/10.1016/S0022-1694(00)00190-6

Dohnal, M., Dušek, J., Vogel, T., Císlerová, M., Lichner, L., Štekauerová, V., 2009. Ponded Infiltration into Soil with Biopores - Field Experiment and Modeling. Biologia (Bratisl). 64, 580–584. https://doi.org/10.2478/s11756-009-0078-7

Dörner, J., 2005. Anisotropie von Bodenstrukturen und Porenfunktionen in Böden und deren Auswirkungen auf Transportprozesse im gesättigten und ungesättigten Zustand. Dissertation. Christian-Albrechts-Universität zu Kiel.

Dörner, J., Horn, R., 2009. Direction-Dependent Behaviour of Hydraulic and Mechanical Properties in Structured Soils under Conventional and Conservation Tillage. Soil Tillage Res. 102, 225–232. https://doi.org/10.1016/j.still.2008.07.004

Eastman, C.M., 2011. Soil Physical Characteristics of an Aeric Ochraqualf Amended with Biochar. Master Thesis. The Ohio State University. https://doi.org/OSU1316548127

EBC, 2012. European Biochar Certificate-Guidelines for a Sustainable Production of Biochar. Arbaz, Switzerland. https://doi.org/10.13140/RG.2.1.4658.7043

Eibisch, N., Durner, W., Bechtold, M., Fuß, R., Mikutta, R., Woche, S.K., Helfrich, M., 2015. Does Water Repellency of Pyrochars and Hydrochars Counter their Positive

Effects on Soil Hydraulic Properties? Geoderma 245–246, 31–39. https://doi.org/10.1016/j.geoderma.2015.01.009

Elrick, D.E., Reynolds, W.D., 1992. Infiltration from Constant-Head Well Permeameters and Infiltrometers, in: Advances in Measurement of Soil Physical Properties: Bringing Theory into Practice. Soil Science Society of America Journal, Special Publication no.30. https://doi.org/10.2136/sssaspecpub30.c1

Essien, O.E., 2011. Effect of Varying Rates of Organic Amendments on Porosity and Infiltration Rate of Sandy Loam Soil. J. Agric. Environ. 12, 51–58.

Eusufzai, M.K., Fujii, K., 2012. Effect of Organic Matter Amendment on Hydraulic and Pore Characteristics of a Clay Loam Soil. Open J. Soil Sci. 2, 372–381. https://doi.org/10.4236/ojss.2012.24044

Factura, H., Bettendorf, T., Buzie, C., Pieplow, H., Reckin, J., Otterpohl, R., 2010. Terra Preta Sanitation: Re-Discovered from an Ancient Amazonian Civilisation - Integrating Sanitation, Bio-Waste Management and Agriculture. Water Sci. Technol. 61, 2673–2679. https://doi.org/10.2166/wst.2010.201

FAO and ITPS, 2015. Status of the World's Soil Resources (SWSR) – Main Report. Food and Agriculture Organization of the United Nations and Intergovermental Technical Panel on Soils. Rome, Italy. https://doi.org/ISBN 978-92-5-109004-6

Fredlund, M.D., Wilson, G.W., Fredlund, D.G., 2002. Representation and Estimation of the Shrinkage Curve, in: de Campos & Marinho (Eds.), Proceedings of the Third International Conference on Unsaturated Soils, UNSAT. Recife, Brazil, March 10-13.

Gardner, W.R., 1958. Some Steady-State Solutions of the Unsaturated Moisture Flow Equation with Application to Evaporation from a Water Table. Soil Sci. 85, 228–232.

Gaskin, J.W., Speir, A., Morris, L.M., Ogden, L., Harris, K., Lee, D., Das, K.C., 2007. Potential for Pyrolysis Char to Affect Soil Moisture and Nutrient Status of a Loamy Sand Soil, in: Proceedings of the 2007 Georgia Water Resources Conference. University of Georgia, March 27-29. https://doi.org/http://hdl.handle.net/1853/48168

Gebhardt, S., Fleige, H., Horn, R., 2012. Anisotropic Shrinkage of Mineral and Organic Soils and its Impact on Soil Hydraulic Properties. Soil Tillage Res. 125, 96–104. https://doi.org/10.1016/j.still.2012.06.017

Ghanbarian-Alavijeh, B., Hunt, A.G., 2012. Unsaturated Hydraulic Conductivity in Porous Media: Percolation Theory. Geoderma 187–188, 77–84. https://doi.org/10.1016/j.geoderma.2012.04.007

Githinji, L., 2014. Effect of Biochar Application Rate on Soil Physical and Hydraulic Properties of a Sandy Loam. Arch. Agron. Soil Sci. 60, 457–470. https://doi.org/Doi 10.1080/03650340.2013.821698

Glaser, B., Haumaier, L., Guggenberger, G., Zech, W., 2001. The "Terra Preta" Phenomenon: A Model for Sustainable Agriculture in the Humid Tropics. Naturwissenschaften 88, 37–41. https://doi.org/10.1007/s001140000193

Glaser, B., Lehmann, J., Zech, W., 2002. Ameliorating Physical and Chemical Properties of Highly Weathered Soils in the Tropics with Charcoal - A Review. Biol. Fertil. Soils 35, 219–230. https://doi.org/10.1007/s00374-002-0466-4

Gray, D.M., Norum, D.I., 1967. The Effect of Soil Moisture on Infiltration as Related to

Runoff and Recharge, in: Proceedings of Hydrology Symposium No. 6 Soil Moisture. Canada. https://doi.org/10.1016/j.bbrc.2008.12.060

Gray, M., Johnson, M.G., Dragila, M.I., Kleber, M., 2014. Water Uptake in Biochars: The Roles of Porosity and Hydrophobicity. Biomass and Bioenergy 61, 196–205. https://doi.org/10.1016/j.biombioe.2013.12.010

Grayson, R.B., Western, A.W., Chiew, F.H.., 1997. Preferred States in Spatial Soil Moisture Patterns: Local and Nonlocal Controls. Water Resour. Res. 33, 2897–2908.

Haghiabi, A.H., Abedi-Koupai, J., Heidarpour, M., Mohammadzadeh-Habili, J., 2011. A New Method for Estimating the Parameters of Kostiakov and Modified Kostiakov Infiltration Equations. World Appl. Sci. J. 15, 129–135.

Hallett, P.D., 2007. An Introduction to Water Repellency, in: Gaskin, R. (Ed.), Proceedings of the 8th International Symposium on Adjuvants for Agrochemicals (ISAA2007). International Society for Agrochemical Adjuvants (ISAA), Columbus, Ohio, USA.

Hallin, I.L., Douglas, P., Doerr, S.H., Bryant, R., 2015. The Effect of Addition of a Wettable Biochar on Soil Water Repellency. Eur. J. Soil Sci. 66, 1063–1073. https://doi.org/10.1111/ejss.12300

Hamidreza Sadeghi, S., Hazbavi, Z., Kiani Harchegani, M., 2016. Controllability of Runoff and Soil Loss From Small Plots Treated by Vinasse- Produced Biochar. Sci. Total Environ. 541, 483–490.

Hardie, M., Clothier, B., Bound, S., Oliver, G., Close, D., 2014. Does Biochar Influence Soil Physical Properties and Soil Water Availability? Plant Soil 376, 347–361. https://doi.org/10.1007/s11104-013-1980-x

Hardie, M.A., 2011. Effect of Antecedent Soil Moisture on Infiltration and Preferential Flow in Texture Contrast Soils. Dissertation. The University of Tasmania.

Hardie, M.A., Cotching, W.E., Doyle, R.B., Holz, G., Lisson, S., Mattern, K., 2011. Effect of Antecedent Soil Moisture on Preferential Flow in a Texture-Contrast Soil. J. Hydrol. 398, 191–201. https://doi.org/10.1016/j.jhydrol.2010.12.008

Hartge, K.H., 1966. Ein Haubenpermeameter zum schnellen Durchmessen zahlreicher Stechzylinderproben. Z. Kult. und Flurbereinigung 7, 155–163.

Hartge, K.H., Horn, R., 2016. Essential Soil Physics. Schweizerbart Science Publishers, Stuttgart.

Hartge, K.H., Horn, R., 2009. Die physikalische Untersuchung von Böden. 4th Ed. Schweizerbart´sche Verlagsbuchhandlung, Stuttgart.

Hasan, M., Chowdhury, T., Drabo, M., Kassu, A., Glenn, C., 2015. Modeling of Infiltration Characteristics by Modified Kostiakov Method. J. Water Resour. Prot. 7, 1309–1317.

Herath, H.M.S.K., Camps-Arbestain, M., Hedley, M., 2013. Effect of Biochar on Soil Physical Properties in Two Contrasting Soils: An Alfisol and an Andisol. Geoderma 209–210, 188–197.

Hillel, D., 1998. Environmental Soil Physics. Academic Press, USA.

Horn, R., 2004. Time Dependence of Soil Mechanical Properties and Pore Functions for Arable Soils. Soil Sci. Soc. Am. J. 68, 1131–1137. https://doi.org/10.2136/sssaj2004.1131

Horn, R., 1994. Effect of Aggregation of Soils on Water, Gas and Heat Transport, in: Schulze (Ed.), Flux Control in Biological Systems. Academic Press, pp. 335–364.

Horn, R., Kutilek, M., 2009. The Intensity – Capacity Concept — How Far is it Possible to Predict Intensity Values with Capacity Parameters. Soil Tillage Res. 103, 1–3.

Horn, R., Peng, X., Fleige, H., Dörner, J., 2014. Pore Rigidity in Structured Soils - only a Theoretical Boundary Condition for Hydraulic Properties? Soil Sci. Plant Nutr. 60, 3–14. https://doi.org/10.1080/00380768.2014.886159

Huang, M., Rodger, H., Barbour, S.L., 2015. An Evaluation of Air Permeability Measurements to Characterize the Saturated Hydraulic Conductivity of Soil Reclamation Covers. Can. J. Soil Sci. 95, 15–26. https://doi.org/10.4141/cjss-2014-072

Igbadun H.E., Othman M. K., Ajayi A. S., 2016. Infiltration Characteristics of Organic Amended Soils. Glob. J. Res. Eng. 16, 35–39.

Imhoff, P.T., Akbar Nakhli, S.A., 2017. Reducing Stormwater Runoff and Pollutant Loading with Biochar Addition to Highway Greenways. Final Report for NCHRP IDEA Project 182, University of Delaware, Washington, DC.

Instron, 2008. Instron Series 5560A: Reference manual.

Itsukushima, R., Ideta, K., Iwanaga, Y., Sato, T., Shimatani, Y., 2016. Evaluation of Infiltration Capacity and Water Retention Potential of Amended Soil using Bamboo Charcoal and Humus for Urban Flood Prevention, in: Proceedings of the 11th International Symposium on Ecohydraulics. Feb 7-12, Melbourne, Australia.

Jačka, L., Pavlásek, J., Pech, P., Kuráž, V., 2016. Assessment of Evaluation Methods using Infiltration Data Measured in Heterogeneous Mountain Soils. Geoderma 276, 74–83. https://doi.org/10.1016/j.geoderma.2016.04.023

Jeffery, S., Meinders, M.B.J., Stoof, C.R., Bezemer, T.M., van de Voorde, T.F.J., Mommer, L., van Groenigen, J.W., 2015. Biochar Application does not Improve the Soil Hydrological Function of a Sandy Soil. Geoderma 251–252, 47–54. https://doi.org/10.1016/j.geoderma.2015.03.022

Jindo, K., Mizumoto, H., Sawada, Y., Sanchez-Monedero, M.A., Sonoki, T., 2014. Physical and Chemical Characterization of Biochars Derived from Different Agricultural Residues. Biogeosciences 11, 6613–6621. https://doi.org/10.5194/bg-11-6613-2014

Jones, B.E.H., Haynes, R.J., Phillips, I.R., 2010. Effect of Amendment of Bauxite Processing Sand with Organic Materials on its Chemical, Physical and Microbial Properties. J. Environ. Manage. 91, 2281–2288. https://doi.org/10.1016/j.jenvman.2010.06.013

Joseph, S.D., Camps-Arbestain, M., Lin, Y., Munroe, P., Chia, C.H., Hook, J., van Zwieten, L., Kimber, S., Cowie, A., Singh, B.P., Lehmann, J., Foidl, N., Smernik, R.J., Amonette, J.E., 2010. An Investigation into the Reactions of Biochar in Soil. Aust. J. Soil Res. 48, 501–515.

Jury, W.A., Gardner, W.R., Gardner, W.H., 1991. Soil Physics, 5th ed. John Wiley & Sons, USA.

Jury, W.A., Horton, R., 2004. Soil Physics, 6th ed. John Wiley & Sons, USA.

Kameyama, K., Miyamoto, T., Shiono, T., Shinogi, Y., 2012. Influence of Sugarcane

Bagasse-Derived Biochar Application on Nitrate Leaching in Calcaric Dark Red Soil. J. Environ. Qual. 41, 1131–1137. https://doi.org/10.2134/jeq2010.0453

Khabbazi, A.E., Hinebaugh, J., Bazylak, A., 2016. Determining the Impact of Rectangular Grain Aspect Ratio on Tortuosity–Porosity Correlations of Two-Dimensional Stochastically Generated Porous Media. Sci. Bull. 61, 601–611. https://doi.org/10.1007/s11434-016-1020-3

Kinney, T.J., Masiello, C.A., Dugan, B., Hockaday, W.C., Dean, M.R., Zygourakis, K., Barnes, R.T., 2012. Hydrologic Properties of Biochars Produced at Different Temperatures. Biomass and Bioenergy 41, 34–43. https://doi.org/10.1016/j.biombioe.2012.01.033

Kutílek, M., Jendele, L., Panayiotopoulos, K.P., 2006. The Influence of Uniaxial Compression upon Pore Size Distribution in Bi-Modal Soils. Soil Tillage Res. 86, 27–37. https://doi.org/10.1016/j.still.2005.02.001

Laird, D.A., Rogovska, N., Garcia-Perez, M., Collins, H., Streubel, J., Smith, M., 2011. Pyrolysis and Biochar-Opportunities for Distributed Production and Soil Quality Enhancement, in: Newell, K. (Ed.), Sustainable Alternative Fuel Feedstock Opportunities, Challenges and Roadmaps for Six U.S. Regions. United States Department of Agriculture, USDA.

Lal, R., Shukla, M.K., 2005. Principles of Soil Physics. Taylor & Francis e-Library, New York, USA.

Lee, S.S., Shah, H.S., Awad, Y.M., Kumar, S., Ok, Y.S., 2015. Synergy Effects of Biochar and Polyacrylamide on Plants Growth and Soil Erosion Control. Environ. Earth Sci. 74, 2463–2473. https://doi.org/10.1007/s12665-015-4262-5

Lehmann, J., 2009. Terra Preta Nova-Where to from Here?, in: Woods, W.I., Teixeira, W.G., Lehmann, J., Steiner, C., Winklerprins, A.M.G.A., Rebellato, L. (Eds.), Amazonian Dark Earths: Wim Sombroek's Vision. Springer, Dordrecht. https://doi.org/10.1007/978-1-4020-9031-8_28

Li, Y., Ren, X., Hill, R., Malone, R., Zhao, Y., 2017. Characteristics of Water Infiltration in Layered Water-Repellent Soils. Pedosphere 28, 775–792. https://doi.org/10.1016/S1002-0160(17)60414-4

Lianes, E., Marchamalo, M., Roldán, M., 2009. Evaluación del Factor C de la RUSLE para el Manejo de Coberturas Vegetales en el Control de la Erosión en la Cuenca del Río Birrís, Costa Rica. Agron. Costarric. 33, 217–235. https://doi.org/0377-9424

Liang, B., Lehmann, J., Solomon, D., Kinyangi, J., Grossman, J., O'Neill, B., Skjemstad, J.O., Thies, J., Luizão, F.J., Petersen, J., Neves, E.G., 2006. Black Carbon Increases Cation Exchange Capacity in Soils. Soil Sci. Soc. Am. J. 70, 1719–1730. https://doi.org/10.2136/sssaj2005.0383

Lim, T.J., Spokas, K.A., Feyereisen, G., Novak, J.M., 2016. Predicting the Impact of Biochar Additions on Soil Hydraulic Properties. Chemosphere 142, 136–144. https://doi.org/10.1016/j.chemosphere.2015.06.069

Liu, Z., Dugan, B., Masiello, C.A., Gonnermann, H.M., 2017. Biochar Particle Size, Shape, and Porosity Act Together to Influence Soil Water Properties. PLoS One 12, e0179079. https://doi.org/10.1371/journal.pone.0179079

Lopez-Capel, E., Zwart, K., Schackley, S., Postma, R., Stenstrom, J., Rasse, D.P., Budai, A., Glaser, B., 2016. Biochar Properties, in: Shackley, S., Ruysschaert, G., Zwart,

K. & Glaser, B. (Eds.), Biochar in European Soils and Agriculture : Science and Practice. Routledge, Abingdon, UK.

Lopez, V.D., 2014. Biochar as a Soil Amendment: Impact on Hydraulic and Physical Properties of an Arable Loamy Sand Soil. Master Thesis, University of California.

Lu, S.G., Sun, F.F., Zong, Y.T., 2014. Effect of Rice Husk Biochar and Coal Fly Ash on Some Physical Properties of Expansive Clayey Soil (Vertisol). Catena 114, 37–44. https://doi.org/10.1016/j.catena.2013.10.014

Major, J., Rondon, M., Molina, D., Riha, S.J., Lehmann, J., 2010. Maize Yield and Nutrition During 4 Years After Biochar Application to a Colombian Savanna Oxisol. Plant Soil 333, 117–128. https://doi.org/10.1007/s11104-010-0327-0

Mašek, O., Ronsse, F., Dickinson, D., 2016. Biochar Production and Feedstock, in: Shackley, S., Ruysschaert, G., Zwart, K. & Glaser, B. (Eds.), Biochar in European Soils and Agriculture : Science and Practice. Routledge, Abingdon, UK.

Masiello, C.A., Dugan, B., Brewer, C.E., Spokas, K., Novak, J.M., Liu, Z., Sorrenti, G., 2014. Biochar Effects on Soil Hydrology, in: Lehmann, S.J. (Ed.), Biochar for Environmental Management Science, Technology and Implementation. Routledge, pp. 541–560.

Masís-Meléndez, F., Chamindu Deepagoda, T.K.K., de Jonge, L.W., Tuller, M., Moldrup, P., 2014. Gas Diffusion-Derived Tortuosity Governs Saturated Hydraulic Conductivity in Sandy Soils. J. Hydrol. 512, 388–396. https://doi.org/10.1016/j.jhydrol.2014.02.063

Mbagwu, J., 1994. Soil Physical Properties Influencing the Fitting Parameters in Philip and Kostiakov Infiltration Models. Miramare-Trieste.

Miyata, S., Kosugi, K., Gomi, T., Onda, Y., Mizuyama, T., 2007. Surface Runoff as Affected by Soil Water Repellency in a Japanese Cypress Forest. Hydrol. Process. 21, 2365–2376. https://doi.org/10.1002/hyp

Mohawesh, O., Janssen, M., Maaitah, O., Lennartz, B., 2017. Assessment the Effect of Homogenized Soil on Soil Hydraulic Properties and Soil Water Transport. Eurasian Soil Sci. 50, 1077–1085. https://doi.org/10.1134/S1064229317090046

Moldrup, P., Olesen, T., Komatsu, T., Schjønning, P., Rolston, D.E., 2001. Tortuosity, Diffusivity, and Permeability in the Soil Liquid and Gaseous Phases. Soil Sci. Soc. Am. J. 65, 613–623. https://doi.org/10.2136/sssaj2001.653613x

Moldrup, P., Yoshikawa, S., Olesen, T., Komatsu, T., Rolston, D.E., 2003. Air Permeability in Undisturbed Volcanic Ash Soils: Predictive Model Test and Soil Structure Fingerprint. Soil Sci. Soc. Am. J. 67, 32–40. https://doi.org/10.2136/sssaj2003.0032

Mualem, Y., 1976. A New Model for Predicting the Hydraulic Conductivity of Unsaturated Porous Media. Water Resour. Res. 12, 513–522.

Mukherjee, A., Lal, R., 2013. Biochar Impacts on Soil Physical Properties and Greenhouse Gas Emissions. Agronomy 3, 313–339. https://doi.org/10.1016/S0268-0890(99)90085-3

Nartey, O.D., Zhao, B., 2014. Biochar Preparation, Characterization, and Adsorptive Capacity and its Effect on Bioavailability of Contaminants: An Overview. Adv. Mater. Sci. Eng. 1–12. https://doi.org/10.1155/2014/715398

Neitsch, S.L., Arnold, J.G., Kiniry, J.R., Williams, J.R., 2009. Soil & Water Assessment Tool. version 2009. Texas Water Resources Institute Tech.

Nimmo, J.R., 2004. Porosity and Pore Size Distribution, in: Hillel, D. (Ed.), Encyclopedia of Soils in the Environment. Elsevier, pp. 295–303. https://doi.org/10.1016/B978-0-12-409548-9.05265-9

Novak, J., Sigua, G., Watts, D., Cantrell, K., Shumaker, P., Szogi, A., Johnson, M.G., Spokas, K., 2016. Biochars Impact on Water Infiltration and Water Quality Through a Compacted Subsoil Layer. Chemosphere 142, 160–167. https://doi.org/10.1016/j.chemosphere.2015.06.038

Novak, J.M., Busscher, W.J., Watts, D.W., Amonette, J.E., Ippolito, J.A., Lima, I., Gaskin, J., Das, K.C., Steiner, C., Ahmedna, M., Rehrah, D., Schomberg, H., 2012. Biochars Impact on Soil-Moisture Storage in an Ultisol and Two Aridisols. Soil Sci. 177, 310–320.

Novak, J.M., Lima, I., Xing, B., Gaskin, J.W., Steiner, C., Das, K.C., Ahmedna, M., Rehrah, D., Watts, D.W., Busscher, W., Schomberg, H., 2009. Charaterization of Designer Biochar Produced at Different Temperatures and their Effects on a Loamy Sand. Ann. Environ. Sci. 3, 195–206.

Obia, A., Børresen, T., Martinsen, V., Cornelissen, G., Mulder, J., 2017. Effect of Biochar on Crust Formation, Penetration Resistance and Hydraulic Properties of Two Coarse-Textured Tropical Soils. Soil Tillage Res. 170, 114–121. https://doi.org/10.1016/j.still.2017.03.009

Obia, A., Mulder, J., Martinsen, V., Cornelissen, G., Børresen, T., 2016. In Situ Effects of Biochar on Aggregation, Water Retention and Porosity in Light-Textured Tropical Soils. Soil Tillage Res. 155, 35–44. https://doi.org/10.1016/j.still.2015.08.002

Oh, T.K., Choi, B., Shinogi, Y., Chikushi, J., 2012. Characterization of Biochar Derived from Three Types of Biomass. J. Fac. Agric. Kyushu Univ. 57, 61–66.

Ortiz-Malavassi, E., 2014. Atlas de Costa Rica 2014 [WWW Document]. URL (accessed 01.12.2018). https://repositoriotec.tec.ac.cr/handle/2238/6749

Ouyang, L., Wang, F., Tang, J., Yu, L., Zhang, R., 2013. Effects of Biochar Amendment on Soil Aggregates and Hydraulic Properties. J. Soil Sci. Plant Nutr. 13, 991–1002. https://doi.org/10.4067/S0718-95162013005000078

Peake, L.R., Reid, B.J., Tang, X., 2014. Quantifying the Influence of Biochar on the Physical and Hydrological Properties of Dissimilar Soils. Geoderma 235–236, 182–190.

Peng, X., Horn, R., 2013. Identifying Six Types of Soil Shrinkage Curves from a Large Set of Experimental Data. Soil Sci. Soc. Am. J. 77, 372–381. https://doi.org/10.2136/sssaj2011.0422

Peng, X., Horn, R., 2005. Modeling Soil Shrinkage Curve Across a Wide Range of Soil Types. Soil Sci. Soc. Am. J. 69, 584–592. https://doi.org/10.2136/sssaj2004.0146

Peng, X., Horn, R., Smucker, A., 2007. Pore Shrinkage Dependency of Inorganic and Organic Soils on Wetting and Drying Cycles. Soil Sci. Soc. Am. J. 71, 1095–1104. https://doi.org/10.2136/sssaj2006.0156

Peng, X., Zhang, Z.B., Gan, L., Yoshida, S., 2016. Linking Soil Shrinkage Behavior and Cracking in Two Paddy Soils as Affected by Wetting and Drying Cycles. Soil Sci. Soc. Am. J. 80, 1145–1156. https://doi.org/10.2136/sssaj2015.07.0273

Peth, S., 2004. Bodenphysikalische Untersuchungen zur Trittbelastung von Böden bei der Rentierweidewirtschaft an borealen Wald- und subarktisch-alpinen Tundrenstandorten Auswirkungen auf thermische, hydraulische und mechanische Bodeneienschaften. Dissertation. Christian-Albrechts-Universität zu Kiel.

Ritzema, H.P., 2006. Drainage Principles and Applications. Wageningen, Alterra, ILRI Publication no. 16. https://doi.org/10.1016/0378-3774(96)84103-5

Ronsse, F., van Hecke, S., Dickinson, D., Prins, W., 2013. Production and Characterization of Slow Pyrolysis Biochar: Influence of Feedstock Type and Pyrolysis Conditions. GCB Bioenergy 5, 104–115. https://doi.org/10.1111/gcbb.12018

Ruysschaert, G., Nelisesen, V., Postma, R., Bruun, E., O´Toole, A., Hammond, J., Rödger, J.M., Hylander, E., Kihlberg, T., Zwart, K., Hauggaard-Nielsen, H., Shackley, S., 2016. Field Applications of Pure Biochar in the North Sea Region and Across Europe, in: Shackley, S., Ruysschaert, G., Zwart, K. & Glaser, B. (Eds.), Biochar in European Soils and Agriculture: Science and Practice. Routledge, Abingdon, UK.

Saravanathiiban, D.S., Kutay, M.E., Khire, M. V, 2014. Effect of Macropore Tortuosity and Morphology on Preferential Flow Through Saturated Soil: A Lattice Boltzmann Study. Comput. Geotech. 59, 44–53. https://doi.org/10.1016/j.compgeo.2014.02.006

Selker, J.S., Keller, C.K., McCord, J.T., 1999. Vadose Zone Processes. CRC Press LLC, USA.

Sohi, S., Lopez-Capel, E., Krull, E., Bol, R., 2009. Biochar, Climate Change and Soil: A Review to Guide Future Research, CSIRO Land and Water Science Report 05/09. https://doi.org/10.1139/Z03-132

Soil Survey Staff, 2014. Soil Survey Field and Laboratory Methods Manual. Soil Survey Investigations Report no. 51, Version 2.0.

Spokas, K.A., Cantrell, K.B., Novak, J.M., Archer, D.W., Ippolito, J.A., Collins, H.P., Boateng, A.A., Lima, I.M., Lamb, M.C., McAloon, A.J., Lentz, R.D., Nichols, K.A., 2012. Biochar: A Synthesis of its Agronomic Impact Beyond Carbon Sequestration. J. Environ. Qual. 41, 973. https://doi.org/10.2134/jeq2011.0069

Sun, F., Lu, S., 2014. Biochars Improve Aggregate Stability, Water Retention, and Pore-Space Properties of Clayey Soil. J. Plant Nutr. Soil Sci. 177, 26–33. https://doi.org/10.1002/jpln.201200639

Sun, Z., Moldrup, P., Elsgaard, L., Arthur, E., Bruun, E.W., Hauggaard-Nielsen, H., Wollesen de Jonge, L., 2013. Direct and Indirect Short-Term Effects of Biochar on Physical Characteristics of an Arable Sandy Loam. Soil Sci. 178, 465–473.

Tammeorg, P., Simojoki, A., Mäkelä, P., Stoddard, F.L., Alakukku, L., Helenius, J., 2014. Biochar Application to a Fertile Sandy Clay Loam in Boreal Conditions: Effects on Soil Properties and Yield Formation of Wheat, Turnip Rape and Faba Bean. Plant Soil 374, 89–107. https://doi.org/10.1007/s11104-013-1851-5

Tang, C., Shi, B., Liu, C., Suo, W., Gao, L., 2011. Experimental Characterization of Shrinkage and Desiccation Cracking in Thin Clay Layer. Appl. Clay Sci. 52, 69–77.

Teβin, A.K., 2016. Biochar in Soil: Effect on Physical, Chemical and Hydrological Properties in Differently Textured Soils. Master Thesis. Aarhus Universitet.

Tillman, R.W., Scotter, D.R., Wallis, M.G., Clothier, B.E., 1989. Water-Repellency and its Measurement by Using Intrinsic Sorptivity. Aust. J. Soil Res. 27, 637–644. https://doi.org/10.1071/SR9890637

Uloma, A.R., Samuel, A.C., Kingsley, I.K., 2014. Estimation of Kostiakov's Infiltration Model Parameters of Some Sandy Loam Soils of Ikwuano–Umuahia, Nigeria. Open Trans. Geosci. 1, 34–38.

Uzoma, K.C., Inoue, M., Andry, H., Zahoor, A., Nishihara, E., 2011. Influence of Biochar Application on Sandy Soil Hydraulic Properties and Nutrient Retention. J. Food, Agric. Environ. 9, 1137–1143. https://doi.org/10.5530/pj.2018.1.27

van De Genachte, G., Mallants, D., Ramos, J., Deckers, J.A., Feyen, J., 1996. Estimating Infiltration Parameters from Basic Soil Properties. Hydrol. Process. 10, 687–701. https://doi.org/doi:10.1002/(sici)1099-1085(199605)10:5%3C687::aid-hyp311%3E3.0.co;2-p

van Genuchten, M.T., 1980. A Closed-Form Equation for Predicting the Hydraulic Conductivity of Unsaturated Soils. Soil Sci. Soc. Am. J. 44, 892–898.

van Genuchten, M.T., Leij, F.J., Yates, S.R., 1991. The RETC Code for Quantifying the Hydraulic Functions of Unsaturated Soils, EPA/600/2-91/065. Washington, WA, USA. https://doi.org/10.2136/vzj2009.0017

Verheijen, F., Jeffery, S., Bastos, A.C., van der Velde, M., Diasfas, I., 2010. Biochar Application to Soils: A Critical Scientific Review of Effects on Soil Properties, Processes and Functions, EUR 24099 EN, Office for the Official Publications of the European Communities. Luxembourg. https://doi.org/10.2788/472

Villagra-Mendoza, K., Horn, R., 2018a. Effect of Biochar Addition on Hydraulic Functions of Two Textural Soils. Geoderma 326, 88–95.

Villagra-Mendoza, K., Horn, R., 2018b. Effect of Biochar on the Unsaturated Hydraulic Conductivity of Two Amended Soils. Int. Agrophysics 32, 373–378. https://doi.org/10.1515/intag-2017-0025

Villagra-Mendoza, K., Ortiz-Malavassi, E., Otterpohl, R., 2017. Role of Charcoal Addition on Infiltration Processes and Soil Water Content Characteristics of a Sandy Loam Soil. Agric. Eng. Int. CIGR J. 19, 9–15.

Warrick, A.W., 2003. Soil Water Dynamics. Oxford University Press, New York, USA.

Wesseling, J.G., Stoof, C.R., Ritsema, C.J., Oostindie, K., Dekker, L.W., 2009. The Effect of Soil Texture and Organic Amendment on the Hydrological Behaviour of Coarse-Textured Soils. Soil Use Manag. 25, 274–283. https://doi.org/10.1111/j.1475-2743.2009.00224.x

White, I., Sully, M.J., 1987. Macroscopic and Microscopic Capillary Length and Time Scales from Field Infiltration. Water Resour. Res. 23, 1514–1522.

Xing, X., Kang, D., Ma, X., 2017. Differences in Loam Water Retention and Shrinkage Behavior: Effects of Various Types and Concentrations of Salt Ions. Soil Tillage Res. 167, 61–72. https://doi.org/10.1016/j.still.2016.11.005

Xue, J., Gavin, K., 2008. Effect of Rainfall Intensity on Infiltration into Partly Saturated Slopes. Geotech. Geol. Eng. 26, 199–209. https://doi.org/10.1007/s10706-007-9157-0

Yargicoglu, E.N., Sadasivam, B.Y., Reddy, K.R., Spokas, K., 2015. Physical and

Chemical Characterization of Waste Wood Derived Biochars. Waste Manag. 36, 256–268. https://doi.org/10.1016/j.wasman.2014.10.029

Zhang, H.Q., Hartge, K.H., 1995. Mechanical Properties of Soils as Influenced by the Incorporated Organic Matter, Advances in Soil Science: Soil Structure, its Development and Function. CRC Press Inc., Boca Raton, FL., pp.93-108.

Zhang, J., Chen, Q., You, C., 2016. Biochar Effect On Water Evaporation and Hydraulic Conductivity in Sandy Soil. Pedosphere 26, 265–272. https://doi.org/10.1016/S1002-0160(15)60041-8

Zhang, Z.B., Zhou, H., Zhao, Q.G., Lin, H., Peng, X., 2014. Characteristics of Cracks in Two Paddy Soils and their Impacts on Preferential Flow. Geoderma 228–229, 114–121. https://doi.org/10.1016/j.geoderma.2013.07.026

Zhao, Y., De Maio, M., Vidotto, F., Sacco, D., 2015. Influence of Wet-Dry Cycles on the Temporal Infiltration Dynamic in Temperate Rice Paddies. Soil Tillage Res. 154, 14–21. https://doi.org/10.1016/j.still.2015.06.009

Zhi-guo, L., Chi-ming, G., Run-hua, Z., Mohamed, I., Guo-shi, Z., Li, W., Run-qin, Z., Fang, C., Yi, L., 2017. The Benefic Effect Induced by Biochar on Soil Erosion and Nutrient Loss of Slopping Land Under Natural Rainfall Conditions in Central China. Agric. Water Manag. 185, 145–150.

Zolfaghari, Z., Mosaddeghi, M.R., Ayoubi, S., 2016. Relationships of Soil Shrinkage Parameters and Indices with Intrinsic Soil Properties and Environmental Variables in Calcareous Soils. Geoderma 277, 23–34. https://doi.org/10.1016/j.geoderma.2016.04.022

Zong, Y., Chen, D., Lu, S., 2014. Impact of Biochars on Swell – Shrinkage Behavior, Mechanical Strength, and Surface Cracking of Clayey Soil. J. Plant Nutr. Soil Sci. 177, 920–926.

Zornoza, R., Moreno-Barriga, F., Acosta, J.A., Muñoz, M.A., Faz, A., 2016. Stability, Nutrient Availability and Hydrophobicity of Biochars Derived from Manure, Crop Residues, and Municipal Solid Waste for their Use as Soil Amendments. Chemosphere 144, 122–130. https://doi.org/10.1016/j.chemosphere.2015.08.046

Curriculum Vitae

Karolina Villagra Mendoza

Born on January 26, 1976,

In Puntarenas, Costa Rica,

Central America.

University Studies

03/2007 – 10-2019

Technische Universität Hamburg-Harburg, Hamburg (TUHH), Germany.
Doctoral studies on "Effect of Biochar Amended Soils on Infiltration Processes".

10/2004 − 10/2006

Technische Universität Hamburg-Harburg, Hamburg (TUHH), Germany.
Master of Science in Environmental Engineering.
Thesis on "Refined Modelling of Infiltration Processes into the Upper Soil Layer".

12/2000 − 12/2003

Technical University of Costa Rica (ITCR), Cartago, Costa Rica.
Master of Business Administration.

02/1994 − 08/1999

Technical University of Costa Rica (ITCR), Cartago, Costa Rica.
Bachelor in Agricultural Engineering. Graduated with distinction.

Professional and Academic Experience

Since 07/2012

Technical University of Costa Rica (ITCR), Cartago, Costa Rica.
Adjunct Instructor at the Agricultural Engineering School.

01/2017 – 03/2017

Christian-Albrechts-Universität zu Kiel, Kiel, Germany.
Intern at the Institute of Plant Nutrition and Soil Science.

12/2006 − 12/2011

Technische Universität Hamburg-Harburg (TUHH), Hamburg, Germany.

Research Assistant at the Institute of River and Coastal Engineering (Wasserbau).

09/2005 – 11/2005

Björnsen Beratende Ingenieure GmbH. Koblenz, Germany.

Intern at the Hydraulic Engineering Group.

09/2000 – 01/2004

Procter & Gamble (P&G) Global Financial Services.

Financial Accountant.

01/1999 – 07/1999

National Service of Groundwater, Irrigation and Drainage (SENARA).

Consultant at the Hydraulic Engineering Group.

Hamburg, 07.01.2019